STUDIES OF CLASSICAL AND RECURRENT NOVAE

A Thesis
Submitted for the Degree of
Doctor of Philosophy in the Faculty of Science
BANGALORE UNIVERSITY

By

G.C. ANUPAMA

INDIAN INSTITUTE OF ASTROPHYSICS
BANGALORE 560034
INDIA

1990 NOVEMBER

Declaration

I hereby declare that the matter contained in this thesis is the result of the investigations carried out by me at the Indian Institute of Astrophysics, Bangalore and the Department of Physics, Bangalore University, Bangalore, under the supervision of Dr. T.P. Prabhu and Prof. B.C. Chandrasekhara. This work has not been submitted for the award of any degree, diploma, associateship, fellowship, etc. of any university or institute.

Anupama

G.C. Anupama

Candidate

Tushar Prabhu

T.P. Prabhu

Supervisor

B.C. Chandrasekhara

B.C. Chandrasekhara

Supervisor

Bangalore 560034

1990 November 23

Acknowledgement

I am extremely grateful to Dr. T.P. Prabhu for suggesting the topic, and for his constant guidance and encouragement throughout the work. I am also grateful to Prof. B.C. Chandrasekhara for the invaluable help rendered by him towards the successful completion of this thesis.

I thank the Director, IIA for providing all the facilities needed for this study. Prof. J.C. Bhattacharyya took a keen interest in this work. I gratefully acknowledge the encouragement given by him and also by Prof. K.R. Sivaraman; both of them protected me from mundane problems and helped me to concentrate fully on research. The time allocation committee generously allotted observing time on the 102 cm telescope. Mr. K. Kuppuswamy, Mr. A. Muniyandi, Mr. M. Appakutty and others offered much help during observations. It would not have been possible to accumulate the data used in this thesis without all this help. I thank Prof. H.W. Duerbeck for kindly providing the ESO data on Nova Scuti 1989 and T Pyx, and Dr. A. Cassatella for providing the IUE data on RS Oph. I also thank them for many inspiring discussions and correspondence.

All the reductions were performed at the VAX 11/780 system at VBO, Kavalur. I thank Dr. R. Srinivasan, Mr. A.V. Ananth, Dr. K.K. Ghosh, Mr. K.N. Kutty and others at the computer centre. Most of the final figures and text were prepared on personal computers at the computer centre at IIA. I thank Prof. A. Peraiah, Dr. K.E. Rangarajan and Mr. Baba Verghese for the ready help provided by them. Availability of unlimited computer time at both these centres have helped in completing this work in reasonable time frame, and to my satisfaction.

I thank Dr. Ashok Pati for inspiration and for several useful suggestions. Thanks are due to Divakara Mayya for his image processing programs, and Dr. A.V. Raveendran for the program to fit truncated Fourier series. K.S. Balasubramanian, Vasundhara Raju, Divakara Mayya and other friends provided the much-needed moral support. I also thank Prof. N.K. Rao, Dr. K.K. Ghosh, Dr. S. Giridhar, Prof. R.K. Kochhar, Dr. R.C. Kapoor and Dr. S.K. Jain for their support and encouragement.

Ms. A. Vagiswari, Ms. Christina Louis, Mr. H.N. Manjunath and other staff of IIA library made books, journals, references and xerox copies readily available. All the staff of the Director's secretariat were also helpful in every respect. Mr. J.H. Inbaraj prepared the line drawings, Mr. A. Elangovan prepared the photographic prints, and Mr. P.N. Prabhakara made the xerox copies. Mr. D. Kanagaraj, Mr. P. Bose and Mr. M. Subramani bound the copies of the thesis. My thanks are due to all of them. I thank again all those staff members of IIA, Bangalore and VBO, Kavalur, who made it a pleasure to work at the Institute.

Finally, I am immensely grateful to my parents, grandparents, sister, brother-in-law, nephew and other family members for their strong support, encouragement and affection.

Summary

Novae belong to the cataclysmic variable class of objects, which includes dwarf novae, recurrent novae and classical novae. These systems undergo outbursts ranging from $\Delta m \sim$ 2–5 mag for dwarf novae, $\Delta m \sim$ 7–9 mag for recurrent novae, to $\Delta m \sim$ 9–> 14 mag for classical novae, with the inter-outburst periods being $\sim$ weeks to years for dwarf novae, $\sim$ decades for recurrent novae and $\sim 10^4$ years for classical novae. Cataclysmic variables are interacting binary star systems consisting of a Roche-lobe filling secondary, on or near main sequence, losing hydrogen-rich material through the inner Lagrangian point onto an accretion disc that surrounds the primary, which is a white dwarf in most cases. A classical nova outburst is caused by a thermonuclear runaway on the surface of the white dwarf primary, whereas in dwarf novae the outburst is due to accretion disc instabilities, caused by factors such as enhanced mass transfer.

Novae serve as valuable astrophysical laboratories. The physics of accretion onto compact, evolved objects, thermonuclear runaways on semi-degenerate surfaces, line formation and transfer processes in moving atmospheres, and formation of dust in the ejected matter are some of the astrophysical problems that can be understood better by detailed studies of novae. Such problems are also encountered in other instances of ejection of matter such as supernovae and planetary nebulae.

In this study we present optical spectroscopic data of the classical novae LW Serpentis 1978, Nova Scuti 1989 and of the recurrent nova RS Ophiuchi 1985, obtained during outbursts. Spectroscopic data of the recurrent novae T Coronae Borealis, RS Ophiuchi and T Pyxidis and the classical nova GK Persei 1901 obtained during quiescence are also presented. Also, CCD images of the shells of GK Persei, and T Pyxidis are presented. Most of the data used in the study were obtained with the 102 cm reflector at the Vainu Bappu Observatory (VBO). In addition, some data obtained at the European Southern Observatory (ESO), kindly made available by H.W. Duerbeck and also some archival data from the International Ultraviolet Explorer (IUE), kindly made available by A. Cassatella are made use of. All data were reduced at VBO using the locally developed RESPECT software package, as also the STARLINK package with locally developed application routines. These data have been used to study the physical conditions in the nova envelopes, and the components of the binary system.

Chapter I contains a general introduction to the field, and the outline of the

dissertation. Chapter II describes the procedure of data reduction.

Results on three classical novae are presented in Chapter III. The outburst spectrum of the moderately slow nova LW Serpentis 1978 compares well with that of a typical nova. Based on moderate-resolution Hα-line profile, a kinematical model for the shell of LW Serpentis is proposed. The spectrum of Nova Scuti 1989, also a moderately slow nova, compares well with LW Serpentis at similar epochs. The fluxes in emission lines have been used in determining the physical conditions in the ejected material. Spectra observed during oscillations in the light curve show that the variations are mostly in the continuum, and hence imply a change in photospheric radius.

CCD images of the shell of nova GK Persei obtained in the lines of [N II] and [O III] are used to determine the expansion of the shell by comparison with data available in literature. The shell is asymmetric with bulk of the emission arising in the southwest quadrant in the [N II] image. There is a difference in the distribution of [O III] and [N II] emission indicating chemical inhomogeneities. The spectrum at quiescence is decomposed into those of K0-2 IV secondary and the hot accretion disc. The mass transfer rate is estimated to be $\sim 10^{-10}\ M_{\odot}\ \mathrm{yr}^{-1}$. The He/H abundance in the accretion disc is ≤ 0.24.

Results on three recurrent novae are presented in Chapter IV. Although the outburst characteristics of recurrent novae are similar to those of classical novae, the cause of the outburst in these systems is rather uncertain. Outburst in most cases appears to be due to thermonuclear runaways on massive white dwarfs. However, in the case of recurrent novae RS Ophiuchi and T Coronae Borealis, alternative explanations also exist, according to which the primary in these systems is a main sequence star, with outbursts attributed to instabilities in the disc.

The fluxes in the Hα, He I and He II emission lines during the outburst of RS Ophiuchi have been used to determine the electron density and helium abundance (He/H= 0.16) in the envelope. Based on an estimate of the number of hydrogen and helium ionizing photons, the temperature and radius of the ionizing source have been determined. The results obtained during the late stages of outburst are consistent with the primary being a white dwarf rather than a main sequence star. The coronal line fluxes have been used to determine the temperature in the shocked ejecta. Spectra obtained during quiescence indicate that the secondary is an M0 $\pm$ 1 giant. The presence of strong O I 8446 Å emission line implies presence of Lyβ fluorescence and a high temperature for the ionizing source. The presence of O I 7774 Å line in absorption indicates that the accretion disc is optically thick. The quiescence spectrum is decomposed into the spectra of cool secondary and hot accretion disc. The mass transfer rate is estimated to be $\sim 10^{-6}\ M_{\odot}\ \mathrm{yr}^{-1}$. Spectra of the recurrent nova T Coronae Borealis obtained during its quiescence phase (1985–1990) show that the secondary is an M4 $\pm$ 1 giant. The emission lines in the spectra are variable in strength. The Hα flux shows a long term variation with a period $\sim$ 2400 days. Superposed over this is an orbital phase dependent variation with maxima at ~ 0.5 and ~ 0.9 phase. The estimated mass transfer rate is $\sim 10^{-7}\ M_{\odot}\ \mathrm{yr}^{-1}$.

Images of T Pyxidis in [N II] and [O III] reveal a bright shell ejected in the 1944 outburst and a faint extension due to the 1920 outburst. Comparison of VBO and ESO images shows that the bright shell expanded by 0.2 ± 0.1 arcsec in 3 years. The differences in [O III] and [N II] images suggest the presence of chemical inhomogeneities as in the case of GK Persei. The spectrum at quiescence is dominated by the accretion disc, and has a high degree of excitation. The estimated mass transfer rate is $\sim 10^{-8}\ M_{\odot}\ \mathrm{yr}^{-1}$, and He/H abundance is ≤ 0.24.

The results of the study are summarized in Chapter V. A mention is also made of the problems that require further investigation using medium and large telescopes, and multiwavelength long-term monitoring.

The tables, figures and equations are numbered sequentially in each section, with the chapter and section numbers indicated by suffixes.

Contents

I. Introduction

A nova explosion is accompanied by violent ejection of matter causing a spectacular increase in luminosity, occasionally leading to a temporary appearance of a naked eye star where none was known before — hence the historic name *nova stella.*

Novae belong to the group of Cataclysmic Variables — a name first suggested by the Gaposchkins (see Payne-Gaposchkin 1977). These objects are interacting binary star systems consisting of a Roche-lobe filling secondary, on or near main sequence, losing hydrogen-rich material through the inner Lagrangian point onto an accretion disc that surrounds the white dwarf primary. This group also comprises of, in addition to novae, dwarf novae, nova-like variables, AM Herculis stars and intermediate polars. The primary in AM Her and intermediate polars is a magnetic white dwarf. The magnetic field is (i) strong enough to affect the flow of gas from secondary (AM Her type), or, (ii) weaker and only capable of disrupting the accretion disc close to the white dwarf's surface (intermediate polars) (Starrfield 1988). Originally, supernovae were also considered to be cataclysmic variables. The low-mass x-ray binaries, where the primary is a neutron star instead of a white dwarf, are referred to as cataclysmic binaries. Novae are often referred to as classical novae, in order to distinguish them from dwarf novae and also from its sister subgroup recurrent novae described in §I.5.

Novae serve as valuable astrophysical laboratories. The matter accreted by the white dwarf reaches a critical amount, the temperature at the base of the envelope rises sufficiently to ignite thermonuclear reactions, which lead to a runaway reaction. This thermonuclear runaway results in the explosive ejection of the envelope. One observes the evolution of the spectrum formed in this expanding envelope. The physics of accretion onto compact, evolved objects, thermonuclear runaways on semi-degenerate surfaces, which give an insight into nuclear reaction networks, and line formation and transfer processes in moving atmospheres are some of the astrophysical problems that can be understood better by detailed studies of novae. Observations over the past two decades have shown that many novae develop strong infrared emission characteristic of dust formation. The fact that only some novae form dust indicates that conditions for nucleation are just marginal and consequently provides an opportunity to investigate what constitutes favourable conditions. An understanding of physical conditions in the expanding nova envelope in the light of line formation has implications in other environments such as

Table I.1.1 Eruption characteristics of novae.

Class	Range (mag)	Energy (erg)	Recurrence time
Novae			
(a) Classical	$9- > 14$	$10^{45} - \geq 10^{46}$	$10^3 - 10^4$ years (estimated)
(b) Recurrent	$7-9$	$10^{43} - 10^{45}$	$10 - 100$ years
Dwarf novae	$2-6$	$10^{38} - 10^{39}$	$15 - 500$ days
Nova-like			no eruptions (old novae?)

supernovae and Wolf-Rayet stars, while studies of grain formation has implications in environments such as supernovae and planetary nebulae. Other astrophysical processes of relevance to novae are the evolution of individual component stars of the interacting binary system and the effect of magnetic fields on all processes mentioned above.

In this chapter some of the basic, general properties of novae are presented. An early comprehensive review is available in the classic work of C. Payne-Gaposchkin (1957), *The Galactic Novae.* Gallagher & Starrfield (1978), Gerhz (1988), Starrfield (1988) and the book *Classical Novae* (eds. Bode & Evans 1989) contain reviews on recent developments in the field.

1. Observational Properties of Novae

The outburst characteristics of novae, as compared with other cataclysmic variables (Gallagher & Starrfield 1978) are given in Table I.1.1.

1.1 Optical Light Curve

The outbursts of all novae are similar to the extent that all novae show a rapid rise to maximum light followed by a decline to preoutburst magnitude. The temporal evolution of the optical light, *i.e.* timescale and behaviour of decline, however, distinguishes between novae. The overall timescale of a nova outburst is described by the 'speed class', first introduced by Payne-Gaposchkin (1957). The speed class of a nova depends on t_n, the time taken for the nova to diminish by n = (2 or 3)

Table I.1.2 Speed classes of novae.

Speed class	t_2 (days)	Rate of decline (mag/day)
Very fast	$\lesssim 10$	> 0.20
Fast	11–25	0.18–0.08
Moderately fast	26–80	0.07–0.025
Slow	81–150	0.024–0.013
Very slow	151– ≥ 250	0.013– ≤ 0.008

magnitudes below maximum visual brightness or, in other words, the rate of decline during that time. Table I.1.2 gives the speed classes of novae as classified by Payne-Gaposchkin (1957).

The evolution of the optical light curve of a nova is given below. Novae have generally not been observed in their prenova stage. However, sparse preoutburst magnitudes are available for many novae from sky survey observations. These data indicate that V533 Her, LV Vul, CP Lac, BT Mon, GK Per and V1500 Cyg had a significant rise in brightness 1–5 years prior to outburst. Also, nova V446 Her showed dwarf-nova-like eruptions prior to outburst (Warner 1989, Livio 1989).

The initial brightening from the prenova level to two magnitudes below maximum takes place within two or three days. Many novae show a pause during the rise — the premaximum halt — at about two magnitudes below maximum. The nova then brightens to (visual) maximum over a period of one to two days for fast novae and upto several weeks for the slowest. The duration of the maximum phase is of the order of hours for fast novae and a few days in slow novae. The difference between the magnitude in the prenova stage and at maximum gives the range of the nova.

Although the light curve is broadly similar for all novae, there exist several differences in the evolution of individual novae. In the early decline phase, the light curves of very fast and fast novae are generally smooth. The light curves of moderately fast and slow novae decline with minor or major irregularities. Very slow novae have an extended premaximum phase with a delayed maximum. The maximum phase is often structured, with several light maxima.

At about three magnitudes below maximum, the nova enters the 'transition phase'. This phase is of particular interest as novae show their greatest diversity in behaviour during this period. Some novae show large-scale, quasiperiodic oscillations, whereas others enter into a deep minimum phase lasting a few months after which the nova brightens to follow its late decline, while some others have a smooth transition phase without any noticeable pecularity. Fast novae GK Per and V603 Aql showed oscillations with periods of the order of 5 days with a range of 1.5 mag and of the order of 12 days with a range of $\sim$ 1 mag respectively (Warner 1989). A minimum is seen in several moderately fast and slow novae during the transition phase. This minimum is associated with dust formation in the ejecta. Obscuration by dust as an explanation of the deep minimum observed in the optical light curve of nova DQ Her during the transition phase was originally proposed by McLaughlin (1936). Observation of dust in a classical nova was however not directly made until infrared photometry was obtained for the moderately slow nova FH Ser in 1970 (Hyland & Neugebauer 1970). Subsequent infrared observations of several other novae (*e.g.* NQ Vul: Ney & Hatfield 1978, LW Ser: Gerhz *et al.* 1980) confirmed dust formation accompanied by an infrared excess during the transition phase.

Table I.1.3 gives the classification scheme for nova light curves developed by Duerbeck (1981), based on the observed light curve properties of several novae.

The final decline to the postnova stage progresses steadily from the end of the transition phase. During this phase, the photometric and spectroscopic features of the postnova phase gradually emerge. The light curve variations during the postnova quiescence is used in the study of the nova binary system.

The ideal optical light curve of a nova is shown in Figure I.1.1 (McLaughlin 1960; also reproduced by Warner 1989). This figure illustrates the three possible behaviours during the transition phase.

1.2 Spectral Development

Based on a large collection of observational data, McLaughlin developed a classification scheme for the development of the optical spectra of novae. The classification (McLaughlin 1960) exemplifies the differences in the dominant spectral appearances and is related to different phases of the optical light curve variations. The spectral stages are: prenova (quiescence), premaximum (initial rise to maximum), principal (immediate postmaximum, early decline), diffuse enhanced (continued decline), Orion (continued decline), Nitrogen flaring (transition), and nebular (late decline). The spectrum generally consists of broad absorption features at the premaximum,

Table I.1.3 Light curve classification.

Type	Description	Example	Speed class
A	Smooth, fast decline without major disturbances	V1500 Cyg, CP Pup	Very fast
A0	A + oscillations in the transition stage	GK Per, V603 Aql	Fast
B	Decline with or without major irregularities		Moderately fast
Ba	Decline with standstills or other minor irregular fluctuations	V555 Her, LV Vul	
Bb	Decline with major fluctuations	DN Gem, NQ Vul	
C	Extended maximum, deep minimum in transition with		Slow
Ca	small variations of visual brigtness at maximum (< 2 mag)	T Aur, DQ Her	
Cb	strong brightness decline during maximum	FH Ser, LW Ser	
D	Slow evolution, extended pre-maximum, delayed maximum, often several light maxima	HR Del, RR Pic	Very slow

and changes into P-Cygni type emission lines during the principal stage. The diffuse enhanced and Orion stages are characterized by larger velocity absorption systems. Forbidden and permitted lines of nitrogen increase in intensity during the nitrogen flaring stage. The spectrum is that of a photoionized nebula during the nebular stage. Different spectral stages are reached at definite brightness levels of the nova with respect to the maximum light. Permitted and forbidden lines of the resolved shell may be seen several years after outburst during the postnova stage. The nova spectrum in the postnova stage is composite with contribution from the accretion disc and the cool secondary.

The spectral evolution of a nova closely follows the light curve. In the following,

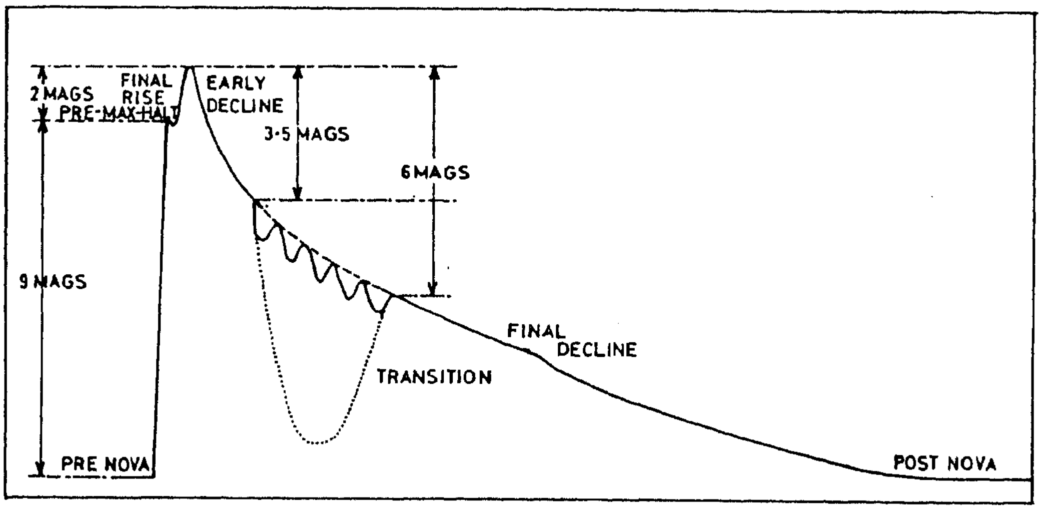

Fig. I.1.1 Ideal optical light curve of a nova (reproduced from Warner 1989).

the evolution is briefly described, following the classification scheme of McLaughlin (1960). The difference in magnitudes, Δm, between the maximum magnitude and the magnitude at the stage in question, and the relative time interval, Δt, measured from date of maximum is also given for each stage.

The prenova spectrum

This stage corresponds to the quiescent phase of the nova prior to its outburst. Only three low resolution objective prism prenova spectra are available taken two (V533 Her), seven (HR Del) and nineteen (V603 Aql) years prior to outburst. The prenova spectrum of these objects is very similar to the postnova spectrum except for emission lines from the ejected shell seen in the postnova spectrum (Seitter 1989). The prenova spectra show a very blue continuum with no or weak emission lines not clearly detectable on the low resolution spectra.

The premaximum spectrum

Premaximum spectra, at $\Delta m = 1.5$ and $\Delta t = -0.1$, are available for a relatively large number of novae (*e.g.* HR Del, V1500 Cyg). In this stage, the spectrum is characterized by strong continuum and blueshifted absorption lines. Emission lines are comparatively weak or absent. The spectrum resembles that of an early type star (*e.g.* B0 for V1500 Cyg: Seitter 1977). The absorption lines due to the elements C, N and O are more pronounced with respect to normal star spectra (McLaughlin 1960). The absorption-line radial velocities usually remain constant or decrease slightly and are generally lower than those of the principal spectrum. Lines consist of a single component with the line width corresponding to the velocity of expansion. The velocities may range from -1300 km s^{-1} for very fast novae like V1500 Cyg (Andrillat 1977) to -72 km s^{-1} for slow novae like RR Pic (Payne-Gaposchkin 1957).

The spectral observations indicate that the premaximum phase of a nova outburst is a period of uniform expansion of an optically thick envelope. It is also observed that the spectrum shifts to later stellar types during this phase, indicating that the envelope cools as it expands.

The principal spectrum

The principal spectrum appears in the immediate postmaximum phase at $\Delta m = 0.6$, $\Delta t = 0.04$. At maximum, the spectrum is characterized by strong absorption lines and resembles the spectrum of an A or F supergiant with the lines of C, N and O being enhanced. The absorption velocities range from 500–$\geq$ 1200 km s^{-1} for fast novae to 150–$\geq$ 300 km s^{-1} for slow novae. At, or immediately after maximum, an emission-line component appears in the principal spectrum. The strongest lines are due to H, Ca II, Na II, and Fe II. Emissions due to [O I] and [N II] soon appear.

The ultraviolet spectrum obtained with the International Ultraviolet Explorer, (IUE), shows strong emission lines, primarily arising from the resonance and lowest lying intercombination lines of abundant elements like He II; Mg II; Al II, Al III; Si II, Si III; N III, N IV, N V; O III, O IV, O V; C II, C III, C IV (Friedjung 1989).

The diffuse enhanced spectrum

This stage appears at $\Delta m = 1.2$, $\Delta t = 0.16$ and is the third absorption system, with broad diffuse absorption lines of species similar to those in the principal system. The velocities of these blueshifted absorptions are twice those of the principal system, ranging from -1200 km s^{-1} to -700 km s^{-1}, depending on the speed class. The absorptions reach a maximum at $\Delta m = 2$, $\Delta t = 4.2$. Lines show P-Cygni profiles with broad emissions of the diffuse enhanced system underlying those of the principal spectrum. In the later phases of this stage, the lines often split into narrow components.

The Orion system

The nova spectrum, which is now a mixture of the principal and diffuse enhanced system, is further complicated by the presence of yet another absorption system — the Orion system. This absorption system develops at $\Delta m = 2.1$, $\Delta t = 0.46$. The absorption component of this system is blue shifted by atleast as much as the diffuse enhanced system, with velocities ranging from -2700 km s^{-1} to -1000 km s^{-1}. The absorption lines are diffuse and remain so until they disappear, at $\Delta m = 3.3$, $\Delta t = 1.25$, with their velocities increasing before disappearance. The maximum of this absorption system occurs at $\Delta m = 2.7$, $\Delta t = 0.8$ and is accompanied by the emergence of N III absorptions. The diffuse enhanced system disappears prior to the Orion system, at $\Delta m = 3.0$, $\Delta t = 1.0$.

The excitation and ionization increase with time all through the Orion stage, as indicated by the N III and N IV (at later times) absorptions. The emission lines associated with this system are broad and grow in strength as the nova declines and the absorption strengths decrease. There are distinctive stages in the development of the Orion emission during which particular species become exceptionally strong. These are the [O I] flash occurring at $\Delta m = 2.6$, $\Delta t = 0.7$ and the [N II] flash at $\Delta m = 3.3$, $\Delta t = 1.25$. Nitrogen flaring or the '4640 stage' is another, most frequent example of line enhancement. This feature appears due to blending of lines of the N III multiplet at 4640 Å and other N II and N III lines. This stage emerges at $\Delta m = 3.0$, $\Delta t = 1.0$ and persists into the late nebular stage. The '4640 stage' corresponds to the transition phase of the optical light curve. In the Orion stage, the lines are generally structured.

In the ultraviolet region, the line spectrum remains roughly the same throughout the principal, diffuse enhanced and Orion stages, with an increase in line-to-continuum ratios, as the continuum fades faster.

The nebular stage to post nova

This final spectral phase of a nova outburst is characterized by forbidden lines which make an appearance even when the principal spectrum is strong. The first forbidden lines to appear are those of [O I]. These lines are characteristic of high density and low temperatures. The lines of [O I] are followed by [Fe II]. At about the time the Orion spectrum begins to fade out, lines of [N II] and [O III] appear. Lines of [Ne III] and [Ne V] are characteristic of the Orion stage. During transition, lines of highly ionized metals appear. Also, coronal lines of [Fe VI], [Fe X], [Fe XI], [Fe XIV], [A X] and [A XI] appear in some novae. In this 'nebular stage', the spectrum consists of emission lines of H, He I, He II, N II, N III and the forbidden lines, all of the same width as the absorption lines in the principal system.

The principal absorption system disappears, during the evolution of the nebular

Table I.1.4 Emission line spectral phases.

Spectral phase	$T_{\rm rad}$ K	N_e cm^{-3}	Prominent lines (λ in Å)
Neutral	10^5	$> 10^9$	O I 1304, C II 1335, Fe II 5169
Auroral	10^5	10^8	[O III] 4363, [O I] 5577, [N II] 5755
Coronal	10^6	10^8	[Si IX] 2150, [Fe X] 6374, [Al IX] 20400
Nebular	10^5	10^7	[Ne III] 3869, [O III] 5007, [N II] 6584

spectrum, at $\Delta m = 4.1$, $\Delta t = 2.2$. The optical spectrum evolves towards that of a planetary nebula with the N III absorption disappearing at $\Delta m = 4.4$, $\Delta t = 2.7$ and the '4640' diffuse emission disappearing at $\Delta m = 4.7$, $\Delta t = 3.5$. The density in the ejecta steadily decreases, with the temperature of the ionizing source steadily increasing, as seen by the appearance and strengthening of highly ionized lines in the spectrum. At $\sim$ 5 magnitudes below maximum, the [O III] 5007 Å line equals Hβ in strength.

In the ultraviolet region also, forbidden lines of highly ionized species like those due to [Ne III], [Ne IV], [Ne V]; [Na V], [Na VI]; [Mg V], [Mg VII]; [Al VI], [Al VIII] and [Si VII], [Si IX] appear in the nebular phase.

The highly ionized forbidden lines seen in the nebular phase of a nova spectrum arise in an expanding shell photoionized by the central remnant (*e.g.* V693 CrA: Williams *et al.* 1984; GQ Mus: Krautter & Williams 1988). In some novae, the coronal lines, like those due to [Fe X], [Fe XI], [Fe XIV], [A X] arise in the ejecta shock heated to temperatures $\sim 10^6$ K either by dissipation of turbulence within the ejecta (*e.g.* V1500 Cyg: Shields & Ferland 1978), or by interaction with a pre-existing circumstellar material (*e.g.* RS Oph: Gorbatskii 1972, 1973; Bode & Kahn 1985).

The emission spectrum in a nova outburst is seen to evolve as density declines. The characteristics of ionization and emission spectrum are determined essentially by the radiation temperature ($T_{\rm rad}$) and the number density (N_e). The emission line spectral phases, and prominent lines in each phase, as also the corresponding $T_{\rm rad}$ and N_e (Williams 1989) are shown in Table I.1.4.

In the infrared 1–4 μm region, during the free-free stage of nova development, the spectrum is dominated by lines of H I and He I, with contributions from C I, O I and Na I. In addition, some novae show lines due to diatomic molecules like CO (Bode & Evans 1989). The 8–13 μm region is also dominated by lines of H I. [Ne II] is present in the case of 'neon' novae (Gerhz, Grasdalen & Hackwell 1985). Coronal lines are seen in the infrared also during the coronal line phase in the optical. During the dust formation phase in the 'dusty' novae, the spectrum is essentially featureless. However some novae (V1370 Aql and QU Vul) have shown a prominent excess around 10 μm, attributed to the silicate signature (Bode & Evans 1989).

The emission lines in the nebular phase show highly structured profiles. These line profiles can be used to interpret the geometry of the nova outburst and the nova shell. Coarse structure can be interpreted in terms of an equatorial ring and a pair of polar blobs based on early stage line profile studies (*e.g.* V603 Aql: Weaver 1974; DQ Her: Mustel & Boyarchuk 1970; LW Ser: Prabhu & Anupama 1987). Later profiles show increasing fine structure in the emission lines, indicating breaking up of the shell into numerous small cloudlets (Seitter 1989).

Velocities gradually decrease due to the snow-plow effect caused by sweeping up of interstellar medium. The ionization decreases with decrease in temperature of the ionizing source as the white dwarf cools down. Density also decreases and appears to remain constant at $N_e \sim 10^3$ cm^{-3} or less, indicating that the shell has reached a stable state (Seitter 1989).

As the nova fades to its preoutburst magnitude, spectrum characteristic of the binary system begins to appear. The spectrum shows a strong blue continuum superposed by emission lines characteristic of an accretion disc. The red-infrared region is dominated by the secondary spectrum. Superposed on this spectrum are the permitted and forbidden lines from the steadily dispersing nova shell.

1.3 Interrelationship between Observational Properties

From the studies of novae in M31, Hubble (1929) noticed that bright novae fade faster than fainter novae. Later work on Galactic novae by McLaughlin (1945) showed the same correlation between peak luminosity and the rate of decline. The relatively easily observable rate of decline is thus a luminosity and hence a distance indicator, making novae one of the standard candles for extragalactic distance modulus estimates. The rate-of-decline–magnitude relationship is usually written in the form (Warner 1989)

$$M = b_n \log t_n - a_n \tag{I.1.1}$$

where t_n is the time taken to decline n magnitudes from maximum brightness, M is the absolute magnitude (V, B or pg) at maximum light and $n = 2$ or 3. The linearity in the above relationship breaks down for the fastest and slowest novae (Arp 1956). Recently, based on their studies of M31 novae, Capaccioli *et al.* (1989) proposed a new form of relationship that incorporates the deviations from linearity for largest and smallest values of t_2. The relationship is expressed as

$$M_V(\max) = -7.89 - 0.81 \arctan\left(\frac{1.32 - \log t_2}{0.19}\right). \tag{I.1.2}$$

Observations show that all novae, irrespective of speed class have the same absolute magnitude 15 days past maximum (*e.g.* van den Bergh & Younger 1987; Cohen 1985; Warner 1989). This empirical relationship $M(t_{15}) = K$ (const) is also used as an extragalactic distance indicator.

The expansion velocities observed in novae are also related to the speed class. The correlation of t_n with $v_{\rm exp}$, the mean expansion velocity (km s^{-1}) deduced from the principal and diffuse enhanced absorption spectra as expressed by McLaughlin (1960) is

$$\begin{aligned} \log v_{\rm exp} &= 3.70 - 0.5 \log t_3 \\ &= 3.57 - 0.5 \log t_2 \qquad \text{principal} \end{aligned} \tag{I.1.3}$$

and

$$\begin{aligned} \log v_{\rm exp} &= 3.81 - 0.4 \log t_3 \\ &= 3.71 - 0.4 \log t_2 \qquad \text{diffuse enhanced.} \end{aligned} \tag{I.1.4}$$

1.4 Multiwavelength Aspects

The observational properties of novae discussed in the earlier sections were based on optical studies. Observations of novae in the x-ray, ultraviolet, infrared and radio regions over the last two decades have vastly improved the understanding of these systems.

The correlation of the peak luminosities and the ejection velocities with the timescales of outburst, give an impression that faster novae are overall more energetic than the slower novae. But, the time integrated optical luminosities of the fast novae are lower than those of slow novae (Payne-Gaposchkin 1957). This shows the unreliability of the optical light curve as a measure of the bolometric variation during outburst. Analysis of the ultraviolet flux measurements on FH Ser (1970) (Gallagher & Code 1974) and subsequent observations of novae in the ultraviolet (see *e.g.* Friedjung 1989) showed that while a nova decreases in the optical, the ultraviolet flux is redistributed towards the shorter wavelength in such a way that the total (ultraviolet+optical) remains nearly constant. Also, the infrared observations of FH Ser (Hyland & Neugebaur 1970; Geisel, Kleinmann & Low 1970) and subsequent infrared observations of novae (*e.g.* Gerhz 1988; Bode & Evans 1989) showed that during the transition phase when the optical light curve drops by several magnitudes, an infrared excess develops. The excess is such that the total (infrared+optical) luminosity is maintained at approximately same level as the (optical+ultraviolet) luminosity earlier. The constant bolometric luminosity behaviour is true of both fast and slow novae. For fast novae a constant luminosity plateau is found at a luminosity considerably lower than that at maximum brightness (Gallagher & Starrfield 1976; Martin 1989).

The total luminosity of a nova is often compared with the Eddington luminosity expressed as (Rybicki & Lightman 1986)

$$L_{\rm ed} = \frac{4\pi G M c m_{\rm H}}{\sigma_T} = 1.25 \times 10^{38}\ \ {\rm erg\ s^{-1}} \left(\frac{M}{M_\odot}\right)$$

where $\sigma_T = 6.65 \times 10^{-25}$ cm^2 is the Thomson cross-section. Eddington limit is the maximum luminosity that a central mass M can have. During the constant bolometric luminosity phase the nova emits at $L \simeq L_{\rm ed}$ for 1 $M_\odot$. The total radiant energy emitted by a nova lies in the range 10^{45}–10^{46} erg (Gallagher & Starrfield 1978).

Ultraviolet observations of old novae at quiescence give results concerning the underlying binary, especially the accretion disc and about the possibility of continuing activity of the hot component of the binary. The ratio of ultraviolet He II 1640 Å and 3203 Å lines is a good indicator of interstellar reddening. The strength of the 2200 Å absorption is also an indicator of interstellar absorption.

The development of novae in the infrared closely follows the photomteric and spectral development at visual wavelengths. The sequence of infrared development as a function of decline from the visual maximum is (Bode & Evans 1989) as follows: During the first $\sim$ 0.5–1 mag from maximum, the remnant is optically thick. The transition to optically thin occurs after a decline $\sim$ 1 mag. The time of this transition is however wavelength dependent. The observed continuum flux from a nova is of thermal origin. The main contributor to the opacity is the free-free absorption which varies as ν^{-2}. Hence the envelope remains optically thick in the infrared for a longer duration than in the optical. Immediately prior to — and around — visual maximum, the infrared flux is simply the Rayleigh–Jeans tail of the optical pseudo-photosphere. The infrared maximum is hence somwhat delayed relative to visual maximum. When the remnant is optically thick, its angular diameter may be determined assuming that it radiates as a blackbody. The rate of change of the angular diameter with time together with the expansion velocity give an estimate of the distance to the nova. Within a few days of visual maximum, the expanding envelope becomes optically thin and the infrared flux distribution is characteristic of thermal bremsstrahlung with emission lines superimposed. Some novae (slow ones) show an excess in the infrared due to dust formation, when they have declined by ~3–4 mag. The visual light curve enters a minimum at this phase, indicating an optical depth > 1 to optical radiation. The absorption in this case is attributed to the dust formed in the envelope. The dust temperature for the novae having the 'optically thick' shell falls initially and then rises to a maximum, which coincides precisely with maximum infrared luminosity and the minimum in the visual light curve (*e.g.* FH Ser, NQ Vul). Some novae have dust shells that are optically thin to visible radiation (*e.g.* V1668 Cyg). In this case the dust temperature falls monotonically and the visual light curve is smooth. The grains formed contain either carbon in the form of graphite, or silicon carbides, or silicates. Silicates are more likely to be formed in 'neon' novae, where the primary is a O-Ne-Mg white dwarf, whereas, for a C-O white dwarf primary the grains are comprised of carbon (Bode & Evans 1989).

The first classical novae to be detected at radio wavelengths were HR Del 1967 and FH Ser 1970 (Hjellming & Wade 1970). The characteristic timescales of the radio variation in novae is several years, and the maximum radio flux density occurs much later than optical maximum ($\sim$ 100 days later) (Seaquist 1989). During the rising part of the radio light curve, the radio spectral index is $\alpha > 0$ ($f_\nu \propto \nu^\alpha$), whereas, during the decay $\alpha \sim -0.1$. These characteristics are consistent with thermal bremsstrahlung emission from an ionized gas shell ejected at the time of the outburst. The prolonged timescale of radio emission is because the emitting gas remains optically thick at radio wavelengths long after optical maximum. The radio data, combined with optical data provide estimates of distances, masses and kinetic energies of the nova envelopes (the kinetic energies are of the order 10^{44}–10^{45} erg s^{-1}, $\sim$ 10 percent of the total radiant energy). Since the shell is fully ionized during the radio emitting phase, the mass estimated is more accurate than estimates using optical lines. In addition, radio measurements are unaffected either by interstellar dust or the dust formed within the nova envelope. The development of the radio emission detected from the recurrent nova RS Oph during its 1985 outburst was, on the other hand, different from classical novae. This is explained as a result of interaction of the ejecta with circumstellar matter formed due to wind from the secondary (Bode & Kahn 1985).

Three classical novae — GQ Mus, QU Vul, PW Vul (Ögleman, Beuermann & Krautter 1984; Ögleman, Krautter & Beuermann 1987) and one recurrent nova — RS Oph (Mason *et al.* 1987) are the only novae detected in the x-ray during outburst. GK Per was detected as an x-ray source during its dwarf-nova-like outbursts (King, Ricketts & Warwick 1979; Watson, King & Osborne 1985). About 9 novae have been positively detected as x-ray sources in their post-outburst quiescence (Becker 1989). The EXOSAT observations of the three classical novae made at late times in the outburst ($\gtrsim$ 200 days) indicate that the source of emission is the hot white dwarf radiating at $L \sim L_{\rm ed}$, at a temperature $\sim 3 \times 10^5$ K. In GQ Mus, the x-ray emission is consistent with nuclear burning of around 10^{-6} $M_\odot$ on a surface of a 0.8–0.9 $M_\odot$ white dwarf (Becker 1989). X-ray emission during the early times of the outburst of RS Oph arise from the shock-heated, radio emitting region of the ejecta. The x-ray flux detected at late times around day 250 however is from the hot white dwarf, as in the classical novae (Mason *et al.* 1987). The hard x-ray flux from quiescent novae arises from the boundary layer of the accretion disc, whereas the soft x-rays may originate from the white dwarf primary itself or from an optically thin boundary layer.

1.5 Recurrence of Nova Outbursts

The statistics on space densities of interacting white dwarf binaries in the Galaxy and M31, and the observed rate of discovery of novae suggests that classical nova systems have an eruption once every 10^4–10^5 years (Ford 1978; Bath & Shaviv 1978). The mass ejected during a nova outburst is $\sim 5 \times 10^{-5}$ $M_\odot$ (Pottasch 1959). This implies a mean mass transfer rate of $\sim 5 \times 10^{-9}$–5×10^{-10} $M_\odot$ yr^{-1} between outbursts. A classical nova system can undergo $\sim 10^4$ outbursts in its lifetime of $\sim 10^9$ years (Ford 1978; Bath & Shaviv 1978). A few novae are known to have outbursts every few decades, in contrast with the recurrence period of $\sim 10^4$ years for classical novae. These systems are known as recurrent novae. The mean recurrence period of ~ 40 years for the recurrent novae implies a mean mass transfer rate $\sim 10^{-6}\ M_\odot\ \mathrm{yr}^{-1}$. The lifetime of these systems is estimated as $\sim 10^5$ years (Bath & Shaviv 1978).

The higher mass transfer rates for recurrent novae imply that secondaries in these systems are giants instead of main sequence stars as in the dwarf and classical nova systems. The secondaries of the recurrent novae T CrB, RS Oph and V745 Sco are indeed M-giants (*e.g.* Webbink *et al.* 1987; Duerbeck & Seitter 1989), and the mass transfer rates in T CrB and RS Oph are of the order $10^{-6}\ M_\odot\ \mathrm{yr}^{-1}$ (see Chapter IV, this study). On the other hand the colours of the recurrent nova T Pyx is extremely blue at quiescence indicating that the secondary is probably not a giant. The speed class designations of the recurrent novae span the range from slow to very fast. Although only a few recurrent novae are known, they seem to be quite a heterogeneous class of objects with different configurations and histories. Since more than half of the known recurrent novae were discovered only during the past 50 years, it is likely that more classical novae will be found, in the future, to be recurrent in nature. It would be of interest to know whether the distribution of periodicities is bimodal with peaks at a few decades and a few tens of thousands of years, or on the other hand form a continuous distribution.

2. Interacting Binary Models of Novae

The first indication that novae are binary systems was provided by the photometric observations by Walker (1954), whereas it was the classic work of Kraft (1964) that established the fact that all novae occur in binary systems. The interacting binary model for cataclysmic variables that is universally accepted now was first proposed by Crawford & Kraft (1956). In the restricted three body problems worked out for such binary systems, the most important feature is the figure-of-eight equipotential surface surrounding both stars. This surface gives a dumb-bell shape when rotated about the line of centres. The lobes of the dumb-bell are called the 'Roche lobes' and their point of contact, which is a saddle point is the inner Lagrangian point.

In a nova system, one member of the binary is a white dwarf (primary) and the other member a larger, cooler star (secondary) that fills its Roche lobe. The separation of the white dwarf and its companion is small enough that a combination of gravitational and centrifugal forces causes a flow of gas through the inner Lagrangian point into the lobe of the white dwarf. The material transferred has

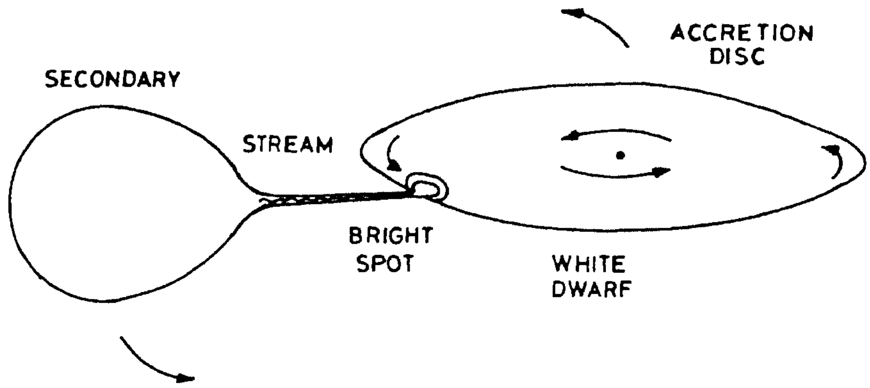

Fig. I.1.2 Schematic representation of a cataclysmic binary system.

high specific angular momentum and hence does not strike the primary directly, but follows an elliptical orbit. The effect of the Roche potential and Coriolis forces causes this ellipse to precess slowly about the white dwarf. However internal dissipation within the gas stream causes it to lose energy through radiation. The timescale for energy dissipation being much shorter than that for angular momentum redistribution, the stream reaches the orbit of lowest energy consistent with its specific angular momentum, *i.e.* a circular one. However, the presence of internal dissipation processes even after circularization causes the circulating gas to lose energy. This loss of gravitational binding energy results in the gas sinking deeper into the gravitational potential of the primary by orbiting it more closely. This in turn causes a loss of angular momentum in the form of a redistribution of the angular momentum in the stream. Thus the gas elements near the white dwarf surface, with their higher circular velocities transfer their angular momentum to the more slowly rotating material further out. In this way the inner parts of the matter spiral in towards the white dwarf giving up their binding energy to supply the losses caused by internal dissipation, while their angular momentum is transferred outwards to the edge of the matter distribution. The outer parts of matter gaining angular momentum spiral outwards. Ultimately a disc-like distribution of circulating matter lying in the orbital plane and extending down to the white dwarf surface is formed. This disc is known as the accretion disc. Figure I.1.2 (from King 1989) is a schematic representation of a cataclysmic binary system.

It is relatively easy to model the physical parameters of the accretion disc when it is in a steady state. The kinetic energy present in the circulating matter close to the white dwarf surface is given up in a 'boundary layer' of radial extent $b \ll R_1$, before accretion onto the white dwarf occurs. The boundary layer has extremely high temperatures, of the same order or greater than the white dwarf temperature, and emits hard and soft x-rays. In the presence of magnetic field strong enough to disrupt the disc flow near its inner edge, accretion occurs only on to small regions of the white dwarf near the magnetic poles, resulting in pulsed emission, as in intermediate polars and AM Her stars. Details of the formation of the accretion disc and its properties are available in King (1989).

3. Theory of Outburst

Theoretical models with thermonuclear runaway reactions on the surface of the white dwarf have been extremely successful in reproducing the observed energetics of a nova outburst. The presence of a significant fraction of close binaries among 10 old novae studied by Kraft (1964) led him to propose that the nova outburst was caused by thermonuclear reactions occurring in the accreted envelope of the white dwarf. The nuclear reactions that occur during the resulting evolution were first described in detail by Starrfield *et al.* (1972), Starrfield, Sparks & Truran 1974). Basing their work on the hydrostatic accretion studies, Starrfield *et al.* (1972) treated the thermonuclear runaway by means of a nuclear reaction network and showed that the outburst originated as a product of the nonequilibrium β^+ decays in combination with enhanced CNO nuclei in the envelope. Reviews of the early work on the thermonuclear studies are found in Gallagher & Starrfield (1978) and Starrfield, Sparks & Truran (1976). Bath & Shaviv (1976) showed that radiation pressure can drive winds from novae for extensive periods. The early work has been extended and supported in the recent years by a number of analytic and semi-analytic studies of accretion processes. Numerical simulations of the envelope accretion and evolution were first carried out by Kutter & Sparks (1980), Nariai, Nomoto & Sugimoto (1980) and by Prialnik *et al.* (1982). The thermonuclear runaway reactions and the nova outburst models are explained in detail by Starrfield, and Bath & Harkness in the book *Classical Novae* (eds. Bode & Evans 1989).

The accretion layer near the white dwarf surface grows in thickness with constant mass transfer from the secondary, until it reaches a temperature high enough for thermonuclear burning of hydrogen to begin at the bottom. The degenerate nature of the white dwarf surface causes a steady increase in the temperature as the nuclear reactions proceed, causing a steady increase in the reaction. This heats the gas still further, finally giving rise to a thermonuclear runaway. Energy production rapidly increases, culminating in an explosive outburst. Factors such as white dwarf mass and luminosity, mass accretion rate, and the chemical composition of the reacting layer all strongly influence the evolution of the outburst. In the outbursts of novae, CNO reactions at high temperatures and densities impose severe constraints on the energetics of the outburst, as they provide the required energies for a nova outburst and shell ejection (Starrfield, Sparks & Truran 1974). The most important aspect of the CNO reactions is the heating of the envelope by the decay of the four β^+ unstable nuclei— $^{13}_{17}$N, $^{14}_{8}$O, $^{15}_{8}$O and $^{17}_{9}$F. In the initial phases of the evolution, the lifetimes of the CNO nuclei against proton capture are much longer than the decay times of the β^+ unstable nuclei allowing for their decay so that proton capturing by the daughter nuclei can keep the reactions cycling. As the temperature in the shell source increases, the CNO lifetimes against proton capture continuously decrease, until at temperatures of $\sim 10^8$ K they become shorter than the β^+ decay lifetime and every proton capture is followed by a waiting period before the β^+ decay occurs followed by another proton capture. During the evolution to the peak temperature a convective region forms just above the shell source and encompasses the entire accreted envelope. This implies that at the peak of the outburst the β^+ unstable nuclei are the most abundant CNO nuclei. Since CNO reactions do not create new nuclei but only redistribute them among the various CNO isotopes (Starrfield *et al.* 1972), the rate of energy production at maximum temperature depends only on the half-lives and numbers of the β^+ decay nuclei initially present in the envelope. The convective timescale in the envelope being shorter than the β^+ decay time, these nuclei reach the surface without decaying. Once the peak temperature is reached and the envelope begins to expand, the rate of energy generation drops. The decline in energy generation is dependent on the decay of the β^+ unstable nuclei as their decay is independent of temperature and density. The decay of the β^+ unstable nuclei provides the delayed source of energy ultimately responsible for both ejecting the shell and producing the luminous output of the outburst. Enhancement of CNO abundance leads to an increase in peak energy generation and more energy is stored for release at outburst. The energy released in this case is sufficient to eject material with expansion velocities similar to those observed and also reproduce the observed light curves of fast novae (Starrfield 1989 and references therein).

Hydrodynamic simulations also predict a phase of constant bolometric luminosity following the initial outburst. This is because only a fraction of the accreted envelope is ejected during the initial nova explosion. The remaining material quickly returns to quasistatic equilibrium (Prialnik, Shara & Shaviv 1978). Since the shell source is still burning at the bottom of the envelope, the luminosity is $\sim L_{\rm ed}$, and therefore the temperature exceeds 10^5 K. This material is slowly ejected by radiation-pressure-driven mass loss. This remnant present on the white dwarf radiates at a constant bolometric luminosity. Once the nova attains the constant bolometric luminosity, its evolution is somewhat slower, with the evolution back to minimum taking a few years. The least studied and least understood phase of a nova outburst is the final turnoff phase when the white dwarf rids itself of enough material to halt nuclear burning in the shell. It is also during this time that the accretion disc re-establishes itself so that the system can begin to evolve to another outburst in 10^4–10^5 years.

Recently, Starrfield, Sparks & Truran (1987), Starrfield, Sparks & Webbink (1989), Webbink *et al.* (1987), Kato (1990a, 1990b, 1990: preprint) have shown that the outbursts of recurrent novae U Sco, T Pyx and RS Oph can be explained as a consequence of thermonuclear runaways on white dwarfs with mass approaching the Chandrasekhar limit. As an alternative to the thermonuclear mechanism on white dwarfs, Webbink (1976) and Livio, Truran & Webbink (1986) have suggested that the outbursts of the recurrent novae T CrB and RS Oph are accretion events on a main sequence primary. The secondary in RS Oph is assumed to be a bloated main sequence star (Livio, Truran & Webbink 1986). In the models of Webbink (1976) and Livio, Truran & Webbink (1986), the outburst is caused by an episodic transfer of a chunk of matter from the secondary onto the main sequence primary. The energy released during the circularization of this matter is responsible for the outburst. It is not yet clear which of these two models represents the reality.

4. Novae among other Eruptive Variables

Variables related to classical novae can be divided into three main classes (Vogt 1989): (i) potential novae — dwarf novae and novalike variables; (ii) stars which share some outburst characteristics with novae — symbiotic novae; and (iii) stars which are evolutionarily related to classical novae, *i.e.* possible progenitors and successors of novae — progenitors could be binary nuclei of planetary nebulae and close, but detached, white dwarf–red dwarf pairs; successors could be type Ia supernovae and their remnant nuclei.

Spectra of old novae, as seen earlier, are generally characterized by Balmer and He II emission, as well as high excitation emission lines such as He II 4686 Å and the C III/N III '4640' complex. The spectra of nova-like variables are very similar to old novae. These objects are probably old novae whose outbursts occurred in pre-historic times. They could also be novae in a pre-outburst phase. Dwarf novae in quiescence show a spectrum very similar to that of old novae, except that lines of high excitation are weaker or absent. These systems undergo outbursts with amplitudes between 2–6 magnitudes, the outbursts repeating in semi-regular time intervals. The risetime for an outburst is very short, but decline takes much longer. Some dwarf novae also show standstills for days, months or years, during which period the star remains at a constant luminosity between that of quiescence and outburst maximum. The outbursts of dwarf novae are a consequence of accretion disc instabilities (Vogt 1989; Bath 1978). The disc instability could be caused by an episodic mass transfer from the secondary. The excess infalling mass is immediately transferred onto the white dwarf surface, releasing energy in the process. Alternatively, the mass transfer rate is constant and mass is accreted in a torus, forming the outer disc. As soon as its total mass and viscosity reaches a certain critical value, part of the torus becomes unstable and there is an infall of matter onto the white dwarf, releasing energy in the process.

Several novae have shown dwarf-nova-like activity in their post outburst quiescence phase. The best studied case is GK Per 1901, for which more than 10 dwarf nova outbursts have been recorded. Another well documented case is V1017 Sgr. This system was earlier classified among recurrent novae. However, in recent years it has become more evident that it is a classical nova with one recorded nova eruption (1919) and two dwarf-nova-like outbursts (1901, 1973) (*e.g.* Vogt 1989). Fragmentary data exist for other cases such as WY Sge and Q Cyg. Nova V446 Her 1960 and V3890 Sgr 1962 have shown dwarf-nova-like activity prior to nova outburst. A recent nova outburst of V3890 Sgr (1990: *AAVSO Alert Not. No.* 125) classifies it among the recurrent novae.

Postoutburst quiescence observations of novae have revealed the presence of magnetic white dwarfs in some nova systems: *e.g.* DQ Her, GK Per, V1500 Cyg. Quiescence observations of DQ Her exhibit oscillations in the light curve with a stable period of 71 seconds (Patterson, Robinson & Nather 1978; Martin 1989). Time resolved spectroscopy also reveals similar periodicities (Chanan, Nelson & Margon 1978). The stability in the periodicity is attributed to the rotation of the white dwarf with magnetic field of strength $\sim 6 \times 10^5$ G (Lamb & Patterson 1983) associated with it. This field strength disrupts the accretion disc only near the white dwarf surface. The magnetic properties of this system lead to its classification as an intermediate polar (Warner 1983; Martin 1989). It is also a prototype of the 'DQ Her' class of objects (Lamb & Patterson 1983). GK Per also has a similar white dwarf (Bianchini & Sabadin 1983; Watson, King & Osborne 1985). V1500 Cyg on the other hand, exhibits a spectrum similar to that of AM Her (Hutchings 1979; Kaluzny & Chlebowski 1988). Polarization studies reveal a $\pm 5\%$ variable circular polarization with a periodicity of 0.137154 day indicating that the white dwarf has a surface magnetic field of $\sim 10^7$ G (Stockman *et al.* 1988; Horne & Schneider 1989). V1500 Cyg is the first nova eruption to be recognized as having originated in an AM Her type system.

The symbiotic novae are similar to the very slow novae which undergo single nova-like eruptions (2–7 magnitudes amplitude) and fade over a period of several years. The spectral development is similar to that of classical novae *e.g.* RR Tel, PU Vul. The quiescence spectra of the recurrent novae T CrB, RS Oph and V745 Sco are very similar to the spectra of symbiotic stars. The spectrum is a typical combination spectrum consisting of molecular absorption lines of a late-type giant and emission lines of high ionization. The symbiotic stars are long period binaries. Both T CrB and RS Oph have long periods (227.5 and 230 days respectively: Kenyon & Garcia 1986; Garcia 1986). The light variations of symbiotic stars resemble those of cataclysmic variables in many respects.

In the studies of recurrent nova outbursts as a consequence of thermonuclear runaways, Starrfield, Sparks & Truran (1987), Starrfield, Sparks & Shaviv (1989) and Kato (1990a) have shown that during the outburst only a small fraction of the matter accreted onto the massive white dwarf is ejected. The mass of the white dwarf, which is already approaching the Chandrasekhar limit, increases following each outburst. It has been suggested that these systems will end as supernovae of type Ia, and such a supernova explosion would not disrupt the system, but would leave behind a low-mass x-ray binary system (Vogt 1989).

5. The Cyclic Evolution Scenario

Novae and dwarf novae have essentially the same binary configuration. The space densities of these two class of objects is also of the same order. Also a number of novae exhibit dwarf nova eruptions. Based on these similarities Vogt (1982) suggested classical novae and dwarf novae are the same stars. According to Vogt, the post nova gradually develops through different dwarf nova stages which mainly differ in accretion rate and density of the disc. The cycle is closed with a permanent standstill in which the white dwarf accumulates sufficient material to initialize a new nova explosion. Recently, a similar scenario has been elaborated in more detail by Shara *et al.* (1986), Prialnik & Shara (1986), Livio & Shara (1987) and Livio (1989). The cyclic evolution scenario for classical novae is described below.

The accretion rate in nova systems varies as a function of time (Livio 1988, 1989; Shara 1989). During a nova outburst, high luminosities ($\gtrsim L_{\rm ed}$) are reached, and mass ejection continues for weeks or months. As seen earlier, during the constant $L_{\rm bol}$ phase, the white dwarf effective temperature increases and the photosphere shrinks. The mass ejection rate from the white dwarf decreases and finally stops. However, the nova remnant remains hot and luminous for 50–300 years (Livio & Shara 1987). This is because the hot white dwarf irradiates the secondary causing enhanced mass loss from it (Kovetz, Prialnik & Shara 1988). It has been observed that a number of novae, *e.g.* V1229 Aql, IV Cep, HR Del, FH Ser, V1500 Cyg, CP Pup, did not return to their preoutburst brightness for a long time (Robinson 1975; Warner 1985).

As the white dwarf cools, the rate of mass transfer $\dot{M}$ decreases. When $\dot{M}$ drops below a critical value $\dot{M} \lesssim 10^{-9}\ M_\odot\ {\rm yr}^{-1}$, accretion disc instabilities occur and old classical novae undergo dwarf nova eruptions (Shara 1989; Livio 1989). Several old novae exhibit dwarf nova activity. Mass transfer rates further decrease to the point that dwarf nova eruptions become infrequent or stop altogether. After a long interval of very low $\dot{M}$ ('hibernation') the mass transfer rate starts increasing and dwarf nova eruptions begin again (Shara 1989). Further increase in $\dot{M}$ suppresses dwarf nova eruptions when $\dot{M} \gtrsim 10^{-9}\ M_\odot\ {\rm yr}^{-1}$. At this rate of $\dot{M}$ the system appears as a nova-like variable, as it would have spectroscopic properties of an old nova with no sign of a visible shell and no history of a recent thermonuclear runaway. Eventually the nova-like variable erupts again as a classical nova when the pressure and temperature at the envelope base become large enough to trigger a thermonuclear runaway (Shara 1989; Livio 1989).

A cataclysmic binary can thus recycle itself several times, becoming in turn a dwarf nova, a hibernating system, a born again dwarf nova, a nova-like variable and finally a classical nova.

6. Outline of the Present Investigation

This work deals with a study of classical and recurrent novae at outburst and postoutburst quiescence. In what follows, an outline of the study is given.

The second chapter describes the observational techniques and the data reduction procedure. The reduction methods for both photographic and CCD spectra are described. The methods of detector calibration, wavelength and flux calibration of the spectrum, correction for atmospheric extinction and measurement of line fluxes are discussed in detail. The spectroscopic data reduction package, *RESPECT*, developed locally is also described. This chapter also deals with the methods of reduction of CCD image data of nova shells, which includes flat field correction, alignment and stacking of different frames.

In the third and fourth chapters the individual systems studied are presented. Chapter III deals with Classical Novae and Chapter IV with Recurrent Novae. In Chapter III, studies of three classical novae — Nova LW Ser 1978, Nova Scuti 1989 and GK Per 1901 are presented. Previously unpublished outburst data on the moderately slow nova LW Ser 1978 is utilized to study its spectral evolution during the diffuse enhanced and onset of [O I] flash phase. A kinematic model for the nova shell is proposed based on the Hα line profile. Spectra of Nova Scuti 1989 also obtained during its diffuse enhanced and [O I] flash phase are used to study its spectral evolution in correlation with the outburst light curve. Based on the observed emission line fluxes, the reddening and distance to the nova and physical conditions in the envelope such as density and temperature are estimated. The last section in this chapter deals with the study of the old nova GK Per at quiescence. The quiescent spectrum is used to determine the spectral type of the secondary. An estimate is made of the accretion disc spectrum. Based on emission line fluxes, the temperature, radius and mass of the white dwarf primary, size of accretion disc and helium abundance in the disc are estimated. Narrow band images of the nebular remnant of GK Per are used to study the differences in the spatial distribution of oxygen and nitrogen in the shell. Also, based on proper motion measurements the shell expansion velocity is determined.

Chapter IV contains the study of three recurrent novae — RS Oph, T CrB and T Pyx. RS Oph is studied in both outburst (1985) and quiescence phases. The outburst data is used to study the temporal evolution of the spectrum and physical conditions such as density and mass in the ejected envelope. Temperature in the shock-heated region is determined using the coronal line ratios. Helium abundance and the physical parameters of the primary are estimated using hydrogen and helium lines. The quiescence spectrum is used to determine the type of the secondary. An estimate of the accretion disc contribution to the optical spectrum is made. Based on the estimated accretion disc spectrum mass transfer rate in this system and the size of the accretion disc is estimated. The quiescence spectrum of T CrB is used to determine the spectral type of the secondary. The orbital phase dependance of the emission line flux variability is brought out. Quiescent spectrum of T Pyx is presented in the last section of this chapter. The fluxes of hydrogen and helium emission lines are to estimate the helium abundance in the accretion disc and the temperature of the primary. Also presented in this section are the narrow band images of the shell. These images are used to determine the differences in the spatial distribution of oxygen and nitrogen in the shell, which has a slow expansion.

The fifth and final chapter discusses the results obtained in this investigation, and also presents the future prospects.

II. Observational Techniques

Instruments used in astronomical observations are light collecting and analysing devices. The light collector is the telescope. This is followed by an analyser, such as a spectrograph or a band-selecting filter, and finally a light detector-recorder device or a system such as a photographic plate or a charge-coupled device (CCD).

Astronomical telescopes use either refraction or reflection to gather light over a large collecting surface and focus it onto a much smaller area. Refractors use lenses and are hence affected by chromatic aberration. Reflecting telescopes make use of paraboloidal reflecting surfaces. In reflectors, the prime focus is in front of the mirror. This means that an appreciable amount of light is blocked by focal plane instruments. In order to reduce this, a secondary mirror placed before the primary focus is used to bring light to a focus either at the side of the telescope tube (Newtonian focus) or to a focus behind the telescope tube through a hole in the primary (Cassegrain). In yet another type of focus — the coudé arrangement — light is brought down the polar axis of the telescope drive by a series of secondary mirrors to a fixed focus often in a room below the telescope. This arrangement is convenient for the use of large, heavy instruments.

1. Spectroscopy

A spectrum of light radiated by the star can be obtained by passing the light through a spectrograph. The starlight dispersed by the grating is then recorded either on photographic plates or on solid state detectors such as CCD.

1.1 Instrumentation

Observations of novae included in this work were made with the 102 cm Carl Zeiss reflector at Vainu Bappu Observatory (VBO), Kavalur. A spectrograph at the f/13 Cassegrain focus of the telescope was employed to obtain spectra. The detectors used in recording the spectra were (a) photographic plates, (b) CCD. Two different spectrographs were used. (i) A Cassegrain spectrograph fabricated at the Indian Institute of Astrophysics (IIA). This spectrograph consists of a mirror collimator of focal length 70 cm, with the camera-grating-collimator angle being 60°. Cameras with focal length 175 mm and 150 mm are available with the spectrograph. A set of gratings: 80 g mm^{-1}, 300 g mm^{-1}, 400 g mm^{-1}, 600 g mm^{-1} and 1800 g mm^{-1} is available for various dispersions. (ii) The Carl Zeiss Universal Astronomical Grating Spectrograph (UAGS). This spectrograph consists of a catadioptric collimator system of effective focal length 83 cm. The camera-grating-collimator angle is 48°. Cameras of focal length 110 mm, 150 mm, 175 mm and 250 mm are available for use with the spectrograph. A set of gratings: 150 g mm^{-1}, 300 g mm^{-1}, 651 g mm^{-1} and 1800 g mm^{-1} is available for various dispersions.

In the case of photographic data, Kodak IIaD, 103aD and 098-02 plates were employed for recording the spectrum. A Varo 8605 image intensifier was employed to intensify the starlight before recording onto the photographic plate held in contact with the fiber-optic output face plate of the image intensifier. Calibration of photographic densities to a relative intensity scale is achieved by the calibration plate obtained using an auxiliary calibration spectrograph equipped with a rotating sector to yield twelve 1 mm steps at relative exposure intervals of $\Delta \log E = 0.1$. CCD spectra were obtained using the Photometrics CCD system which has a Thomson-CSF TH7882 CCD chip coated for ultraviolet enhancement as the detector. More details of observations of novae included in this study are given in sections of Chapters III and IV where they are discussed individually.

1.2 Data Reduction

Procedure

Reductions of spectroscopic data involve the following operations

(a) detector calibration,
(b) wavelength calibration,
(c) atmospheric extinction correction,
(d) instrumental response correction,
(e) flux calibration,
(f) computation of line fluxes/equivalent widths.

A spectrum recorded on a photographic plate is digitized using a microdensitometer. This spectrum is contaminated by emulsion grain noise caused due to clumping of individual grains of the photosensitive silver halide emulsion into more or less dense clusters with areas of lower density between them. The nonuniformity of sensitivity to light over the surface of the grain also contributes to noise. Noise needs to be removed to facilitate evaluation of weaker features in data. Noise removal can be done in measurement domain by convolution of data with a weighting function, or in Fourier domain by multiplying with an appropriate filter. If one obtains the power spectrum of data, it is seen that noise power decreases exponentially with frequency. The signal power falls faster at higher frequencies due to the degrading effects of factors such as resolution of the instrument. On a well-exposed spectrum, signal dominates at the lower Fourier frequencies, whereas noise dominates at higher frequencies. Noise can hence be filtered out in Fourier space. Filtering can be achieved by multiplying the Fourier spectrum of data with either a low-pass filter or an optimal filter (Anupama 1990). Low-pass filter is one which has a strength of 1 upto frequencies over which signal is dominant and strength 0 at frequencies corresponding to noise. The Fourier transform of such a filter with sharp cutoff, however, has sidelobes, which would cause 'ringing' in the data after multiplication. The edges of the filter are, in practice, rounded using a cosine-bell function to suppress ringing. A low-pass filter leaves the low-frequency noise intact. The use of a weighted, optimal filter (Brault & White 1971; Lindgren 1975) removes an estimated proportion of variations caused by low-frequency noise. Photographic noise is found to increase linearly with signal. To enable better accuracy in noise removal at higher densities, the observed densities can be transformed to 'modified densities' such that noise remains nearly constant at all density levels (Lindgren 1975; Anupama 1990).

Noise removed data is converted to intensity values using a calibration curve given by

$$\log I = \sum_{i=1}^{n} a_i (\log \omega)^i, \tag{II.1.1}$$

where $\omega = \log(10^D - 1)$ is the Baker density, and $D = -\log(I_t/I_o)$ is the ordinary density, I_o and I_t being the intensities incident on the photographic emulsion and transmitted by it, respectively. The calibration curve is determined from the calibration plate where density step values are registered for known values of relative intensities. The intensity of the image tube thermal background is then subtracted in log (Intensity) domain to get the intensities in the stellar spectrum.

A CCD detector has a two-dimensional format, high quantum efficiency, and linearity. The last two properties, together with the fact that it is re-usable and can hence be calibrated better, make the use of a CCD detector in stellar spectroscopy more advantageous than photographic plates. A CCD detector has flaws which includes charge-transfer inefficiencies at low exposure levels, sensitivity to cosmic ray particle hits, cosmetic defects and read-out noise. The raw CCD image needs to be corrected for electronic bias, thermal noise, pixel-to-pixel sensitivity difference (flat-fielding) and sky background. If $R(x,y)$ is the raw CCD image, with $B(x,y)$ the bias image, $F(x,y)$ the flat-field image and $S(x,y)$ the sky background, then the actual stellar counts $D(x,y)$ are given by

$$D(x,y) = \frac{R(x,y) - B(x,y)}{F(x,y)} - S(x,y). \qquad \text{(II.1.2)}$$

In the following, we use the coordinate system with x increasing in the direction of dispersion, and y along the slit.

Electronic bias needs to be subtracted to eliminate signal registered by the detector in the absence of exposure to light. The required bias image B is constructed by averaging a series of zero-exposure images. Averaging is done to reduce the statistical noise introduced by bias subtraction. A pixel-by-pixel bias subtraction is then performed to obtain a bias subtracted data.

Pixel-to-pixel variations are compensated for, and long-scale response variations are removed through division by a flat field image factor F. This image factor is constructed from several flat-field images obtained by exposing the CCD to a spatially-uniform continuum source. The flat images are individually de-biased and 'stacked' together by weighted averaging. The use of several well-exposed flat images to construct the template image reduces statistical errors introduced during division. The procedure generally adopted for flat-fielding varies slightly between imaging and spectroscopy. In the case of spectroscopy vignetting in the direction parallel to the slit is corrected by flat-fielding in the usual fashion *i.e.* division of image by flat image, whereas the vignetting in the direction of dispersion, which is distorted by varying efficiency of optical elements and the detector to light of different wavelengths, is corrected by instrumental response correction. Thus, only pixel-to-pixel sensitivity variations are corrected for by flat-fielding in the direction of dispersion. In order to acheive this, the flat-field is divided by a low-order polynomial in x, resulting in an image with values of order unity. Division by such an image approximately preserves the relationship between data counts and detected photons, but corrects for pixel-to-pixel variations.

The recorded stellar spectrum is often contaminated by sky background consisting of both continuous and emission spectrum. This needs to be subtracted out. The sky background S is derived from the de-biased and flat-fielded image by smoothly interpolating sky data on each side of the object spectrum. A least-squares low-order polynomial fit to the sky data at each y is obtained. The sky background interpolated for the position of the spectrum is then subtracted from the de-biased and flat-fielded image to obtain the stellar counts $D(x,y)$.

The de-biased, flat-fielded, sky-subtracted, one-dimensional stellar spectrum now needs to be extracted out from the two-dimensional image. This can be done by summing contributions from a range of spatial pixels y_1 through y_2 containing the object spectrum. Such a sum would extend far into the wings of the starlight profile $P(x, y)$, where the signal is weak compared with background noise. This delivers a noisy spectrum. This can be avoided by using an optimal extraction method. In this method, the spatial profile $P(x, y)$ of the starlight, varying very slowly with wavelength (x direction) is constructed. The contribution $f(x, y)$ to the spectrum at wavelength x by a pixel (x, y) is given by

$$f(x,y) = \frac{D(x,y)}{P(x,y)}. \tag{II.1.3}$$

The total spectrum is obtained by taking a weighted average

$$f(x) = \frac{\sum_y w(x,y) f(x,y)}{\sum_y w(x,y)}, \tag{II.1.4}$$

where $w(x, y)$ are the weights, inversely proportional to the variances,

$$w(x,y) = \frac{P^2(x,y)}{V^2(x,y)}. \tag{II.1.5}$$

The variance is determined as $V(x, y) = V_0 + D(x, y)Q$, with $\sqrt{V_0}$ the root-mean-squared readout noise, $D(x, y)$ the registered counts, Q the effective number of photons per data number and hence $N = QD$ the number of incident photons and $\sqrt{N}$ the rms noise in photons.

The spectrum $f(x)$ thus obtained is the optimal estimate of stellar spectrum. This method of extraction is equivalent to performing an inverse-variance weighted least-squares fit at each x of a known spatial profile to data points with known uncertainties. An optimal extracted spectrum has a better signal-to-noise ratio as lower weights are given to noisy pixels in the wings of the starlight profile.

The extraction of CCD spectrum as described above closely follows the method of Horne (1986, 1988). Reduction procedure common to photographic and CCD spectroscopy is described below.

The spectrum is calibrated to a wavelength scale using the coefficients obtained by fitting a low-order polynomial to the comparison source spectrum and binned at equal wavelength intervals by spline interpolation.

The observed counts or relative intensities $I_{\nu,\mathrm{obs}}$ at frequency ν are related to the true spectrum f_ν by the relation

$$I_{\nu,\mathrm{obs}} = a f_\nu R_\nu e^{-\tau\nu}, \qquad \text{(II.1.6)}$$

where a is a constant scale factor relating the observed spectrum to actual energy flux, R_ν is the relative efficiency of the telescope, instrument and detector system to the light of frequency ν, and τ is the attenuation of starlight by the earth's atmosphere.

Extinction in the earth's atmosphere is caused by Rayleigh scattering of light by O_2 and H_2O molecules in the atmosphere. The wavelength calibrated spectrum is corrected for extinction using the relation

$$I_{\mathrm{cor}} = I_t e^{kX/\lambda^4}, \qquad \text{(II.1.7)}$$

where k is the constant determining the fraction of light scattered and is site dependant, whereas X measures the length of the atmosphere traversed by the starlight and is given by

$$X = \sec Z - 0.0018167(\sec Z - 1)^2 - 0.002875(\sec Z - 1)^3 - 0.0008083(\sec Z - 1)^4, \qquad \text{(II.1.8)}$$

where Z is the zenith distance of the star (Hardie 1962).

Instrumental response curve R_ν is determined from the standard stars for which spectral energy distribution is accurately known. A correction curve, as a function of wavelength is determined by dividing the observed fluxes of the standard star by its actual fluxes. Division of the program star spectrum by this correction curve yields stellar spectrum corrected for the instrumental response.

Telluric absorption bands are present in the near infrared region with band heads at 6867 Å and 7594 Å due to O_2; 7168 Å, 8200 Å and 9050 Å due to H_2O. These bands affect the stellar fluxes in that region of the spectrum. They are removed by the following method: the stellar features and continuum ranges devoid of the telluric bands in the standard star spectrum are set to unity; the telluric absorption features in this template are then suitably scaled such that division of the program star spectrum by the template smooths out the atmospheric features in the stellar spectrum.

Using photometric *UBVRI* magnitudes of the star, it is possible to calibrate the spectrum for absolute fluxes. The spectrum is convolved with the response curves of *UBV* (Allen 1973) and *RI* (Bessel 1986) bands and the observed magnitude ($m_\lambda = -2.5 \log f_\lambda$) at the effective wavelength corresponding to each of these bands is obtained. A correction curve is obtained from the photometric magnitudes which, when applied to the observed flux, gives absolute fluxes.

To determine the equivalent widths of stellar lines, the spectrum is first normalized to a pseudo-continuum level. This is done by interactively determining the continuum points in the spectrum. A fit through these points determines the continuum. Division by this continuum yields a continuum-normalized spectrum. Line equivalent widths are obtained by integrating the line flux above (below) the continuum level for emission (absorption) lines. Total flux in an emission line is obtained by integrating the total area covered by the line. In this case, spectrum is not normalized by the continuum level. However, while obtaining the line fluxes, a baseline determined by the adjacent continuum levels is subtracted out to correct for the contribution due to continuum.

Software

A software package *RESPECT* (Prabhu, Anupama & Giridhar 1987; Prabhu & Anupama 1990, in preparation) was developed for interactive spectrophotometric data reduction. This software package was developed in the VAX VMS 11/780 computer system environment at VBO. The *RESPECT* package consists of a large number of short executable images of routines originally written in Fortran 77, including Digital run-time library of VAX. Each image is activated through a command defined using the Digital Command Language Definition utility. The commands are acronyms of the operation to be performed. For example the command

$$\$\text{ADDC} \qquad infile \qquad outfile \qquad c$$

adds a constant value c to all data points in $infile$ and writes the new data values into $outfile$. The operating system allows grouping a string of such commands as a command procedure and activating this procedure through another command defined using symbol definition, symbol substitution and parameter passing utilities.

Display on terminals is achieved through the basic command set of the Tektronix Interactive Graphics Library (IGL). The plotting routine on the Printronix printer/plotter utilizes Digital PLXY software. The interactive graphic commands employ the IGL routines.

The *RESPECT* commands can be subdivided into (i) entry into and exit from the *RESPECT* environment; (ii) the basic command set consisting of (a) reformatting commands, (b) graphic action commands, (c) pixel-finding routines, (d) averaging and convolving routines, (e) file manipulation commands, (f) arithmetic operations, (g) curve-fitting and curve-generating commands, (h) fast Fourier transform, (i) coordinate scaling commands, (j) calculator command, and (k) spherical astronomy commands; (iii) spectroscopic extension commands used to perform operations required for spectrophotometry. A majority of the last set of commands activate command procedures which contain a series of basic commands needed to perform the required operation.

Reductions

The photographic spectrograms of the program stars and standard stars along with their calibration plates were digitized using the Perkin Elmer PDS 1010M microdensitometer at IIA. Digitization was done at 3–5 μm intervals using a slit of 7.5–10 μm width and height corresponding to the width of the spectrum. The digitized spectra were reduced following the procedure described earlier.

All spectra were smoothed using a low-pass filter with cut-off frequency 15 cycles mm^{-1} except when the data was too noisy, a cut-off frequency 12 cycles mm^{-1} was used. The densities were converted to 'modified densities' before smoothing and converted back to densities after smoothing. The smoothed data were converted to relative intensities by fitting a third-order polynomial to the calibration $\log I$ vs $\log \omega$ step values. In case of image tube plates, the image-tube thermal background has been corrected for. The spectrum was wavelength calibrated by fitting a third-order polynomial to the comparison source spectra. Spectra have been corrected for atmospheric extinction using a value of $k = 0.014$ mag μm^4 determined for VBO site using standard stars (Shylaja 1986). The observed spectrum has been corrected for instrumental response and brought to a relative flux scale whenever standard stars were observed. In the absence of standard star data, the spectrum has been normalized to a pseudo-continuum level and brought to (I/I_c) scale. Spectra have been brought to an absolute flux scale whenever $UBVRI$ magnitudes were available.

The reductions of CCD spectra have been performed using the methods described earlier. All spectra were de-biased and flat-fielded. Flat-field images were obtained by (a) illuminating the spectrograph slit by a Xe lamp, and (b) observing a uniformly illuminated portion of the dome through the telescope. It was found that Xe flats gave rise to nonuniformity in the direction perpendicular to dispersion (y-direction), whereas dome flats were uniform. Hence, only dome flats were used subsequently. Sky subtraction was carried out to remove contributions from night sky emissions due to [O I] and [N II]. Star spectrum was then extracted using the optimal extraction method described earlier. The value of 10 for Q, as estimated for the CCD system in use, was used in the determination of variance V. Wavelength calibration was done by fitting a third-order polynomial to comparison source spectra taken before and after the stellar exposures. All spectra have been corrected for atmospheric extinction, and corrected for instrumental response using standard stars observed on the same night.

All reductions were carried out at the VAX 11/780 system at VBO, using the *RESPECT* software.

2. Imaging

Portions of the sky can be imaged onto a dectector either by collimating the light collected by the telescope and passing it through a camera fixed at the focus of the telescope, or by fixing the detector directly at the focus. In the former case the telescope acts as a telephoto lens, and in the latter case, it acts as a camera. The detector could either be a photographic plate, film or a solid-state array such as CCD. Imaging in different wavelengths can be achieved by the usage of appropriate filters.

2.1 Instrumentation

Images of nova shells included in this work were obtained using the 102 cm Carl Zeiss reflector at VBO. A CCD detector placed at the f/13 Cassegrain focus of the telescope was used to image the nova shells.

The instrumental set-up consisted of a locally fabricated offset guiding unit with a filter holder wheel, to which the Photometrics CCD dewar was fixed. The CCD array is of size 384×576 pixels, each pixel 23 μm square. The f/13 Cassegrain beam provides an image scale of 16 arcsec mm^{-1} corresponding to 0.36 arcsec per pixel. Hα+[N II] (160 Å bandpass; 50 Å bandpass) and [O III] (50 Å bandpass) interference filters were used to image the shells of novae GK Persei and T Pyxidis.

2.2 Observations and Reductions

CCD images of the shell of the classical nova GK Per were obtained through both

Hα+[N II] (160 Å BP) and [O III] (50 Å BP) interference filters, whereas the shell of the recurrent nova T Pyx was imaged through only Hα+[N II] (50 Å BP) interference filter.

The CCD images need to be corrected for electronic bias and pixel-to-pixel sensitivity differences (flat-fielding). Electronic bias needs to be subtracted to correct the data counts for the mean DC voltage bias given to the detector electronics for an efficient charge transfer. The bias image is constructed by averaging several zero-exposure images obtained during a single run of observations. A pixel-by-pixel bias subtraction of the raw CCD image is then performed to obtain a bias subtracted data. Alternatively, a mean value of the bias image obtained by rejecting deviants beyond 3σ may be subtracted from all pixels to obtain the bias subtracted data.

The images also need to be corrected for the signal registered by the detector in the absence of exposure to light *i.e.* dark counts due to detector white noise. A dark image is obtained by exposing the CCD with the shutter closed for a duration similar to the exposure times of the object images. Several such dark images obtained during one observing run are then stacked to construct a mean dark image. This mean dark image is bias corrected and then subtracted from the bias corrected object frame either pixel-by-pixel or using a mean dark value.

In the case of the Photometrics CCD system in use, it was found that for an operating temperature of $\sim 120°$ C the mean dark count value was not significantly higher than the mean bias value even for a half-hour dark image. Also intrinsic pixel-to-pixel variations of bias and dark values appear insignificant. Hence, a mean of the bias and dark values was subtracted out from the raw data image.

Pixel-to-pixel sensitivity variations are corrected for through division of the dark subtracted image by a flat field image. A flat field image is obtained by exposing the CCD to a spatially uniform continuum source. Flat field images were obtained by exposing the CCD to twilight sky. Several such well exposed flat images obtained during a single observing run were individually de-biased, dark subtracted and normalized by the maximum value. The normalized flat images were then stacked. Stacking several images reduces the statistical errors introduced during division. Pixel-by-pixel division of the dark subtracted data image by the normalized mean flat image preserves the relationship between data counts and detected photons, but corrects for pixel-to-pixel variations. The de-biased, flat-fielded data is now on a relative flux scale.

In order to improve the signal-to-noise ratio in the data, whenever more than one frame of an object was available, the images were stacked. Each image was individually de-biased and flat-fielded. The images were then aligned with respect to the best image. More than 6 stars in the field, common to all the images, were identified and the XY positions of their centroids determined. A transformation of the type

$$X' = C(1) + C(2)X + C(3)Y \tag{II.2.1}$$

$$Y' = C(4) + C(5)X + C(6)Y \tag{II.2.2}$$

was used to align the images. The coefficients $C(1)$–$C(6)$ were determined individually for each frame. The aligned images were then averaged. The averaged data image was used in further analysis.

It was found that the [O III] and Hα+[N II] (50 Å BP) filters produced "ghost images" due to a slight inclination of the filter with respect to the optical axis of the incoming beam. These "ghost images" were detected at 2% of the original intensity level of only the bright stars in the field. A ghost of the central star was detected in the [O III] image of GK Per. Since it had a star-like appearance, a Lorentzian profile was computed for the ghost, and the model fit subtracted out. It was found that the stars fainter than GK Per did not show the ghost. The faint nebulosity around GK Per is hence unaffected. In the case of T Pyx Hα+[N II] image, the ghost was detectable only for one of the bright field stars. The ghost due to the central star of T Pyx was below the limit of detectability. The shell of T Pyx is certainly unaffected. No attempt was made to remove the ghost in this case.

All reductions have been made with the VAX 11/780 system at VBO using STARLINK/EDRS package. The image processing unit COMTAL VISION 1 available at VBO is not compatible with the STARLINK image display and interaction software. User application programs locally developed under STARLINK environment (Y.D. Mayya & T.P. Prabhu 1990, in preparation) were used for display on COMTAL, obtaining the X, Y positions of the stars, blinking, and such other operations requiring the image processing system.

III. Classical Novae

1. Introduction

Classical novae are prominent members of the class of cataclysmic variables characterized by their well-known large amplitude outbursts, accompanied by the ejection of an expanding shell. The outbursts are a consequence of thermonuclear runaways in the accreted matter on the surface of the white dwarf primary. Most of the known properties of novae were until recently, based on optical studies of these objects during outburst. In the recent times, it has increasingly become evident that multi-wavelength observations are essential for a clear understanding of these systems, both theoretically and observationally.

According to theoretical models, maximum bolometric luminosity is reached before much expansion of the degenerate envelope can take place. Visual maximum occurs only after considerable hydrodynamic expansion. The luminosity at this stage is still at or above the Eddington luminosity. Initial mass loss occurs through continuum radiation pressure. An optically thick shell is ejected at this time. As the ejected envelope expands, it becomes optically thin first at optical wavelengths, then in the infrared and later in the radio wavelengths. The nova spectrum at maximum is an absorption spectrum since it is optically thick to lines as well. The optical thickness to lines reduces faster than for the continuum, and emission lines soon appear. As the nova declines, lines requiring lower electron densities and higher electron temperatures gradually dominate the spectrum (Gallagher & Starrfield 1978; Lance, McCall & Uomoto 1988; Martin 1989). This is due to the photosphere receding and getting hotter as the envelope becomes optically thin. As the shell expands the effective temperature of the central source rises, typically from 10^4 to 10^5 K.

The evolution of the spectrum is as described in §I.1.2. The fluxes in emission lines can be used to study the physical conditions in the envelope as it expands. Two parameters that are desirable to this end are the estimates of interstellar reddening and distance to the nova. As the outburst is complete and the system reaches its quiescent state, it is possible to study the different components individually — the primary, secondary, the accretion disc around the primary and the nebulosity surrounding the system. In the following, a few generalities are described, before we proceed to the study of three individual systems: LW Serpentis 1978 and Nova

Scuti 1989 during the diffuse-enhanced-[O I] flash stage, and GK Persei 1901 during its quiescence.

1.1 Interstellar Extinction and Distance

The observed fluxes can be used to determine the physical conditions only after they are corrected for interstellar extinction, and an estimate of distance to the nova is made. The interstellar extinction is inversely proportional to the wavelength of radiation and is often expressed as

$$A_\lambda = E(\lambda - V) + R \tag{III.1.1}$$

where A_λ is the interstellar extinction on a magnitude scale, $R = A_V/E(B-V)$ is a constant, and the symbol $E(\lambda - V)$ denotes the observed colour excess over the intrinsic colour $(\lambda - V)$. The observations indicate $R = 3.1$ in the mean with some variation about the mean value. The observed mean values of $A_\lambda/E(B-V)$ are tabulated by Savage & Mathis (1979).

The best estimates of interstellar extinction result from the ultraviolet observations of 2200 Å bump. If the nova is bright enough in the radio region, the absorption of the 21 cm line may be observed to determine the column density of neutral hydrogen in the line of sight to the nova, and an estimate of interstellar extinction made using the mean dust/gas ratio. The observed flux ratios of recombination lines, or of forbidden emission lines originating in the same upper level, may also be compared with theoretical ratios in determining extinction if they are sufficiently well spaced in wavelength. However, forbidden lines are observed only in nebular stage, and reliable theoretical H I recombination line intensities are also available only at that stage when the optical depth in these lines is sufficiently low.

In the absence of the above data, *i.e.* when one has only optical spectra near outburst maximum, one can make an estimate of distance, though somewhat inaccurate, by the following means.
(a) The late members of Balmer and Paschen series are less affected by optical depth effects, and these may be compared with the theoretical values. If the spectrum has sufficiently high excitation, then He II lines can also be used.
(b) If an estimate of absolute magnitude M of the nova is made using its observed dependance on the rate of decline, and if a mean value k of extinction per parsec is assumed, then

$$(m - M)_{\rm obs} = 5 \log d - 5 + kd \tag{III.1.2}$$

where m is the apparent magnitude at maximum and d the distance in parsecs. This method would yield an estimate of distance d as well as extinction kd. However, the value of k is highly variable depending on the galactic location, and the absolute magnitude derived above has a large spread.

(c) van den Bergh & Younger (1987) find that the mean intrinsic colour of novae 2 magnitudes below maximum is

$$(B-V)_2^0 = -0.02 \pm 0.04. \qquad \text{(III.1.3)}$$

A comparison of this value with the observed value yields the colour excess.

Direct determination of distance to a nova is possible only through expansion parallax — either from radio and infrared observations when the nova is expanding like a blackbody, or from the observations of expanding nebulosity. Though it is desirable to obtain independant and accurate estimates of interstellar extinction and distance to the nova towards an understanding of the physical conditions as also of the luminosity of the nova, one has to be satisfied with estimates (a)–(c) above in the absence of multiwavelength observations over the entire duration of the outburst.

1.2 Physical Conditions in the Nova System

The expanding envelope is the first component that becomes available for analysis following the outburst. After the outburst decays the nova system reaches its quiescent state when the individual components of the central system embedded in the ejecta — the hot primary surrounded by an accretion disc, and the cool secondary transferring mass through the inner Lagrangian point — can be separated. In the following these components are discussed individually.

1.2.1 The Ejecta

The expanding envelope

Collisionally excited forbidden lines can be used as probes of electron density n_e and electron temperatures T_e. Due to stratification of physical conditions, however, the information derived applies only to the region emitting the line (Martin 1989). During the nebular stage the conditions in the ejecta are similar to those seen in planetary nebulae and photoionized by the hot nova remnant. Emission line diagnostics as used for planetary nebulae (Osterbrock 1974) may be used. The most useful line ratios are [O III] (4959+5007)/[O III] 4363; [O III] (4959+5007)/[Ne III]

3869 and [O III] (4959+5007)/He I 5876 in the optical (Starrfield 1988) and Si III] 1892/Si IV 1397; C III] 1909/C IV 1549; Si IV 1397/ C IV 1549 in the ultraviolet (Snijders *et al.* 1987).

The above mentioned optical forbidden lines are however not available during the initial stages of the outburst when the density in the line forming region is high, similar to those in active galactic nuclei. In the high density limit, during the early decline the ratio of [O I] 5577/6300 can be used to determine the temperature (Martin 1989), using the relation

$$[\mathrm{O\ I}]\ 5577/6300 = 43 \exp\left(-2.58/T_e^4\right). \tag{III.1.4}$$

As the density declines, 5577 Å line fades relative to the 6300 Å line. However, these lines themselves become available only after the density is reduced below the critical density for their formation. Also, it is likely that such conditions are met initially only in a part of the envelope. In the ultraviolet region, Si III] 1892/C III] 1909 ratio can be used for density determination (Nussbaumer & Stencel 1987).

Electron densities may also be estimated from the recombination lines using the relationship

$$f_\lambda = \epsilon_\nu n_e n_A V/d^2 \tag{III.1.5}$$

if an estimate of the line-emitting volume V can be made. Here, f_λ is the observed flux in the emission line, $\epsilon_\nu = (4\pi j_\nu / n_e n_A)$ the emissivity, j_ν the emission coefficient, n_e and n_A are the electron and ionic densities and d is the distance to the nova.

Hydrogen Balmer lines Hα and Hβ are the most commonly used recombination lines. During early phases of the outburst when matter is radiation bound and density is high, optical depth in Lyman and Balmer series is also high. Under high optical depth conditions, self absorption becomes important. The Hβ photons are absorbed and converted to Hα plus Paschen Pα, whereas the Hα photons are merely scattered only to be quickly converted back to Hα (Osterbrock 1974). The Balmer decrement is very high and normal Case B conditions cannot be employed for line emissivities. On the other hand, at densities $\gtrsim 10^{10}$ cm^{-3}, as seen in the immediate post-maximum and later in the accretion disc at quiescence, the Balmer decrement is flatter than Case B.

The high density and optical depth conditions in the nova envelopes are similar to those seen in active galactic nuclei. The effect of high optical depths in Lyman and Balmer lines have been incorporated in the calculations of hydrogen spectrum by several workers (*e.g.* Netzer 1975; Krolik & McKee 1978; Drake & Ulrich 1980). These models are also sensitive to factors such as dilution of incident radiation, which is often represented by an ionization parameter. The available models are only exploratory in nature, and not sufficiently detailed for an undisputed application. In this study, we hence use the recombination coefficients calculated for normal Case B conditions by Hummer & Storey (1987), and only make qualitative comments on the effect of optical depth.

The volume of the shell may be computed from spectroscopically determined expansion velocities $v_{\rm exp}$ as

$$V = \frac{4}{3}\pi(v_{\rm exp}t)^3\phi \qquad \text{(III.1.6)}$$

where t is the time since outburst, $v_{\rm exp}t$ is the radius of the shell and the filling factor ϕ is the fraction of the sphere with radius $v_{\rm exp}t$ that is filled with matter. For a spherical shell of thickness a tenth of radius, $\phi \sim 0.1$. However, the shells observed many years after outburst have an ellipsoidal shape with equatorial ring and polar cones, and ϕ may actually be close to 0.01.

When recombination lines of H are used, $n_A = n_{\rm H^+}$ may be calculated from

$$\begin{aligned} n_e &\simeq n_{\rm H^+} + n_{\rm He^+} + 2n_{\rm He^{++}} && \text{(III.1.7)} \\ &= n_{\rm H^+} \qquad \text{in low ionization conditions} \\ &= (1+2A)n_{\rm H^+} \qquad \text{in high ionization conditions} \end{aligned}$$

A being the abundance of He with respect to H by number (typically ~ 0.1).

The estimates of $n_{\rm H^+}$ and V lead to the mass of ionized hydrogen ($\simeq$ mass of the ejected shell),

$$M_{\rm H^+} = m_{\rm H} n_{\rm H^+} V \qquad \text{(III.1.8)}$$

where $m_{\rm H}$ is the mass of hydrogen atom.

Abundance determinations are important to the theory of outbursts and in understanding the details of nuclear reactions that take place (Truran 1982). They are also important in explaining many of the pecularities seen in novae (Martin 1989). Abundances have been determined in three distinct ways. Antipova (1974) applied the curve-of-growth method to the absorption spectra near maximum visual light. Collin-Souffrin (1977) has shown that the abundances of heavy elements in novae can in principle be determined through photoionization models of emission line strengths in integrated spectra during the nebular phase. Williams (1977) proposes a third approach, which is based on spatially resolved spectra of old nova shells. He also suggests the curve-of-growth method for abundance determinations in novae is unreliable. Abundances determined from old nova shells have shown enhancements (relative to H) of He, C, N and O.

He/H abundance is obtained using the He I, He II and H recombination lines. Line formation in He I is complicated by the metastability of the lowest triplet level $2s\,^3S$ which can have significant population. Collisional excitations from this level enhance recombination lines used in abundance analysis. Clegg (1987) gives empirical formulae for the collisional contribution to He I recombination lines, as a fraction of the radiative contribution. These correction factors are used whenever He I line fluxes are employed. The radiative recombination emissivities are taken from Brocklehurst (1971) for He I, and from Hummer & Storey (1987) for He II.

The metastability of the $2\,^3S$ level of He I can cause some lines to become optically thick, particularly at densities $n_e \gtrsim 10^{10}$ cm^{-3}. Almog & Netzer (1989) have made detailed calculations of the He I spectrum for a range of densities extending to $n_e = 10^{14}$ cm^{-3} for a range of optical depths in the He I 3889 Å line. In the estimation of helium abundances under density conditions of $n_e > 10^{10}$ cm^{-3}, as encountered in the accretion disc, He I emissivities from Almog & Netzer (1989) have been used.

The nebula

The nebulae formed by the shells ejected by novae can be classified into two types: (i) ones that expand freely into the interstellar medium and are photoionized by the central nova remnant and, (ii) the ones that expand into a higher density circumstellar medium. The circumstellar environment may either be the steady wind from the secondary, or a neutral remnant of the planetary nebula that was ejected at the time of formation of the white dwarf. The nebulosity in this case is ionized by shock heating of the ejecta on interaction with the pre-existing material.

The nebular remnant can be resolved a few years after outburst if the nova is sufficiently nearby. Classic examples of the two categories are (i) DQ Her and (ii) GK Per. In most cases the nebula is barely resolved from ground based observations (see Cohen & Rosenthal 1983), and detailed information is limited to spectroscopic separation of nebular emission lines from the composite spectrum. The studies of line profiles provide clues to the geometric structure of the shell. An example is provided in §III.2.3 on LW Ser.

The few instances of long lasting well-resolved nebulae provide more direct information on the structure of the shell, and hints on elemental startification. The angular expansion (proper motion μ) can be measured by comparing images recorded at different epochs. This information, in conjunction with the spectroscopically determined expansion velocities, yields an estimate of the distance to the nova

$$D = \frac{v_{\rm exp}}{\mu} \tag{III.1.9a}$$

or

$$D_{\rm pc} = \frac{v_{\rm exp}\ ({\rm km\ s^{-1}})}{4.75\mu\ ({\rm arcsec\ yr^{-1}})}. \tag{III.1.9b}$$

In the case of type (ii) remnants, there is a significant deceleration of the remnant as it ploughs through the circumstellar medium. In such an event, the distance needs to be estimated fairly early in the evolution of the nebula, and the deceleration of the nebula can be monitored, which yields information on the physical conditions in the circumstellar matter. This has been exemplified using data on GK Per in §III.4.1.

1.2.2 The Central Binary System

The primary

The quiescent spectrum of novae in the optical region is generally dominated by the accretion disc. The white dwarf spectrum may be visible only in the far ultraviolet. The emission lines in the optical region provide some clues to the nature of the white dwarf if one assumes that they are photoionized by the white dwarf radiation. Some caution is necessary since the ionizing radiation may have contribution from the boundary layer between the white dwarf and the accretion disc, and also from the inner, hot regions of the disc itself.

The temperature of the white dwarf may be determined using the estimates of H and He ionizing fluxes based on the strengths of recombination lines of H and He. In particular, for hydrogen,

$$\begin{aligned} Q({\rm H}^0, T_s) &= n_{{\rm H}^+} n_e \alpha_B({\rm H}^0, T_e) V \\ &= N_{{\rm H}^+} n_e \alpha_B({\rm H}^0, T_e). \end{aligned} \tag{III.1.10}$$

A corresponding equation may be written for He^+. Here

$$Q = \int_{\nu_1}^{\infty} L_\nu \, d\nu, \tag{III.1.11}$$

ν_1 being the ionization edge and L_ν the luminosity of the source. Q is the total number of ionizing photon luminosity, T_s is the temperature of the central source,

n is the number density, V is the volume of ionized region, α_B is the recombination coefficient and N the total number of ions in the nebula (Osterbrock 1974). It is assumed that all the ionizing photons are absorbed within the volume V.

For the ratio of ionizing photons, one can write

$$\frac{Q(\mathrm{He}^0, T_s)}{Q(\mathrm{H}^0, T_s)} = \frac{\alpha_B(\mathrm{He}^0, T_e)}{\alpha_B(\mathrm{H}^0, T_e)} \equiv A\frac{N_{\mathrm{He}^+}}{N_{\mathrm{H}^+}}, \tag{III.1.12}$$

and from Equation III.1.5,

$$\frac{Q(\mathrm{He}^0, T_s)}{Q(\mathrm{H}^0, T_s)} = A\frac{\epsilon_\nu(\mathrm{H}^+, n_e, T_e)}{\epsilon_\nu(\mathrm{He}^+, n_e, T_e)}\frac{f(\mathrm{He}^+)}{f(\mathrm{H}^+)} \equiv B\frac{f(\mathrm{He}^+)}{f(\mathrm{H}^+)}. \tag{III.1.13}$$

Similar equations can be written for the ratio $Q(\mathrm{He}^+, T_s)/Q(\mathrm{H}^0, T_s)$. At $T_e = 10^4$ K, we have $A = 1.05$ for He^0 and H^0, and $A = 5.94$ for He^+ and H^0. In the case of Equation III.1.13, using He II 4686 Å and Hβ lines, at $T_e = 10^4$ K and $n_e = 10^{10}$ cm^{-3}, $B = 0.69$. In the above equations, it is sufficient to use the ratios of the surface emissivities q of ionizing radiation instead of $Q = 4\pi R_s^2 q$, R_s being the radius of the ionizing source, since the ratios are independent of R_s.

Using consistent values of line emissivities based on model calculations, the ratio of ionizing photon luminosities can be estimated. A comparison with an estimate based on model atmospheres or blackbody radiation yields the temperature of the central source known as Zanstra temperature. Using an estimate for the distance to the nova, individual ionizing photon luminosities may be computed, and from a comparison with the model atmospheric or blackbody emissivities, the radius of the white dwarf can be estimated. In particular,

$$Q(\mathrm{H}^0, T_s)\delta = 4\pi R_s^2 q(\mathrm{H}^0, T_s)\delta \equiv \frac{f(\mathrm{H}^+)4\pi d^2 \alpha_B(\mathrm{H}^0, T_e)}{\epsilon_\nu(\mathrm{H}^+, n_e, T_e)} \tag{III.1.14}$$

where δ is the fraction of the ionizing radiation intercepted by the nebula, assumed to be 0.1 in the following, since the envelopes of novae are not spherically symmetric, but are composed of equatorial rings and polar cones.

The secondary

The spectrum of the secondary is often seen in the red–infrared region. The secondary is generally a late-type star. A quantitative estimate of the spectral type is made from the observations of strengths of absorption lines and bands in the spectrum, as also from the shape of the continuous energy distribution. It is necessary to correct for the contribution from the accretion disc and primary before applying quantitative criteria. These are discussed below.

The accretion disc

The spectrum of an optically thick but physically thin accretion disc in steady state can be computed based on energy dissipation considerations (King 1989). The observed continuum flux f_λ is (Kenyon & Webbink 1984)

$$f_{\lambda,\mathrm{acc}} = \frac{2hc^2}{\lambda^5}\left(\frac{R_1}{D}\right)^2 \cos i \int_1^{R_2/R_1} \frac{2\pi x\, dx}{\exp[hc/\lambda kT(x)] - 1} \qquad \text{(III.1.15)}$$

where $x = R/R_1$, $T(x) = \frac{3GM_1\dot{M}}{8\pi\sigma R_1^3} x^{-3/4}(1 - x^{-1/2})^{1/4}$ is the effective temperature of the disc at R, $\cos i$ the projection factor, R_1 is the white dwarf radius and R is the radial position within the disc. For $R \gg R_1$ we have

$$T(R) = \left(\frac{3GM_1\dot{M}}{8\pi\sigma}\right)^{1/4} R^{-3/4} \qquad \text{(III.1.16)}$$

or

$$T(R) = T_*\left(\frac{R}{R_1}\right)^{-3/4} \qquad \text{(III.1.17)}$$

where

$$T_* = \left(\frac{3GM_1\dot{M}}{8\pi\sigma R_1^3}\right)^{1/4} = 4.7\times 10^5 \left(\frac{M_1}{M_\odot}\frac{\dot{M}}{M_\odot\ \mathrm{yr}^{-1}}\right)^{1/4}\left(\frac{R_1}{R_\odot}\right)^{-3/4} \mathrm{K}. \qquad \text{(III.1.18)}$$

The spectrum has a sharp cutoff at shorter wavelengths due to a finite inner radius R_1 and at longer wavelengths due to a finite outer radius R_2.

For accretion rates $\geq 10^{-9}\ M_\odot\ \mathrm{yr}^{-1}$ the disc radiates as a blackbody out to its maximum radius. Beall *et al.* (1984) compute the thermal spectrum of the infrared and optical emission from an accretion disc around a compact object, assuming an optically thick, finite disc and a power-law dependence of disc temperature on radius *i.e.* $T(R) = T_0 r^{-3/4}$ where $r = R/R_0$. R is the radial position within the disc and R_0 is the Schwarzschild radius ($2GM/c^2$) for a 6 $M_\odot$ star. From equations III.1.17 and III.1.18, we have

$$T_0 = \left(\frac{3GM_1\dot{M}}{8\pi\sigma}\right)^{1/4} R_0^{-3/4} = T_*\left(\frac{R_1}{R_0}\right)^{3/4} \qquad \text{(III.1.19)}$$

At intermediate wavelengths the flux follows a power law

$$f_{\nu,\mathrm{acc}} \propto \nu^{1/3}$$

or

$$f_{\lambda,\mathrm{acc}} \propto \lambda^{-2.33} \tag{III.1.20}$$

Assuming the white dwarf contribution to be negligible, the total observed flux can be written as a sum of the flux from the accretion disc and the flux from the cool secondary,

$$\begin{aligned} f_{\lambda,\mathrm{obs}} &= f_{\lambda,\mathrm{acc}} + f_{\lambda,\mathrm{cool}} \\ &= A\lambda^{-2.33} + Bf^{\mathrm{rel}}_{\lambda,\mathrm{cool}} \end{aligned} \tag{III.1.21}$$

where A and B are constants and $f^{\mathrm{rel}}_{\lambda,\mathrm{cool}}$ is a relative energy distribution curve from a library of stellar spectra. A separation of the accretion disc and cool component spectra may be made by matching the observed spectra with different model spectra subject to the constraints on the cool star spectral type determined from absorption line and band indices. The separation is particularly easy since the accretion disc is a hot source whereas the secondary is cool.

The luminosity of the accretion disc being dependent on the mass accretion rate $\dot{M}$, the standard accretion disc models may be used to estimate $\dot{M}$. Webbink *et al.* (1987) derive a relation between the absolute magnitude M_V of the disc and $\dot{M}$ as

$$M_V(\mathrm{obs}) = -9.48 - \frac{5}{3}\log(M_1\dot{M}) - \frac{5}{2}\log(2\cos i), \tag{III.1.22}$$

where M_1 is the mass of the white dwarf in solar units and i is the inclination of the disc axis to the line of sight.

Based on all the above considerations, fits of theoretical accretion disc spectrum are obtained for the quiescence spectra of GK Per (§III.4.2) and RS Oph (§IV.1.2.2). Estimates of mass transfer rates are made for GK Per (§III.4.2) and RS Oph, T CrB and T Pyx (Chapter IV).

2. LW Serpentis 1978

Nova LW Serpentis was discovered by Honda (1978: *IAU Circ. No.* 3186) on 1978 March 1 at a photographic magnitude of 9.0. It reached a maximum recorded brightness of $m_{\mathrm{pg}} = 8.3$ on March 4 (Kozai 1978: *IAU Circ. No.* 3188). The nova was well observed in the infrared band and the formation of its optically thick dust shell has been well studied (Szkody *et al.* 1979; Gehrz *et al.* 1980). The nature of the light curve of LW Ser places it among the moderately slow class of novae,

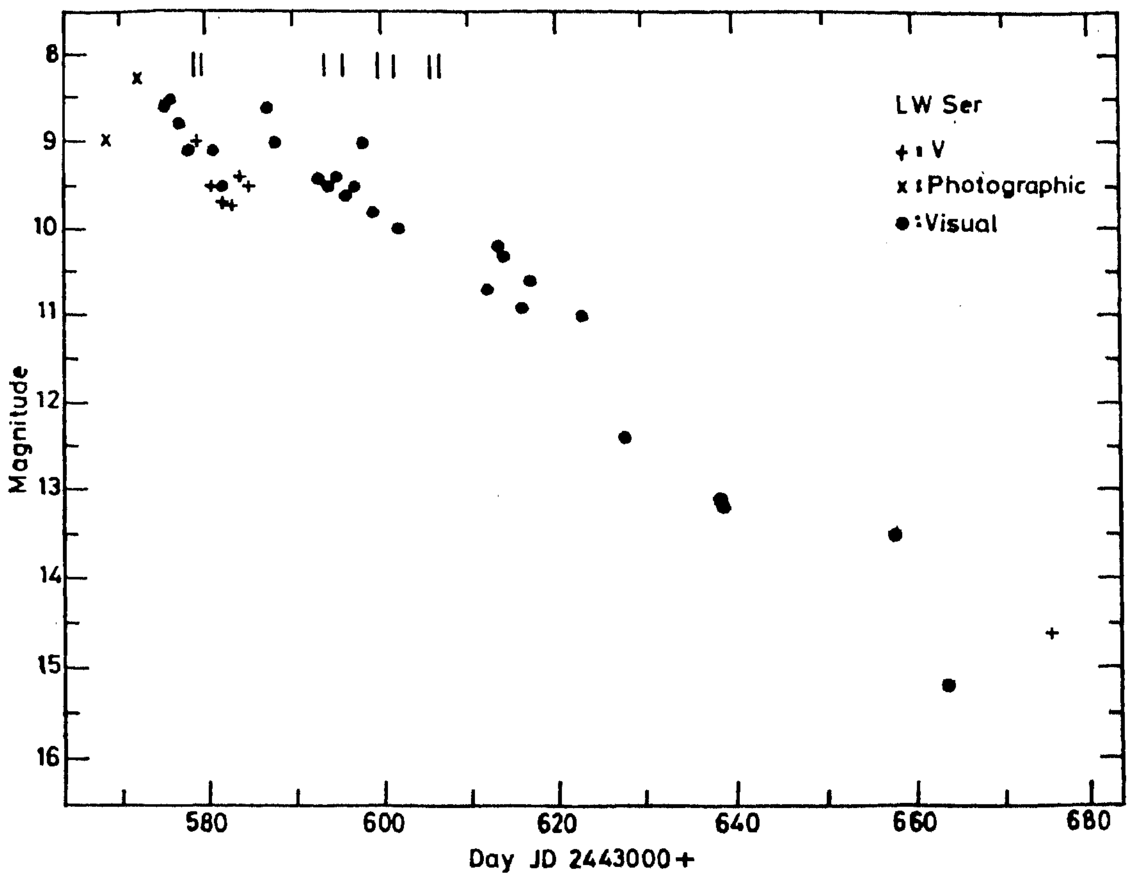

Fig. III.2.1 The light curve of LW Ser. Vertical bars indicate the epochs of spectroscopic observations. JD2443580 = 1978 March 12.5.

exhibiting structured light curve, or in other words, oscillations near maximum light. It has been ascribed the type Cb (Duerbeck 1981), similar to nova FH Ser 1970. The light curve of LW Ser is also similar to that of NQ Vul 1976 (Bb). All the three novae developed a fairly deep minimum during the transition phase and exhibited well-developed dust shells. The development of the dust shell in LW Ser bore a striking resemblence to that of NQ Vul (Bode & Evans 1983).

The discovery magnitude of $m_{\rm pg} = 9$ on March 1 and the value of $m_{\rm pg} = 8.3$ on March 4.82 suggest that LW Ser reached its maximum between March 1 and 4. Following Gerhz *et al.* (1980) 1978 March 1.5 has been assumed as maximum. The nova has not been studied extensively in the optical. The available *UBV* data on LW Ser has been compiled by van den Bergh & Younger (1987). The optical spectrum of LW Ser was briefly described by Herbig (1978: *IAU Circ. No.* 3198) and Prabhu (1978: *IAU Circ. No.* 3201). The light curve based on *UBV* data as well as visual estimates is shown in Figure III.2.1.

Table III.2.1 LW Ser: Journal of observations.

1978 UT		Wavelength Range Å	Dispersion Å mm^{-1}
March	10.90	4600–8800	675
	10.92	4000–8800	166
	10.94	4000–8800	166
	10.96	$H\alpha$	30
March	11.00	3900–6700	166
	11.01	3900–6700	166
	11.91	7000–8800	83
	11.97	7000–8800	83
March	12.00	4900–7300	83
March	25.90	$H\alpha$	30
March	27.88	$H\alpha$	30
	27.94	7000–8800	83
March	31.89	$H\alpha$	30
April	2.91	$H\alpha$	30
April	6.94	4600–8700	675
April	7.94	4600–8700	675

In the following the spectroscopic data obtained during its decline from $V \simeq 9.0$ to $\simeq 10.2$ mag are presented (see also Prabhu & Anupama 1987). The epochs of observations are marked in Figure III.2.1.

2.1 Observations and Reductions

Post-maximum spectra in the range 3900–8800 Å were recorded between 1978 March 10 and April 7, using the 102 cm reflector and the Cassegrain spectrograph equipped with the 175 cm focal length camera and a Varo 8605 single-stage image intensifier,. at VBO. Spectra were recorded at dispersions 675, 166 and 83 Å mm^{-1}. In addition, the $H\alpha$ line was recorded at 30 Å mm^{-1}. The journal of observations appears in Table III.2.1. The spectra were recorded on Kodak IIaD plates and calibrated to relative intensity using the auxiliary calibration spectrograph. No spectrophotometric standard star was observed and hence no attempt is made to correct the spectra for instrumental response. The spectrograms were digitized at 5 μm intervals using a 10 μm wide aperture and reduced following the procedure described in Chapter II. Fe+Ne comparison source spectrum was used for wavelength calibration. All spectra were reduced to continuum. The continuum was slightly underexposed on March 27 and considerably so on April 7. The line equivalent widths are rather uncertain on these days.

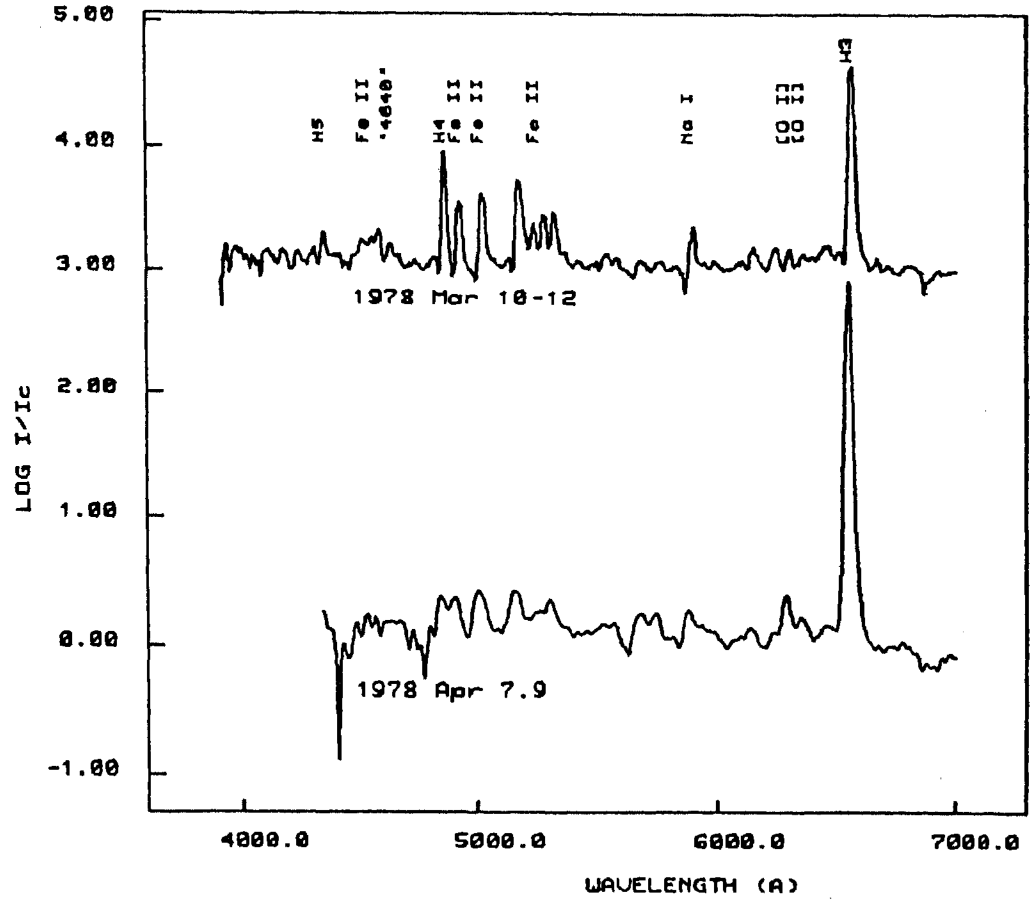

Fig. III.2.2 Spectra of LW Ser in the region 3900–7000 Å on days 10 (top) and 37 (bottom), normalized to continuum. A bias of 3 has been added to the log (I/I_c) scale for day 10 spectrum.

2.2 The Optical Spectra

Description of spectra

Spectroscopic observations of LW Ser in the range 3900–8800 Å were made at phases (i) 9–11 days after maximum at $V \simeq 9.0$, (ii) 26 days after maximum at $V \simeq 9.8$, and (iii) 36 and 37 days after maximum at $V \simeq 10.2$. Hα profile was recorded 9, 24, 26, 30 and 32 days after maximum. The spectra are shown in Figures III.2.2 and III.2.3. Tables III.2.2 and III.2.3 list the line identifications and emission-line equivalent widths at each phase. Lines were identified using the catalogue of Meinel, Aveni & Stockton (1975) and also by comparing with the spectra of novae published in the literature. In the following the spectrum at each phase is described.

Phase 10 (1978 March 10–12): The spectrum is dominated by strong, broad emission lines (FWHM $\sim$ 1200 km s^{-1}) of hydrogen and Fe II. The prominent lines are Balmer lines of hydrogen Hα–Hϵ, lines of Fe II multiplets 42, 48 and 49, Na I D, Ca II infrared triplet at 8498, 8542 and 8662 Å, O I 7774 and 8446 Å, the '4640'

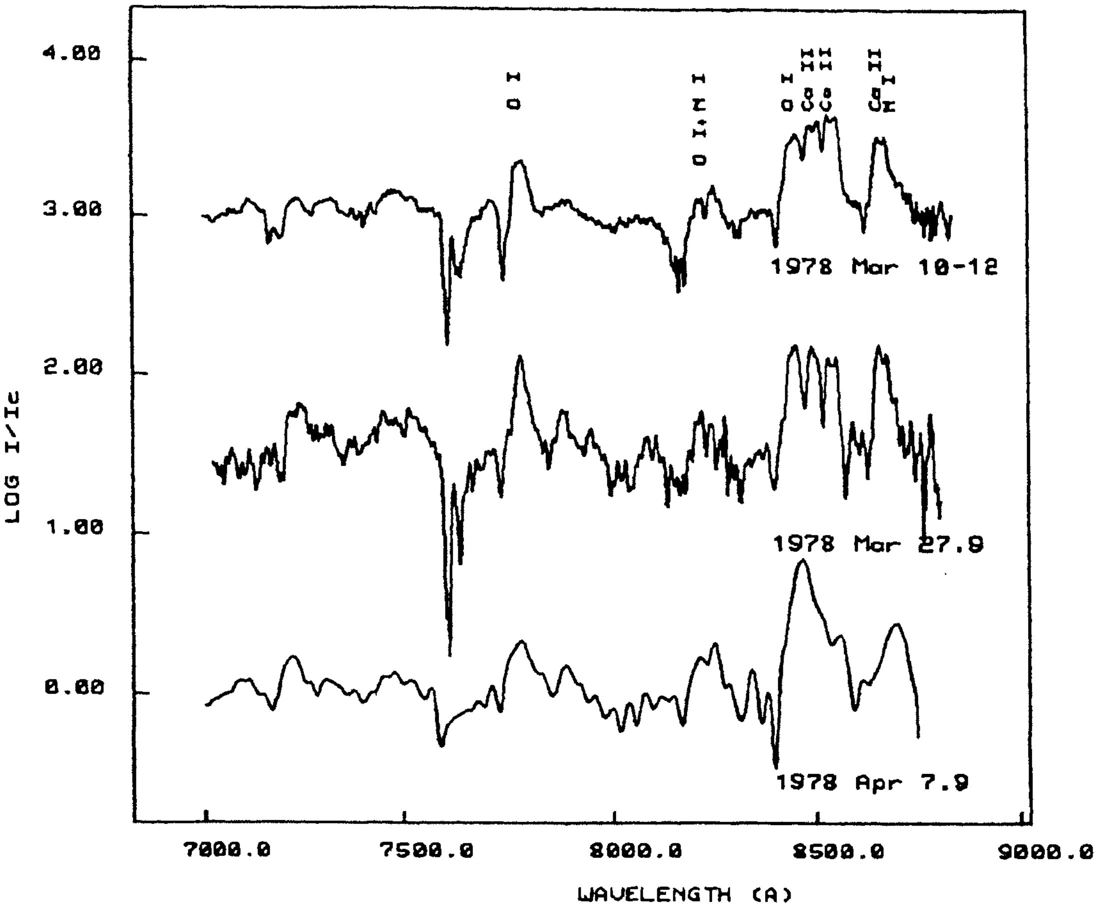

Fig. III.2.3 Spectra of LW Ser in the region 7000–8800 Å on days 10 (top), 26 (centre) and 37 (bottom), normalized to continuum. A bias of 3 and 1.5 have been added to the log (I/I_c) scale for the day 10 and day 26 spectra, respectively.

N/O complex. N II 5462–5495 Å, 5666–5710 Å and 5931–5941 Å are also clearly present and fairly strong. N I 8680–8728 Å is blended with Ca II 8662 Å, whereas N I 8184–8242 Å is clearly present, though affected by atmospheric absorption and blended with O I (34). N I 7423–7468 Å is blended with Fe II (73); N I 8594 Å and 8629 Å, if present, are blended with Ca II triplet. Lines of C II 7231 Å, 7236 Å, 7112–7119 Å are also present. C I 8335 Å could be present, but underexposure of the spectrum in that region makes identification difficult. Ca II H and K are present, with Ca II H blended with Hϵ. Lines of Si II and Ti II are likely to be present, but would be blended with other lines. The lines at 4478 Å, and 7882 Å are identified with Mg I 4481 Å and 7877–7896 Å respectively.

All the permitted lines may have a P-Cygni profile. However, the lines being broad and blended, the P-Cygni absorptions are not clearly visible except in the lines of Fe II 5018 Å, Na I D, O I 7774 Å, 8446 Å and Ca II 8862 Å. Forbidden lines

Table III.2.2 LW Ser: Line identifications and emission equivalent widths in the region 3900–6800 Å.

λ_m Å	Identification		Equivalent width (Å) Day 10	37
3934	3933.66	Ca II K (1)	8	
3971	3968.47	Ca II H (1)		
	3970.07	Hϵ	27	
4056	4056.21	Ti II (11)	7	
4108	4101.74	Hδ	23	
4180	4178.86	Fe II (28)	31	
4240	4233.17	Fe II (27)		
	4236.93, 4237.05		27	
	4241.79	N II (48)		
4300	4296.57	Fe II (28)	23	
	4303.17	Fe II (27)		
4351	4340.47	Hδ	36	
	4351.76	Fe II (27)		
4413	4385.38	Fe II (27)	22	
	4416.82	Fe II (27)		
4446	4443.80	Ti II (19)		
	4447.03	N II (15)	4	
4478	4481.13	Mg II (4)	14	
	4481.33	Mg II (4)		
4520	4515.34	Fe II (37)		
	4520.23	Fe II (37)	26	
	4522.63	Fe II (38)		
4556	4549.47	Fe II (38)	25	
	4555.89	Fe II (37)		47
4587	4583.83	Fe II (38)	32	
4636	'4640'	N/O complex	25	44
	4629.34	Fe II (37)		
4730	4731.44	Fe II (43)	6	2
4817	4825.71	Fe II (30)	14	3
4866	4861.33	Hβ	180	45
4926	4923.92	Fe II (42)	83	44
5018	5018.43	Fe II (42)	132	65
5174	5169.03	Fe II (42)		
	5175.89	N II (66)	178	71
	5179.50	N II (66)		
	5197.57	Fe II (49)		
5236	5234.62	Fe II (49)	52	

Table III.2.2 Continued.

λ_m Å	Identification	Equivalent width (Å) Day 10	37
5281	5275.99 Fe II (49)	69	
	5284.09 Fe II (41)		88
5319	5316.61 Fe II (49)	86	
	5316.78 Fe II (48)		
5365	5362.86 Fe II (48)	23	
5423	5414.09 Fe II (48)	14	
5481	5462.62, 5480.10,	10	
	5495.70 N II (29)		24
5539	5534.86 Fe II (55)	19	
5581	5577.35 [O I] (3)	11	14
5685	5666.64, 5676.02, 5679.56, 5686.21, 5710.76 N II (3)	10	27
5755	5754.80 [N II] (3)	8	26
5901	5889.95 Na I (1)	52	33
	5895.92 Na I (1)		
5945	5931.79 N II (28)	8	
	5941.67 N II (28)		21
5989	5991.38 Fe II (46)	8	
6100	6084.11 Fe II (46)	6	7
	6113.33 Fe II (46)		
6157	6147.74 Fe II (74)		
	6149.24 Fe II (74)		
	6155.99, 6156.78	27	18
	6158.19 O I (10)		
6250	6247.56 Fe II (74)	34	9
6302	6300.23 [O I] (1)	16	71
6366	6363.88 [O I] (1)	16	45
	6379.63 N II (2)		
	6347.09 Si II (2)		
	6371.36 Si II (2)		
6460	6456.38 Fe II (74)		
	6453.64 O I (9)		
	6456.01 O I (9)	44	
	6432.65 Fe II (40)		39
6511	6516.05 Fe II (40)	14	
6568	6562.82 Hα	1074	over-exposed

Multiplet numbers appear in parentheses

Table III.2.3 LW Ser: Line identifications and emission equivalent widths in the region 7100–8800 Å.

λ_m Å	Identification	Equivalent width (Å) Day 10	26	37
7116	7112.36, 7115.13	9		19
	7119.45 C II (20)			
7236	7224.51 Fe II (73)			
	7231.12 C II (3)			
	7236.19 C II (3)	10	46	43
	7254.19 O I (20)			
	7254.47 O I (20)			
7314	7307.97 Fe II (73)	14	23	
	7320.70 Fe II (73)			
	7291.46 Ca II] (1)			12
	7323.88 Ca II] (1)			
7423	7423.63 N I (3)	1	6	
7479	7442.28 N I (3)			
	7468.29 N I (3)			
	7476.45, 7479.06,	32	69	20
	7480.66 O I (55)			
	7462.38 Fe II (73)			
7707	7711.71 Fe II (73)	7	under-exposed	
7782	7771.96, 7774.18,	47	107	44
	7775.40 O I (1)			
7882	7877.14 Mg II (18)	14	30	8
	7896.37 Mg II (18)			
8215	8184.80, 8187.95,			
+	8216.28, 8223.07,			
8249	8242.34 N I (2)	18	28	43
	8227.64, 8230.01,			
	8232.99 O I (34)			
8448	8446.35 O I (4)	86	110	
	8446.76 O I (4)			
8499	8498.02 Ca II (2)			356
	8502.49 P_{16}	119	85	
8544	8542.09 Ca II (2)	149	75	
	8545.38 P_{15}			
8666	8662.14 Ca II (2)	90		
8711	8680.24, 8683.38,		130	91
	8686.13, 8703.24,			
	8711.69, 8718.82,	24		
	8728.88 N I (1)			

Multiplet numbers appear in parentheses

of [N II] 5755 Å, [O I] 5577, 6300, 6363 Å are clearly present. [N II] 6548, 6584 Å could be present blended with Hα.

Phase 26 (1978 March 27): Lines of oxygen and nitrogen have increased in strength, whereas the strengths of Fe II lines, hydrogen lines and lines of other elements have decreased. Ca II] 7291, 7324 Å has appeared, blended with Fe II(73). The blue-shifted absorptions have shifted to higher velocities.

Phase 37 (1978 April 6, 7): The strengths of Fe II lines, hydrogen lines and lines of other elements have further decreased. The decrease in the strengths of oxygen and nitrogen lines is however not as significant. Ca II] 7291, 7324 Å and [O I] 6300, 6363 Å have considerably strengthened, as also O I 8446 Å, whereas O I 7774 Å has decreased. The blue-shifted absorptions have further shifted to higher velocities.

The velocities

Expansion velocities obtained from the P-Cygni absorptions are listed in Table III.2.4. The magnitude of velocity, measured on day 10, is seen to decrease with increasing quantum number for the Balmer lines. This phenomenon is well observed in novae. Velocities from lines of Fe II, Na I D and O I 7774 Å, on day 10, yield a mean absorption velocity of -1300 ± 60 km s^{-1}. Hα gives a velocity of -1480 km s^{-1} in agreement with the value of -1500 km s^{-1} on day 12, measured by Herbig (1978: *IAU Circ. No.* 3198). This absorption system is identified with the diffuse-enhanced system.

The line profiles of O I 7774, 8446 Å show weak absorption at -820 km s^{-1} (day 10) and -690 km s^{-1} (day 26). The Hα line profiles obtained between days 9–33 show a similar system at -700 km s^{-1}. These absorptions are identified with the principal velocity system. The Hα line also showed an absorption at ~ -1770 km s^{-1} on April 2 (day 32). The O I lines showed absorption at similar velocities on days 26 and 37. These absorptions are ascribed to the Orion absorption system.

The velocities of the absorption systems seen in LW Ser are in accordance with those observed in novae of moderate speed class (Gallagher & Starrfield 1978).

Hα line profile

The Hα profiles on days 10, 24, 26 and 32 are shown in Figure III.2.4, reduced to continuum intensity, based on spectrograms obtained at 30 Å mm^{-1}. The continuum is generally underexposed. The absorption at -1480 km s^{-1} is barely visible on March 11. The profile of April 2 shows a shallow and broad absorption at -1770

Table III.2.4 LW Ser: Absorption line velocities.

Emission line		Absorption velocity (km s^{-1}) Day 10	26	37
4101	Hδ	−1460		
4340	Hγ	−870		
4629	Fe II (37)	−1270		
4861	Hβ	−1319		
4924	Fe II (42)	−1401		
5018	Fe II (42)	−1416		
5169	Fe II (42)	−1281		
5893	Na I (1)	−1265		
6563	Hα	−1482		−1770
		−700	−700	−760
7774	O I (1)	−1279	−1620	−1770
		−813	−662	
8446	O I (4)	−1395	−1646	−1797
		−830	−769	
8662	Ca II (2)	−1330		

km s^{-1}. The principal absorption is also visible.

The Hα profile is seen to be asymmetric with more emission towards the red. The centre of the profile lies at 300 km s^{-1}. Though the profile is very nearly flat-topped, some structure is evident near the peak, particularly after March 25. Figure III.2.5 shows the mean of the observed profiles. It is likely that [N II] 6548, 6584 Å contribute to the emission, but it is estimated that the contribution is not more than ten percent.

2.3 Geometric Structure of the Shell

High resolution imaging and spectroscopy of shells around old novae indicate that a typical nova shell consists of an equatorial ring, a pair of polar caps, and possibly a few rings at intermediate latitudes. Particular examples are DQ Her and V603 Aql (Mustel & Boyarchuk 1970; Weaver 1974), and HR Del (Solf 1983). It also appears that these components are confined within a prolate ellipsodal shell, the expansion velocity being smaller at the equator than at the poles. A typical nova shell thus appears to consist of rings of matter at different latitudes with respect to an axis of symmetry. In the event of continuous ejection of matter, these rings take the shape of hollow cones with different angles of opening with respect to a common

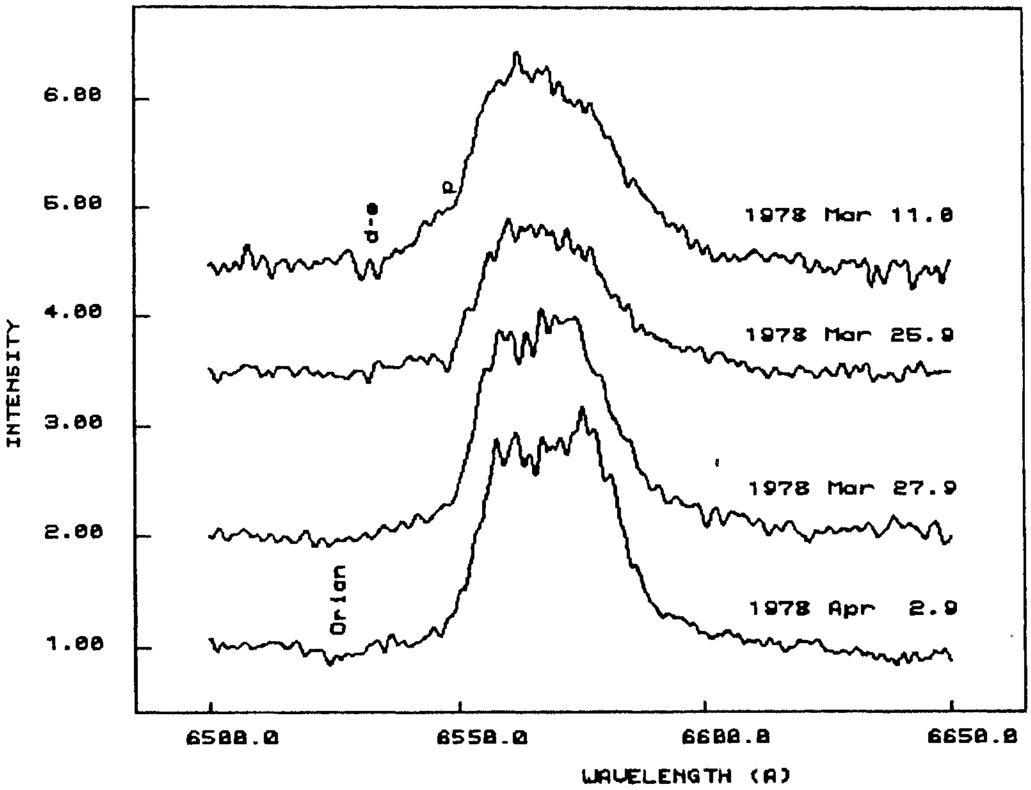

Fig. III.2.4 Hα line profiles in LW Ser between 1978 March 11 (day 10) and April 2 (day 32),, normalized to continuum. The principal (p), diffuse-enhanced (d-e) and Orion absorptions are marked. Bias of 3.5, 2.5 and 1 are added to the respective intensities of the first three spectra.

axis (Solf 1983). The polar cap can be considered as a cone with a small angle of opening. In the following the different components of the shell will be referred to as cones.

General considerations

The emission profile due to an individual cone is generally double-peaked, and is sharply bounded by the velocities

$$v_{\mathrm{r,b}} = v_0 + v \cos(\phi \pm i), \tag{III.2.1}$$

where v_{r}, v_{b} are the red and blue limits of the profile, v_0 is the systemic velocity, ϕ the semi-angle of opening, i the inclination of the polar axis to the line of sight and v the velocity of expansion of the cone. With the assumption that the cones are embedded in a prolate ellipsoidal shell, v can be expressed as

$$v = (v_{\mathrm{p}}^2 \cos^2 \theta + v_{\mathrm{e}}^2 \sin^2 \theta)^{1/2}, \tag{III.2.2}$$

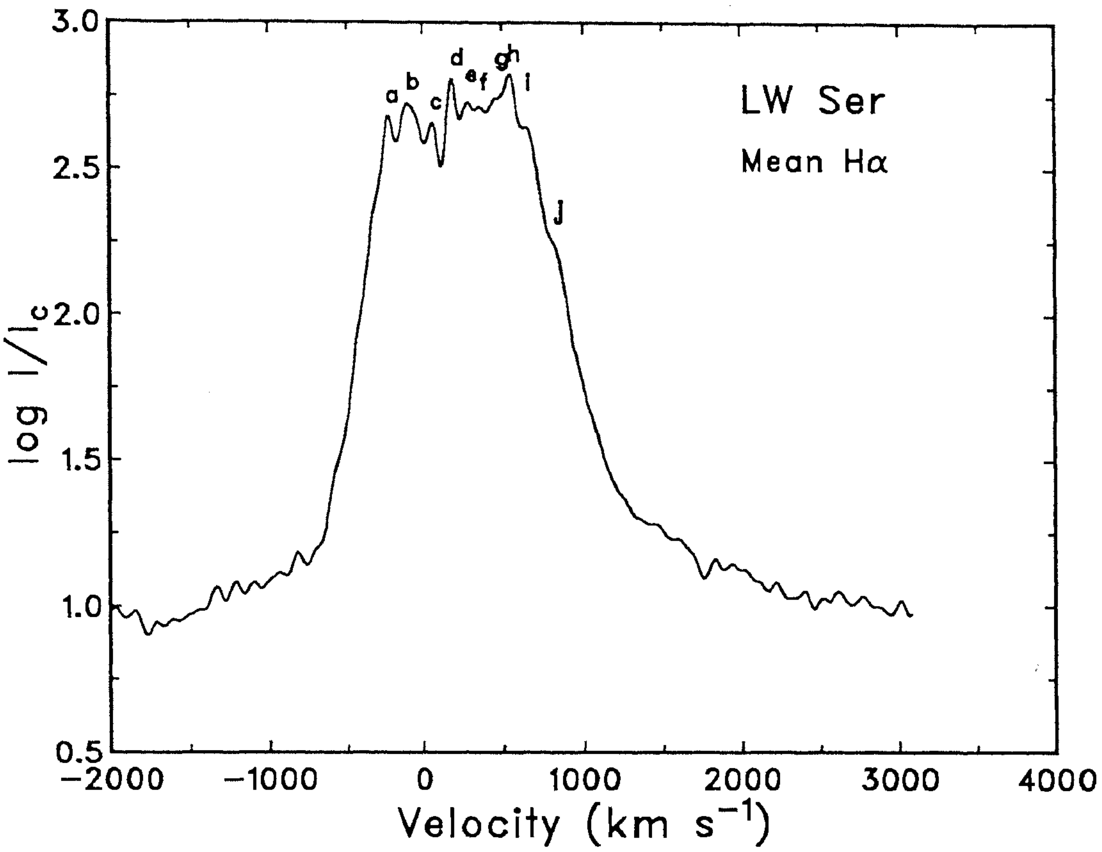

Fig. III.2.5 Mean Hα profile in LW Ser. Peaks referred to in the text and Table III.2.5 have been marked a–j.

where v_p, v_e are the polar and equatorial expansion velocities and θ is the parametric angle given by

$$\tan\theta = \frac{v_p}{v_e}\tan\phi. \tag{III.2.3}$$

Assuming the longer axis of the ellipsoidal shell makes an angle i with the line of sight, the section of the ellipsoid in the plane defined by the line of sight and the longer axis would be an ellipse. The expansion velocities along the perimeter of the ellipse can be parametrized by

$$v_x = v_p \cos\theta \cos i - v_e \sin\theta \sin i, \tag{III.2.4a}$$

$$v_y = v_p \cos\theta \cos i - v_e \sin\theta \cos i, \tag{III.2.4b}$$

where the x-axis is chosen along the line of sight. The maximum velocity component along the line of sight would then be given by v_x such that

$$\frac{dv_x}{d\theta} = 0, \tag{III.2.5a}$$

whereas the absorption velocity would correspond to v_x at

$$v_y = 0. \tag{III.2.5b}$$

Obtaining the corresponding values of θ, and substituting in Equation III.2.4a, it can be shown that the emission from the shell is contained within

$$v_{\rm max} = v_{\rm p}(\cos^2 i + f^2 \sin^2 i)^{1/2}, \tag{III.2.6}$$

where $f = v_{\rm e}/v_{\rm p}$, and that the absorption component is at

$$v_{\rm abs} = -\frac{v_{\rm e}}{(f^2 \cos^2 i + \sin^2 i)^{1/2}}. \tag{III.2.7}$$

Eliminating ϕ and θ from Equations III.2.1–III.2.3, one obtains the condition

$$(x - \delta)^2 + y^2 = 1, \tag{III.2.8}$$

where $x = \frac{1}{2}(v_{\rm r} + v_{\rm b})/v_{\rm p} \cos i$, $y = \frac{1}{2}(v_{\rm r} - v_{\rm b})/v_{\rm e} \sin i$, $\delta = v_0/v_{\rm p} \cos i$. Thus, if the observed profile is separated into components corresponding to different cones, the values (x_i, y_i) lie on a unit circle with centre at $(\delta, 0)$. A least-squares fit can hence be obtained to derive optimal values of v_0, $v_{\rm p}$, $v_{\rm e}$ and i. The values of ϕ can then be derived from

$$\tan\phi = \frac{fy}{x - \delta}. \tag{III.2.9}$$

A kinematic model

The fact that Hα profile showed structure suggests that the shell had already broken into equatorial rings and polar cones. Since the material was still optically thick to line radiation, it is difficult to model the line profiles in terms of contributions due to individual cones. However, the velocities of peaks may be used to obtain a qualitative kinematical model following the previous section.

The averaged Hα profile is used so that the effect of residual noise is reduced in the identification of peaks. The most prominent peaks lie at velocities −240, −110, +50, +180, +270 and +530 km s^{-1}, and fainter peaks appear at +360 and +460 km s^{-1}. There are several undulations on the red wing of the Hα profile. Prominent among these are those at +640 and +840 km s^{-1}. All these features are marked a–j in Figure III.2.5.

Least-squares fits to the circle (Equation III.2.8) were obtained for all possible combinations of pairs $(v_{\rm r}, v_{\rm b})$ chosen from among the prominent six peaks, and the rms residuals defined as

$$\langle(\Delta s)^2\rangle^{1/2} = \left\langle\left[(\Delta x v_{\rm p} \cos i)^2 + (\Delta y v_{\rm e} \sin i)^2\right]\right\rangle^{1/2} \tag{III.2.10}$$

Table III.2.5 Model parameters for the shell of LW Ser.

			Model 1	Model 2
v_p (km s^{-1})			800	1100
f			0.67	0.67
v_0 (km s^{-1})			40	−10
i			16	11
v_{max} (km s^{-1})			783	1089
v_{abs} (km s^{-1})			−765	−1076
Identification	Peak velocities (km s^{-1})		ϕ (deg)	
	v_b	v_r		
(a,c)	−240	50	101	98
(b,d)	−110	180	86	87
(e,h)	270	530	48	59

were computed. The parameter v_p was varied between 600 and 1600 km s^{-1}, i between 1° and 89°, and v_0 between −100 and +100 km s^{-1}. The value of f was fixed at 0.67 in analogy with the observed shell of DQ Her. The model with the least rms residual was chosen as the best model. It was found that the residuals are sensitive to the choice of (v_r, v_b) pairs, but rather insensitive to the values of v_p. The best fit was obtained for pairs $(-240, 50)$, $(-110, 180)$, $(270, 530)$ km s^{-1}. The rms residual was $\lesssim 20$ km s^{-1} over the entire range of v_p.

The choice of v_p was made by constraining the model value of v_{abs} to the observed value of −750 km s^{-1}. The best fit model thus obtained is listed in Table III.2.5. The model (model 1) is asymmetric with no polar cone on the hemisphere facing the earth. The polar axis subtends a small angle ~ 11°–16° to the line of sight. Furthermore, two of the rings are equatorial and the third could be termed polar. The minor peaks can be attributed to structure in the polar cone.

The presence of significant emission at Hα beyond ~ 800 km s^{-1} suggests that the value of v_p could be larger than this value. If the constraint on v_{abs} is removed, one obtains the alternative model (model 2) listed in Table III.2.5 with $v_p = 1100$ km s^{-1}. The emission shortward of the dip at ~ −750 km s^{-1}, as also the emission at $\gtrsim$ 800 km s^{-1}, can then be ascribed to the polar regions. However, this results in excess emission at $\phi \sim 60°$ with only weak emission at $\phi \sim -60°$.

2.4 LW Serpentis among other Novae

LW Ser belongs to a class of novae that exhibit a moderate rate of decline, and a transition phase associated with infrared emission due to an optically thick dust shell.

Using the absolute magnitude–rate of decline relationship, Gehrz *et al.* (1980) obtained an absolute maximum magnitude of $M_V = -7.2$. Assuming $A_V = 1.0$ and $m_v(\max) \simeq 7.9$, they arrive at a distance of $D = 6.3$ kpc. Their infrared observations, however, yielded an angular diameter of 22.7 milliarcsec 75 days since maximum. This value implies an expansion velocity of ~ 1650 km s^{-1}, at assumed distance. van den Bergh & Younger (1987) derive mean values of $(B-V)_0 = -0.02 \pm 0.04$ and $M_V(15) = -5.23 \pm 0.16$ fifteen days after maximum for all but the fastest novae. The observed values of $(B-V)_0 = 0.50$ and $V = 9.5$ for LW Ser fifteen days after maximum imply $E(B-V) = 0.52$, $A_V = 1.6$ and $D = 4.2 \pm 0.4$ kpc. This value of distance agrees better with the observed expansion velocity (Gerhz *et al.* 1980). The expansion velocity of the principal shell, however, is more likely to be around 600 km s^{-1} (Cohen & Rosenthal 1983). This reduces the implied distance to LW Ser by a factor of two, based on the observed angular diameter of the optically thick dust shell. The reduced distance implies that LW Ser reached only $M_V \simeq -5.0$ at recorded maximum. From Cohen & Rosenthal (1983), it appears that both NQ Vul and LW Ser were subluminous at maximum. Alternatively, distances derived from the infrared blackbody angular diameter and the expansion velocity are underestimated. The extinction estimate for the relatively nearby nova FH Ser is 2.8 mag which brings it close to the standard absolute magnitude rate of decline relationship. NQ Vul would also fit in well assuming a value of $A_V = 2.5$ mag (Duerbeck 1981) based on polarization measurements, instead of 1.4 mag assumed by Cohen & Rosenthal. There is no evidence yet that the extinction to LW Ser is larger than 1.6 mag, whereas, a value ~ 3 is needed to make it appear normal at the nearer distance derived by Cohen & Rosenthal. On the other hand, it is possible that the nova was discovered after maximum, and it was brighter than $V \sim 8.0$ at the actual maximum.

The spectrum of LW Ser may be compared with that of a typical nova, as described by McLaughlin (1960), and also with other novae that exhibited a similar light curve — DQ Her (Stratton & Manning 1939), FH Ser (Anderson, Borra & Dubas 1971), NQ Vul (Yamashita *et al.* 1977; Shcherbakov 1977). Assuming $m_v \sim 8.0$ for maximum, the three epochs of our observations would correspond to 1.0, 1.5 and 2.2 mag below maximum. For a typical nova spectrum, these stages would correspond approximately to (i) the principal spectrum, (ii) advanced stages of the diffuse-enhanced spectrum, and (iii) Orion absorption stage close to the onset of [O I] flash. On the other hand, comparison with the evolution as a function of time expressed in units of t_3, the time required to decline by three visual magnitudes, (McLaughlin 1960) and using a value of $t_3 = 50$ days (Duerbeck 1981), we obtain, for the three epochs (i) 10 days after maximum the diffuse enhanced absorption had just appeared, (ii) 26 days after maximum the nova was past the maximum of diffuse enhanced phase, and the Orion absorption had just appeared, and (iii) 37 days after maximum [O I] flash had just occured.

The evolution of the spectrum of LW Ser agrees generally with other novae of similar speed class. The major difference is in the weakness of the principal absorption.

The velocity structure of the Hα profile suggests that the shell of LW Ser consists of equatorial disc and polar cones. The polar axis is inclined at a small angle ($\sim 15°$) to the line of sight. The line profile, however does not give a clear indication of a polar cone at the pole nearer to the earth. Such a cone could indeed be present, but may not be contributing significantly near the peak Hα emission. The geometry in terms of a prolate ellipsoid with equatorial rings and polar cones is similar to those of the shells of DQ Her (Weaver 1974) and HR Del (Solf 1983). A nova envelope is radiation bound in the early stages of outburst (Ferland 1977; Martin 1989). In such a case, one expects to see the nearer polar cone through considerable amount of neutral hydrogen. The neutral hydrogen may trap significant amount of Lyα radiation resulting in an enhanced population of $n = 2$ level of H (Strittmatter *et al.* 1977). This would imply a higher amount of absorption of Hα from the nearer polar cone. Since the line emission from the farther polar cone is redshifted considerably with respect to the nearer cone, it passes through the neutral matter without any absorption. Similar effect was observed in V1500 Cyg (Strittmatter *et al.* 1977). Also, in the case of V1500 Cyg, the blue peaks brightened relative to the red ones between 25–115 days from maximum in the nebular stage (Prabhu 1977). It is possible that a similar evolution would have taken place in LW Ser at epochs later than our observations, and probably shown the nearer polar cap.

3. Nova Scuti 1989

Nova Scuti 1989 was discovered on 1989 September 20 by Wild (1989: *IAU Circ. No.* 4861) at a magnitude of $\sim$ 10.5 (1989 September 21). Pre-discovery photographic magnitudes by McNaught (1989: *AAVSO Alert Notice Nos.* 119, 121; *IAU Circ. No.* 4862): 9.5 on 1989 September 8.65, 8.5 on September 17.41 and 9.0 on September 18.49 indicate the nova was discovered in the post-maximum phase. The outburst light curve places it among the moderately slow novae, exhibiting oscillations near maximum light. The light curve based on the magnitudes in IAU Circulars and AAVSO Circulars is plotted in Figure III.3.1. The observed maximum was on 1989 September 17.41 with $m_{\rm pg} = 8.5$. A smooth light curve indicates the maximum lies between the observations of 1989 September 8.65 and 1989 September 17.41. No star in the location of the nova was detected on the Palomar Sky Survey, ESO B fields and UK Schmidt J, R and I plates, indicating an outburst range of atleast 13 magnitudes (McNaught 1989: *IAU Circ. No.* 4862).

Spectra obtained by Barbon & Rosino (1989: *IAU Circ. No.* 4862) on 1989 September 23.8 indicate that the nova was in its early decline, showing broad emission lines of H, O I 7774 Å, He I 5876 Å, Fe II, N II and a faint blend of N III at 4640 Å. The halfwidth of the Hα line corresponds to an expansion velocity of $\sim$ 1400 km s^{-1}. The average expansion velocity derived by the halfwidths of other lines is $\sim$ 915 km s^{-1}. Spectra obtained on September 25.00 by Huchra, Olowin and Layden (1989: *IAU Circ. No.* 4862) show strong emission lines of Balmer series, Ca II H and K, and Fe II lines. The full width at half maximum and the full width at zero intensity, measured for Hβ are 1600 km s^{-1} and 2500 km s^{-1} respectively.

Spectroscopic observations of the nova between 1989 September 25 and 1989 December 4 obtained from VBO are presented here. Also presented are the spectra obtained on 1989 September 25 and October 8 by H.W. Duerbeck and collaborators from ESO.

3.1 The Spectrum

Observations and reductions

Photographic spectra in the wavelength range 4000–8800 Å were recorded from VBO between 1989 September 25 and October 3 using the 102 cm reflector and the UAG spectrograph equipped with the 150 mm camera and a Varo 8605 image intensifier. Kodak 103aD plates were used. CCD spectra at 5.5 Å per pixel res-

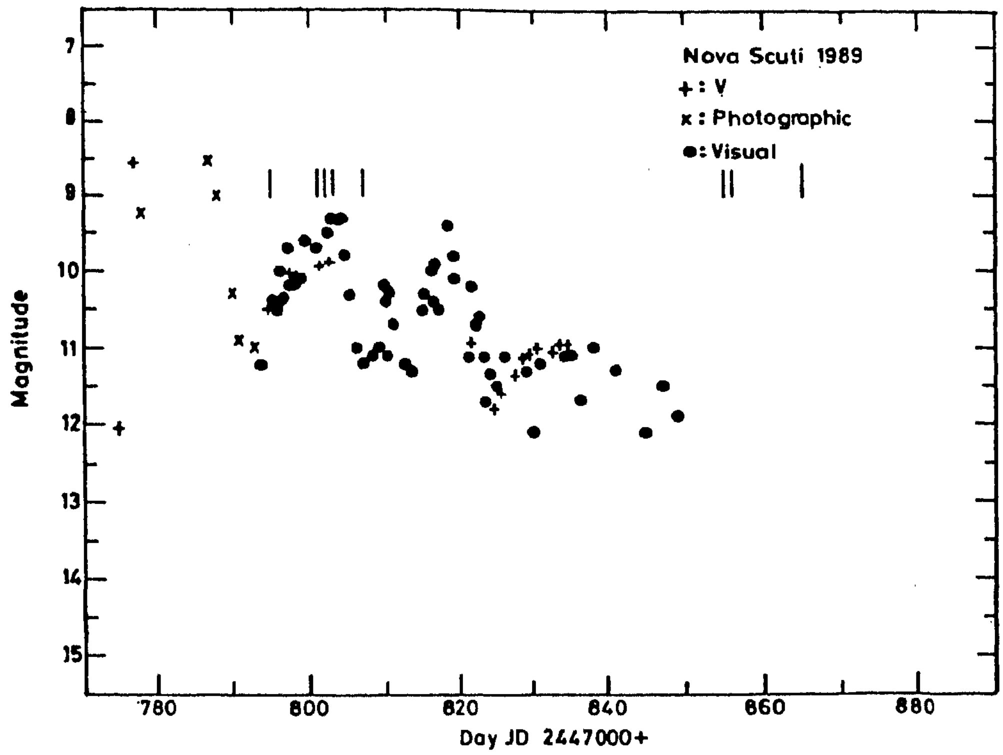

Fig. III.3.1 The light curve of Nova Scuti 1989. Vertical bars indicate the epochs of spectroscopic observations. JD2447780 = 1989 September 10.5.

olution were obtained on November 25 in the wavelength range 4400–7600 Å and on December 4 in the wavelength range 6000–9200 Å using the UAG spectrograph with 250 mm camera at the 102 cm reflector. The ESO spectra on September 25 and October 8 were obtained with the ESO 1.5 m telescope and a Boller & Chivens spectrograph, and were made available in flux calibrated form by H.W. Duerbeck. Table III.3.1 gives the journal of observations.

The photographic data were digitized on the PDS 1010M microdensitometer at 5 μm intervals and reduced to a relative intensity scale following the procedure in Chapter II. All spectra were Fourier smoothed using a low pass filter with cutoff at 15 cycles mm^{-1}. A Fe+Ne comparison source was used for wavelength calibration. Spectrophotometric standards HD 19445 and HR 8681 were used for flux calibration. Zero point corrections to the observed fluxes were applied using the published *VRI* magnitudes (*IAU Circ. Nos.* 4862, 4868, 4873 & 4902), as described in Chapter II. The VBO CCD data were individually de-biased, flat field corrected and the one dimensional spectrum extracted following the procedure in Chapter II. Fe+Ne comparison source was used for wavelength calibration. Spectrophotometric

Table III.3.1 Nova Scuti 1989: Journal of observations.

Date 1990 UT		Wavelength range Å
Sep	25.00*	3200–10500
	25.58	4500–8900
Oct	1.58	5000–8900
	1.62	4000–8000
	1.66	5000–8900
	1.69	4000–8000
Oct	2.57	4000–8000
	2.60	5000–8900
	2.62	5000–8900
Oct	3.56	5000–8900
	3.62	4000–8000
Oct	8.*	3200–7100
Nov	25.55	4600–7600
	25.57	4600–7600
Dec	4.56	6100–9200
	4.58	6100–9200

* ESO data

standard star HD 19445 was used for flux calibration. Since standard fluxes beyond 8300 Å were not available for the standard star, an estimated correction for the instrumental response was applied to the spectrum beyond 8300 Å, and the fluxes are somewhat uncertain.

Description of spectrum

The spectra of Nova Scuti 1989 used here cover four epochs — (i) on September 25 when the nova was recovering from a local dip in the light curve, soon after maximum, at a magnitude $m_v = 10.5$; (ii) October 1–3 during a subsequent maximum in the light curve, at magnitude $m_v = 9.5$; (iii) October 8 at a subsequent local dip, $m_v = 11.1$ and; (iv) November 25 and December 4 during the final decline ($m_v \sim 12.2$). The dates of observations are marked on the light curve in Figure III.3.1. The spectra are shown in Figures III.3.2–III.3.4.

The spectrum at all epochs consists of strong emission lines characteristic of a nova spectrum. The evolution of the emission line spectrum is similar to that of moderately slow novae *e.g.* , LW Ser (see §III.1) and V1819 Cyg (Whitney & Clayton 1989). Tables III.3.2 and III.3.3 list the line identifications and fluxes relative to Hβ. In what follows, the spectrum at each epoch is described.

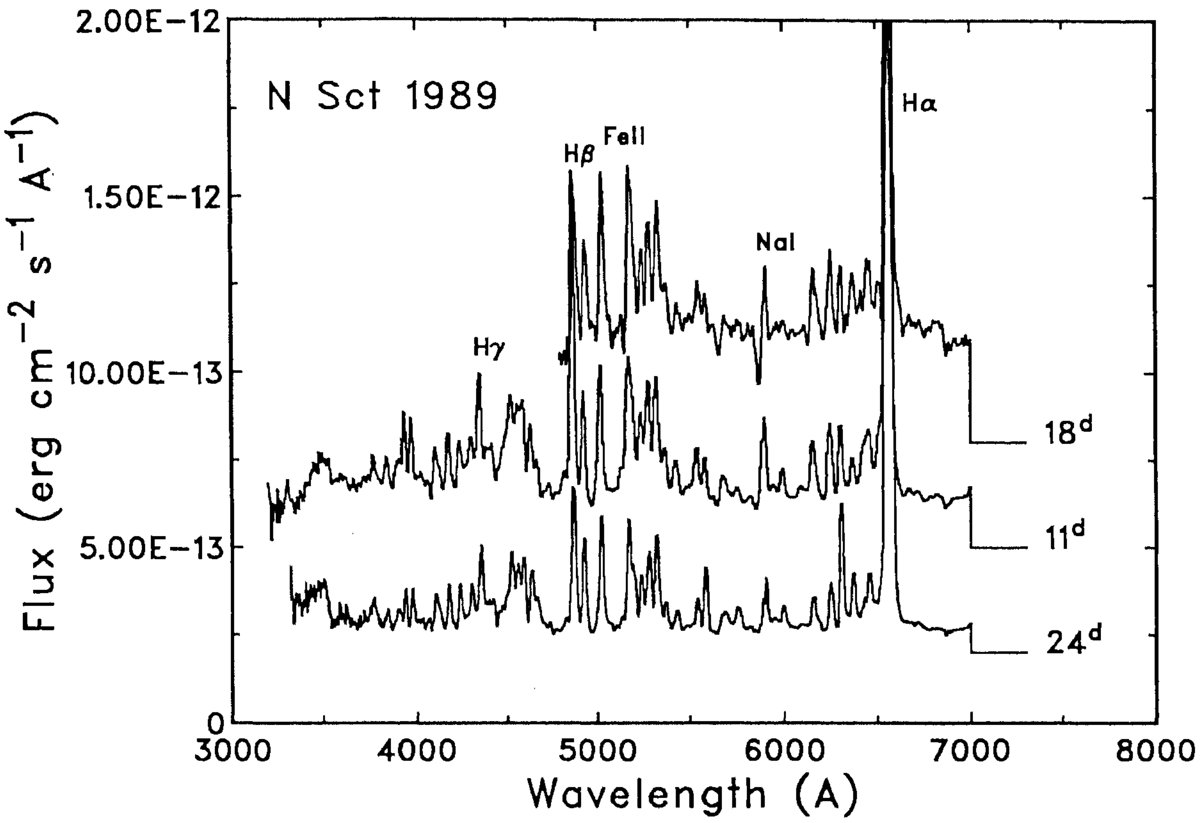

Fig. III.3.2 Spectra of Nova Scuti in the region 3200–7000 Å on 1989 September 25 (middle), October 1–3 (top) and October 8 (bottom). Bias of 0.5×10^{-12}, 0.8×10^{-12} and 0.2×10^{-12} erg cm^{-2} s^{-1} $Å^{-1}$ is added to the spectra of the three epochs, respectively. The zero point is shown by the horizontal line at the right, together with the day number since maximum. Note that the continuum was brighter on day 18 compared to days 11 and 24.

Epoch I (1989 September 25): The spectrum is dominated by strong broad emission lines (average FWHM $\sim$ 1200 km s^{-1}). The prominent lines in the spectrum are Balmer lines of hydrogen Hα–H_{14}; lines of Fe II multiplets 27, 37, 38, 42, 48, 49, 72, 73 and 74; Na I D 5893 Å; O I 6156, 6158, 7774, 8446 Å, Ca II H and K and the infrared triplet. Lines of nitrogen are also quite strong. N II 5462–5492 Å, 5666–5710 Å, 5941 Å and N I 8184–8242 Å are strong and unblended, whereas N I 8594, 8629 and 8728 Å are blended with the Ca II infrared triplet. N I 7423–7468 Å is blended with Fe II (73). Lines of C II 7231, 7236, 7112–7119 Å are also present. Lines of Si II and Ti II are probably present, but blended with other lines. Mg I 7877–7896 Å is clearly present. Hydrogen Paschen lines from P_7 10049 Å are present. P_{12} 8750 Å and P_{14} 8598 Å are blended with N I, and P_{13} 8662 Å and P_{15} 8542 Å with Ca II. P_7 is blended with Fe II 9999 Å. Forbidden lines are also

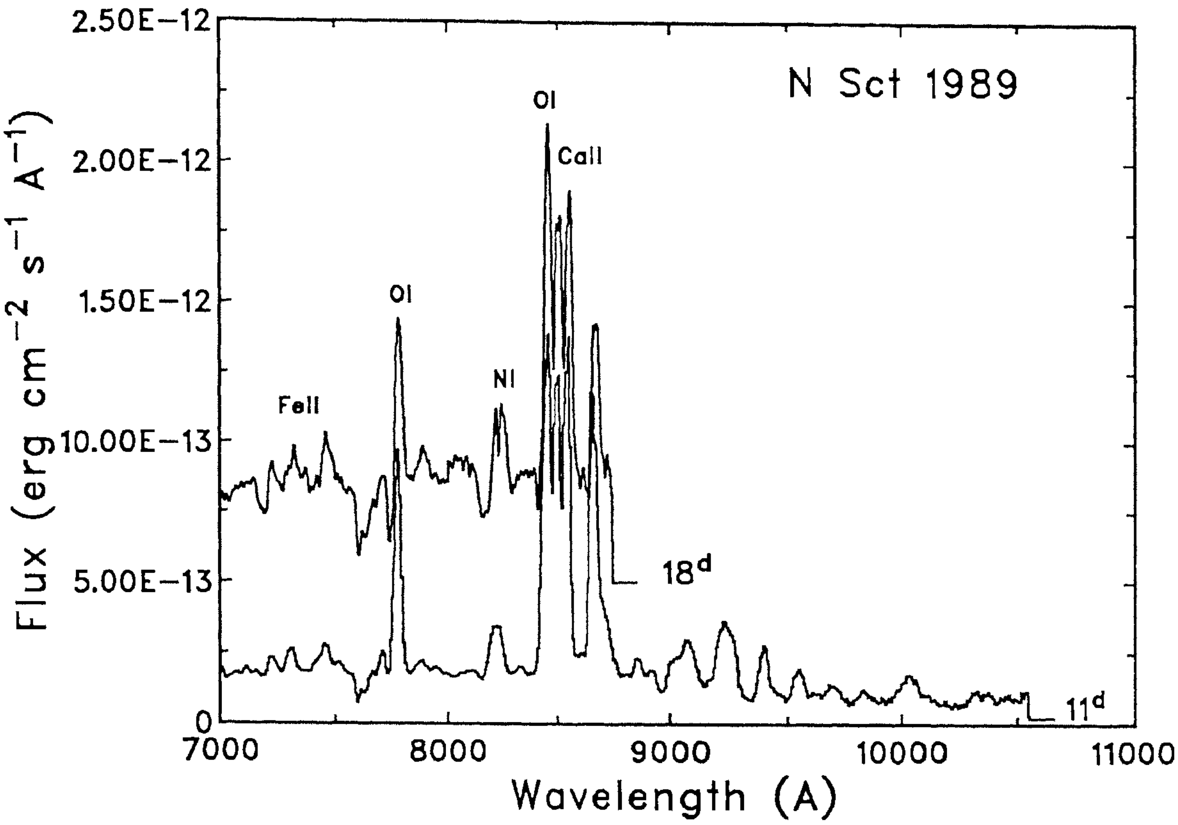

Fig. III.3.3 Spectra of Nova Scuti in the region 7000–10500 Å on September 25 (bottom) and October 1–3 (top). Bias of 0.2×10^{-12} and 0.5×10^{-12} erg cm^{-2} s^{-1} Å^{-1} is added to the two spectra, respectively. The zero point is shown by the horizontal line at the right, together with the day number since maximum. Note that the continuum was bright on day 18 compared to day 11.

present. [O I] 5577 Å and 6300 Å are fairly strong. [N II] 5755 Å is weaker. [O I] 6363 Å is present blended with Fe II(74), Si II(2). He I 5876, 6678, 7065 Å could be weakly present, with 5876 Å blended with Na I D. The P-Cygni absorption of Na I D is the only absorption clearly seen; absorptions of other lines are affected by blending.

Epoch II (1989 October 1–3): There is an increase in the continuum level as compared to Epoch I. The increase in the continuum is about 0.9 mag. Fe II lines have increased in strength, as also the strengths of oxygen and nitrogen lines. An increase of 1.2 mag was observed in the light curve at this epoch (see Figure III.3.1). The increase in the 0.9 mag continuum level accounts for most of the visual magnitude rise. The increase in the emission line strengths accounts for the

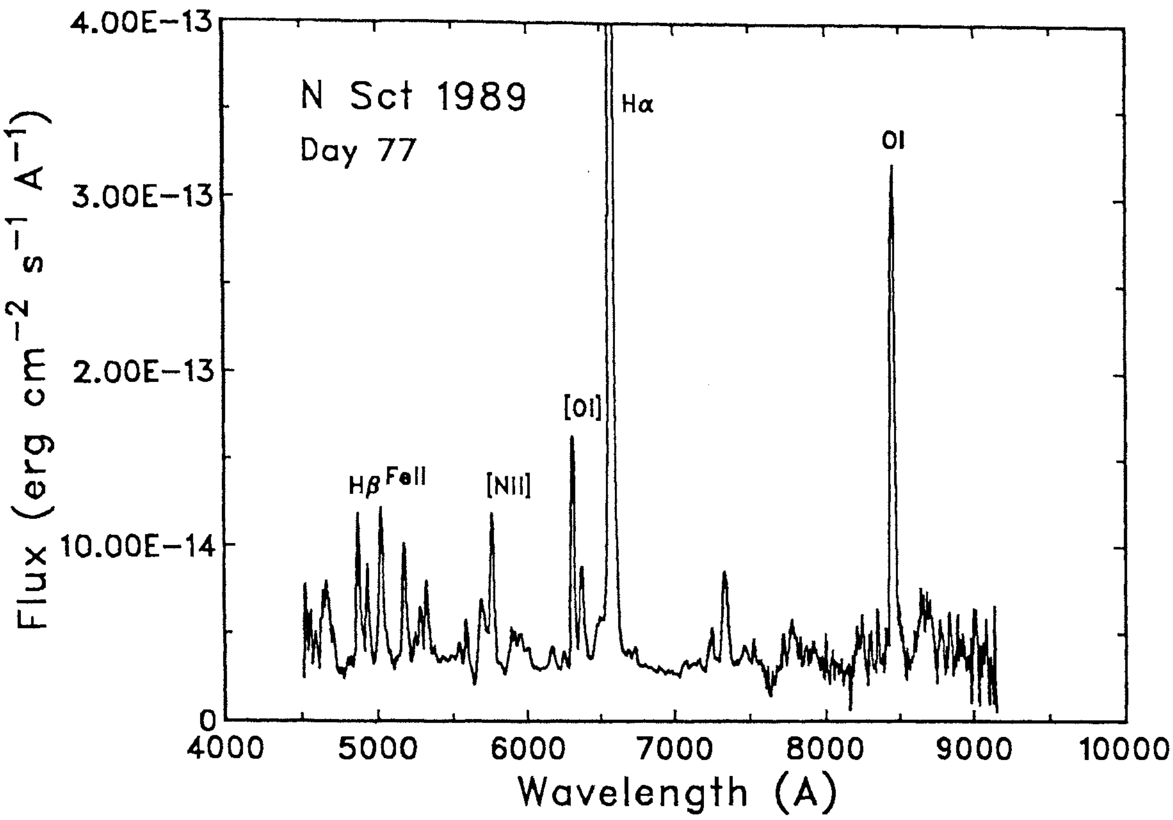

Fig. III.3.4 Spectrum of Nova Scuti on November 25–December 4, in the region 4500–9200 Å.

remaining 0.3 mag rise. P-Cygni absorptions appear stronger, as clearly seen from the Na I D absorption. The Hα line gives an absorption velocity of -1580 ± 40 km s^{-1}, whereas the mean absorption obtained from Na I, Fe II lines and O I permitted lines is -1300 ± 90 km s^{-1}.

Epoch III (1989 October 8): The continuum level has decreased. Lines of oxygen and nitrogen continue to increase in strength, whereas lines of hydrogen, Fe II and Na I D have decreased. The decrease in the continuum level is about 1.9 mag which is in proportion with the 2 mag decrease in the light curve.

Epoch IV (1989 November 25, December 4): This stage marks the decline of the nova. The continuum level has further decreased. Lines of Fe II, Ca II, Na I D have weakened considerably. The decrease in the strength of the permitted lines of oxygen and nitrogen is however not very significant. The strengths of the forbidden lines have increased. Ca II] appears to be the major contributor to the blend at 7185 Å. There is a dramatic increase in the strength of [O I] 6300, 6363 Å and [N II] 5755 Å, whereas the increase in the strength of [O I] 5577 Å is marginal. O I

Table III.3.2 Nova Scuti: Line identifications and observed fluxes relative to Hβ, in the region 3400–6000 Å.

λ_m	Identification		Flux			
Å			Day 11	18	24	77
3450	3416.02	Fe II (16)				
	3494.67	Fe II (16)	0.424		0.563:	
	3456.93	Fe II (76)				
3593	3596.05	Ti II (15)	0.161		0.046:	
3716	3721.94	H_{14}	0.041			
3739	3734.37	H_{13}	0.040			
3763	3750.15	H_{12}	0.149		0.164	
	3770.63	H_{11}				
3840	3835.39	H_9	0.122		0.103	
3902	3889.05	H_8	0.144		0.131	
3937	3933.66	Ca II (1) K	0.496		0.153	
3976	3968.47	Ca II (1) H	0.163		0.174	
	3970.07	Hϵ				
4018	4012.37	Ti II (11)	0.094		0.079	
4109	4101.74	Hδ	0.165		0.259	
4175	4173.45	Fe II (27)	0.267		0.227	
4233	4233.17	Fe II (27)	0.170		0.253	
4302	4303.17	Fe II (27)	0.187		0.284	
4345	4340.47	Hγ	0.381		0.519	
	4351.76	Fe II (27)				
4386	4385.38	Fe II (27)				
+			0.248		0.312	
4408	4416.82	Fe II (27)				
4529	4515.34, 4520.23,					
	4555.89	Fe II (37)				
+	4522.63	Fe II (38)	1.187	1.421	0.795	0.960
	4549.47	Fe II (38)				
4582	4583.83	Fe II (38)				
4635	4629.34	Fe II (37)	0.381	0.576	0.327	
	'4640'	N/O complex				1.341
4864	4861.33	Hβ	1.000	1.000	1.000	1.000
4925	4923.92	Fe II (42)	0.272	0.879	0.553	0.557

Table III.3.2 Continued.

λ_m Å	Identification	Flux Day 11	18	24	77
5018	5018.43 Fe II (42)	0.427	1.400	0.767	1.354
	5005.14 N II (19)				
5172	5169.03 Fe II (42)	0.660	1.713	0.939	0.951
	5197.57 Fe II (49)				
5236	5234.62 Fe II (49)	0.242	0.635	0.295	0.170
5276	5275.99 Fe II (49)	0.377	0.847	0.493	0.414
5316	5316.61 Fe II (49)	0.402	1.151	0.590	0.615
	5316.78 Fe II (48)				
5365	5362.86 Fe II (48)	0.197	0.396	0.152	0.045
5423	5425.27 Fe II (49)	0.212	0.354	0.103	0.041
	5414.09 Fe II (48)				
5486	5495.70, 5480.10,	0.103	0.283	0.022:	0.173
	5462.62 N II (29)				
5533	5534.86 Fe II (55)				
	5530.27 N II (63)	0.223	0.211	0.451	0.119
	5535.39 N II (63)				
5577	5577.35 [O I] (3)	0.193	0.324	0.341	0.398
5680	5666.64, 5676.02,				
	5679.56, 5686.21,	0.210	0.191	0.200	0.385
	5710.76 N II (3)				
5755	5754.80 [N II] (3)	0.053	0.171	0.208	0.708
5903	5889.95 Na I (1)	0.263	0.380	0.257	
	5895.92 Na I (1)				1.248*
5945	5941.67 N II (28)	0.039	0.072	0.058	
5989	5991.38 Fe II (46)	0.084	0.139	0.144	0.221
	5995.28 O I (44)				
$F_{H\beta}$ (10^{-11} erg cm^{-2} s^{-1})		2.804	1.102	1.258	0.226

Multiplet numbers appear in parentheses.

* Contribution from He I 5876 Å also.

Table III.3.3 Nova Scuti: Line identifications and observed fluxes relative to Hβ, in the region 6000 Å – 1.1 μm.

λ_m Å	Identification	Flux Day 11	18	24	77
6084	6084.11 Fe II (46)	0.041	0.023	0.020	
6152	6155.99, 6156.78,				
	6158.19 O I (10)	0.214	0.648	0.220	0.203
	6147.74 Fe II (74)				
6247	6247.56 Fe II (74)	0.235	0.711	0.263	0.104
6303	6300.23 [O I] (1)	0.226	0.444	0.775	1.748
6365	6363.88 [O I] (1)	0.144	0.571	0.396	1.115
	6416.91 Fe II (74)				
	6347.09 Si II (2)				
	6371.36 Si II (2)				
6455	6456.38 Fe II (74)	0.428	0.560	0.496	0.889
	6453.64, 6454.48,				
	6456.01 O I (9)				
6563	6562.82 Hα	10.895	12.701	7.144	15.695
6676	6678.15 He I (46)	0.032	0.077		0.065
6827	6812.26 N II (54)	0.023	0.103	0.010	
	6836.2 N II (54)				
7069	7065.19 He I (10)	0.014	0.012		0.121
7114	7112.36, 7115.13,	0.033	0.056		
	7119.45 C II (20)				
7136	7135.8 [A III] (1)		0.087		0.145
7224	7222.39 Fe II (73)	0.090	0.282		0.304
	7231.12 C II (3)				
	7236.19 C II (3)				
7317	7307.97 Fe II (73)	0.181	0.189		
	7320.70 Fe II (73)				
	7291.46 Ca II] (1)				1.456
	7323.88 Ca II] (1)				
7457	7462.38 Fe II (73)	0.306	0.746		0.329
7778	7771.96, 7774.18,	1.006	1.729		0.289
	7775.40 O I (1)				
7884	7877.13 Mg II (8)	0.065	0.465		0.145
	7896.37 Mg II (8)				

Table III.3.3 Continued.

λ_m Å	Identification		Flux			
			Day 11	18	24	77
8217	8184.80, 8187.95, 8216.28, 8223.07, 8242.34	N I (2)	0.448	1.229		0.895
8446	8446.35 8446.76	O I (4) O I (4)	1.864	4.139		6.679
8502	8498.02 8502.49	Ca II (2) P_{16}	1.391	3.238		
8541	8542.09 8545.38	Ca II (2) P_{15}	1.539	3.420		
8602	8594.01 8598.39	N I (8) P_{14}	0.085	0.213		0.644
8663	8662.14 8665.02	Ca II (2) P_{13}	1.494	2.283		
8717	8703.24, 8711.69, 8718.82	N I (1)	0.039			2.417
8857	8862.79	P_{11}	0.073			
9065	9060.6	N I (15)	0.395			
9239	9228.11 9237.49	S I (1) S I (1)	0.685			
9400	9405.77	C I (9)	0.286			
9545	9545.97	P_8	0.151			
10026	9999 10049.38	? P_7	0.339			
10116	10113.4	N I (18)	0.085			
$F_{H\beta}$ (10^{-11} erg cm^{-2} s^{-1})			2.804	1.102	1.258	0.226

Multiplet numbers appear in parentheses.

8446 Å has also strengthened, whereas O I 7774 Å has decreased. Although the hydrogen line strengths have decreased, the Hα/Hβ ratio has increased. P-Cygni absorptions are either absent or very weak.

The spectrum during the first three epochs resembles that of the diffuse enhanced stage, whereas the spectrum at the last epoch is that of the [O I] flash and nitrogen flaring stage.

3.2 Absolute Magnitude, Reddening and Distance

The light curve of Nova Scuti 1989 (Figure III.3.1) indicates the maximum had reached between the two preoutburst observations of 1989 September 8.64 and September 17.41. The photographic magnitude of the nova on these days was $m_{pg} = 9.5$ and $m_{pg} = 8.5$ respectively. From the light curve, the maximum is estimated to have reached on 1989 September 14 at a magnitude $m_{pg} = 8.3$. Early UBV observations indicate that the $(B - V)$ colour of the nova decreased from 0.49 on September 25 to 0.21 on October 2. Assuming that the nova had $(B-V) = 0.49$ at maximum also, and using the conversion between m_{pg} and V as given by Capaccioli *et al.* (1989), $V_{max} = 8.0 \pm 0.3$ is estimated; the error estimate is based on colour curves of different novae (van den Bergh & Younger 1987). A smooth light curve through the oscillations between maximum and early decline gives the following parameters of the light curve: (i) at 15 days from maximum (1989 September 29) $V = 10.0$; (ii) the time taken for a decline of 2 mag in the V light curve, $t_2 = 16 \pm 5$ days; (iii) the time taken for a decline of 3 mag in the V light curve $t_3 = 46 \pm 9$ days. Using these parameters the absolute magnitude of the nova at maximum can be estimated. Using the different calibrations found in the literature, the absolute magnitude at maximum is determined as listed in Table III.3.4. The values range from $M_V = -7.2$ to $M_V = -8.3$, with a simple average of

$$M_V = -7.8 \pm 0.4$$

which implies an apparent distance modulus of

$$(m - M)_V = 15.8 \pm 0.5.$$

Early in the outburst, based on optical observations, we have only methods (a)–(c) described in §III.1.2 for estimating interstellar extinction. The ESO spectrum of September 25 contains the lines P_8, P_{11}, H_{13} and H_{14} without severe blending with other lines. Using the ratios of H_{14}/P_{11} and H_{13}/P_8, and the tables of Hummer & Storey (1987) for $T_e = 10^4$ K, $n_e = 10^{10}$ cm^{-3} (a value to be justified in §III.3.3), the reddening is estimated to be

$$E(B - V) = 0.39 \pm 0.02.$$

The resulting corrected distance modulus is $(m - M)_V^0 = 14.6$ and the implied distance 8.3 kpc. The observed colour at two magnitudes below maximum,

Table III.3.4 Nova Scuti: Absolute magnitude estimates.

No.	Relation	Ref.	$M_V(\max)$
1	$M_B(\max) = -10.67 + 1.80 \log t_3$ $\pm 0.30 \quad \pm 0.20$	1	-7.9 ± 0.8
2	$M_V(\max) = -10.70 + 2.41 \log t_3$ $\pm 0.30 \quad \pm 0.23$	2	-7.8 ± 0.9
3	$M_V(t_{15}) = -5.60 \pm 0.45$	2	-7.6 ± 0.5
4	$M_V(t_{15}) = -5.23 \pm 0.39$	3	-7.2 ± 0.4
5	$M_V(\max) = -7.89 - 0.81 \arctan\left(\frac{1.32 - \log t_2}{0.19}\right)$	4	-8.3 ± 0.4

1: Pfau (1976); 2: Cohen (1985); 3: van den Bergh & Younger (1987);
4: Capaccioli *et. al.* (1989).

$(B-V)_2 = 0.23 \pm 0.03$ suggests a value of $E(B-V) = 0.25$. The colours corrected for $E(B-V) = 0.39$ fall within the range of observed colours of novae two magnitudes below maximum. In particular, the values $(B-V)_2^0 = -0.18$ and $(U-B)_2^0 = -1.07$ are very similar to the values of V533 Her 1963: $(B-V)_2^0 = -0.13$ and $(U-B)_2^0 = -1.06$ (van den Bergh & Younger 1987). It may be noted that the light curves of Nova Scuti 1989 and V533 Her are quite similar.

The well-studied globular cluster M11 (=NGC 6705) lies 21 arcmin east of Nova Scuti. The cluster has an apparent distance modulus of $(m-M)_V = 12.7$ (Lee *et al.* 1989) and a reddening $E(B-V) = 0.44$ (Anthony-Twarog *et al.* 1989), resulting in a distance estimate of 1.8 kpc. Assuming the reddening per kpc to be $0.44/1.8 = 0.24$ along the line-of-sight, Nova Scuti is estimated to be at a distance of 3.7 kpc with reddening $E(B-V) = 0.9$. At its galactic latitude (-3.3 deg), the nova crosses the galactic plane at about 3 kpc. Also, substantial reddening is not expected beyond the Aquila-Carina arm at 2 kpc. Hence, the above estimate of reddening is an upper limit, and the distance a lower limit. The nova apparently belongs to the central bulge of the galaxy. In what follows a reddening correction of $E(B-V) = 0.40$ and distance of 8.3 kpc are assumed.

3.3 Physical Conditions

Nova Scuti had not yet reached the nebular phase during our observations, and lines of [O III] are not yet easily detectable in our spectra. However, an estimate of

Table III.3.5 Nova Scuti: Electron density, temperature and mass.

Day	Electron density 10^8 cm^{-3}	Temperature K	Mass 10^{-5} $M_\odot$
11	27.0	7000	0.53
18	8.8	6800	0.77
25	4.4	6000	1.00
77	0.5	5000	3.50

density may be obtained using the hydrogen line fluxes (see §III.1.2). The observed Hα line fluxes dereddened using $E(B-V) = 0.4$ are used to estimate the density. The volume of the line emitting region is estimated using the observed velocity of -1300 km s^{-1} and a filling factor $\phi \sim 0.1$. Taking the emissivity for Hα from Hummer & Storey (1987) at $T_e = 10^4$ K, the electron density is estimated to decrease from a value 3×10^9 cm^{-3} on day 11 (Epoch I) to 5×10^7 cm^{-3} on day 77 (Epoch IV). The derived densities are listed in Table III.3.5. The densities decreased as $n_e = 3.2 \times 10^{11} t_d^{-2.02}$ cm^{-3}, where t_d is the time, in days, since maximum. The mass of the envelope is estimated as $M_H = 3.5 \times 10^{-5}$ $M_\odot$ on day 77. The estimates on different days lead to $M_H \sim 4.6 \times 10^{-7} t_d^{0.98}$ $M_\odot$.

The observed dereddened fluxes of [O I] 5577 Å and 6300 Å imply, from Equation III.1.4, that the temperature decreased from 7000 K on day 11 to 5000 K on day 77. The derived temperatures are also tabulated in Table III.3.5.

On day 77, He I 6687 Å is weakly present. He I 5876 Å is also present, blended with Na I D. The He I line fluxes may be used to estimate $n(\mathrm{He}^+)/n(\mathrm{H})$ in the ejecta. Since He I 5876 Å is blended with Na I D, its flux estimate is uncertain. Hence only 6678 Å is used to estimate He$^+$ abundance. The ratios 6678/Hβ and 6678/Hα have been used. Taking the emissivities for Hα and Hβ from Hummer & Storey (1987) and for He I 6678 Å from Brocklehurst (1972) at $T_e = 10^4$ K and $n_e = 10^7$ cm^{-3}, $n(\mathrm{He}^+)/n(\mathrm{H})$ is estimated. He I 6678 Å emissivity has been corrected for collisional effects following Clegg (1987). Hβ gives $n(\mathrm{He}^+)/n(\mathrm{H}) = 0.15$, whereas H$\alpha$ gives $n(\mathrm{He}^+)/n(\mathrm{H}) = 0.04$. The observed, reddening corrected, Hα/Hβ ratio has a value 10.4 on day 77. This implies a high Lyα optical depth. The observed ratio of Hα/Hβ on day 77 agrees well with the model in Drake & Ulrich (1980) for which $\tau(\mathrm{Ly}\alpha) = 10^6$, $n_e = 10^8$ cm^{-3} and $T_e = 10^4$ K. Using the emissivities for Hα and Hβ from Drake & Ulrich, $N(\mathrm{He}^+)/N(\mathrm{H}) = 0.043$ from Hβ and $N(\mathrm{He}^+)/N(\mathrm{H}) = 0.054$ from Hα is obtained. He II lines are not easily detectable in the spectra. This, together with the fact that He I lines are still weak indicates that ionization in the ejecta is still low and most of the helium is still in neutral form. It is hence too early for an abundance estimate of He. Using Equation III.1.12 the temperature of the source of ionization in the envelope can be estimated. The deduced value is 8.7×10^4 K. The radius of the source determined from the observed Hβ flux, for an assumed distance of 8.3 kpc, and using Equation III.1.14 is 1.9×10^{11} cm$= 2.8\ R_{\odot}$. It is thus possible to infer the presence of a hot, bloated white dwarf within the expanding envelope.

3.4 Discussion

The optical light curve indicates Nova Scuti 1989 is a slow nova, somewhat similar to V1819 Cyg (Whitney & Clayton 1989) and V533 Her (van den Bergh & Younger 1987). The rate of decline is $t_2 = 16 \pm 15$ days and $t_3 = 46 \pm 9$ days, implying an absolute maximum brightness $M_V = -7.8 \pm 0.04$. The foreground reddening towards the nova is estimated to be $E(B - V) = 0.39$–0.9 and the distance is between 3.7–8.3 kpc. At maximum, nova V533 Her had a sharp peak of about one magnitude (Chincarni & Rosino 1964). It is possible to accomodate such a peak in Nova Scuti 1989 between the prediscovery photographic observations of September 8 and 17. In such an event, a distance of ~ 5 kpc would agree with $E(B-V) \sim 0.4$. We have, however, assumed a distance of 8.3 kpc in accordance with the recorded maximum.

The evolution of the spectrum is similar to that of slow novae. The nova was in the diffuse enhanced phase during the first three epochs of observations — 1989 September 25, October 1-3, October 8; and in the of O I flash, nitrogen flaring phase during the last epoch — 1989 November 25, December 4. The absorption velocities measured on October 1–3 give -1600 km s^{-1} for Hα line and a mean value of -1300 km s^{-1} for other lines. The spectrum of September 25 was obtained as the nova was recovering from a local dip in the light curve soon after maximum; that of October 1–3 during a subsequent maximum and that of October 8 at a subsequent local dip. A variation was seen in the spectral continuum proportional to the light curve variations. On October 1–3, the continuum flux increased by a constant value of 0.9 mag, whereas a 1.2 mag increase was observed in the light curve. Subsequently, the continuum flux decreased by 1.9 mag on October 8 in proportion with a 2 mag decrease in the light curve. During this period, the colours of the nova did not show any significant variations. The light curve and continuum flux variations are hence not due to temperature variations, but caused by a variation in the photospheric radius.

The density in the envelope, as estimated from observed Hα flux decreased from 3×10^9 cm^{-3} on day 11 to 5×10^7 cm^{-3} on day 77. The derived hydrogen mass in the envelope increased from 5×10^{-6} $M_\odot$ to 3.5×10^{-5} $M_\odot$. The temperature as estimated from the [O I] line ratios steadily decreased from 7000 K on day 11 to 5000 K on day 77. The observed, dereddened ratios of Hα/Hβ, Hβ/Hγ and Hγ/Hδ depart considerably from the theoretical values of Case B, but can be explained on the assumption of high optical depths in Lyman and Balmer lines. A comparison of observed ratios with the theoretical models of Netzer (1975), Krolik & McKee (1978) and Drake & Ulrich (1980) indicates that Lyα optical depth was in the range 10^5–10^6 and Hα optical depth in the range 10–100 during the period of our observations. The effect of high initial optical depth and its decrease with time imply that one is progressively viewing deeper and deeper into the envelope. This explains the slower decrease of densities (t^{-2}) as compared to the assumed increase of volume (t^3), as also the increase in derived mass almost in proportion to time. The high optical depth in Lyα, on the other hand, increases the Hα emissivity by a larger factor in early days, and a lower factor later. A correction for this effect would decrease the early estimates of densities and augment the effect of Hα optical depth.

A velocity of 1300 km s^{-1} was assumed for the calculation of the volume of the envelope. This is likely to be the diffuse enhanced system, the principal system having a lower velocity $\sim$ 1000 km s^{-1}. The filling factor of the envelope is also likely to be smaller than the assumed value of 0.1. These two factors decrease the estimate of volume, and increase the densities. The Lyα optical depth, on the other hand, tends to decrease the derived densities. The derived densities are hence optimal values. These densities are higher than the critical densities for the observed forbidden lines of [O I] 5577 Å (1.1×10^8 cm^{-3}), [N II] 5755 Å (1.8×10^7 cm^{-3}) and [O I] 6300 Å (1.8×10^6 cm^{-3}). These lines orginate near the edge of H$^+$ region where the densities are apparently lower.

A value $N(\mathrm{He}^+)/N(\mathrm{H}^+) \sim 0.05$ is estimated on day 77. The lack of detection of He II indicates a low abundance of He^{++}/H$^+$. There is hence a considerable extent of He^0/H$^+$ region. This is attributed to high optical depth in the Lyman continuum. As the density of the envelope decreases the degree of ionization will increase.

The estimates of the amount of ionizing radiation yield an estimate of $T_s = 8.7 \times 10^4$ K and $R_s = 2.8\ R_\odot$ for the central ionizing source on day 77.

4. GK Persei

GK Persei (Nova Persei 1901) was the first bright nova of the twentieth century and was subjected to very detailed spectroscopy and photographic photometry (Payne-Gaposchkin 1957). It was discovered on 1901 February 22 by Anderson (1901), and reached a maximum of $V = 0.2$ mag. Subsequent decline, at a rate of 0.23 magnitude per day classifies it among the very fast novae. The outburst light curve was characterized by rapid semi-periodic fluctuations during the transition phase (Payne-Gaposchkin 1957). It presently resides at a typical magnitude of $V = 13.1$. In contrast with other old novae, GK Per exhibits dwarf nova like outbursts of ~ 3 mag, the latest of which was in 1989 (*IAU Circ. No.* 4819). These dwarf nova like outbursts are thought to start at the inner edge of the accretion disc where an unstable region could occasionally be formed due to modulation of the mass transfer rate from the secondary (Cannizzo & Kenyon 1986; Bianchini *et al.* 1986). Most of the optical outbursts of GK Per occur at time intervals given by $\Delta t = n(400 \pm 40)$ days, where $n = 1, 2, 3$ and 5 (Sabbadin & Bianchini 1983).

Apart from its dwarf nova like activity, GK Per is unusual in several other respects. It has a very long orbital period: 1.904 days (Bianchini, Hamzaoglu & Sabbadin 1981); 1.997 days (Crampton, Cowley & Fisher 1986). Unlike other known classical novae, GK Per has an evolved secondary of type K0–K2IV (Crampton, Cowley & Fisher 1986; Kraft 1964; Gallagher & Oinas 1974). The eccentricity of the orbit is uncertain. Bianchini, Hamzaoglu & Sabbadin (1981) suggest a highly eccentric orbit, $e = 0.39$, whereas Crampton, Cowley & Fisher (1986) determine an essentially circular orbit. The primary is a white dwarf of mass $> 0.72\ M_\odot$ (Watson, King & Osborne 1985), 0.9 $M_\odot$ (Crampton, Cowley & Fisher 1986) or 1.3 $M_\odot$ (Bianchini, Hamzaoglu & Sabbadin 1981). The mass of the secondary is estimated as 0.25 $M_\odot$ by Crampton, Cowley & Fisher (1986) and 0.9 $M_\odot$ by Bianchini, Hamzaoglu & Sabbadin (1981). The orbital inclination is uncertain, but the absence of obvious eclipses indicates it cannot be very high. Bianchini & Sabbadin (1983) suggest $i = 66°$, and Crampton, Cowley & Fisher (1986) give $i \leq 73°$. A long term solar type activity of the secondary has been detected. This solar type cycle has a periodicity of ~ 7 years (Bianchini 1990).

Based on Ariel 5 sky survey instrument observations of an x-ray flare lasting ~ 45 days from the vicinity of GK Per in 1978 which coincided with ~ 1 mag optical outbursts, King, Ricketts & Warwick (1979) proposed GK Per as a hard x-ray source, which was subsequently confirmed by observations in quiescence by the Einstein Observatory (Becker & Marshall 1981; Cordova & Mason 1984). Bianchini & Sabbadin (1983) suggested that the accreting white dwarf in this system must have a strong magnetic field in order to explain the hard x-ray emission from the system, and the form of the accretion disc emission. EXOSAT observations during the 1983 outburst (Watson, King & Osborne 1985) showed the x-ray flux to be modulated at a period of 351 seconds. In addition, the hard x-ray emission also varied aperiodically on timescales ~ 3000 seconds. The dominant hard x-ray component had an unprecedently flat ($L_\nu \propto \nu^{-0.5}$) spectrum for a cataclysmic variable. The 351 second periodicity is associated with the spin period of the magnetized white dwarf.

A month after the 1901 outburst, expanding nebulosities were seen in the vicinity of the nova (*e.g.* Ritchey 1901; Perrine 1902). This first recorded 'light echo' was explained by Couderc (1939) in terms of reflection from dust grains lying in a plane crossing the line of sight to the nova. The fact that no other nova (with the exception of V732 Sgr 1936: Swope 1940) has shown such a phenomenon led Schaefer (1988) to the suggestion that the grain density in the light echo region of GK Per is upto 10^4 times that in the general interstellar medium.

The expanding ejecta from the 1901 outburst was first discovered by Barnard in 1916 and photographed by Pease (1917). The expanding ejecta has been intermittently followed ever since. The asymmetry and longevity of this remnant is quite unusual and unique among novae. During the outburst, matter was ejected with an initial velocity of 1200 km s^{-1} (McLaughlin 1960). The total mass ejected has been estimated to be 7×10^{-5} $M_\odot$ (Pottasch 1959). The evolution of the optical nebulosity over several decades indicates the expanding ejecta is interacting with the ambient medium (Oort 1951; Seaquist *et al.* 1989). The remnant of GK Per and its environs have been studied in great detail by Seaquist *et al.* (1989).

An extended emission associated with GK Per has been detected in the far infrared (Bode *et al.* 1987; Seaquist *et al.* 1989). The 60 μm and 100 μm IRAS images show the presence of an elongated structure running roughly northwest–southeast through the position of the nova. This extension which is about 40 arcmin is coincident with the H I emission (Seaquist *et al.* 1989). The IR extension is double peaked and the nova resides on a saddle point between these peaks. There is no significant change in temperature across this extension (Bode *et al.* 1987). Bode *et al.* and Seaquist *et al.* suggest that the IR and H I emission arise from a torus of material surrounding GK Per viewed almost edge-on The distribution of the CO emission (Hessman 1987) also matches very well with the IR and H I emission. Bode *et al.* and Seaquist *et al.* suggest that the toroid is most likely the result of planetary nebula ejection from the central binary during its common envelope phase of evolution. The age of the planetary nebula as estimated by Bode *et al.* is 3×10^4 to 1.3×10^5 years.

The remnant of GK Per has been imaged in broad band as well as in the emission lines ([N II], [O III], [O II]) photographically, and in recent times using CCDs. Optical images of the expanding ejecta obtained over several decades show that the shell is highly asymmetric and has evolved into a series of knots. The bulk of the emission arises in the southwest quadrant. [O III] images, however, do not show any emission in this region. Recent images of the shell (Seitter & Duerbeck 1987; Seaquist *et al.* 1989) suggest a box shaped morphology, with evident flattening in the southwest and northeast. This flattening is due to deceleration of the ejecta on interaction with the ambient medium. In a 4.86 GHz radio image obtained by Seaquist *et al.* (1989), the ridge of maximum radio brightness coincides with the flattened southwest portion of the optical shell, indicating interaction between the nova ejecta and the ambient gas. The radio emission is nonthermal with synchrotron radiation being the predominant emission mechanism. Based on radio observations, Seaquist *et al.* (1989) and Reynolds & Chevalier (1984) conclude that in many respects the remnant of GK Per behaves like a supernova remnant.

The density of optical knots is maximum in the region of the radio-emitting ridge. The fact that [O III] emission is absent in the knots in the radio-ridge while [N II] and [O II] are bright can be used to determine the physical conditions in the knots in the ridge. The absence of [O III] emission has led Seaquist *et al.* (1989) to infer that reverse shock speed in the radio emitting region must be less than 100 km s^{-1}. For a shock velocity < 100 km s^{-1} they estimate the density of knots in this region to be about 2×10^3 cm^{-3}. In the non-radio-emitting region, where [O III] is detected in the blobs, the shock speeds are presumably higher and densities much lower.

The angle subtended at the nova by the southwest interaction zone has remained constant over the several decades suggesting that the interacting circumstellar gas is confined to a polar cone with an opening angle of 90° and axis perpendicular to

III.4.1 Journal of observations of the shell of GK Persei.

Date UT		Exposure time min	Filter	Bandpass Å
1988 Dec	8.81	30	Hα+[N II]	160
1989 Feb	5.64	45	[O III]	50
	5.67	45	[O III]	50
1990 Jan	17.65	30	Hα+[N II]	160
	17.70	30	Hα+[N II]	160
1990 Feb	20.63	30	Hα+[N II]	160

the axis of the bipolar nebula (Seaquist *et al.* 1989). If this polar cone is a part of the planetary nebula, then it possesses much lower mass than the main shell.

Bode *et al.* (1987) and Seaquist *et al.* (1989) suggest that GK Per exploded into its own planetary nebula accounting for its unique characteristics.

4.1 Nebular Remnant

Optical CCD images of the nebular shell around GK Per were obtained from VBO using the 102 cm reflector and Photometrics CCD system, in Hα+[N II] and [O III] emission lines. The [O III] images were obtained on 1989 February 5 and the Hα+[N II] images on 1988 December 8, 1990 January 17 and 1990 February 20. Table III.4.1 gives the details of observations.

All images were individually de-biased and flat field corrected following the procedure in Chapter II. Flat field images were obtained from twilight sky exposures. The de-biased and flat-fielded images were aligned using a shift+rotation transformation (*i.e.* coefficients $C_2 = C_6 = 1$ in equations II.2.1 and II.2.2). The [O III] images were aligned with respect to the Hα+[N II] images. The aligned Hα+[N II] images of 1990 January 17 and 1990 February 20 were then averaged to obtain a mean Hα+[N II] image. Likewise a mean [O III] image was obtained. The 'ghost' in the [O III] image was removed as described in Chapter II. The image was smoothed using a 3×3 Gaussian filter ($\sigma = 1$).

Figure III.4.1 shows the mean Hα+[N II] image. This image predominantly contains [N II] emission which is at least 20 times as strong as Hα (Seaquist *et al.* 1989). The shell is asymmetric. It is flattened in the southwest and northeast directions. The bulk of the emission arises from the southwest quadrant. This is

Fig. III.4.1 Image of GK Per shell through [N II] emission. North is at the top and east to the left. Scale: 1 mm = 1.58 arcsec.

coincident with the radio emitting ridge (Seaquist *et al.* 1989). Comparison of the [N II] and [O III] images shows that the knots in both emissions generally coincide except for the radio emitting region. Difference in the [N II] and [O III] distributions have been noticed by Duerbeck & Seitter (1987) and also by Seaquist *et al.* (1989) and have been attributed to spatial variations in the physical conditions of the knots. An enhancement of [O III] emission over [N II] is seen along position angles 132° and 295° (Figure III.4.2). This coincides with the direction of H I emission and the IR torus. The knots in [O II] emission also generally coincide with the [N II] emission (Seaquist *et al.* 1989). However, it is seen that there is strong emission from [O III] and [O II] in the east where [N II] is weak or absent. Similar [O II] enhancement is seen in the west along the direction of [O III] enhancement. This indicates an enhancement of oxygen over nitrogen in these regions, *i.e.* along the equatorial torus. Differences in the chemistries of polar and equatorial regions in nova shells have been suggested by Duerbeck & Seitter (1987). A combination of the [O II] and [O III] images shows a symmetric distribution of oxygen in the shell, whereas the distribution of nitrogen is asymmetric. Similar differences in the distribution of oxygen and nitrogen have been noticed in the shell of T Pyx also (Shara *et al.* 1989, see also §IV.3.1).

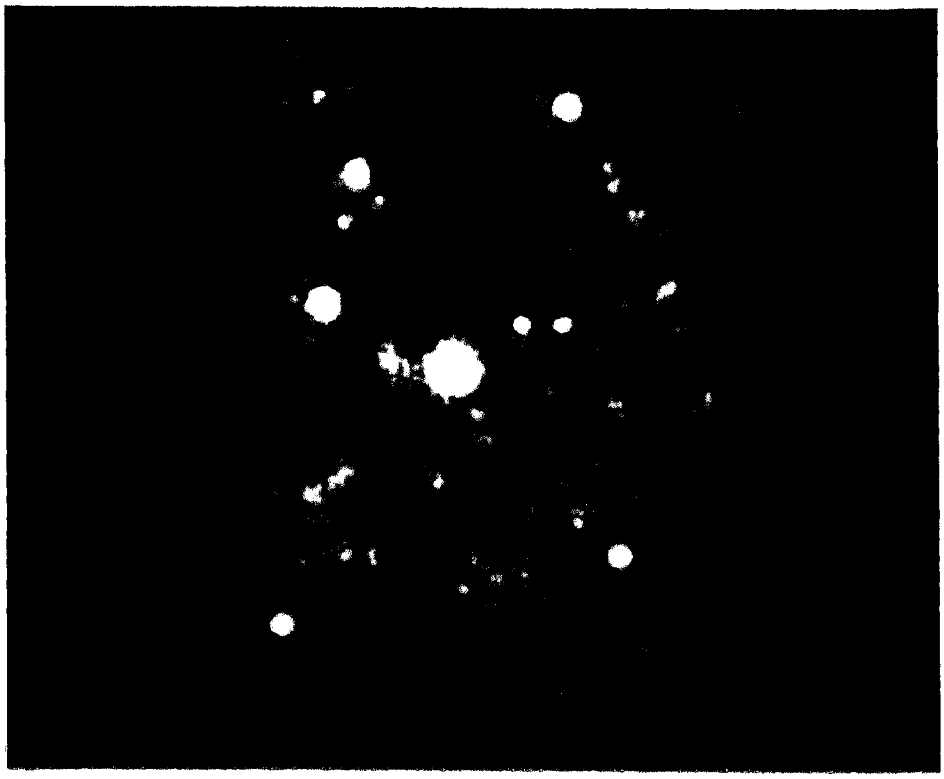

Fig. III.4.2 True colour image of GK Per shell. Red: [N II] emission; Green: [O III] emission. North is at the top and east to the left. Scale: 1 mm = 1.21 arcsec.

Comparison with the [N II] images published by Seaquist *et al.* (1989) indicate an expansion of the nebula. We have measured the proper motions (μ arcsec yr^{-1}) of about 60 individual knots in the [N II] image, by comparing our image with the 1984 August 19 image of Seaquist *et al.* (1989). Figure III.4.3 is the contour diagram of the [N II] image with the knots numbered. The measured proper motions and position angles of the knots are listed in Table III.4.2. Measurement of stars in the field give a measurement error 0.06 arcsec. The mean proper motion is 0.227 ± 0.104 arcsec yr^{-1}. The scatter in the proper motion is significantly larger than the measurement error. If we assume the knots to be distributed near the periphery of a spherical shell, the space velocity may be obtained as $v_{\rm sp} = \mu \cos\theta$, where θ is the angle subtended by the knot radius vector with the sky plane. The measured radial distance of the knot is $r = R\cos\theta$ where R is the radius of the spherical shell. The space velocity is thus given by

$$v_{\rm sp} = \mu \frac{R}{r}(4.75 D_{\rm pc}) \quad {\rm km\ s^{-1}} \qquad \text{(III.4.1)}$$

where the factor in parenthesis converts the proper motion in units of arcsec yr^{-1} to space velocity in units of km s^{-1}, $D_{\rm pc}$ being the distance to the nova in parsecs. The

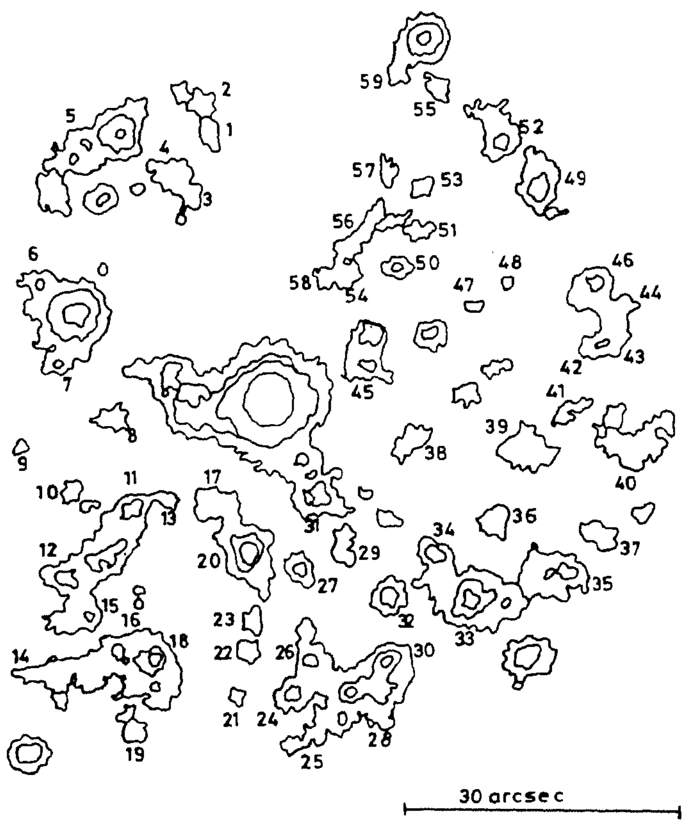

Fig. III.4.3 Contour diagram of [N II] image of GK Per shell. Knots for which proper motion is measured are marked. North is at the top and east to the left.

space velocities computed for the knots assuming a distance 470 pc and $R = 42.3$ arcsec are also listed in Table III.4.2. The mean space velocity is 500 ± 230 km s^{-1}.

Figure III.4.4 shows the distribution of proper motions as a function of position angle. There appears to be a bimodal distribution of velocities. The velocities are lower in the interaction zone (southwest) and also on the opposite side. These low velocity knots lie along the region of the polar cone identified by Bode *et al.* (1987) and Seaquist *et al.* (1989). The mean proper motion in the polar cone region is 0.173 ± 0.047 arcsec yr^{-1}. The velocity of the knots in sectors 60°–150° and 240°–300° is almost twice as high as the velocity of the knots in the interaction region. The high velocity knots coincide with the [O III] enhancement. From the published images of the shell, deceleration of the shell in the interaction zone is evident. If v_0 is the initial expansion velocity, the present velocity v is

$$v = v_0 - at \tag{III.4.2}$$

where a is the deceleration and t is the time elapsed since the outburst. The radius

Table III.4.2 Radius, position angle, proper motion and space velocity of bright [N II] knots in GK Per shell.

#	r arcsec	θ deg	μ arcsec yr^{-1}	v_{sp} km s^{-1}
1	32.02	15.0	0.263	587
2	34.19	15.5	0.217	484
3	24.42	25.0	0.136	304
4	27.68	26.0	0.147	328
5	34.73	39.0	0.100	223
6	29.14	67.5	0.370	826
7	24.15	84.0	0.170	380
8	17.64	101.0	0.176	393
9	28.76	104.0	0.281	627
10	24.96	118.0	0.176	393
11	20.08	131.5	0.255	569
12	31.20	133.0	0.228	509
13	16.55	137.0	0.198	442
14	41.52	141.0	0.314	701
15	32.02	142.0	0.159	355
16	33.10	151.5	0.240	536
17	13.57	155.0	0.105	234
18	32.02	158.0	0.131	292
19	40.70	159.5	0.157	351
20	17.35	174.0	0.155	346
21	33.92	175.0	0.216	482
22	28.22	176.5	0.134	299
23	24.96	177.5	0.045	100
24	33.10	186.0	0.186	415
25	36.90	191.0	0.159	355
26	29.30	191.0	0.188	420
27	19.54	192.5	0.162	362
28	33.65	198.0	0.176	393
29	18.99	207.0	0.224	500
30	12.21	208.0	0.231	516
31	32.29	210.0	0.107	239
32	25.78	214.0	0.134	299
33	31.20	223.0	0.228	509
34	25.51	230.0	0.193	431
35	37.99	242.5	0.347	775
36	28.49	244.5	0.339	757
37	39.07	250.5	0.428	956
38	17.09	260.0	0.160	357
39	28.49	262.0	0.338	755

Table III.4.2 Continued.

#	r arcsec	θ deg	μ arcsec yr^{-1}	v_{sp} km s^{-1}
40	40.59	265.5	0.426	951
41	32.83	271.0	0.324	723
42	36.36	283.0	0.381	851
43	39.07	283.0	0.479	1069
44	40.15	288.5	0.509	1136
45	11.67	291.0	0.119	226
46	38.53	293.0	0.440	982
47	24.96	297.0	0.309	693
48	29.58	299.0	0.236	527
49	38.53	311.5	0.281	627
50	20.62	318.0	0.138	308
51	25.51	321.0	0.219	489
52	39.07	321.0	0.297	663
53	29.58	327.0	0.159	355
54	16.28	329.0	0.152	339
55	40.16	333.5	0.300	670
56	19.27	334.0	0.141	315
57	29.03	334.0	0.141	315
58	15.20	335.0	0.045	100
59	40.43	341.0	0.136	304

of the shell is

$$r = v_0 t - \frac{1}{2}at^2. \tag{III.4.3}$$

From the above equations the deceleration may be obtained as

$$a = \frac{2}{t}(\frac{r}{t} - v). \tag{III.4.4}$$

Using the above equations and the measured velocities, a deceleration of 1.5 km s^{-1} yr^{-1} and an initial velocity of 1100 km s^{-1} is obtained for the high velocity system. In the direction of the southwest interaction zone, a deceleration of 12.8 km s^{-1} yr^{-1} and an initial velocity of 1500 km s^{-1} are obtained. The initial velocity of 1100 km s^{-1} obtained for the high velocity systems, which lie along the equatorial torus, is similar to the spectroscopic expansion velocity of 1200 km s^{-1} observed during outburst (McLaughlin 1960). The initial velocity in the polar region is however much higher. The initial and final velocities in the polar region agree with the energy conserving expansion model derived by Seaquist *et al.* (1989).

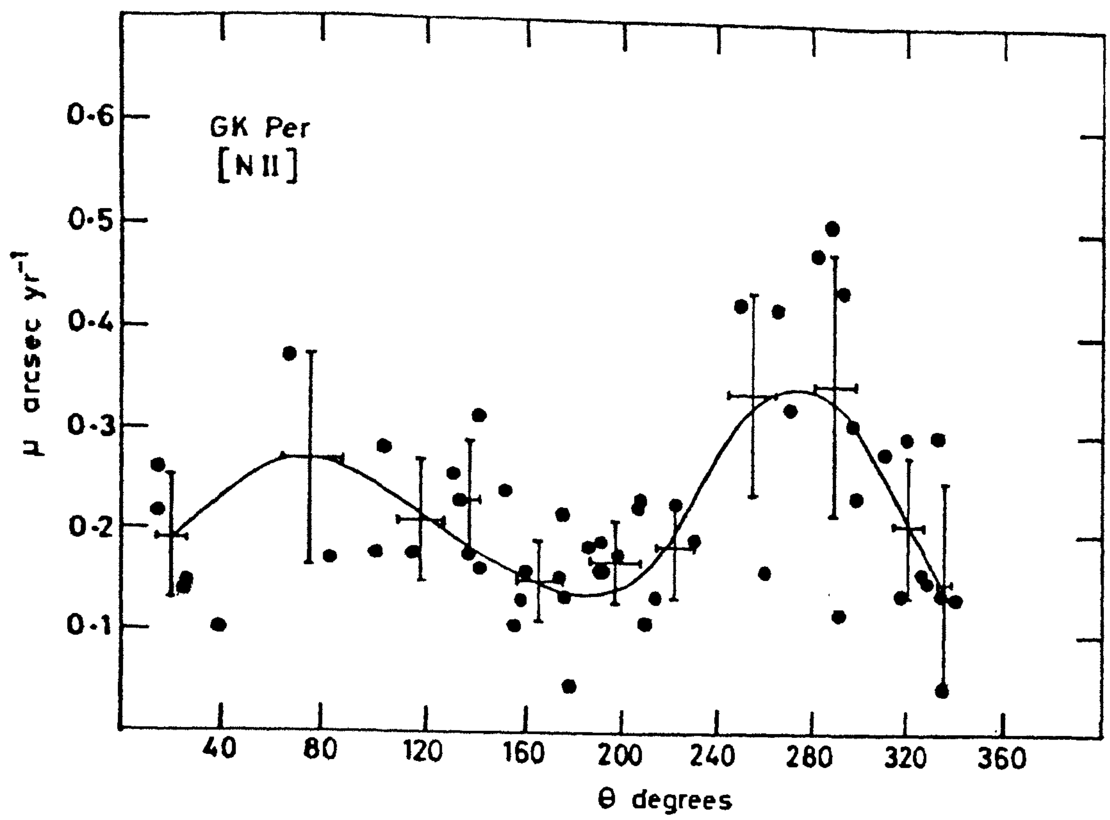

Fig. III.4.4 Proper motion of the knots in the shell of GK Per as a function of position angle. The polar cone region is between 150°–220° and 330°–40°

4.2 The Optical Spectrum

The optical spectrum of GK Per contains strong emission lines of H, He I and He II from the accretion disc around the primary (Gallagher & Oinas 1974). Ca II 3934 Å is also weakly present in emission. Absorption features due to the secondary are also present. Na I D and Ca I 4227 Å are the strongest absorption features; a majority of the absorption lines are due to Fe I. Lines of Cr I, Ti I and Mg I are also present (Kraft 1964; Gallagher & Oinas 1974). Based on the Ca I 4227 Å equivalent width, and the strength of the absorption lines, Gallagher & Oinas (1974) assign a spectral type K2 V-IV for the secondary, in agreement with Kraft (1964). Crampton, Cowley & Fisher (1986) classify the secondary as K0IV. The secondary is estimated to contribute about 33 percent to the total light in the blue (Gallagher & Oinas 1974; Crampton, Cowley & Fisher 1986).

Table III.4.3 GK Persei: Journal of spectroscopic observations.

Date UT		Wavelength range Å
1989 Nov	25.75	4400–7600
	25.78	4400–7600
1989 Dec	4.79	6100–9200
	4.82	6100–9200
1989 Dec	31.79	4400–7600
	31.83	4400–7600
1990 Jan	2.68	4400–7600
	2.70	4400–7600
1990 Jan	15.59	4400–7600
	15.62	4400–7600
	15.64	4400–7600
	15.68	4400–7600
1990 Jan	16.58	6100–9200
	16.60	6100–9200
	16.63	6100–9200
	16.67	6100–9200
1990 Feb	21.64	4400–7600
	21.66	4400–7600

Observations

Spectra of GK Per in the region 4500–7600 Å and 6100–9200 Å were obtained during 1989 November 25–1990 February 21 using the 102 cm telescope at VBO. Spectra were recorded at 5.5 Å per pixel resolution at the Cassegrain focus using the Photometrics CCD system + 250 mm camera + UAG spectrograph. Table III.4.3 gives the details of observations.

The spectrum frames were individually de-biased and flat-fielded and the one-dimensional spectrum extracted following the procedure in Chapter II. Night sky emission lines were removed. Fe+Ne comparison spectrum was used for wavelength calibration. Spectrophotometric standards HD 217086, HD 19445, HD 60778, Feige 15 and EG 99 were used for flux calibration. The flux calibrated spectra were averaged to improve signal-to-noise ratio. Spectra in the two regions were combined and the mean spectrum was corrected for interstellar reddening using $E(B-V) = 0.3$ (Wu *et al.* 1989) and the Savage & Mathis (1979) law.

Spectrum

Figure III.4.5 shows the mean, dereddened spectrum in wavelength region 4500–9200 Å. The spectrum is composite consisting of strong emission lines — Hβ, Hα,

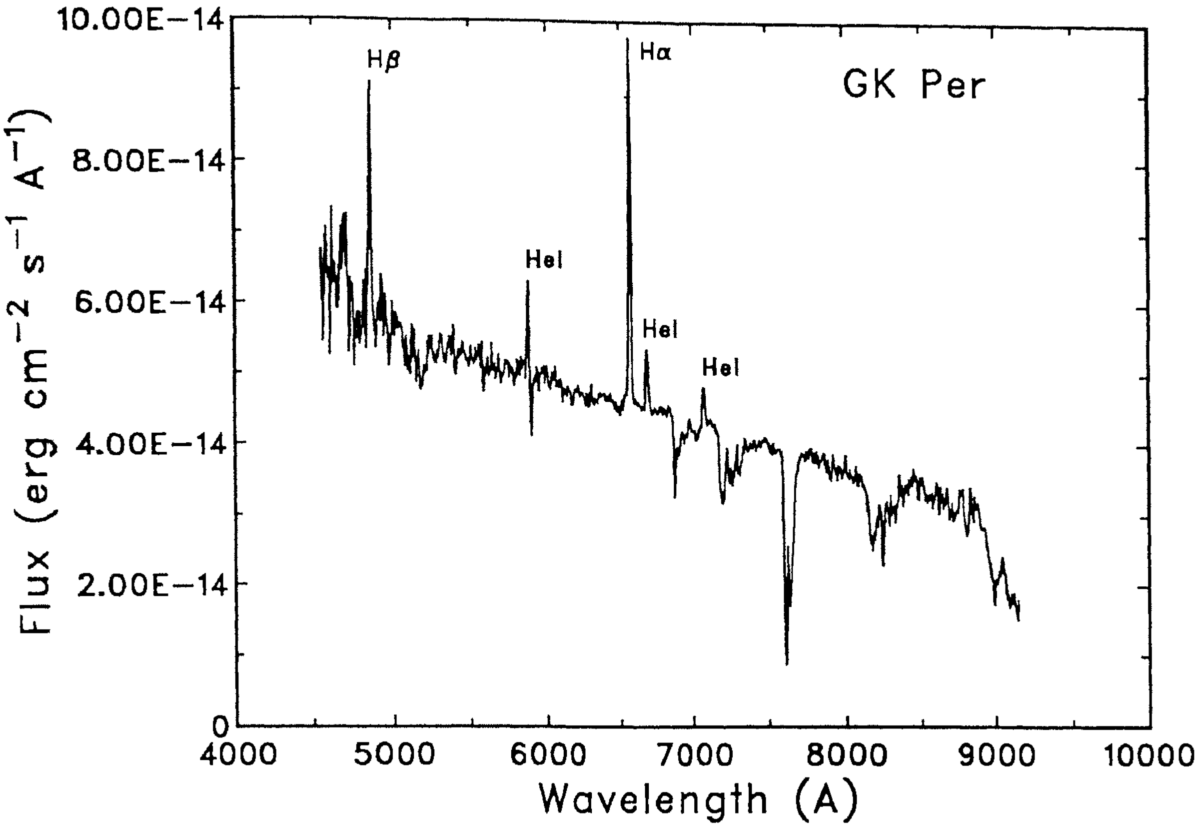

Fig. III.4.5 Quiescent spectrum of GK Per in the region 4500–9200 Å, corrected for $E(B-V)$ = 0.3. Epoch: 1989 November 25–1990 February 21.

He I 5876, 6678, 7065 Å — over a blue continuum. He II 4686 Å and He I 7281 Å are weakly present. Na I D absorption is strong. The strong blue continuum and emission lines arise in the accretion disc around the white dwarf primary. Table III.4.4 lists the emission line fluxes corrected for reddening.

The Balmer decrement is flat with Hα/Hβ $\sim$ 1.9, indicating high densities in the emitting medium. In the models of Drake & Ulrich (1980) such a ratio is reproduced for $T_e \gtrsim 10^4$ K, $n_e \gtrsim 10^{12}$ cm^{-3} and $\tau_{\mathrm{Ly}\alpha} \gtrsim 10^4$. An estimate of He abundance and the Zanstra temperature of the central ionizing source may be obtained using the He I, He II and hydrogen line fluxes.

The observed He I 5876/7065 = 1.9 ratio is reproduced for $n_e \approx 10^{12}$ cm^{-3}, $T_e = 10^4$ K and low values of $\tau(3889)$ in the models of Almog & Netzer (1989). Using the observed line ratios of He I 5876/Hβ, 5876/Hα, He I 7065/Hβ, 7065/Hα an estimate of He^+/H^+ is made. The emissivities for He I lines are from Almog & Netzer (1989) for $n_e = 10^{12}$ cm^{-3}, $T_e = 10^4$ K and $\tau(3889) = 3.8$. Hα and

Table III.4.4 GK Persei: Emission line fluxes corected for $E(B-V) = 0.3$.

Line identification λ in Å		Flux 10^{-13} erg cm^{-2} s^{-1}
4686	He II	1.06:
4861	Hβ	2.58
5876	He I	1.19
6563	Hα	4.87
6678	He I	1.00
7065	He I	0.63
7281	He I	0.20

Hβ emissivities from Hummer & Storey (1989) for $n_e = 10^{10}$ cm^{-3} have been used, since hydrogen emissivities for $n_e > 10^{10}$ cm^{-3} have not been calculated. An average $\langle He^+/H^+ \rangle = 0.204 \pm 0.031$ is estimated. Taking emissivities for He II 4686 Å from Hummer & Storey (1989), $He^{++}/H^+ = 0.036$ is obtained. The derived helium abundance is He/H $= 0.24 \pm 0.02$.

In the models of Drake & Ulrich (1980), the Hβ emissivity drops steeply from 7.02×10^{-25} erg cm^3 s^{-1} at $T_e = 10^4$, $n_e = 10^{12}$, $\tau_{\mathrm{Ly}\alpha} = 10^4$ through 0.019×10^{-25} erg cm^3 s^{-1} at $T_e = 2 \times 10^4$, $n_e = 10^{12}$, $\tau_{\mathrm{Ly}\alpha} = 10^6$ to 0.005×10^{-25} erg cm^3 s^{-1} at $T_e = 2 \times 10^4$, $n_e = 10^{15}$, $\tau_{\mathrm{Ly}\alpha} = 10^6$. It thus appears that the above estimate of helium abundance is an upper limit. As an example, using emissivities from Drake & Ulrich (1980) for $n_e = 10^{12}$ cm^{-3}, $T_e = 1.5 \times 10^4$ K, $\tau_{\mathrm{Ly}\alpha} = 3.5 \times 10^4$, the helium abundance would be reduced to ~ 0.1.

For $T_e = 10^4$ K, $n_e = 10^{10}$ cm^{-3}, using the observed ratio of He II 4686/Hβ, the temperature of the ionizing source is estimated from Equation III.1.12 to be $T_s = 1.3 \times 10^5$ K. This estimate of temperature and the observed Hβ luminosity imply a radius $R_s \sim 0.01\ R_\odot$ for the ionizing source (from Equation III.1.14).

Gallagher & Oinas (1974) estimate the secondary contributes only 33 percent to the total light in the blue. The total observed spectrum is thus a combination of the accretion disc spectrum and the secondary spectrum. Using standard fluxes for a K1IV star from O'Connell (1973), and assuming the spectrum to be of the form given in Equation III.1.21, an estimate of the accretion disc spectrum has been made. The standard K1IV fluxes were scaled to match the observed spectrum at $\lambda \sim 9000$ Å and subtracted from the observed spectrum. A suitably scaled theoretical disc spectrum of the form given by Equation III.1.20 was then fit to the

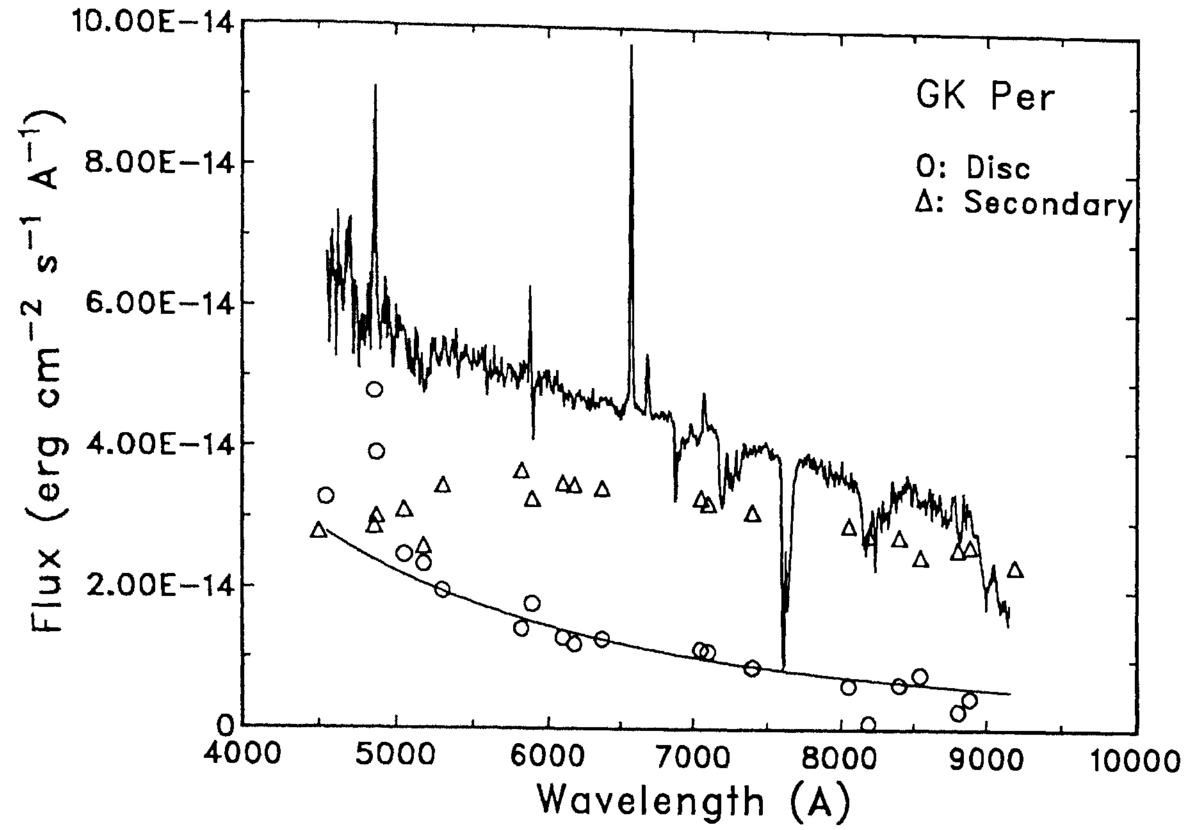

Fig. III.4.6 The quiescent spectrum of GK Persei decomposed into the K1IV secondary, and the accretion disc spectrum.

residual flux. The contribution from the individual components were estimated by an iterative determination of the constants A and B in Equation III.1.21 such that their total matches the observed flux within 10 percent. The best fit accretion disc spectrum was estimated as $f_\lambda = 10^{-5.02}\lambda^{-2.33}$ erg cm^{-2} s^{-1} Å^{-1}. Figure III.4.6 shows the decomposition of the observed spectrum into the secondary and accretion disc components.

The dereddened continuum flux of the secondary at 5500 Å, $f_{5500} = 3.4 \times 10^{-14}$ erg cm^{-2} s^{-1} Å^{-1}, corresponds to an absolute magnitude $M_V = +4.24$, at a distance of 470 pc, consistent with the K0-2IV estimates for the secondary (Crampton, Cowley & Fisher 1986; Warner 1976; Gallagher & Oinas 1974). The estimated disc spectrum implies $M_V = +4.93$ for the accretion disc, at a distance of 470 pc. With the above estimate of the accretion disc spectrum, the secondary contributes 40 percent of the total flux at 4400 Å.

The ultraviolet–optical spectrum of the disc in GK Per is found to have a maximum at 3000 Å (Bianchini & Sabbadin 1983; Wu *et al.* 1989). The fall in the disc spectrum at wavelengths below 3000 Å has been attributed to a disruption of the inner regions of accretion disc close to the white dwarf by the white dwarf's magnetic field. From the estimate of M_V for the accretion disc and Equation III.1.22, a mass transfer rate $\dot{M} = 2 \times 10^{-10}$ $M_\odot$ yr^{-1} is estimated. Using the above estimates of $\dot{M}$, $M_{\rm WD} \sim 1$ $M_\odot$, and the models of Beall *et al.* (1984) for the accretion disc flux distribution, the fall in the spectrum shortwards of 3000 Å is reproduced for an inner radius $R_i \sim 10^9$ cm. These values may be compared with $\dot{M} = 3 \times 10^{-10}$ $M_\odot$ yr^{-1} and $R_i = 1.2 \times 10^9$ cm derived by Bianchini & Sabbadin (1983) by fitting a model to the ultraviolet and *UBV* fluxes.

4.3 Summary

Optical CCD images of the nebular shell of GK Per in [N II] and [O III] emission lines are presented. The shell is clumpy and asymmetric. In [N II], it is flattened in the southwest and northeast directions. The bulk of the emission arises from the southwest quadrant, coincident with the radio emitting ridge observed by Seaquist *et al.* (1989). This implies the remnant is interacting with the interstellar medium in that region. The knots in [N II] and [O III] generally coincide in all regions except the radio ridge region. This difference has been attributed to spatial variations in the physical conditions of the knots (Duerbeck & Seitter 1987; Seaquist *et al.* 1989). An enhancement of [O III] emission over [N II] is seen along position angles 132° and 295°. This [O III] enhancement is along the direction of H I emission and the IR torus. A comparison of the published [O II] images (Seaquist *et al.* 1989) shows that the knots in [O II] emission generally coincide with the [N II] emission. There is however an enhancement of [O II] emission along the direction of [O III] enhancement, indicating an enhancement of oxygen over nitrogen along the equatorial torus. A combination of [O III] and [O II] images show a symmetric distribution of oxygen in shell, whereas the distribution of nitrogen is asymmetric.

Proper motion measurements of the knots in [N II] give a mean expansion rate of 0.227 ± 0.104 arcsec yr^{-1}. A bimodal distribution of velocities is seen, with the velocities being lower in the southwest interaction zone and also in the northeast. These low velocity knots lie along the polar cone identified by Bode *et al.* (1987) and Seaquist *et al.* (1989). The high velocity knots lie in sectors 60°–150° and 240°–300° along the equatorial torus. The measured velocities indicate a deceleration of 1.5 km s^{-1} yr^{-1} and an initial velocity of 1100 km s^{-1} for the high velocity system, similar to the spectroscopically determined outburst expansion velocity of 1200 km s^{-1} (McLaughlin 1960). In the direction of the southwest interaction zone, a deceleration of 12.8 km s^{-1} yr^{-1} and an initial velocity of 1500 km s^{-1} is obtained, indicating a higher initial velocity in the polar region. The initial and final velocities obtained for the interaction zone are consistent with the energy conserving model of Seaquist *et al.* (1989).

The optical quiescence spectrum of GK Per central system is also presented. The spectrum is composite consisting of hydrogen and helium emission lines superposed over the absorption spectrum from the secondary. The emission lines arise in the accretion disc around the white dwarf primary. The Hα/Hβ ratio of ~ 1.9 and also the observed He I line ratios indicate high densities $\sim 10^{12}$ cm^{-3} and $T_e \geq 10^4$ K. Using the He II 4686/Hβ line ratio, a temperature 1.3×10^5 K is obtained for the accretion disc ionizing source. The observed $H\beta$ luminosity together with this estimate of temperature imply a white dwarf of radius 0.01 $R_\odot$. A helium abundance He/H $\leq 0.24 \pm 0.02$ in the accretion disc has been estimated. Assuming an optically thick, steady disc, a spectrum of the form $f_\lambda = 10^{-5.02}\lambda^{-2.33}$ erg cm^{-2} s^{-1} Å^{-1} is estimated for the accretion disc. The estimated $M_V = +4.93$ for the disc, at a distance of 470 pc implies a mass transfer rate of $\dot{M} = 2 \times 10^{-10}$ $M_\odot$ yr^{-1}. The ultraviolet–optical spectrum of the accretion disc shows a maximum at 3000 Å (Bianchini & Sabbadin 1983; Wu *et al.* 1989); the fall in the flux at wavelengths below 3000 Å being caused by a disruption of the inner regions of the accretion disc close to the white dwarf by its magnetic field. For a white dwarf with mass ~ 1 $M_\odot$ and mass transfer rate as estimated, a disc with inner radius $R_i \sim 10^9$ cm reproduces the observed fall in the disc spectrum shortwards of 3000 Å.

IV. Recurrent Novae

The recurrent novae constitute a small group of objects which are intermediate between classical novae and dwarf novae in terms of their recurrence timescales ($\sim$ 10–80 years) and magnitude ranges in outburst ($\sim$ 7–11 mag). Their speed class designations span the range from slow (T Pyx) to very fast (*e.g.* U Sco, V394 CrA, T CrB). Recurrent novae are cataclysmic variables satisfying the following criteria (Webbink *et al.* 1987): (i) two or more distinct recorded outbursts, reaching absolute magnitude at maximum comparable with those of classical novae and (ii) ejection of a discrete shell in outburst, at velocities comparable with those of classical novae ($V_{\rm exp} \gtrsim 300$ km s^{-1}). Based on this definition, seven objects are recognized as recurrent novae — T Pyx, U Sco, V394 CrA, T CrB, RS Oph, V745 Sco and V3890 Sgr.

A recurrent nova outburst could either be an accretion powered event as in the case of dwarf novae or, a consequence of thermonuclear runaway as in the case of classical novae. The success of thermonuclear runaway in explaining classical nova outbursts suggests the possibility that a similar mechanism might be operating in recurrent novae. The basic problem to be solved in the context of recurrent novae is that of the recurrence timescales $\tau_{\rm rec}$, which are much shorter in recurrent novae. The most important parameters determining $\tau_{\rm rec}$ are the white dwarf mass and the accretion rate (Starrfield 1989; Webbink *et al.* 1987; Livio 1988). In order to obtain the recurrence times observed in recurrent novae, accretion rates greater than 10^{-8} $M_\odot$ yr^{-1} are required. Also, the white dwarf must be massive (Starrfield, Sparks & Truran 1985; Webbink *et al.* 1987; Livio 1988). Starrfield, Sparks & Truran (1985), Starrfield, Sparks & Shaviv (1989) and Kato (1990a) have been able to reproduce the outburst of U Sco using thermonuclear runaway models for accretion rates $\sim 10^{-7}$–10^{-6} $M_\odot$ yr^{-1} on white dwarfs of mass $M_{\rm WD} \geq 1.3$ $M_\odot$. Webbink *et al.* (1987), Livio (1988) and Kato (1990b) have shown that the outbursts of T Pyx also can be explained as a consequence of thermonuclear runaway on the surface of a massive white dwarf: $M_{\rm WD} \sim 1.3$–1.37 $M_\odot$.

Accretion powered outbursts can occur in three different ways: (i) an instability associated with the mass losing component, causing bursts of mass transfer; (ii) an instability in the disc; (iii) a time dependent accretion rate modulated by orbital eccentricity. However, all these mechanisms suffer from large uncertainties, making their predictive power uncertain (Livio 1988). Webbink (1976) and Livio, Truran

& Webbink (1986) have suggested that the outbursts of T CrB and RS Oph are accretion powered events. The models are essentially identical and involve the episodical transfer of a chunk of matter of $\Delta M \sim 10^{-4}$–10^{-3} $M_\odot$ from the red giant onto an accreting main sequence star. The differences in the outburst light curves of these two systems, according to Livio, Truran & Webbink (1987) arise simply because of the difference in the evolutionary status of the accreting star. In RS Oph, the main sequence accretor is assumed to be in a bloated configuration as a consequence of higher, effective accretion rate and a larger total accreted mass. The accretion stream hence strikes the stellar surface directly resulting in a single outburst. In T CrB, the stream passes around the accreting star, either skimming its surface or colliding with itself and circularizing, giving rise to the first maximum. A disc is formed and the subsequent decay of this disc produces the second maximum.

Observations of RS Oph during its 1985 outburst and subsequent quiescence do not show any evidence for the presence of a bloated main sequence accretor. The observations are, however, consistent with a white dwarf accretor (see §IV.1). Shaviv & Starrfield (1988) have shown that episodic mass transfer onto a bloated main sequence star cannot explain the outburst of RS Oph. M. Kato (1990; preprint) has recently been able to theoretically reproduce the outburst ultraviolet and optical light curves using an optically thick wind method based on the thermonuclear runaway model. The light curves are reproduced for a white dwarf mass of 1.36–1.37 $M_\odot$, with hydrogen abundance 0.52–0.6. Based on IUE observations of T CrB, Cassatella & Selvelli (1988) and Selvelli (1989) conclude that the primary in T CrB is an accreting white dwarf rather than a main sequence star. It is hence possible that the outbursts of RS Oph and T CrB are also a consequence of thermonuclear runaways on massive white dwarfs.

Based on their observational properties, the recurrent novae may be subclassified (Webbink 1989) as follows:

T Pyx class: T Pyxidis is the only known member of this class. It is characterized by slow outburst timescales, with a faithful repetition of the light curve at each outburst and an emission line spectrum at maximum. The system is extremely blue at minimum, has a short orbital period, high mass transfer rates and is located far from the galactic plane. Outbursts are powered by thermonuclear runaway on an extremely massive white dwarf.

U Sco class: This class consists of two members: U Scorpii and V394 Coronae Austrinae. The outburst light curves of these objects decline at an extremely fast rate: $t_3 \sim 5$ days. Modest light curve variations from outburst to outburst have been detected. During outbursts, matter is ejected at very high velocities. There is an under-abundance of hydrogen in these systems. In both outburst and quiescent spectra, helium lines are much stronger than hydrogen lines: N(He)/N(H)~ 2 (twenty times solar) in U Sco. The white dwarf could hence be a helium white dwarf. The secondary is of spectral type G3-6 III in U Sco and K in V394 CrA. Both these systems are at very large distances and far from the galactic plane. Thermonuclear runaway on massive white dwarf is the outburst mechanism.

T CrB class: T Coronae Borealis, RS Ophiuchi, V745 Scorpii and V3890 Sagittarii constitute this subgroup. These objects also have a fast rate of decline during outburst. The outburst light curves repeat faithfully. The outburst ejection velocities are initially very high ~ 4000 km s^{-1} and decrease with time. Intense high excitation coronal lines develop in the outburst spectrum during decline from maximum. These are long period binary systems consisting of an M giant secondary. The secondary in T CrB is M3-4 III, M0-2 III in RS Oph (see §IV.1 and IV.2), and M6III in V745 Sco (Duerbeck & Seitter 1989; Sekiguchi *et al.* 1990). Outburst mechanism is either accretion powered on a main sequence accretor or due to thermonuclear runaway on a massive white dwarf.

In this study we discuss three of the seven known recurrent novae — RS Oph, T CrB and T Pyx. Our discussions are based mainly on the data obtained from VBO. The methods employed are similar to the ones for classical novae and have already been discussed in §III.1. The exception is with the coronal lines, and these are discussed in §IV.1.1.3 on RS Oph.

1. RS Ophiuchi

The recurrent nova RS Ophiuchi has had five recorded outbursts in 1898, 1933, 1958, 1967 and 1985. The nova reaches an outburst magnitude of $m_v \sim 5$ from its mean quiescence magnitude of $m_v \sim 11.5$. It has a rate-of-decline of $t_3 \sim 18$ days and is classified among fast novae. The optical light curve and spectrum are remarkably similar during all outbursts (Rosino 1987). Detailed spectroscopic observations in the optical region exist for the 1933 (see Payne-Gaposchkin 1957) and 1958 (*e.g.* Dufay *et al.* 1964) outbursts. A wealth of information was brought in during the 1985 outburst. The outburst provided for the first time an opportunity for the study of a recurrent nova at all wavelengths: radio, infrared, optical, ultraviolet and x-ray.

A comprehensive discussion of the preliminary results of the 1985 outburst is given by Bode (1987).

Using the M_v–t_3 relation for classical novae, Pottasch (1967) arrived at a distance of 5.8 kpc. However, he did not consider the interstellar reddening towards RS Oph. The flux ratio of He II 1640 Å and 3203 Å estimated from IUE spectra obtained during the 1985 outburst yields an interstellar reddening of $E(B-V) = 0.73$ (Cassatella *et al.* 1985). Applying this extinction to the estimate by Pottasch would reduce the distance to 2 kpc. Duerbeck (1981) quotes a distance of 1.8 kpc. The 21cm H I absorption measurement (Hjellming *et al.* 1986) gives a column density of $(2.4 \pm 0.6) \times 10^{21}$ H atoms cm^{-2} to RS Oph. This, compared to that for a neighbouring, more distant source gives a distance 1.6 kpc to RS Oph. It is interesting to note here that Payne-Gaposchkin (1957) derived a distance of 1.7 kpc based on the M_v–t_3 relation, with a rather uncertain estimate for the interstellar extinction.

The optical spectrum of RS Oph during outbursts is characterized by strong emission in coronal lines. The coronal lines arise in the gas which is shock-heated as the ejected envelope expands supersonically into the circumstellar matter accumulated through steady stellar wind (Gorbatskii 1972, 1973). The shock-heated region also emits synchrotron radiation in the radio region (Hjellming *et al.* 1986), and thermal radiation in soft x-rays (Mason *et al.* 1987). The theoretical model of the envelope proposed by Bode & Kahn (1985) is similar in many respects to that of supernovae, but has much shorter timescales. Coronal as well as other high excitation lines, radio, and x-ray emissions reach a peak at about 60 days from the outburst and then decline. After about 100 days since outburst, a remnant radio and x-ray source is still present, which probably represents the hot component.

The VLA as well as VLBI (Hjellming *et al.* 1986; Taylor *et al.* 1989) sizes imply an average expansion rate (rate of change of total size) of 0.0026–0.0030 arcsec per day, or expansion velocities of $\sim$ 4000 km s^{-1} at a distance of 1.6 kpc. Initial velocities of this order are also apparent in the optical and ultraviolet lines (Rosino & Iijima 1987; Snijders 1987). The VLBI structure consists of a central component of size 0.06 arcsec, and fainter extension to ± 100 milliarcsec in east-west direction, the thickness ranging from 10–30 milliarcsec.

Infrared photometric and spectroscopic data have been used by Evans *et al.* (1988) to conclude that the remnant consisted of four components: the outer region at 2×10^4 K represents unshocked stellar wind; the two middle regions at $\sim 10^5$ K contain the shocked stellar wind and ejecta; the inner region at 2×10^4 K contains unshocked stellar ejecta. Evans *et al.* also conclude that an additional source of infrared radiation, possibly a bright spot on the accretion disc, was present prior to outburst, vanished soon afterwards, and reappeared subsequently. The middle shocked regions are expected to contain still hotter material that does not contribute to the infrared radiation, but manifests itself through radio, x-ray and coronal emission.

RS Oph developed intrinsic linear polarization between days 20 and 80 following the outburst (Cropper 1990). By day $\sim$ 500 the polarization dropped to its pre-outburst level, which is mostly interstellar. Intrinsic polarization of 0.62% at 76° position angle was detected during days 80–114. This position angle is in agreement with that of the radio jets ($\sim$ 84°) at 1.7 GHz detected by Porcas, Davis & Graham (1987).

The visual maximum of RS Oph during the 1985 outburst appears to lie between the discovery on 1985 January 26 and the next observation on January 28. Following Rosino & Iijima (1987), 1985 January 27.5 has been assumed as the day of maximum.

RS Oph is an interacting binary system. The cool component is a giant of spectral type M0–M2 (Sanduleak & Stephenson 1973; Barbon, Mammano & Rosino 1968; Rosino, Bianchini & Rafanelli 1982; Bruch 1986). Duerbeck & Seitter (1989) determine the spectral type as K5–K7. Evans *et al.* (1988) determine K8$\pm$2 as the spectral type based on their CO measurememts, whereas Kenyon & Fernandez-Castro (1987) classify it as K5.7 I-II. The nature of the hot component is, however, more uncertain. Livio, Truran & Webbink (1986) suggest the hot component to be a bloated main sequence star, with episodic mass transfer event onto this star as the cause of outburst. Observations of the 1985 outburst however, show no evidence for the presence of a bloated main sequence star. Alternatively, the hot component is a white dwarf with thermonuclear runaway on the surface of this accreting white dwarf as the cause of the outburst. For thermonuclear runaway models to give the short recurrence time between outbursts as seen in RS Oph, the accretion rate must be high. Also, the accreting star has to be a high mass white dwarf. Indirect evidence for the existence of a white dwarf primary in RS Oph comes from the 1985 October EXOSAT observations, and the remnant radio emission detected about 100 days after the outburst. Hjellming *et al.* (1986) suggest the radio emission is of gyrosynchrotron origin as in magnetic cataclysmic variables. The remnant x-ray radiation implies a temperature of 3.5×10^5 K and a luminosity of 10^{37} erg s^{-1}

(Mason *et al.* 1987). The inferred blackbody radius of 10^9 cm is comparable to that of a white dwarf. Further evidence for thermonuclear runaway on a white dwarf is the sustained bolometric luminosity plateau lasting over 57 days from outburst (Snijders 1987; Bode 1987), similar to that seen in a classical nova outburst, where thermonuclear runaway on a white dwarf is the generally accepted cause of outburst.

The radius and temperature of the central ionizing source, as inferred from the VBO observations (§IV.1.1.2; also Anupama & Prabhu 1989) are comparable to that of a white dwarf during late stages of the outburst.

An orbital period of 230 days has been determined by Garcia (1986). The mass function has been derived as $q = 0.017\ M_\odot$. Assuming M0III spectral type for the secondary with a typical radius $R_2 \sim 50\ R_\odot$ and taking $M_s = M_2 = .1\ M_\odot$, Garcia (1986) finds $\sin i = 0.41$, $a = 196\ R_\odot$ and $r(q) = 74\ R_\odot$, where a is the separation between the two components and $r(q)$ is the Roche radius of the secondary. It is thus seen that the secondary fills its Roche lobe substantially. Based on his estimated absolute magnitude $M_V = -0.65$ mag and spectral type M2III for the secondary, with a bolometric correction -1.6 mag and $T_{\rm eff} = 3620$K appropriate for an M2III star, Bruch (1986) estimates $R_2 = 63 \pm 14\ R_\odot$, indicating a Roche lobe filling giant. A Roche lobe filling secondary implies a mass $\leq 1\ M_\odot$ (Bruch 1986) since the secondary will not fill its Roche lobe for mass much greater than $1\ M_\odot$. If the primary is a white dwarf, then the Chandrasekhar limit to the white dwarf mass limits the orbital inclination to $\geq 30°$ (Bruch 1986). However, the inclination cannot be greater than 70° since no eclipses have been observed in RS Oph.

Results based on spectroscopic observations from VBO, between days 32 and 108 since the 1985 outburst maximum are presented here. Also presented are the results based on spectra obtained during the years 1986–1990 in its post-outburst quiescence phase.

1.1 The 1985 Outburst

1.1.1 Spectroscopic Data

Observations and data reduction

Post-maximum spectra in the range 4300–8900 Å were recorded between 1985 February 27 and May 15, using the 102 cm reflector at VBO and the Cassegrain spectrograph equipped with the Varo image-intensifier. The dispersions of the spectra are 194 and 132 Å mm^{-1}. All spectra were recorded on Kodak IIaD plates, and calibrated using the auxiliary calibration spectrograph. Spectrophotometric

Table IV.1.1 RS Oph: Journal of 1985 outburst observations.

UT 1985		Wavelength range Å	Dispersion Å mm^{-1}
Feb	27.99	6300–8900	194
Mar	27.89	6300–8900	194
	27.93	6300–8900	194
	27.97	6300–8900	194
Mar	28.89	4300–5600	132
	28.95	4300–5600	132
	28.99	4300–5600	132
Apr	26.96	6300–8900	194
Apr	28.86	5700–8000	194
	28.99	6300–8900	194
May	15.87	6300–8900	194
	15.94	5700–8000	194

standards 57 Ser, ι Vir and γ Gem were used for flux calibration. Table IV.1.1 gives the details of observations made during the outburst.

The spectrograms were digitized at 3–5 μm intervals using 7.5–10 μm wide apertures on the PDS 1010M microdensitometer at IIA. Reductions were carried out following the procedure described in Chapter II. Photographic grain noise was filtered using a low-pass filter (cut-off = 15 cycles mm^{-1}) in Fourier space. Wavelength scale was determined using a Fe+Ne comparison source spectrum. All spectra were corrected for the atmospheric absorption features and flux calibrated. SAAO *BVRI* photometric observations (P. Whitelock 1988, personal communication; Evans *et al.* 1988) were used for absolute flux calibration.

Data at the spectrum ends are generally noisy and affected by image-tube distortions, rendering instrumental response correction in these areas uncertain. The derived fluxes of the emission lines have an overall error of 20%, with larger errors at the ends and for weak features. The Hα emission is overexposed on some plates, particularly so on 1985 April 28.99. An average value of the fluxes is taken for each epoch with less weightage given to the overexposed lines. Wavelength calibration in the region 4300–4800 Å is inaccurate due to underexposure of comparison lines in that region. Line identifications have, however, been made by comparing our spectrum with that of Rosino & Iijima (1987). The region around Hγ is noisy and poorly resolved due to image-tube distortion. Instrumental response was unsatisfactory in a few cases and the fluxes in these instances are not used in the analysis.

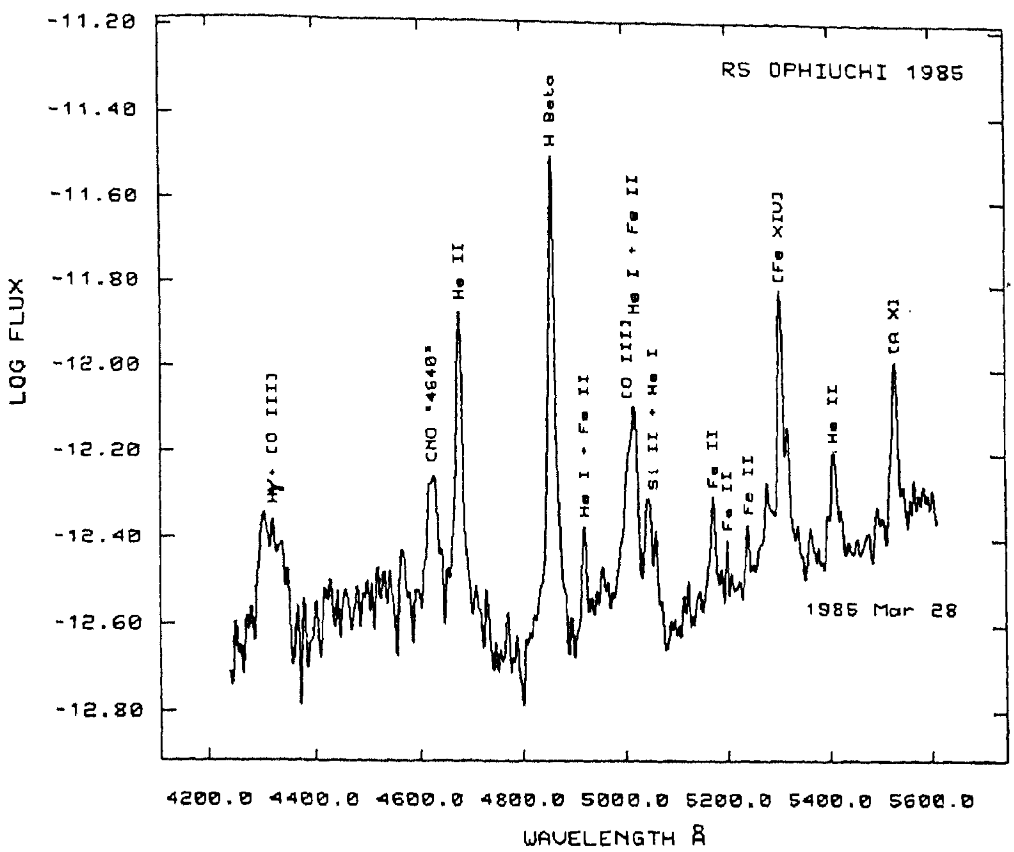

Fig. IV.1.1 Spectrum of RS Oph on day 60 in the range 4200–5600 Å. Flux is in units of erg cm^{-2} s^{-1} Å^{-1}

Description of spectra

Spectroscopic observations of RS Oph were made at phases (i) 32 days after maximum when the nova had declined to $V \sim 8.8$, (ii) 59 and 60 days after maximum at $V \sim 9.8$, (iii) 89 and 91 days after maximum at $V \sim 10.5$, and (iv) 108 days after maximum at $V \sim 10.9$. The spectra are shown in Figures IV.1.1–IV.1.3. Tables IV.1.2 and IV.1.3 list the line fluxes at each phase. Line identifications have been made based on the identifications of Dufay *et al.* (1964), Rosino & Iijima (1987), Wallerstein & Garnavich (1986), and using the catalogue of Meinel, Aveni & Stockton (1975). In the following, spectra at each phase is described.

Phase 32 (1985 February 27): The spectrum is characterized by strong, broad emission lines. The prominent lines are Hα, He I 6678, 7065, 7281 Å; O I 7774 and 8446 Å, the latter very much stronger than the former. He II 7593 Å is also present. The coronal lines [Fe X] 6374 Å and [Fe XI] 7892 Å are fairly strong, whereas [A XI] 6919 Å is barely visible. Paschen lines P_{11} 8862 Å and P_{12} 8750 Å

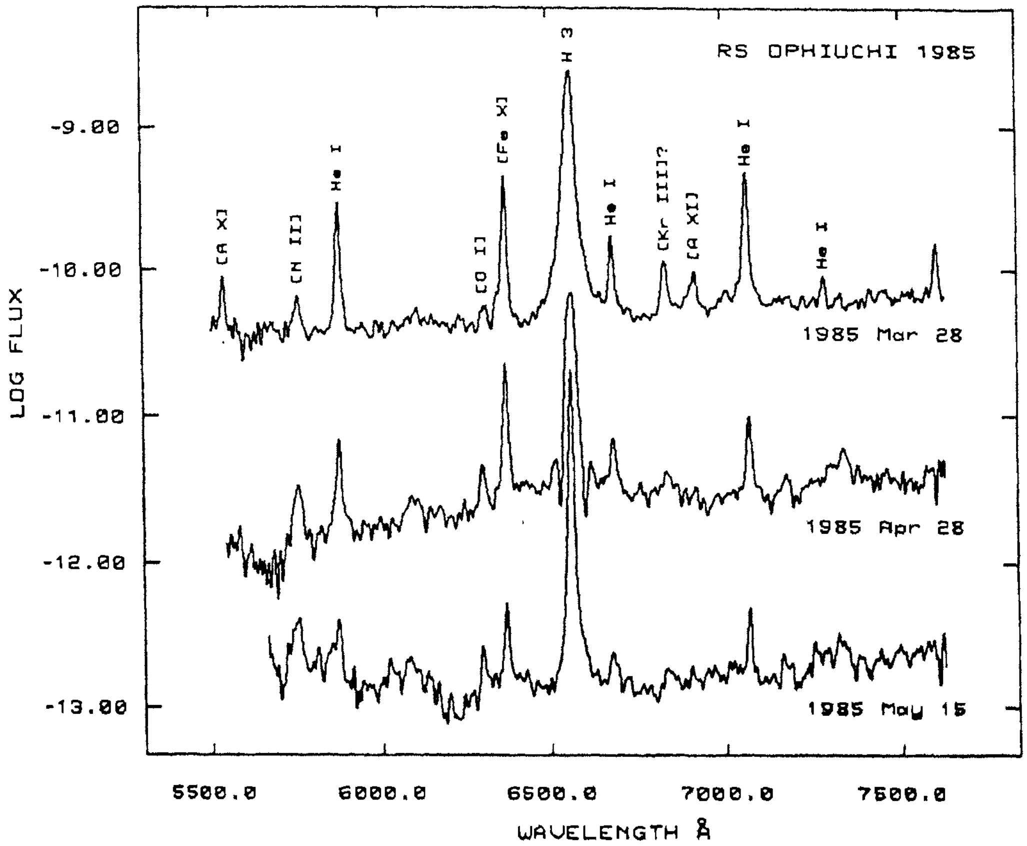

Fig. IV.1.2 Spectrum of RS Oph on days 60, 91 and 108, in the range 5600–7500. Hα is overexposed on April 28. Instrumental response correction on May 15 is uncertain shortward of 6200 Å. Flux is in units of erg cm^{-2} s^{-1} Å^{-1}. Top two spectra are shifted upwards by three and one unit respectively in log (flux).

are strong. P_{13} 8665 Å, P_{15} 8545 Å and P_{16} 8502 Å are blended with the Ca II triplet at 8662, 8542 and 8498 Å. P_{14} 8598 Å is blended with N I 8594 Å. He II 8236 Å could be present, blended with N I 8184–8242 Å complex. N I 8680–8719 Å and 7423–7468 Å could also be present. The lines of Fe II (72, 73) are present with Fe II 7711 Å being strong. There is a strong feature at 6830 Å. This has been attributed to [Kr III] 6826.9 Å by Joy & Swings (1945). Schmid (1989), however, suggests this feature arises due to Raman scattering of O VI 1032 Å line by neutral hydrogen in its ground state. O VI 1038 Å line, which forms a doublet with O VI 1032 Å, Raman scattered by neutral hydrogen, gives rise to 7088 Å feature. This feature is blended with He I 7065 Å, but can be identified in the spectrum of 1985 April 9 (Rosino & Iijima 1987: Fig. 5).

Phase 59 and 60 (1985 March 27, 28): The lines have narrowed and the degree

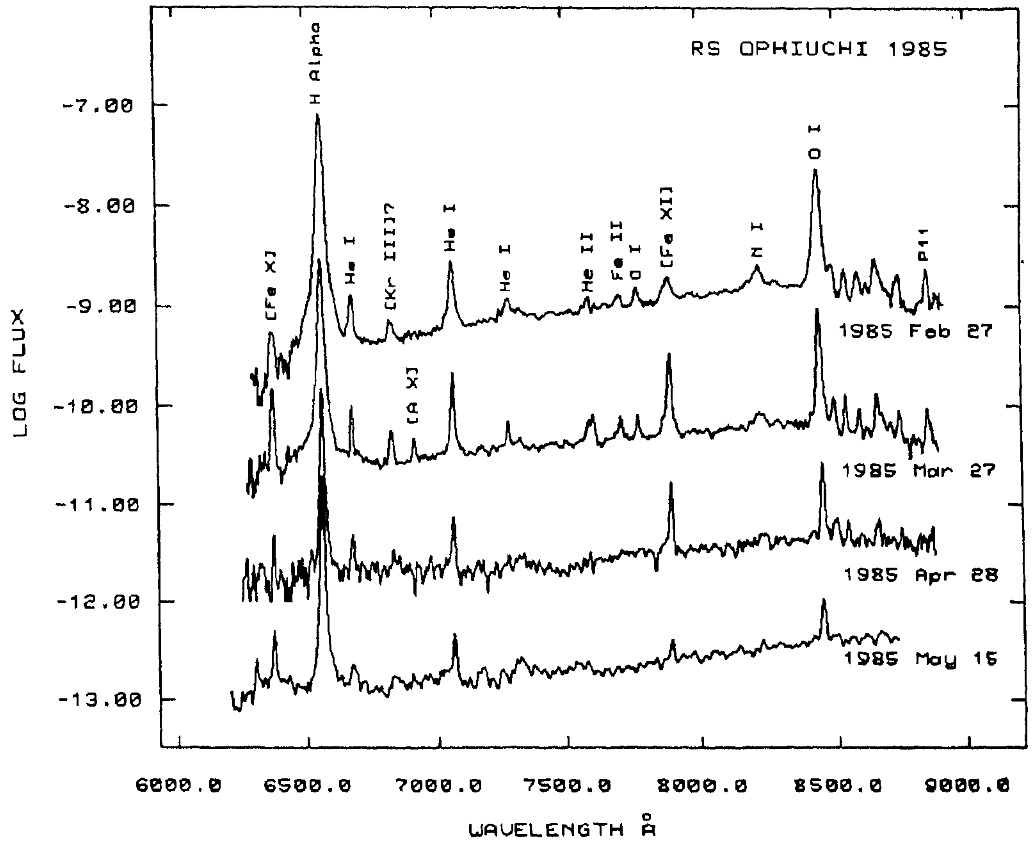

Fig. IV.1.3 Spectrum of RS Oph on days 32, 59, 91 and 108, in the range 6200–8900 Å. He II 7594 Å is uncertain due to overcorrection for atmospheric absorption. Flux is in units of erg $cm^{-2}\ s^{-1}\ Å^{-1}$. Top three spectra are shifted upwards by three, two and one unit respectively in log (flux).

of excitation increased, as seen from the strengthening of coronal and He II lines. Shortward of 6300 Å, the most prominent lines are Hβ, He I 5876 Å, He II 4686 Å, the coronal lines [Fe XIV] 5303 Å and [A X] 5535 Å. Moderately strong are [N II] 5755 Å, the '4640' nitrogen complex, lines of Fe II(42), He II 5411 Å, [O III] 4363, 4959, 5007 Å, Hγ, and Si II 5041, 5056 Å. He I 4922, 5016 Å are blended with Fe II lines at 4924 Å and 5018 Å respectively, and He I 5047 Å is blended with Si II lines. Also present are the lines of Fe II(48, 49), [Ni XIII] 5116 Å, [Fe VII] 6086 Å and [K IV] 6101 Å.

Phase 89 and 91 (1985 April 26, 28): The lines have generally decreased in strength and excitation has decreased. The lines of Hα, He I 5876, 6678, 7065 Å, [N II] 5755 Å are the most prominent lines. O I 8446 Å is also strong although O I 7774 Å has faded to near invisibility. Among the coronal lines, [Fe X] 6374 Å and

Table IV.1.2 RS Oph 1985: Line identifications and observed fluxes, in the region 4300–5600 Å, dereddened for $E(B-V) = 0.73$.

λ_m			Flux(10^{-10}erg cm^{-2} s^{-1})			
Å	Identification		Day 32	59–60	89–91	108
4319*	4340.47	Hγ		1.68		
	4363.21	[O III] (2)				
4565*	4582.84	Fe II (37)				
	4583.83	Fe II (38)				
	4595.68	Fe II (38)		0.32		
4623*	'4640'	N/O complex		0.89		
4676*	4685.68	He II (1)		1.84		
4728	4731.44	Fe II (43)		0.18		
4859	4861.33	Hβ		3.67		
4922	4921.93	He I (48)				
	4923.92	Fe II (42)		0.32		
4957	4958.91	[O III] (1)		0.09		
5012	5006.84	[O III] (1)				
	5015.68	He I (4)				
	5018.43	Fe II (42)		1.12		
5044	5041.06	Si II (5)		0.37		
	5047.74	He I (47)				
	5056.02	Si II (5)				
5116	5116.3	[Ni XIII] (1)		0.08		
5168	5169.03	Fe II (42)		0.20		
5196	5197.57	Fe II (49)		0.09		
5236	5234.62	Fe II (49)		0.10		
5274	5275.99	Fe II (49)		0.10		
	5276.10	[Fe VII] (2)				
5302	5302.86	[Fe XIV] (1)		1.04		
5315	5316.61	Fe II (49)				
	5316.78	Fe II (48)		0.22:		
5362	5362.86	Fe II (48)		0.09		
5409	5411.52	He II (2)		0.32		
5495	5495.82	[Fe II] (17)		0.11		
5530	5534.6	[A X] (1)		0.78		

Multiplet numbers appear in parentheses.
* Wavelength calibration is inaccurate due to comparison lines not being registered in this region. Lines have been identified based on a comparison of our spectrum with that of Rosino & Iijima (1987).

Table IV.1.3 RS Oph 1985: Line identifications and observed fluxes, in the region 5700–8900 Å, dereddened for $E(B-V) = 0.73$.

λ_m Å	Identification		Flux(10^{-10}erg cm^{-2} s^{-1}) Day 32	59–60	89–91	108
5755	5754.80	[N II](3)		0.24	0.32	0.30
5874	5875.63	He I (11)		1.05	0.57	0.17
6084	6085.5	[Fe VII] (1)		0.03	0.18	0.06
6104	6101.1	[K IV] (1)		0.05	0.20	0.05
6301	6300.23	[O I] (1)		0.03	0.19	0.16
6346	6347.09	Si II (2)		0.08	0.06	0.04
6372	6374.51	[Fe X]	0.54	1.30	1.75:	0.28
	6363.88	[O I] (1)				
6562	6562.82	Hα	107.43	29.22	9.26	3.78
6676	6678.15	He I (46)	0.81	0.43	0.21	0.13
6828			0.30	0.26	0.12	0.05
6917	6919.10	[A XI] (1)	0.05	0.14	0.07	0.06
7063	7065.19	He I (10)	1.98	1.27	0.60	0.21
7279	7281.35	He I (45)	0.42	0.17	0.06	0.03
7328	7310.24	Fe II (73)				
	7320.70	Fe II (73)	0.12	0.07		
	7318.6	[O II] (2)				
	7319.4	[O II] (2)				
	7329.9	[O II] (2)				
	7330.7	[O II] (2)			0.13	0.15
7455	7423.63, 7442.28,					
	7468.29	N I (3)				
	7462.38	Fe II (73)				
	7515.88	Fe II (73)	0.11	0.13	0.07	
7593	7592.74	He II (6)	0.18	0.35	0.06	0.03
7711	7711.71	Fe II (73)	0.26	0.14	0.02	
7773	7771.96, 7774.18,					
	7775.40	O I (1)	0.46	0.19	0.06	0.02
7890	7891.94	[Fe XI] (1)	0.71	1.56	0.67	0.18
8187	8184.80, 8187.95,					
+	8216.28, 8223.07,					
8226	8242.34	N I (2)				
	8236.77	He II (6)	0.86	0.29	0.14	0.05
8444	8446.35	O I (4)				
	8446.76	O I (4)	16.38	4.20	0.83	0.37

Table IV.1.3 Continued.

λ_m Å	Identification	Flux(10^{-10}erg cm^{-2} s^{-1}) Day 32	59–60	89–91	108
8500	8498.02 Ca II (2) 8502.49 H P_{16}	0.76	0.37	0.09	0.06
8543	8542.09 Ca II (2) 8545.38 H P_{15}	0.60	0.33	0.07	0.03
8596	8594.01 N I (8) 8598.39 H P_{14}	0.58	0.20	0.08	0.03
8627	8629.24 N I (8)	0.16	0.07	0.05	0.03
8665	8662.14 Ca II (2) 8665.02 H P_{13}	0.85	0.43	0.10	0.04
8680	8680.24, 8683.38, 8686.13 N I (1)	0.20	0.14	0.03	0.02
8715	8703.24, 8711.69, 8718.82 N I (1)	0.11	0.10	0.05	0.02
8745	8750.48 H P_{12}	0.49	0.18	0.08	0.03:
8859	8862.77 H P_{11}	0.49	0.22	0.09	0.05:

Multiplet numbers appear in parentheses.

[Fe XI] 7892 Å are prominent, whereas, [A XI] 6919 Å has weakened considerably. He II, Fe II and N I lines have also considerably weakened. Moderately strong are the lines of [O I] 6300 Å, [Fe VII] 6086 Å, [K IV] 6101 Å and the feature at 6830 Å. [O II] 7319–7331 Å is just visible. The TiO absorption band at 6158 Å from the secondary begins to appear.

Phase 108 (1985 May 15): There is an overall decrease in the emission-line strengths. The degree of excitation has further decreased, with most of the high excitation lines fading. The coronal lines of [Fe X] and [Fe XI] are however still present, whereas [A XI] has almost disappeared. The prominent emission lines in the order of decreasing strength are Hα, [N II] 5755 Å, He I 5876 Å, O I 8446 Å, [O I] 6300 Å, [O II] 7319–7331 Å, He I 7065 Å, [Fe XI] 7892 Å, He I 6678 Å and [Fe X] 6374 Å. Underlying the emission-line spectrum is that of the secondary.

1.1.2 Physical Conditions in the Envelope

The evolution of the envelope of RS Oph using the early radio and x-ray observations has been modelled by Bode & Kahn (1985). They estimate that free expansion phase lasted only a few days, after which the envelope began to expand adiabatically while accreting shock-heated circumstellar matter. Cooling became important after about 60 days. During the latter two phases, the radius and velocity of the envelope vary as

$$r_s = at^{2/3}; \qquad v_s = \frac{2}{3}at^{1/3} \tag{IV.1.1}$$

and

$$r_s = bt^{1/2}; \qquad v_s = \frac{1}{2}bt^{1/2} \tag{IV.1.2}$$

with $a = 3.3 \times 10^{13}$ cm day$^{-2/3}$ and $b = 8.2 \times 10^{13}$ cm day$^{-1/2}$ as estimated by Bode & Kahn. Based on these values of a and b, they estimate a mass loss rate of $\dot{M} = 4 \times 10^{-8}\ M_\odot$ yr^{-1} from the secondary in the form of wind, for an assumed wind velocity of 15 km s^{-1}.

O'Brien & Kahn (1987) suggest that the wind from the companion reached only 7×10^{14} cm since the last outburst of RS Oph and the envelope ejected during the present outburst would overtake it by day 65. The envelope may thus have never reached the momentum-conserving snow-plow stage. The velocities derived from Equation IV.1.1 and those observed as fullwidths at half maximum of the emission lines are compared in Table IV.1.4. There were no significant differences between the widths of permitted and coronal lines. The lines affected by blending have been left out. The tabulated values have been corrected for an average velocity resolution of 300 km s^{-1}, corresponding to the spectra used. The observed values are slightly smaller than predicted between days 60–108. This suggests that the constant a is a slight overestimate, the formal value based on our velocities being $(2.7 \pm 0.5) \times 10^{13}$ cm day$^{-2/3}$.

Electron density

Forbidden emission lines are rather weak and generally blended in our spectra. The only clearly resolved lines are [O I] 6300 Å and [N II] 5755 Å. The presence of these lines indicates that the densities are lower than the corresponding critical densities 1.8×10^6 cm^{-3} and 1.8×10^7 cm^{-3} respectively at 10^4 K. On the other hand, these lines could originate in the outer, low density regions and these densities may not be respresentative of the main shell. Hence, assuming a temperature $T_e = 1.5 \times 10^4$ K consistent with the estimates of Evans *et al.* (1988), the electron density has been derived from Hα line using the relationship III.1.5.

VLBI observations of RS Oph (Taylor *et al.* 1989) indicate that the envelope was disc-shaped rather than spherical. Most of the radio emission originated from a compact component with an angular size of 60 milliarcsec on day 77. Equation

Table IV.1.4 RS Oph 1985: The expansion velocity, electron density and mass.

t_d	v_s (km s^{-1})		n_e	M_H
Day	Obs.	Model	10^8 cm^{-3}	10^{-6} $M_\odot$
32.0	836 ± 192	792	30.6	3.7
59.9	470 ± 107	643	8.8	3.5
90.7	424 ± 127	560	3.4	3.0
108.7	431 ± 99	527	1.8	2.3

IV.1.1 predicts a comparable value of 49 milliarcsec. Though an expanding ring or disc may not follow the equation, the agreement of the envelope size with radio observations, together with the agreement with expansion velocities justifies the usage of the model. Using a value of filling factor $\phi = 0.01$ corresponding to a ring of width a tenth of its radius (given by equation IV.1.1), and covering a tenth of the surface of the sphere of the same radius, the volume of the envelope is described by

$$V = 1.45 \times 10^{39} {t_d}^2 \quad \text{cm}^3, \tag{IV.1.3}$$

where t_d is the time measured in days since outburst. This relationship is different from Equation III.1.6 because the increase in radius is slower due to interaction with the circumstellar wind.

The electron densities in the envelope were computed using the above expression for volume, the Hα fluxes from our data and recombination coefficients tabulated by Hummer & Storey (1987). The computed electron densities are listed in Table IV.1.4. The density varies as

$$n_e = 8.36 \times 10^{12} {t_d}^{-2.26} \quad \text{cm}^{-3}. \tag{IV.1.4}$$

There is an indication that the density decreased slightly slower than that given by Equation IV.1.4 till about day 100. The electron density was also computed using Hβ flux on day 60. Hβ appears fainter than expected. The electron densities computed using the fluxes of P_{11} and P_{12} on all days agree with the tabulated values within the uncertainity of the observed fluxes. Electron densities were also computed using the data of Evans *et al.* (1989) on Pα, Brγ and Brδ. Brδ appeared much brighter than expected, possibly due to a blend with [Si VI] 1.961 μm (Evans *et al.* 1989). Brγ was also somewhat brighter than expected till day 60.

The optical depth in Lyα may be calculated assuming the density derived above, the thickness following our model, and for a neutral hydrogen fraction 10^{-2}. The derived optical depth decreases from 4×10^7 on day 32 to 5×10^6 on day 108. Radiative recombination calculations of H spectrum are not valid at such high optical depths in Lyα. Indeed, on day 59.9, the ratio of Hα/H$\beta \sim 8.0$ instead of 2.62 predicted by radiative recombination case for appropriate density and temperature (Hummer & Storey 1987). The observed line ratios match well with the model BD3 of Krolik & McKee (1978) for an ionization parameter 10^{-2}, electron temperature 1.6×10^4, electron density 10^9 and Lyα optical depth 10^5. Among the models of Drake & Ulrich (1980), the high optical depth and high dilution of incident radiation reproduces the observed ratios. The dilution factor for radiation in RS Oph beyond the first few days is, however, much smaller than encountered in active galactic nuclei. The above models predict a lower value of Hβ emissivity compared to the radiative recombination case. However, the emissivity in Hα differs by less than 50 percent. The derived electron densities would hence change by less than 25 percent.

Nussbaumer & Schild (1979), and Nussbaumer (1986) have shown that C III] 1907, 1909 Å and Si III] 1883, 1892 Å lines in the ultraviolet contain information about density and temperature. The low resolution IUE spectra on RS Oph obtained on days 29, 48, 73, 95, 110 and 258 following the 1985 outburst show the Si III] and C III] lines (Snijders 1987). The C III] and Si III] doublets not being resolved in these spectra, their doublet ratios cannot be used to determine the densities. However, Nussbaumer & Stencel (1987) have shown that Si III] 1892 /C III] 1909 ratio can be used to determine the densities assuming that the observed emission has its origin in a homogeneous gas. Following Nussbaumer & Stencel (1987), assuming solar abundance for a(Si/C); ($a_{\odot}$(Si/C) = 0.1) and a value 0.5 for the ratio of the ionization fractions (f), the electron densities have been computed using the ratio of Si III] 1892/C III] 1909 lines. These are listed in Table IV.1.5.

The densities computed from the ultraviolet lines are consistent with the optical estimates within a factor of 2–4. The densities are quite sensitive to the assumed value of af. A slight change in the assumed value of af from 0.05 to 0.06 would make the two estimates agree better till day 110. Alternatively, a reduction in the volume of the emitting region decreases the discrepancy. This implies that although an accurate estimate for the densities is not possible with the data available, the densities derived from the two different considerations are consistent within the errors of the assumed quantities. The density on day 258 implies a much lower value of $af = 0.02$. The ratio of Si III]/C III] on this day is similar to that observed

Table IV.1.5 RS Oph 1985: Electron density using Si III] 1892/C III] 1909 ratio.

Day	Si III]/C III]	n_e 10^8 cm^{-3}
29	0.48	56.2
43	0.37	34.0
55	0.38	35.5
73	0.31	20.5
95	0.27	12.1
110	0.37:	34.0:
258	0.08	< 0.1

in several planetary nebulae (Feibelman & Aller 1987) with densities $\sim 10^4$ cm^{-3}, and $af \sim$ 0.02–0.03. It would thus appear that the density conditions of the expanding envelope are similar to those in symbiotic stars until about day 100 and more like planetary nebulae around day 250. It is quite likely that the lines arise in different regions during outburst and during inter-outburst period.

Hydrogen mass

The mass of hydrogen in the envelope as estimated using Equation III.1.8 are also listed in Table IV.1.4. The derived value is steadily decreasing. On the other hand, the total mass of the envelope is expected to steadily rise due to accretion from the circumstellar matter. The newly accreted matter is heated to coronal temperatures as it passes through the shock at the edge of the envelope. The hot matter does not contribute significantly to the recombination spectrum. Since the cooling rate is low during the adiabatic phase, one expects the permitted lines to arise mostly from the ejected envelope, and hence the derived mass should have remained constant. The inferred mass varies as the square root of the emitting volume, and hence it would appear that the volume increases faster than indicated by the assumed model. If the filling factor is made to increase as $t_d^{0.6}$ instead of being held constant, the inferred mass will remain constant. This may arise either due to a diffusing out of the thickness of the ring at a rate faster than expected from homologous expansion, or if the emitting gas was initially in the form of condensations which diffused out in time.

Our estimates of the mass of the ejecta agree with the estimate of Bohigas *et al.* (1989) which is based on the total mass of the envelope derived at late stages when most of the shocked matter had cooled down.

Table IV.1.6 RS Oph 1985: The He abundance and physical parameters of the ionizing source.

Day	$\frac{N_{He^+}}{N_{H^+}}$	$\frac{N^*_{He^{++}}}{N_{H^+}}$	T_s	R_s (10^{10} cm)		L_s (10^{38} erg s^{-1})	
			10^5 K	$\delta = 0.1$	$\delta = 1$	$\delta = 0.1$	$\delta = 1$
32.0	0.05	0.00	0.32	200	63	29	3.0
59.9	0.12	0.00	> 0.43	< 44	< 14	28:	2.9:
90.7	0.15	0.01	1.50	4.0	1.3	5.5	0.6
108.4	0.13	0.03	2.6	1.6	0.5	8.5	0.9
204.0†	0.11	0.05	3.6	0.6	0.2	5.0	0.5

* The value for day 204 is derived from observations, the rest of the values are assumed ones.

† Mean epoch of observations of Bohigas *et.al.* (1989) and Bruch (1986).

Chemical abundances

The fact that the envelope in RS Oph contains different regions of shocked and unshocked matter makes it difficult to determine chemical abundances of elements such as oxygen and nitrogen with respect to hydrogen using forbidden lines. The forbidden lines could arise in the shocked region, whereas hydrogen lines are predominently formed by photoionization from the central ionizing source. Helium abundance however poses less problems and can be estimated assuming that He is either singly or doubly ionized all through the H^+ region. Evans *et al.* (1988) suggest that He II lines originated in the cooling, shocked matter at a temperature $\sim 2 \times 10^5$ K, during the early months after outburst. Hence the derived He abundance would be reliable only at later epochs.

He I line emissivities were taken from Broklehurst (1971), with a logarithmic extrapolation to the densities of our interest, at an assumed electron temperature of 1.5×10^4 K. These emissivities have been corrected for collisional effects incorporated by Clegg (1987). He I 6678 Å is recommended as the best line for use in abundance determinations (Clegg 1987). It was found that abundances determined using He I 7065 Å agreed with 6678 Å estimates. Hence, both these lines were used, excluding 6678 Å on day 108 when its intensity was uncertain. He I 5876 Å yields much lower abundance, as also found by Bohigas *et al.* (1989). The He^+/H^+ abundances determined by us using He I 6678, 7065 Å and Hα are listed in Table IV.1.6. The value for day 204 is based on the He I 6678/Hα data of Bruch (1986).

The coronal lines were very faint by day 201, and we may assume that He II emission originated in the unshocked ejecta. Using He II 4686/Hβ from Bohigas *et al.* (1989) and the tables of Hummer & Storey (1987), He^{++}/H^{+} abundance of 0.05 is estimated. This together with $He^{+}/H^{+} = 0.11$ yields a helium abundance

$$n(\mathrm{He})/n(\mathrm{H}) = 0.16.$$

Snijders (1987) has obtained CNO abundances using ratios of selected lines in the ultraviolet, based on data obtained by IUE. Using the N III] 1750/O III] 1663 ratio, $n(\mathrm{O})/n(\mathrm{N}) = 1.10 \pm 0.17$ is estimated. Using the ratio C IV 1549/N IV] 1486 on days 94 and 111, $n(\mathrm{C})/n(\mathrm{N}) = 0.16 \pm 0.04$ is estimated. Also, using N V 1240/He II 1640 line ratio, $n(\mathrm{He})/n(\mathrm{N})$ is estimated to be in the range 3–40. These abundances, which are in the range derived for classical novae suggest a thermonuclear runaway outburst (Snijders 1987).

Radius and temperature of the ionizing source

Theoretical models of thermonuclear runaways on white dwarfs suggest that during the constant bolometric luminosity phase following an outburst, the radius of the ionizing source decreases, whereas, the effective temperature increases (Starrfield, Sparks & Truran 1985). Similar results have been obtained from observations of envelopes of classical novae (Ferland 1979; Krautter & Williams 1988; Martin 1989). Based on an estimate of the number of ionizing photons, the radius and temperature of the ionizing source in RS Oph has been estimated.

Using $N(He^{+})/N(H^{+})$, we derive temperatures of 3.2×10^4 K on day 32 and 4.3×10^4 K on day 60 for the central ionizing source. For temperatures in excess of 4×10^4 K, both He and H compete for ionizing photons and He^{+} and H^{+} Strömgren spheres coincide (Osterbrock 1974). The estimate for day 60 is hence a lower limit. If we further assume that no He^{++} existed in the permitted-line region, we obtain an upper limit of $\sim 10^5$ K.

Beyond day 60, we assume that a reduction in He^{+}/H^{+} below 0.16 is to be compensated by He^{++}/H^{+}. Using the implied values of $N(He^{++})/N(H^{+})$, we obtain the effective temperatures as 1.5×10^5 K (day 90.7), 2.6×10^5 K (day 108.4) and 3.6×10^5 K (day 201). The last estimate agrees with that of Mason *et al.* (1987) for day 250 based on x-ray data.

The radius of the source R_s estimated using the observed Hα flux and Equation III.1.14 for two values of δ, *i.e.*, 0.1 and 1, are listed in Table IV.1.6. For day 201, we have used the Hβ luminosity based on Bohigas *et al.* (1989). The blackbody luminosity of the ionizing source, estimated from R_s and T_s are also listed in Table IV.1.6. There is a sudden drop in the luminosity between days 60 and 90.

1.1.3 The Coronal Lines

Coronal lines appear in the spectrum of RS Oph during the nebular phase, reaching their maximum intensity between days 50–100 (Joy & Swings 1945; Griffin & Thackeray 1958; Dufay *et al.* 1964; Rosino 1987; Rosino & Iijima 1987; Wallerstein & Garnavich 1986). Coronal lines [Fe X] 6374 Å, [Fe XI] 7892 Å and [A X] 6919 Å were seen in our red–infrared spectra. Spectra recorded on day 60 in the wavelength range 4300–5600 Å showed strong [Fe XIV] 5303 Å and [A X] 5535 Å lines. The lines [Ni XIII] 5116 Å, [Ni XI] 6033, 6346 Å and [Ni XV] 6702 Å observed by Wallerstein & Garnavich (1986) could also be present in our spectra, but poor signal-to-noise ratio makes their identification difficult.

The emissivity (total emission per unit volume, per unit time) in a coronal line may be expressed as

$$j_L = n_{\rm H} A f(X, T_e) f_j(n_e, T_e) A_{jk} h\nu_{jk}, \qquad \text{(IV.1.8)}$$

where n_H is the hydrogen number density, A is the abundance of the element, $f(X, T_e)$ is the fraction of the element in the ionization state of interest, f_j is the fraction of ions in the upper level of coronal transition, A_{jk} the transition probability and $h\nu_{jk}$ the energy of the emitted photon.

If one considers ratios of lines due to the same element in different ionization states, $n_{\rm H}$ and A cancel out. $f(X, T_e)$ and $f_j(n_e, T_e)$ can be computed and the consequent theoretical line ratios can be compared with the observed ones. Knowing the value of the electron density n_e, the temperature T_e of the coronal-line emitting region may be determined.

In computing the line ratios, ionization fraction as a function of temperature was obtained from the equilibrium calculations of Jacobs *et al.* (1977) for iron and of Landini & Fossi (1972) for argon. The relative level populations for each of the ionized species were computed using the cascade-matrix method (Mason 1975) to solve the excitation equilibrium.

The identified coronal lines arise from transitions among levels in the ground configuration. In order to interpret the observations it is necessary to include all the terms of atleast the ground and two excited configurations. In addition, terms from higher levels should also be included since cascades from these may influence the populations of lower terms.

The populations of the levels of a given ion are determined, for a fixed temperature and electron density by steady-state equations which balance the rates of population and de-population for each level. In the balance equation for ground configuration all radiative and collisional processes, including cascade via the excited configurations and the effect of autoionizing levels on the electron collision rates have been included. It was shown by Mason (1975) that collisional excitation by protons is important under coronal conditions. Including this, the balance equation may be expressed as (Mason 1975)

$$n_e \sum_{j>i} f_i \alpha^{\text{eff}}(i,j) + \sum_{j>i} f_i B(i,j) + n_p \sum_{j>i} f_i \alpha_p(i,j) = n_e \sum_{j<i} f_i \alpha^{\text{eff}}(i,j) + \sum_{j<i} f_i A(i,j). \tag{IV.1.9}$$

In the above equation, the terms with α^{eff} are the electron collision terms, $B(i,j)$ and $A(i,j)$ include radiative processes and α_p accounts for the proton collision.

The electron collision rate coefficient is given by

$$\alpha_e(i,j) = \frac{8.63 \times 10^{-1}}{T_e^{1/2}} \frac{\Omega(i,j)}{\omega_i} \exp\left[\frac{-\Delta E(i,j)}{kT_e}\right], \tag{IV.1.10}$$

where $\Omega(i,j)$ is the collision cross section. Under coronal conditions, electron de-excitation is negligible compared to spontaneous radiative decay for the excited configurations.

The stimulated absorption coefficient $B(i,j)$ is given by

$$B(i,j) = A(i,j) D(h) \frac{\omega_j}{\omega_i} \left[\exp(\frac{\Delta E(i,j)}{kT_R}) - 1\right]^{-1}; \qquad i < j. \tag{IV.1.11}$$

$D(h)$ is the dilution factor and T_R the temperature of ionizing source. Owing to the high dilution factor in the envelope of RS Oph, the effect of $B(i,j)$ is negligible.

Electron excitation to excited configurations, followed by radiative decay plays a major role in the re-distribution of population in the ground configuration. The rate coefficient for such a cascade process is

$$\alpha_e(i,j) = \frac{8.63 \times 10^{-6}}{T_e^{1/2} \omega_i} \sum_k \Omega(i,k) C(k,j) \exp\left[\frac{-\Delta E(i,k)}{kT_e}\right]. \tag{IV.1.12}$$

$$C(k,j) = \frac{A(k,j)}{\sum_{j'<k} A(k,j')} \tag{IV.1.13}$$

is the cascade coefficient and represents the probability that the ion in an excited configuration k will eventually decay to the level j.

The total electron collisional rate coefficient for transitions within the ground configuration can now be written as

$$\alpha^{\rm eff}(i,j) = \frac{8.63 \times 10^{-6}}{T_e^{1/2}\omega_i}\Omega_{\rm eff}(i,j)\exp\left[\frac{-\Delta E(i,j)}{kT_e}\right], \tag{IV.1.14}$$

with

$$\Omega_{\rm eff}(i,j) = \Omega(i,j) + \sum_k \Omega(i,k)C(k,j). \tag{IV.1.15}$$

The atomic data, Ω and A were taken from Mason (1975) for iron, and from Bhatia, Feldman & Doscheck (1979) for A XI. The transition probability for [A X] 5535 Å was taken from Kastner (1976) and the collision strength was taken to be 0.127 from Czyak, Aller & Euwema (1974).

The proton collision strength α_p was obtained, for each of the ions from the sources listed. Since the proton collision strength was not available for [A X] 5535 line, it was computed as

$$\alpha_p = 10^{-10}(-1.43 + 3.52T_6 - 0.5T_6^2 - 0.024T_6^3); \quad 0.5 \leq T_6 \leq 2, \tag{IV.1.16}$$

where T_6 is the electron temperature in units of 10^6 K. The method of Kastner (1977), and Kastner & Bhatia (1979), was followed using the radial integrals listed by Kastner (1977). Equation IV.1.9 was then solved by matrix methods, using a modified version of the FIVEL program of de Robertis *et al.* (1987) to compute the level populations f_i for a range of temperatures and densities.

The level populations are very sensitive to the electron density. If the coronal lines arise mainly in the shocked circumstellar matter, following the model of Bode & Kahn (1985), we expect electron densities of 10^6, 5×10^5, 3×10^5 and 2×10^5 cm^{-3} at the four epochs. In order to produce the observed line intensities at such densities, one requires more than 10^{-4} $M_\odot$ of shocked matter, assuming solar abundances of iron. An overabundance of iron by a factor > 100 would be needed to bring down the mass of the shocked wind to a value consistent with the estimates of Bode & Kahn (1985). On the other hand, if the lines arise in the shocked ejecta, the densities will be larger, and the observed emission can be explained by $\leq 10^{-6}$ $M_\odot$ of the shocked matter. We thus conclude that coronal lines originate mostly from shocked ejecta. We also assume that the density of the coronal line emitting region is similar to that of unshocked ejecta.

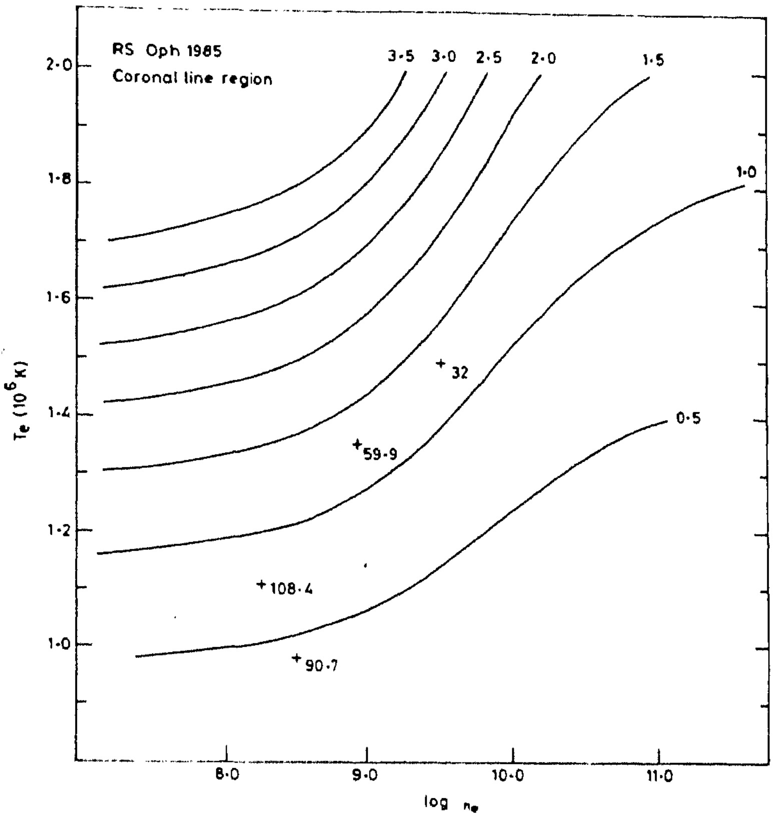

Fig. IV.1.4 Contours of equal ratios of [Fe XI] 7892/[Fe X] 6374 plotted in $(T_e, \log n_e)$ plane. The observed ratios in RS Oph 1985 plotted against the assumed densities, indicate the temperature.

Theoretical line ratios of [Fe XI] 7892/[Fe X] 6374 were computed for the range of temperature and densities: $0.5\times10^6 \leq T_e \leq 2.0\times10^6$ and $7 \leq \log n_e \leq 12$. Figure IV.1.4 shows equal line-intensity ratios of [Fe XI] 7892/[Fe X] 6374 as a function of electron density and temperature. Observed ratios are also plotted. The intensities of [Fe X] 6374 Å were corrected for the contribution due to [O I] 6363 Å, assuming a ratio of [O I] 6300/6363 = 3. The derived temperatures, listed in Table IV.1.7 are close to 10^6 K, with a suggestion of slight cooling with time.

On day 60, we could also use [Fe XIV] 5303 Å, [A X] 5535 Å and [A XI] 6919 Å. We find that the temperature derived from [Fe XIV]/[Fe X] is higher than that from [Fe XI]/[Fe X], whereas [A XI]/[A X] yields a lower temperature. This indicates that there may be temperature inhomogeneities or gradients in the shocked region. A similar suggestion has been made by Wallerstein & Garnavich (1986).

Table IV.1.7 RS Oph 1985: Electron temperatures of coronal line region.

Day	T_e (10^6 K)		
	[Fe XI]/[Fe X]	[Fe XIV]/[Fe XI]	[A XI]/[A X]
32.0	1.50		
59.9	1.34	1.52	1.24
90.7	0.98		
108.4	1.11		

1.2 Quiescence

1.2.1 Optical Spectrum

The optical spectrum of RS Oph in its quiescence resembles those of symbiotic stars. The spectrum is a combination of the cool secondary spectrum, over which strong emission lines are superposed (Walker 1979; Rosino, Bianchini & Rafanelli 1982; Barbon, Mammano & Rosino 1969; Bruch 1986). Balmer lines, He I lines and lines of Fe II are present in emission. Ca II H and K and Na I D lines are strongly present in absorption, whereas, Ca I 4226 Å is absent (Walker 1979). Variability in the emission line strengths has also been noticed (Rosino, Bianchini & Rafanelli 1982).

Observations

Following the 1985 outburst, RS Oph reached the quiescence phase ~ 300 days after the outburst maximum. By this time, lines of high excitation had faded away, and the secondary spectrum was prominent. Observations of RS Oph from VBO were continued well after the outburst during its present quiescence phase. Photographic spectra were obtained at the Cassegrain focus of the 102 cm telescope using the UAG spectrograph during the years 1986–1989. The spectra obtained during 1986–1987 were recorded on Kodak IIaD plates covering a wavelength range 4500–7200 Å at 86 Å mm^{-1} dispersion, whereas the spectra obtained during 1988–1989 were recorded on Kodak 103aD plates and cover a range 4400–8900 Å at 200 Å mm^{-1} dispersion. The Varo 8605 image intensifier was used to intensify the light before recording on the photographic plate. The spectrograms were digitized with the PDS 1010M microdensitometer at 3–5 μm intervals using 7.5–10 μm wide apertures. The digitized spectra were smoothed, converted to intensities and wavelength calibrated following the procedure in Chapter II.

Table IV.1.8 Details of CCD spectra of RS Oph in quiescence.

Date 1990	UT	Wavelength range Å
Feb	21.98	4400–7600
	22.00	4400–7600
Mar	24.92	4400–7600
Mar	30.96	4400–7600
Mar	31.96	4400–7600
Apr	1.89	6100–9200
	1.94	6100–9200
Apr	2.90	6100–9200
	2.98	6100–9200

CCD spectra of RS Oph were obtained from VBO during 1990 February–April at the Cassegrain focus of the 102 cm telescope using the UAG spectrograph with 250 cm camera and 150 g mm^{-1} grating and the Photometrics CCD system. The wavelength ranges covered are 4500–7600 Å and 6100–9200 Å at 5.5 Å per pixel resolution. Table IV.1.8 gives the dates of observations. All spectra were reduced following the procedure described in Chapter II. Spectrophotometric standards HD 117880 and Feige 66 were used for flux calibration. Atmospheric absorption band contributions have been corrected for following the method described in Chapter II. The correction is fairly accurate except for the 7594 Å absorption where the correction has been underestimated.

The photographic spectra being generally underexposed and owing to their poorer quality as compared to the CCD data, we have used them only for line identifications and a general description of the quiescence spectrum. The CCD spectra were averaged and the mean spectrum is used in the analyses. The spectrum has been corrected for interstellar reddening using $E(B-V) = 0.73$ and the Savage & Mathis (1979) law.

Description of the spectrum

The dereddened, quiescent spectrum of RS Oph is shown in Figure IV.1.5. TiO absorption bands, and strong emission lines are present in the spectrum. The presence of TiO absorption bands is indicative of a late-type secondary, although the energy distribution of the spectrum in the wavelength range covered here is bluer than that of a normal late type star. This implies there is contribution to the

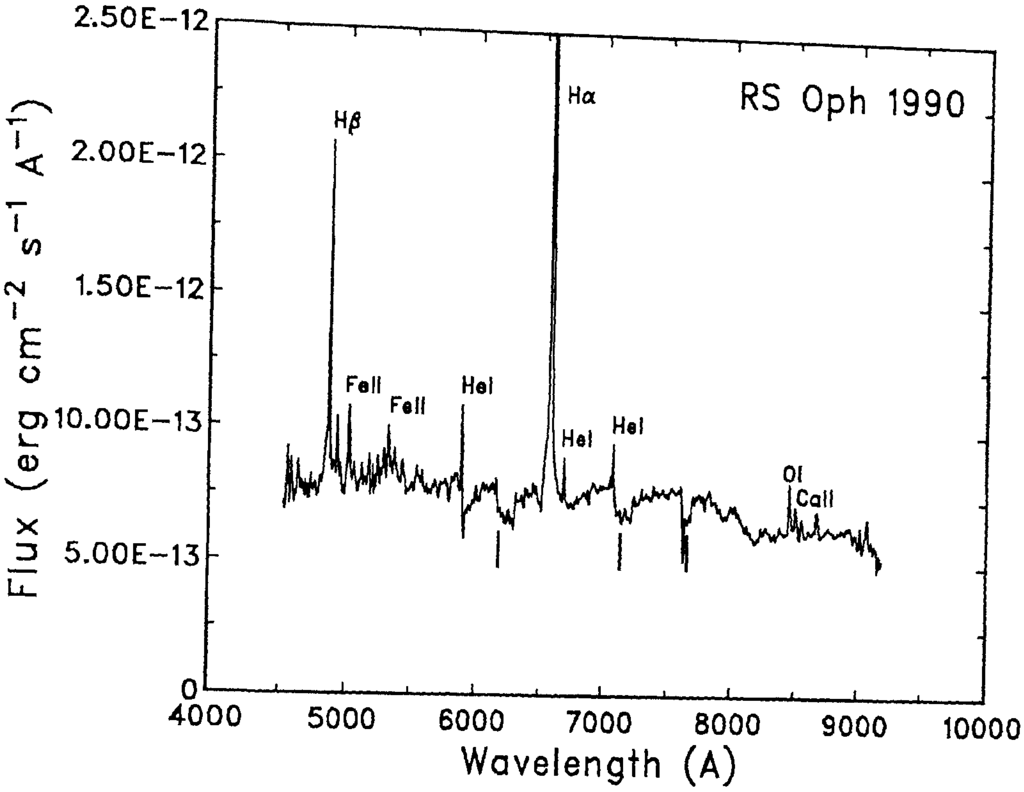

Fig. IV.1.5 Spectrum of RS Oph at quiescence, corrected for $E(B-V)$=0.73. Epoch of observation: 1990 February 21–April 2. Prominent TiO bands are indicated by vertical bars below the spectrum.

continuum spectrum from the hot component at these wavelengths. Hβ, Hα, He I 5876, 6678, 7065 Å, lines of Fe II and the Ca II infrared triplet are in emission. Lines of multiplets 42, 48, and 49 are the most prominent Fe II lines. O I 8446 Å is present in emission, indicating the continued importance of Lyβ fluorescence. O I 7774 Å is however, present in absorption. If the hot component is an accreting white dwarf, then O I 7774 Å in absorption implies an optically thick accretion disc (Friend *et al.* 1988). Na I D absorption is also present.

1.2.2 The Binary Components

Based on optical spectra the secondary in RS Oph has been classified as a giant of spectral type M0–M2 (Sanduleak & Stephenson 1973; Barbon, Mammano & Rosino 1968; Rosino, Bianchini & Rafanelli 1982; Bruch 1986). Walker (1979) classifies the secondary as M3. Duerbeck & Seitter (1989) determine the spectral type as K5–K7, whereas Kenyon & Fernandez-Castro (1987) classify it as K5.7 I–II.

K–M stars show TiO absorption bands in their spectrum which can be used as indicators of spectral type. O'Connell (1973) and Kenyon & Fernandez-Castro (1987) show that the red TiO bands at 6180 Å and 7100 Å are good temperature indicators. These features, in conjunction with the VO 7865 Å band and the Na I infrared doublet at 8190 Å can be used to derive the spectral type, and luminosity class.

The determination of spectral types for giants relies on the measurement of an absorption index defined as the depth of a feature at a wavelength λ relative to an interpolated continuum point (O'Connell 1973; Kenyon & Fernandez-Castro 1987). Thus

$$[I_\lambda] = -2.5\log\{f_\lambda/[f_{\lambda_1} + (f_{\lambda_2} - f_{\lambda_1})(\lambda - \lambda_1)/(\lambda_2 - \lambda_1)]\}, \qquad \text{(IV.1.17)}$$

where λ_1 and λ_2 are continuum wavelengths and f_λ is the flux in a bandpass centred at λ.

Table IV.1.9 gives the wavelength λ of the feature whose indices were measured, its corresponding continuum wavelengths λ_1 and λ_2 and the observed, dereddened fluxes at these wavelengths. The indices for 6180 Å, 7100 Å TiO bands and the VO 7865 Å were defined as

$$[\mathrm{TiO}]_1 = -2.5\log\{f_{6180}/[f_{6125} + 0.2245(f_{6370} - f_{6125})]\} \qquad \text{(IV.1.18)}$$

$$[\mathrm{TiO}]_2 = -2.5\log\{f_{7100}/[f_{7025} + 0.2000(f_{7400} - f_{7025})]\} \qquad \text{(IV.1.19)}$$

and

$$[\mathrm{VO}]_1 = -2.5\log\{f_{7865}/[f_{7400} + 0.7154(f_{8050} - f_{7400})]\}. \qquad \text{(IV.1.20)}$$

A 30 Å bandpass was used to construct these indices, following Kenyon & Fernandez-Castro (1987), as it avoids contamination from the strong emission lines present in the spectrum.

Na I infrared doublet at 8181, 8195 Å can be used as a luminosity discriminant among M stars (Sharpless 1956; Kenyon & Fernandez-Castro 1987). A sodium index defined as

$$[\mathrm{Na}]_1 = -2.5\log\{f_{8190}/[f_{8050} + 0.4000(f_{8400} - f_{8050})]\}. \qquad \text{(IV.1.21)}$$

Table IV.1.9 RS Oph: Absorption band fluxes, indices and the derived spectral type.

Wavelength Å		Flux	Index	Sp. type
Abs. band	Continuum	10^{-13} erg cm^{-2} s^{-1}		
	6125	7.77		
TiO 6180		6.93	0.11	K5.3
	6370	7.45		
	7025	7.91		
TiO 7100		7.02	0.12	K5.4
	7400	7.73		
	7400	7.73		
VO 7865		7.32	−0.03	M0.1
	8050	6.85		
	8050	6.85		
Na 8190		5.97	0.11	
	8400	6.23		

was used for luminosity classification. A 30 Å bandpass was used even in this case as it avoids the strong atmospheric features around 8230 Å as well as the O I 8446 Å emission feature.

Using the observed fluxes listed in Table IV.1.9, $[\mathrm{TiO}]_1$, $[\mathrm{TiO}]_2$, [VO] and [Na] indices were computed, and used to determine the spectral type of the secondary. Fits to standard K and M stars listed in Kenyon & Fernandez-Castro (1987) were used to determine the spectral type ST:

$$ST = -1.75 + 9.31[\mathrm{TiO}]_1 \qquad (\mathrm{IV.1.22})$$

$$ST = -1.83 + 10.37[\mathrm{TiO}]_2 - 3.28[\mathrm{TiO}]_2^2 \qquad (\mathrm{IV.1.23})$$

and

$$ST = 0.74 + 19.3[\mathrm{VO}] - 17.22[\mathrm{VO}]^2 \qquad (\mathrm{IV.1.24})$$

where $ST = -6$ for K0 stars, 0 for M0 stars and +6 for M6 stars.

The indices and spectral types estimated from each of the features are also listed in Table IV.1.9. The value of sodium index suggests a luminosity class more evolved than a giant. However, the sodium fluxes could be in error because of contamination from the weaker atmospheric features in that region. Based on [TiO] indices, we can assign a spectral type K5III to the secondary.

The energy distribution of RS Oph appears bluer than a normal K5III energy distribution. This implies a significant amount of contribution from the hot component. Bruch (1986) estimates the hot component to be about +1.1 mag brighter than the secondary at 5500 Å. This would imply that it contributes significantly to the spectrum even beyond 6000 Å. In such a case the TiO absorption bands in the secondary would be diluted. With his estimate of the primary's contribution, Bruch (1986) classifies the secondary as M2III. Based on infrared observations Evans *et al.* (1988) classify the secondary as K8±2 III. The secondary is thus of spectral type later than K5.

Based on the estimates of Evans *et al.* (1988) and Bruch (1986), assuming the secondary to be M0III and the total spectrum of the form given by Equation III.1.21, the flux from the accretion disc may be estimated. Standard fluxes for the M0III star were taken from O'Connell (1973), where relative relative fluxes are tabulated. As a first approximation, the scale factor B in Equation III.1.21 was chosen such that the standard fluxes matched the observed flux at $\sim$ 9000 Å. This region was chosen as the contribution from the accretion disc was expected to be the least here. The scaled M fluxes were then used to remove contribution from the secondary to the total flux. The excess over the secondary flux is due to the accretion disc. The presence of O I 7774 Å in absorption indicates an optically thick disc (Friend *et al.* 1989). From the optically thick, steady-state model for the accretion disc, a theoretical accretion disc spectrum of the form given by Equation III.1.20 can be fit to the flux excess. The scale factor A was chosen such that the theoretical fit closely matched the observed fluxes (*i.e.* flux excess over the secondary). The scale factors A and B were iteratively determined such that the total of the disc spectrum and the standard M spectrum matched the observed (total) flux at all wavelengths within 10 percent. The best estimate for the accretion disc was found to be $f_{\lambda,\mathrm{acc}} = 10^{-3.55}\lambda^{-2.33}$ erg cm^{-2} s^{-1} Å^{-1}, with λ expressed in Å units. Figure IV.1.6 shows the decomposition of spectrum into secondary and accretion disc components.

The TiO and VO indices were remeasured on the estimated M giant spectrum. The values obtained were $[\mathrm{TiO}]_1 = 0.253$, $[\mathrm{TiO}]_2 = 0.204$ and $[\mathrm{VO}] = -.005$ corresponding to spectral types M0.6, M0.2, M0.6 respectively. The flux of the M star at 5500 Å is $f_{5500,\mathrm{cool}} \approx 6.17 \times 10^{-13}$ erg cm^{-2} s^{-1} Å^{-1} corresponding to an absolute visual magnitude $M_V = -0.62$ mag at a distance of 1.6 kpc. This value is in agreement with that obtained by Bruch (1986). This value of M_V corresponds to an M2III star (Egret, Keenan & Heck 1982). Based on the revised values of

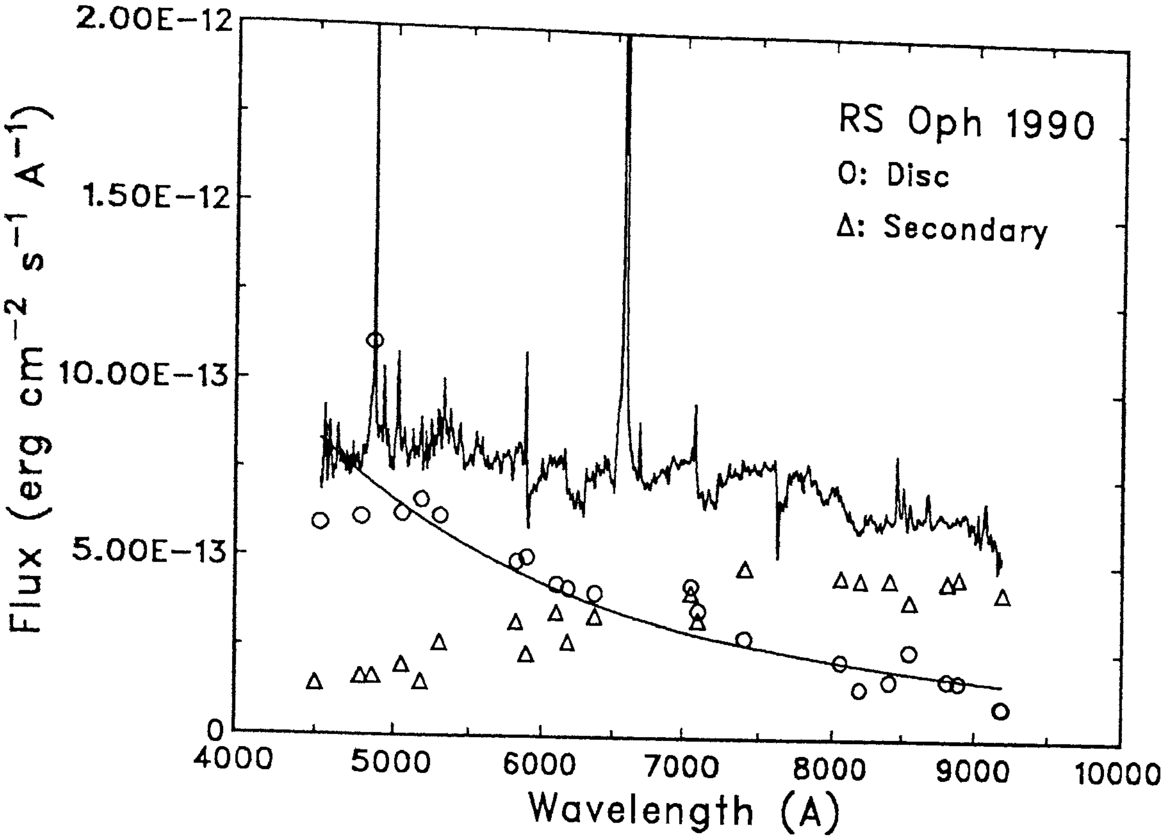

Fig. IV.1.6 The quiescence spectrum of RS Oph, and the decomposed spectra of the accretion disc and the M0III secondary.

TiO and VO indices and the estimate of M_V we reclassify the cool component in RS Oph as an M1±1 III star. The accretion disc flux at 5500 Å corresponds to $M_V = -1.4$ mag. The accretion disc is 0.78 mag brighter than the cool secondary. This result agrees with that of Bruch (1986).

The infrared colours of RS Oph at quiescence are anomalous (Evans *et al.* 1988, Feast & Glass 1974). The mean quiescence (1973–1982) *JHK* magnitudes (dereddened) prior to the 1985 outburst are 7.08, 6.51 and 6.32 mag respectively, giving $(J - H) = 0.57$ and $(H - K) = 0.19$. Post-outburst magnitudes between 1985 June–1986 October give $(J - H) = 0.59$ and $(H - K) = 0.17$. The $(H - K)$ colours imply a spectral type M2III for the secondary, whereas the $(J - H)$ colours imply K2.5III (Frogel *et al.* 1978). In a spectrum obtained on 1987 August 19, Evans *et al.* (1988) find an excess at wavelengths < 1.6 μm, *i.e.* J window, over the flux of a normal M0III star normalized at 1.6 μm, whereas there is no significant excess at $\lambda > 1.6$ μm. The excess flux at J wavelength (1.25 μm) is $\sim 1.0 \times 10^{-13}$ erg cm^{-2}

s^{-1} Å^{-1} corresponding to 0.32 magnitudes. There is thus an excess of 0.32 mag in the $(J-H)$ colour. Our fit to the accretion disc spectrum predicts a flux 0.8×10^{-13} erg cm^{-2} s^{-1} Å^{-1} at J, very close to the observed excess. We hence attribute the excess in J to the accretion disc contribution. Correcting the J flux for the accretion disc contribution, we get mean colours $(J-H) = 0.78$ and $(J-H) = 0.80$ for 1973–1982 and 1985 June–1986 October respectively. These colours, together with the $(H-K)$ colours imply a spectral type M2.5III for the secondary.

The absence of significant excess beyond 1.6 μm implies no/negligible contribution from the accretion disc in that region. This means the accretion disc spectrum has turned over at $\sim$ 1.6 μm. Such a turnover can be caused by the finite size of the disc. Assuming the turnover at H band (1.4 μm) we can estimate the size of the accretion disc following the discussion in §III.1.2.2. The thermonuclear outburst models for recurrent novae (Starrfield, Sparks & Truran 1985) predict the mass of the white dwarf in these systems to be close to the Chandrasekhar limit *i.e.* $M_1 \approx 1.38 M_\odot$. Also, to explain the short recurrence timescales, mass transfer rates of the order 10^{-8} $M_\odot$ yr^{-1} are required. Using Equation III.1.19 for $M_1 = 1.3$ $M_\odot$ and $\dot{M} = 10^{-8}$ $M_\odot$ yr^{-1}, T_0 is estimated as 1.4×10^7 K ($T_* = 1.7 \times 10^5$ K). Extrapolating the values of Beall *et al.* (1984) logarithmically for the value of T_0 obtained for RS Oph, the maximum disc radius is estimated to be $R_{\rm disc} = 1.7 \times 10^{11}$ cm ≈ 2.4 $R_\odot$.

Assuming $M = 1.3$ $M_\odot$ and $i = 30°$ (based on Bruch 1986), and using our estimate of M_V for the disc, we arrive at $\dot{M} \sim 5 \times 10^{-6}$ $M_\odot$ yr^{-1} using Equation III.1.22. This value of $\dot{M}$ implies a value for $T_* = 8 \times 10^5$ K and $R_{\rm disc} = 12$ $R_\odot$. For the derived value of $\dot{M}$ the recurrence rate for nova outbursts would be $\sim$ 2 years (Starrfield, Sparks & Shaviv 1989). The recurrence period can be lengthened by decreasing the mass of the white dwarf in RS Oph to a value lower than 1.3 $M_\odot$. It is also possible that the above estimate of $\dot{M}$ is higher than the actual mean mass transfer rate.

As an alternative to the accreting white dwarf primary, Livio, Truran & Webbink (1986) suggest an accreting bloated main sequence star as the primary with the matter transferred from the secondary directly hitting the main sequence star. In such a case the excess in flux over the M star flux in our observed spectrum would correspond to this main sequence star. The equivalent width of O I 7774 Å absorption has a value $\sim$ 800 mÅ corresponding to an A–F main sequence star (Faraggiana *et al.* 1988). A blackbody (BB) spectrum at 10^4 K has been fit to the excess over the M star fluxes. The flux of the accretion disc in Equation III.1.21 is replaced by $Af_{\lambda,\mathrm{BB}}$ where $f_{\lambda,\mathrm{BB}}$ is the surface flux of the BB at 10^4 K. The total flux is $f_{\lambda,\mathrm{tot}} = Af_{\lambda,\mathrm{BB}} + Bf^{\mathrm{rel}}_{\lambda,\mathrm{std}}$. As in the case of the accretion disc spectrum, the scale factors A and B have been iteratively determined such that the total of the BB flux and the M star flux match the observed flux at all wavelengths within 10 percent. The best fit was achieved by scaling the BB surface fluxes by a factor 1.6×10^{-21}. The scale factor can be used to estimate the radius of the emitting source. It corresponds to an angular size $\theta \approx 5.7 \times 10^{-11}$, which, at the distance of RS Oph (1.6 kpc) yields a radius of $\approx 4\ R_\odot$ for the BB source. The primary would then correspond to a main sequence A0V star with a bloated radius $\approx 4\ R_\odot$ (instead of 2.4 $R_\odot$ for a normal A0V star). The flux of this primary at J band would be 1.2×10^{-14} erg cm^{-2} s^{-1} Å^{-1} corresponding to 13.5 mag. This flux is insufficient to explain the excess observed in the J band. A main sequence primary would thus require an additional source to explain the flux excess at J.

The emission lines

The emission lines in RS Oph could arise either in the accretion disc or in the stellar wind of the M giant secondary. Table IV.1.10 gives the fluxes of the prominent emission lines. On high resolution spectra obtained by Robinson *et al.* (1989) and Garcia (1986), the emission lines are double peaked. Emission lines from an accretion disc also show a double peaked profile. Robinson *et al.* (1989) have computed theoretical line profiles from optically thick accretion discs. They find the theoretical profiles do not match the observed profiles in RS Oph and conclude a non-accretion disc origin for the emission lines. Garcia (1986) suggests the emission lines could originate in a ring around the secondary formed due to the stellar wind. The Hβ flux observed by us is consistent with the size of the ring 60–100 $R_\odot$ as suggested by Garcia. It appears highly probable that the emission lines seen in RS Oph quiescence spectrum arise in the ring around the secondary. In such a case, the line fluxes cannot be used to estimate the temperature of the hot primary. A similar conclusion is also reached by Duerbeck & Seitter (1989).

2. T Coronae Borealis

T Coronae Borealis has undergone two recorded outbursts in 1866 and 1946. The two outbursts have been identical (Campbell 1948). T CrB is visually the brightest recurrent nova, reaching a magnitude $m_v \approx 2$ at maximum. The rate of decline of

Table IV.1.10 RS Oph in quiescence: Emission line fluxes corrected for $E(B-V) = 0.73$.

λ Å	Identification		Flux 10^{-11} erg cm^{-2} s^{-1}
4856	4861.33	Hβ	1.238
4919	4923.92	Fe II (42)	0.255
4958	4958.91	[O III] (1)	0.255
5008	5006.84	[O III] (1)	0.147
	5005.14	N II (19)	
5012	5015.68	He I (4)	0.259
	5018.43	Fe II (42)	
5161	5169.03	Fe II (42)	0.155
5232	5234.62	Fe II (49)	0.127
5276	5275.99	Fe II (49)	0.204
5312	5316.61	Fe II (49)	0.237
	5316.78	Fe II (48)	
5360	5362.86	Fe II (48)	0.192
5872	5875.63	He I (11)	0.270
6144	6141.01	Fe II (46)	0.055
6560	6562.82	Hα	6.604
6674	6678.15	He I (46)	0.194
7062	7065.19	He I (10)	0.133
7283	7281.35	He I (45)	0.030
8445	8446.35	O I (4)	0.417
	8446.76	O I (4)	
8494	8498.02	Ca II (2)	0.256
	8502.49	H P_{16}	
8540	8542.09	Ca II (2)	0.158
	8545.38	H P_{15}	
8595	8594.01	N I (8)	0.071
	8598.39	H P_{14}	
8631	8629.24	N I (8)	0.059
8659	8662.14	Ca II (2)	0.227
	8665.02	H P_{13}	

Table IV.1.10 Continued.

λ Å	Identification		Flux 10^{-11} erg cm^{-2} s^{-1}
8747	8750.48	H P_{12}	0.028
9009	9014.91	H P_{10}	0.105
9061	9060.6	N I (15)	0.253
	9061.33	Fe II (71)	
	9063.40	He I (77)	

Multiplet numbers appear in parentheses.

0.4 mag per day classifies it among very fast novae (Payne-Gaposchkin 1957). Both outbursts were characterized by the appearance, at $\sim$ 106 days since maximum, of a secondary maximum reaching $m_v \approx 8$ (Pettit 1946; Sanford 1949).

The outburst spectrum of T CrB is very similar to that of RS Oph in several respects. Description of the outburst spectra may be found in Payne-Gaposchkin (1957) and references listed there. The salient features from the description in Payne-Gaposchkin (1957) are presented here. The emission spectrum developed almost at maximum with the appearance of strong, broad emission lines. High initial ejection velocities $\sim$ 4500 km s^{-1} were detected around maximum. As in RS Oph, emission lines narrowed with time and the excitation increased. Strong coronal lines due to [Fe X] 6374 Å, [Fe XIV] 5303 Å were present in the spectrum. During the secondary maximum the continuum brightened up tremendously. However, the emission lines faded and also the excitation decreased. The TiO absorption features from the secondary star were seen in the spectrum about a month after the outburst, disappeared during the secondary maximum and appeared again after decline from secondary maximum (Sanford 1949). The emission lines also reappeared after decline from the secondary maximum. The coronal line [Fe X] 6374 Å reappeared a few days after the decline, whereas [Fe XIV] 5303 Å did not reappear.

The quiescent optical spectrum of T CrB is that of the cool secondary, but with emission lines of H I, He I, He II, [O III], [N III] superposed, similar to the spectrum of symbiotic stars (Swings & Struve 1941; Andrillat & Houziaux 1982; Kenyon 1985). The spectral type of the secondary is estimated to be M3III (Berman 1932; Joy 1938). Kenyon & Fernandez-Castro (1987) estimate a type M4.1$\pm$0.3 III, whereas, Duerbeck & Seitter (1989) estimate M5III. Radial velocity variations with a semiamplitude of 21 km s^{-1} and period of 230.5 days were first detected by Sanford

Table IV.2.1 Spectroscopic orbit of T CrB.*

Parameter	Value	
$T_0^{\dagger}$	JD 2,431,933.83 ± 0.13	
P	227.53 ± 0.02	days
V_0	−27.89 ± 0.06	km s^{-1}
K_1	23.32 ± 0.16	km s^{-1}
K_2	33.76 ± 3.21	km s^{-1}
$M_1 \sin^3 i$	2.60 ± 0.54	$M_{\odot}$
$M_2 \sin^3 i$	1.80 ± 0.20	$M_{\odot}$
$a \sin i$	257 ± 14	$R_{\odot}$

* Subscript 1 refers to the M3III star, 2 to its hot companion.

† Epoch of inferior conjunction of the M3III star.

(1949). Kraft (1958) refined the orbital period to 227.6 days with $K_1 = 24.0$ km s^{-1}. He also estimated a mass ratio of 1.4 with the secondary mass being greater. An inclination of 68° has been estimated by Paczyński (1965). The orbital parameters have been recently refined by Kenyon & Garcia (1986). These are listed in Table IV.2.1 (from Webbink *et al.* 1987). The mass estimates for the secondary and primary are $3.34 \pm 0.73\ M_{\odot}$ and $2.31 \pm 0.29\ M_{\odot}$ respectively (Webbink *et al.* 1987).

The spectrum in the ultraviolet is dominated totally by the hot component (Cassatella & Selvelli 1988; Selvelli 1989). The spectrum consists of high and low excitation permitted and intercombination emission lines, P-Cygni profiles and absorption lines of singly ionized metals (Cassatella, Gilmozzi & Selvelli 1985). The most prominent lines are those due to N V, O I, C II, Si IV, N IV] 1486 Å, C IV 1550 Å, He II 1640 Å, O III] 1750 Å, Si III] 1892 Å, C III] 1908 Å and Mg II 2800 Å. The ultraviolet continuum varies significantly both in slope and intensity, and can be fit by a power law spectrum $f_{\lambda} = A\lambda^{-\alpha}$ over the entire IUE range. The spectral index α varies from 0 to 1.5 with a mean value of 1.0 (Cassatella, Gilmozzi & Selvelli 1985; Cassatella & Selvelli 1988; Selvelli 1989). The integrated ultraviolet luminosity varies from 2.6×10^{34} erg s^{-1} at a low state to 2.6×10^{35} erg s^{-1} at a high state. The mean ultraviolet luminosity is 2.2×10^{35} erg s^{-1} (Selvelli 1989).

Photometry of T CrB during quiescence has shown variations in the light curves, more pronounced in the blue (Bailey 1975; Peel 1985; Lines, Lines & McFaul 1988; Peel 1990), attributed to the ellipsoidal variations of the secondary. Peel (1990) has recently analysed several photographic (1892–1911; 1929–1935) and visual (1872–1979) light curves of T CrB at quiescence to look for orbital phase consistency in the variations. Minima in the photographic light curve have been detected at phases 0 and 0.5. The minimum at 0.5 phase is shallower with fluctuations that are generally bright at phases 0.45 and 0.58. Lines, Lines & McFaul (1988) have detected an additional $\sim$ 55 day periodicity in the *UBV* bands with the amplitude being maximum in the U. They attribute this additional variability to semi-regular variations of the secondary.

The nature of the primary and outburst mechanism in T CrB are uncertain. The large lower mass limit deduced for the hot component from radial velocity measurements exceeding the Chandrasekhar limit pose a problem for thermonuclear models of outburst, which presume a white dwarf primary. In spectra obtained in 1943, Minkowski (1943) detected an absorption spectrum bluewards of 4100 Å consisting of lines of H, He I and Ca II, whereas redward of 4100 Å the spectrum has M-type features with emission lines of H and He II 4686 Å superposed. The absorption spectrum is similar to stars of spectral type ~B8 and has the characteristics of the spectra of shells of B-type stars. Harmanec (1974) also found a similar spectrum. Plavec, Ulrich & Polidan (1973) and Harmanec (1974) suggest the primary is more likely a main sequence star, with the cool giant on the brink of dynamical timescale mass transfer. Webbink (1976) shows that an episodic accretion event onto a main sequence star can explain the outburst characteristics of T CrB. The accretion model proposed by Webbink attributes the principal maximum in the outbursts of T CrB to the dissipation of the excess energy of a part of transferred mass as it collapses into a ring in a circular orbit around the accreting star. The density contrast between the stream and the outflowing stellar wind of the giant is sufficient to accelerate the shock waves formed to velocities of the order of 10^4 km s^{-1} (Webbink *et al.* 1987). The circulating accretion ring broadens into a disc due to viscous dissipation within the ring and gradually falls onto the accreting star. As it does so, its luminosity increases, reaching a maximum as its inner edge reaches the surface of the central star. The height of the secondary maximum and the interval between the primary and the secondary maxima are consistent with the viscous timescales for a main sequence star (Webbink 1976). Webbink *et al.* (1987) also point out that the rise in the continuum in the spectrum of T CrB at secondary maximum is similar to the accretion powered events of dwarf novae.

The quiescent ultraviolet spectra on the other hand give indications for the presence of an accreting white dwarf. Cassatella & Selvelli (1988) and Selvelli

(1989) give the following arguments which indicate a white dwarf primary. The bulk of the accretion disc luminosity is estimated in the ultraviolet with negligible contribution in the optical. A main sequence accretor is incompatible with the observed ultraviolet luminosity and spectral distribution, as the accretion rate in this case would have to be high to explain the observed ultraviolet luminosity, which would imply a significant contribution in the optical. Further, the presence of strong He II 1640 Å line indicates a temperature $\sim 10^5$ K in the boundary layer. The mass accretion rate associated with the observed He II flux is $\dot{M} \sim 1.3 \times 10^{-7}$ $M_\odot$ yr^{-1}. This compares well with the lower limit obtained from the ultraviolet continuum luminosity, $\dot{M} \gtrsim 5 \times 10^{-8}$ $M_\odot$ yr^{-1}. An additional argument in favour of a white dwarf primary is the presence of broad wings in the emission lines of C IV and He II. These lines originate in the innermost disc-boundary layer region and are rotationally broadened. The observed velocities of these lines are not compatible with a main sequence accretor. Other indications for the presence of a white dwarf are the presence of flickering in the U band (Walker 1977; Bianchini & Middleditch 1976), and the overabundance of neon in the ejecta similar to the neon novae, where thermonuclear runaway is the outburst mechanism. A decrease in the value of K_2 by 8 km s^{-1} which is within the errors of radial velocity measurements would reduce the mass of the primary to ~ 1.4 $M_\odot$ allowing for a massive white dwarf primary (Selvelli 1989). Orio (1987) has shown that an accretion event on a massive white dwarf can also explain the outburst light curves of T CrB.

A nebular shell around T CrB was detected in 1977 in Hα+[N II] emission (Williams 1977). The shell consists of two small condensations on either side of the stellar system. These condensations extend to $\sim$ 10 arcsec on both sides. A spectrum of the northeast condensation by Williams (1977) did not show an emission line spectrum, but only a reflection spectrum of T CrB, which Williams attributed to scattering of light in the spectrograph due to the brightness of T CrB. No further reports on the detection of the shell are available. An attempt was made from VBO to detect the shell. CCD images in Hα+[N II] were obtained. Owing to the brightness of T CrB, the 'ghost image' due to the interference filter used was very prominent. The ghost was detected at $\sim$ 2% intensity level of the original, whereas no shell was detected upto this intensity level.

2.1 The Optical Spectrum

Observations

T CrB was continually mointored spectroscopically during the years 1985–1990 from VBO using the 102 cm reflector. Low dispersion spectra covering the wavelength range 4400–9200 Å have been obtained during these years. During 1985–1989 photographic image tube spectra of T CrB were recorded. In 1985, spectra at dispersion 200 Å mm^{-1} in the wavelength range 5000–8800 Å were recorded on Kodak IIaD plates using the Cassegrain spectrograph. During 1986–1989 the UAG spectrograph was used. The spectrograms obtained in 1986 and 1987 cover a wavelength range 4600–6800 Å at a dispersion of 86 Å mm^{-1} and were recorded on Kodak IIaD plates. The data obtained in 1988 and 1989 were recorded on Kodak 103aD plates at a dispersion of 200 Å mm^{-1}, covering wavelength regions 4000–8000 Å and 5000–8800 Å.

The spectrograms were digitized at 5 μm interval using the PDS 1010M microdensitometer. The digitized spectra were Fourier smoothed using a lowpass filter with cutoff at 12 cycles mm^{-1}. The smoothed spectra were then brought to a relative intensity scale and wavelength calibrated. Fe+Ne comparison spectrum was used in the wavelength calibration. The spectra were then normalized with respect to a pseudo-continuum level and equivalent widths of the emission lines were measured. The reductions were performed following the procedure in Chapter II.

From 1989 December to 1990 April, CCD spectra of T CrB were obtained at 5.5 Å per pixel resolution in the wavelength range 4400–7600 Å and 6000–9200 Å. The photometrics CCD system was used with the UAG spectrograph. The CCD frames were individually de-biased, flat field corrected, and the one-dimensional spectrum extracted following the procedure in Chapter II. Fe+Ne comparison source was used in wavelength calibration. Spectrophotometric standards Feige 15, HD 60778, HD 109995, HD 19445, EG 99, HD 60778, HD 117880, HD 161817 and Feige 66 were used for flux calibration. The contribution due to telluric absorption bands in the infrared has been removed following the procedure in Chapter II. CCD observations of T CrB were generally made as it was rising, at fairly low hour angles. The continuum in the red region of the spectrum was found to be affected by atmospheric refraction since the slit of the spectrograph was aligned almost perpendicular to the atmospheric dispersion. The spectra obtained during 1990 Feburary to 1990 April were corrected for this effect as follows: T CrB was observed on each night with the spectrograph slit opened to $\sim$ 13 arcsec such that all the light from the star passed

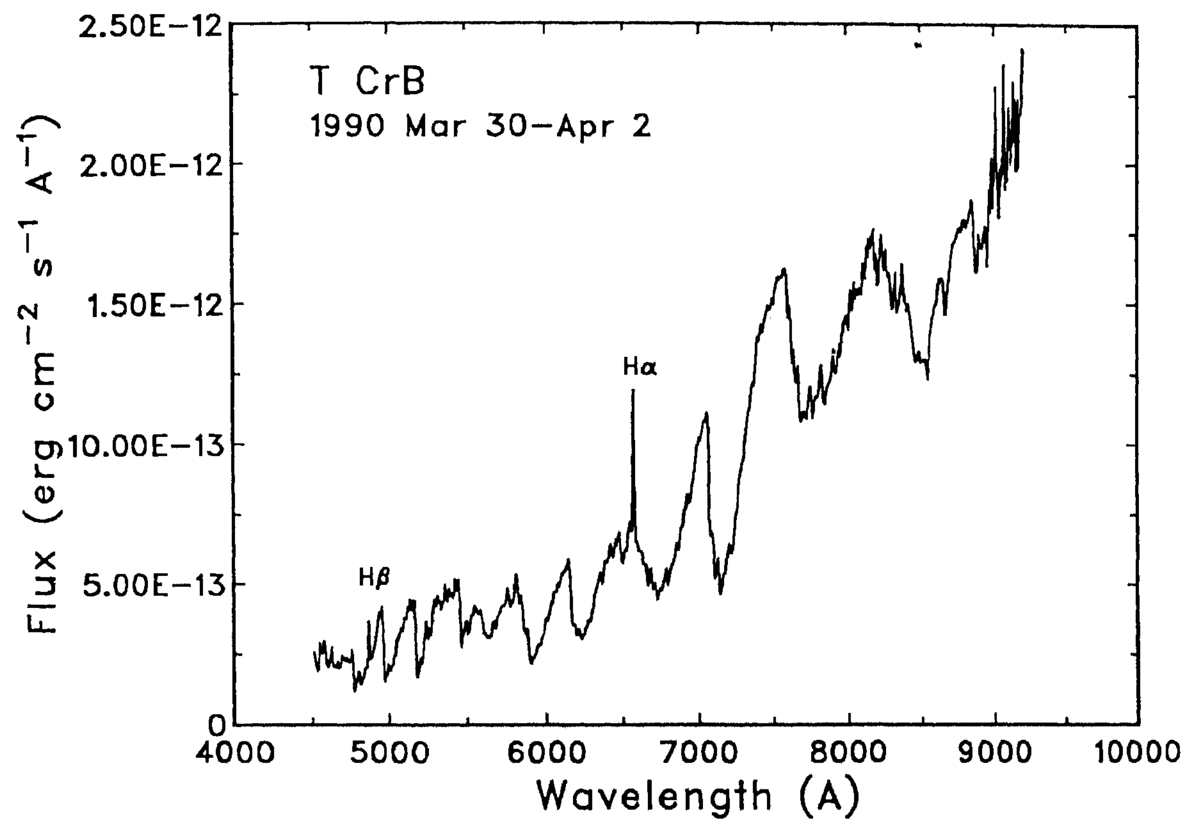

Fig. IV.2.1 Spectrum of T CrB at quiescence, between 1990 March 30–April 2, corrected for $E(B-V)$=0.15.

through the slit. The flux calibrated wide slit spectra were treated as standards and a correction curve was determined to scale the narrow slit spectrum continuum level to match that of the wide slit over the entire range of the spectrum.

Spectrum

Figure IV.2.1 shows the mean of the flux calibrated CCD spectra of T CrB in the wavelength range 4500–9200 Å obtained on 1990 March 30, 31 and 1990 April 1, 2. The spectrum has been corrected for interstellar reddening using $E(B-V) = 0.15$ (Cassatella, Gilmozzi & Selvelli 1985) and the Savage & Mathis (1979) law. The spectrum is dominated by strong TiO absorption features from the M3III secondary. Superposed over this M3III spectrum are the Hβ and Hα emission lines. He I emission lines are weak in the spectrum shown in the figure. Spectra obtained during the latter half of 1985 and in 1986 and 1987 show strong He I 5876, 6678 and 7065 lines. He I lines are also seen in some spectra obtained in 1989. The strengths of the emission lines have been found to be varying over the period of our

Table IV.2.2 Emission line equivalent widths in the T CrB spectrum.

Date (JD)	Emission line (Å)				
2440000+	Hβ 4861	Hα 6563	He I 5876	He I 6678	He I 7065
6124.440		17.09		1.46	0.67:
6183.332		8.02			0.46
6184.309		8.76			
6202.275		9.73	1.62	3.36	
6484.500		15.42	1.83		
6493.347		25.66	3.58	1.76	
6541.234		15.97		0.37:	
6568.224	6.56	19.34	1.33	1.10:	
6574.390	7.65	15.05		1.98	1.36
6639.169	12.80	22.61	1.83	1.81	
6465.483	11.51	31.22	1.29	1.86	0.79
6466.397	8.77	23.30	1.54	2.45	2.95
6859.342	12.42	37.18	2.11	2.11	2.63
6860.330	12.86	35.48	2.40	1.36	1.20
6895.340	5.42	18.81	1.31	1.37	
6936.283	10.94	24.58	3.02	1.80	
6937.203	10.59	23.54	2.18	1.66	
6951.161	4.30	17.48		1.01	1.62
6959.267	5.38	12.82			2.37
6964.220	6.55	19.61	2.06	1.28	1.87
6965.157	8.12	25.96	1.47	1.07	
6999.200	2.85	8.19			
7040.120		9.90			
7042.126		3.68			
7177.470		7.35			
7178.476		5.26			
7211.367		4.99			
7213.368		5.45			
7236.357		7.13			
7268.400		7.19			
7295.250	5.51	10.22			
7304.306		7.07			
7324.144		3.15			
7386.158		4.69			
7527.496		4.89			
7537.475		3.41		0.47	
7538.473		4.28			
7574.390	1.26	2.91			
7575.392		2.31			

Table IV.2.2 Continued.

Date (JD) 2440000+	Emission line (Å) Hβ 4861	Hα 6563	He I 5876	He I 6678	He I 7065
7616.377		3.65			
7617.285	3.62	6.66			
7630.291	2.25	4.93		0.68	
7631.285		5.61			
7659.358		2.31			
7660.240		4.27			
7892.475	1.42	1.89			
7894.482		2.75			
7904.443	0.63	2.70			
7944.438	1.23	3.29			
7975.371	1.70	3.19			
7981.369	3.21	7.02	1.09	0.98	
7982.344	2.65	6.75	1.09		
7983.335		7.99			
7984.291		8.85			

observations. Table IV.2.2 lists the equivalent widths of the emission lines Hβ, Hα, He I 5876, 6678 and 7065 Å.

2.2 The Secondary

The secondary in T CrB has generally been accepted as an M3III giant (*e.g.* Berman 1932; Joy 1938). Recently, based on the strengths of the TiO absorption bands in the red region, Kenyon & Fernandez-Castro (1987) estimated the secondary as M4.1±0.3 III. Duerbeck & Seitter (1989) have estimated it to be M5III. We have used our CCD spectra of 1990 March and April to estimate the type of the secondary. The [TiO] indices described in §IV.1.2.2 were determined from our spectra. These are listed in Table IV.2.3. Using these indices and Equations IV.1.22–IV.1.24 the spectral type has been estimated. This is also listed in Table IV.2.3. The VO band at 7865 Å is affected by the TiO band in that region. An accurate estimate of [VO] index was hence not possible. [Na] index was found similarly affected. However, an estimate of the continuum at 8190 Å by interpolating the nearby continuum points (different from those listed in Table IV.1.9) gives a [Na] index consistent with the estimates for giants by Kenyon & Fernandez-Castro (1987). Based on the [TiO] indices, we classify the secondary in T CrB as M4 ± 1 III. The observed continuum

Table IV.2.3 T CrB: TiO indices and spectral type.

Feature	Index	Sp. type
$[TiO]_1$ 6180	0.58	M3.6
$[TiO]_2$ 7100	0.75	M4.1

flux at 5500 Å: $f_{5500} = 5.2 \times 10^{-13}$ erg cm^{-2} Å^{-1}, implies $M_V = -1.09$ in agreement with the M_V estimates for an M4IIIb star (Corbally, Garrison & Garrison 1988).

No attempt was made to estimate the spectrum of the hot component as the spectral region covered by us is totally dominated by the secondary except for the emission lines. However, based on the mean ultraviolet luminosity, and assuming a $\lambda^{-2.33}$ spectrum, we estimate the hot component to contribute about 10 percent to the flux at 5500 Å, *i.e.* its $M_V = +1.4$. Assuming the primary to be an accreting white dwarf of mass $M_{\rm WD} \gtrsim 1.3\ M_\odot$, from Equation III.1.22, the mass transfer rate is estimated as $\sim 10^{-7}\ M_\odot\ {\rm yr}^{-1}$.

2.3 Hα Variability

The equivalent widths of the emission lines that are listed in Table IV.2.2 are variable. The Hα equivalent width, which is available throughout our observations, has been used here to look for orbital dependance of the emission line strengths. Table IV.2.4 lists the Hα equivalent width as a function of phase reckoned on the ephemeris of Kenyon & Garcia (1986), given in Table IV.2.1. Our data covered about 7 orbital cycles. Figure IV.2.2 gives the Hα light curve based on the equivalent widths. A slow variation is seen in the light curve, with shorter-term variations superposed. To extract the slow variation, a mean value was obtained for each cycle after rejecting the high values. A smooth curve through the mean points (also plotted in Figure IV.2.2) gives the long term variation, the period of which is estimated to be $\sim$ 2400 days. The observed Hα equivalent widths were normalized dividing by the smooth curve corresponding to the long term variation, and are plotted in Figure IV.2.3 as a function of orbital phase. This data was then Fourier analysed using a three term truncated Fourier series:

Table IV.2.4 T CrB: Hα equivalent width as a function of orbital phase.

Phase	Hα equivalent width	
	Observed	Normalized
62.368	17.09	2.34
62.627	8.02	0.96
62.631	8.76	1.04
62.710	9.73	1.09
63.951	15.42	0.97
63.989	25.66	1.60
64.200	15.97	0.93
64.319	19.34	1.10
64.346	15.05	0.85
64.630	22.61	1.21
65.471	31.22	1.82
65.475	23.30	1.36
65.598	37.18	2.35
65.602	35.48	2.25
65.756	18.81	1.36
65.936	24.58	2.16
65.940	23.54	2.07
66.002	17.48	1.63
66.037	12.82	1.26
66.059	19.61	1.96
66.063	25.96	2.60
66.213	8.19	0.96
66.393	9.90	1.36
66.401	3.68	0.50
66.996	7.35	1.50
67.001	5.26	1.07
67.145	4.99	1.10
67.255	7.13	1.70
67.396	7.19	1.36
67.514	10.22	2.76
67.554	7.07	1.91
67.641	3.15	0.90
67.913	4.69	1.47
68.535	4.89	1.88
68.578	3.41	1.31
68.583	4.28	1.65
68.741	2.91	1.16
68.745	2.31	0.92

Table IV.2.4 Continued.

Phase	Hα equivalent width	
	Observed	Normalized
68.925	3.65	1.52
68.929	6.66	2.77
68.986	4.93	2.05
68.991	5.61	2.34
69.114	2.31	0.96
69.118	4.27	1.78
70.139	1.89	0.73
70.147	2.75	1.06
70.191	2.70	1.04
70.367	3.29	1.17
70.503	3.19	1.06
70.529	7.02	2.34
70.534	6.75	2.25
70.538	7.99	2.67
70.542	8.85	2.95

$$\begin{aligned} Eqn =&(1.395 \pm 0.054) + (0.027 \pm 0.062)\cos\phi + (0.498 \pm 0.076)\sin\phi \\ &- (0.184 \pm 0.077)\cos 2\phi - (0.228 \pm 0.090)\sin 2\phi \\ &+ (0.003 \pm 0.075)\cos 3\phi - (0.098 \pm 0.074)\sin 3\phi, \end{aligned} \tag{IV.2.1}$$

where Eqn is the normalized equivalent width and ϕ is the phase in radians. The Fourier fit as given by the above equation is also plotted in Figure IV.2.3. The light curve shows two well defined maxima around phases 0.93 and 0.53. The maximum at phase 0.93 is broader and lower than the 0.53 phase maximum. The Hα light curve obtained by us is out of phase with the broad band light curve.

The orbital phase dependence of the broad band as well as line emission indicates two possibilities: (i) geometrical effects as the system is seen from different aspect angles; (ii) physical effects that switch on and off as a function of orbital phase. It has already been suggested that the broad band light curve is due to ellipsoidal variations of the secondary. However, this cannot explain enhanced emission at phases 0 and 0.5 unless the emission originates along the shorter axis of the secondary itself. It has been generally assumed that T CrB is not an eclipsing binary. The primary does not contribute significantly to the blue band flux and indeed a partial eclipse of the primary cannot explain the depth of light curve at phase zero.

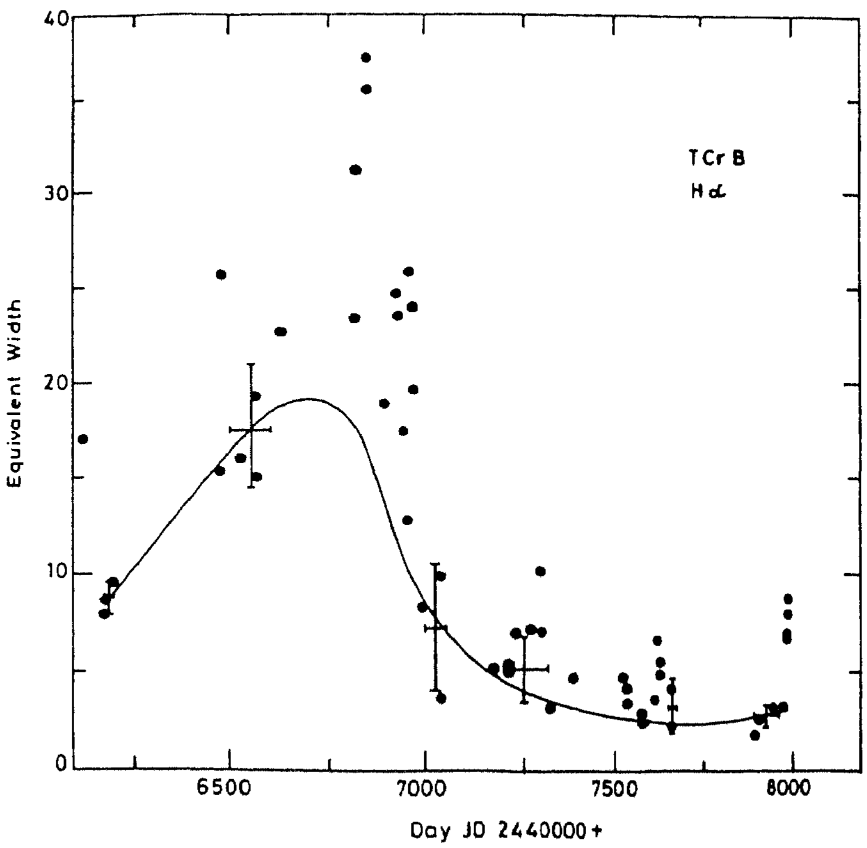

Fig. IV.2.2 Equivalent widths of Hα emission in T CrB. The mean values at different times and a smooth fit to these values are also seen.

The emission line light curve would thus require an explanation independent of the continuum light curve. The dips at 0.25 and 0.75 phase in the emission line curve can be explained if there is a CQ Cephei kind of stream from the secondary to the primary, whose different portions are occulted by the secondary and primary respectively at the above phases. It has been noted that the two outbursts of T CrB in 1866 and 1946 were removed by an exact number of orbital cycles. They occurred at phase 0.68 ± 0.005 (Webbink *et al.* 1987). This has led to the suggestion that there is some kind of phase switching of the mass transfer (Peel 1990). It may also be noted that the secondary maximum in the outburst light curve occurred 106 days (0.47 difference in phase) after the primary maximum. This timescale has been suggested to be the timescale for viscous dissipation of the ring formed at phase 0.68 and its consequent collapse onto the primary (Webbink 1976). In such an event, the interval between phase

tion timescale for the matter ejec

monitoring of the nova from ultraviolet to red region of the spectrum over an entire

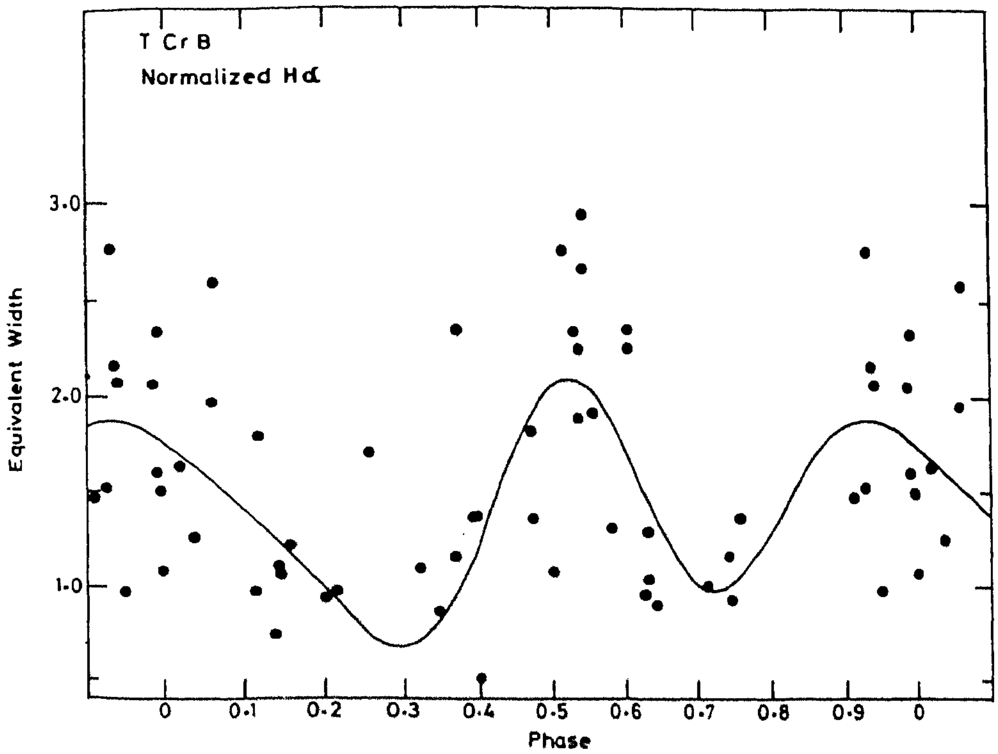

Fig. IV.2.3 Equivalent width of Hα emission in T CrB, normalized by division by the smooth curve in Fig. IV.2.2, folded over orbital phase. The smooth curve in this figure is the truncated Fourier series fit of Equation IV.2.1.

orbital period, and modelling in terms of different components is necessary before one can distinguish between different scenarios.

3. T Pyxidis

This recurrent nova has experienced outbursts in 1890, 1902, 1920, 1944, and 1966, with a mean outburst interval of 19 years. It is the only recurrent nova with an extremely slow development of the optical light curve during outbursts. The outburst is characterized by a slow rise to maximum (32 days) after an initial rapid rise of about three days, a relatively flat maximum and an extremely slow decline at a rate of 0.033 magnitude per day (Landolt 1970; Webbink *et al.* 1987; Payne-Gaposchkin 1957). The spectral development of the 1967 outburst was studied in detail by Catchpole (1969). The development is similar to that of classical novae of similar speed class in many respects. Catchpole (1969) detected different velocity systems at 850 km s^{-1} and 1255 km s^{-1} 12.5 days since initial halt and $\sim$ 2000 km s^{-1} $\sim$ 70 days after initial halt. These velocities have been attributed to the principal, diffuse enhanced and Orion system respectively. T Pyx however differs from classical novae in the formation of high excitation lines in its early stages, a feature commonly observed in recurrent novae. [Fe XIV] 5303 Å coronal line was detected about 50 days after the initial halt (Catchpole 1969). Coronal lines are generally absent in the spectra of slow classical novae. In RS Oph, the coronal lines are formed in the ejecta shock heated as a result of interaction with the pre-existing circumstellar wind. No evidence for such an interaction is present in the 1967 outburst spectrum of T Pyx.

T Pyx is the only known recurrent nova having a discernible nebular shell around it. Narrow band imaging in Hα by Duerbeck & Seitter (1979), Williams (1981, 1982), Duerbeck (1987), Seitter (1987) and Shara *et al.* (1989) has revealed a nebulosity $\approx$ 10 arcsec diameter around T Pyx. A fainter extension at $\approx$ 20 arcsec diameter has been detected by Shara *et al.* . The brighter portion of the shell has been attributed to the 1944 outburst by Seitter (1987), Duerbeck (1987) and Shara *et al.* (1987), the fainter extension is a result of earlier outbursts. Shara *et al.* also find a 2 arcsec radius ring around the central star, which may be the 1966 ejecta. The 10 arcsec shell does not seem to have expanded much since its first detection in 1979 (Seitter 1987; Shara *et al.* 1989). Spectral scans in the range 3500–7000 Å of the northern portion of the shell by Williams (1982) is similar to that of a normal gaseous nebula. Emission lines of [O II] 3727 Å, [O III] 4959, 5007 Å, Hα, Hβ and [N II] 6584 Å are the most prominent. Also present in the spectrum are Hγ, Hδ, He I 5876 Å, [O III] 4363 Å and He II 4686 Å. The relative intensities of the lines indicate excitation conditions similar to those observed in planetary nebulae implying photoionization of the shell by ultraviolet radiation from the stellar nova remnant (Williams 1982). The similarity of the T Pyx shell spectrum with planetary nebulae led Williams (1982) to conclude that the abundances in the shell are roughly solar, but with some nitrogen enhancement. The shell mass is estimated to be $\leq 1 \times 10^{-4}\ M_\odot$ by Shara *et al.* (1989) and $8 \times 10^{-5}\ M_\odot$ by Seitter (1987).

At quiescence, T Pyx lies at a mean magnitude $V_{\rm min} = 15.23$, with mean colours $(B-V)_{\rm min} = +0.099$, $(U-B)_{\rm min} = -0.99$, $(V-R)_{\rm min} = +0.175$ (Webbink *et al.* 1987 and references therein). Bruch, Duerbeck & Seitter (1981) estimate $A_V = 1.12$ corresponding to $E(B-V) = 0.36 \pm 0.05$ (Webbink *et al.* 1987) based on the 2200 Å interstellar feature. The absence of a $(V-R)$ excess excludes the possibility of a luminous red giant secondary in T Pyx (Webbink *et al.* 1987).

The distance estimates of T Pyx are still very uncertain. Based on the equivalent widths of the interstellar calcium K line, Catchpole (1969) arrived at a mean distance of 1050 pc, which may be regarded as a lower limit. Duerbeck (1981), using the M_V–t_3 relationship for classical novae, derived $M_v(\max) = -7.4$. The mean observed magnitude at maximum $V_{\max} = 7.0$ (Catchpole 1969; Landolt 1970) with the extinction given above gives a distance $D = 4500$ pc as an upper limit (Webbink *et al.* 1987). In a spectrum of the shell of T Pyx, Shara *et al.* (1989) detected an expansion velocity of 350 km s^{-1}. This velocity is consistent with a 1 kpc distance if the bright region of the shell is due to the 1944 outburst. If however, the bright shell is due to even older outbursts, then larger distances are implied.

The mean visual luminosity at outburst is an indicator of the outburst mechanism. A distance at the upper limit of the estimate (4500 pc) implies a super-Eddington luminosity ($\log[L_V(\max)/L_\odot] = 5.2$) at maximum, whereas the lower limit gives a luminosity almost at the Eddington limit ($\log[L_V(\max)/L_\odot] = 3.7$). In the thermonuclear runaway models for recurrent novae, which assume the white dwarf mass close to Chandrasekhar limit (Starrfield, Sparks & Truran 1985), nuclear burning in outburst proceeds at a luminosity approaching the Eddington limit ($L_{\rm ed}/L_\odot = 3.8 \times 10^4 M/M_\odot$; Webbink *et al.* 1987). The outburst light curve of T Pyx is very similar to slow classical novae (*e.g.* HR Del, RR Pic, V1816 Cyg). Also, the spectral development and appearance of different velocity systems during outburst is very similar to classical novae. During the rise to maximum, the broad band colours of T Pyx become redder (Eggen, Mathewson & Serkowski 1967). This behaviour is also typical of classical novae. In case the outburst is powered by accretion events, the spectrum should become bluer during rise to maximum, as in the case of dwarf novae. Also the emission-line outburst spectrum is unlike the dwarf novae which normally have absorption-line or continuous spectra during outburst. The timescales of the rise and decline of T Pyx outburst are much longer than the accretion event outbursts. All the above considerations imply a thermonuclear runaway event.

The optical spectrum of T Pyx at quiescence is dominated by the hot component. The continuum is extremely blue. Emission lines characteristic of disc spectrum dominate the spectrum (Williams 1983; Duerbeck & Seitter 1989). Balmer lines, He I lines and He II lines are very prominent. He II 4686 Å is much stronger than Hβ. This implies a hot primary with temperature $\sim 10^5$ K. The colours of T Pyx at

Table IV.3.1 Details of T Pyx shell images.

Date			Filter	Telescope
1986	May	10.04	Hα+[N II]	ESO Danish 1.5 m
		10.05	Hα+[N II]	ESO Danish 1.5 m
1987	Feb	4.	Hα+[N II]	ESO/MPI 2.2 m
		4.	[O III]	ESO/MPI 2.2 m
1989	Apr	1.65	Hα+[N II]	VBO 1.02 m
		1.71	Hα+[N II]	VBO 1.02 m
	Apr	2.63	Hα+[N II]	VBO 1.02 m
		2.68	Hα+[N II]	VBO 1.02 m

minimum are much bluer than would be expected from an extended accretion disc. Two possible explanations for the blue colours consistent with the thermonuclear models are given by Webbink *et al.* (1987): (1) the binary is sufficiently compact and the mass transfer rate sufficiently high so that the temperature of the outer edge of the accretion disc is extremely hot and only the Rayleigh–Jeans tail of the disc luminosity is visible optically. This explanation is feasible only if the mass transfer rate were as high as $\sim 5 \times 10^{-8}\ M_\odot\ \mathrm{yr}^{-1}$ and the binary is an ultrashort period system. (2) it is possible that optically one sees the Rayleigh–Jeans tail of the flux from a bloated white dwarf plus reprocessed radiation from the secondary.

Differential photometry of T Pyx in the B band by Shaefer (1990) indicates an orbital period of 2.3783 hr. In the Fourier transform of his data, Shaefer finds another peak corresponding to 2.6403 hr. Although a definite choice between the two is not possible, Shaefer (1990) puts the odds as roughly 2 to 1 that the 2.3783 hr period is correct, as its peak is 0.6 higher. It is interesting to note that the orbital period for T Pyx is in the middle of the period gap in cataclysmic variables. Shaefer also estimates the mass ratio $M_s/M_p = 0.15$, secondary mass $= 0.20\ M_\odot$ for a white dwarf primary with mass close to Chandrasekhar limit, and secondary radius $R_s = 0.25\ R_\odot$, based on his estimates of $0.00028\ M_\odot$ for the mass function and 27° for the inclination.

3.1 The Shell

Hα+[N II] CCD images of the shell of T Pyx were obtained on 1989 April 1 and 2 at the Cassegrain focus of the 102 cm telescope at VBO. The Hα+[N II] 50 Å

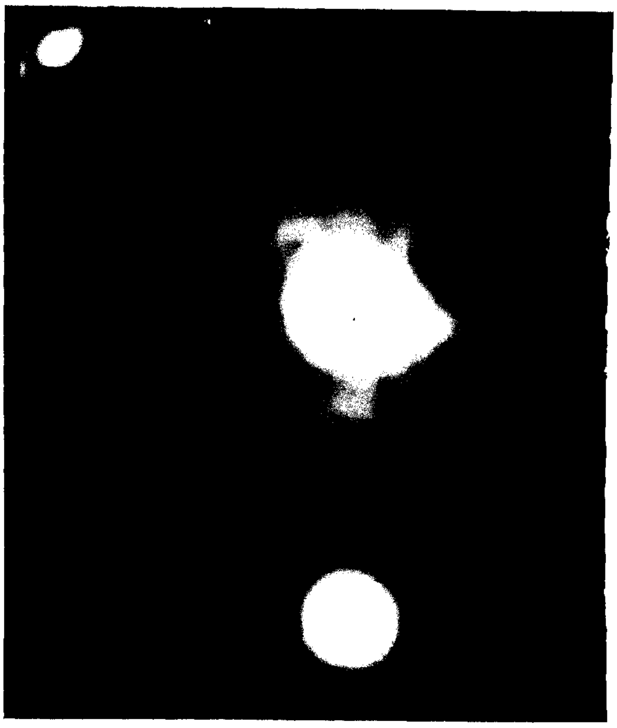

Fig. IV.3.1 T Pyx shell through [N II] emission obtained from VBO on 1989 April 1–2. North is at the top and east to the left. Scale: 1 mm = 0.29 arcsec.

interference filter was used to image the shell onto the Photometrics CCD system. Four frames, each of 30 min exposure were obtained at seeing conditions of 2 arcsec. These frames were individually de-biased and flat fielded as described in Chapter II. Flat field images were obtained from twilight sky exposures. The flat field images of both the nights were 'stacked' and the mean image was used for flat field correction of all the four frames. The frames were aligned and then averaged following the procedure described in Chapter II. A shift+rotation transformation was applied to the frames while aligning. The mean Hα+[N II] image was smoothed using 3×3 Gaussian filter ($\sigma = 1$). Table IV.3.1 gives the details of observations.

Hα+[N II] and [O III] images obtained at ESO by H.W. Duerbeck and his collaborators have also been used in this study. The dates of these observations are also listed in Table IV.3.1. The ESO images were aligned with respect to the VBO image. A six coefficient shift+rotation+shear+stretch transformation as given in Equations II.2.1 and II.2.2 was used to align the images and bring them to the same scale as VBO data (0.36 arcsec per pixel). The Hα+[N II] CCD image obtained at VBO and the 1987 ESO CCD image are shown in Figures IV.3.1 and IV.3.2, respectively. Figure IV.3.3 shows the [O III] image.

In the Hα+[N II] images the shell appears clumpy. It is symmetric along the

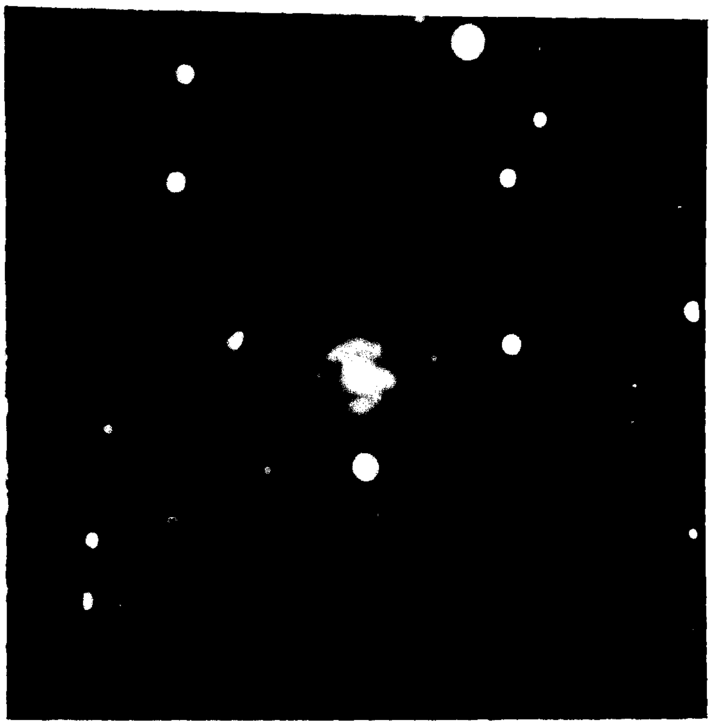

Fig. IV.3.2 T Pyx shell through [N II] emission obtained from ESO on 1987 February 4. North is at the top and east to the left. Scale: 1 mm = 0.98 arcsec.

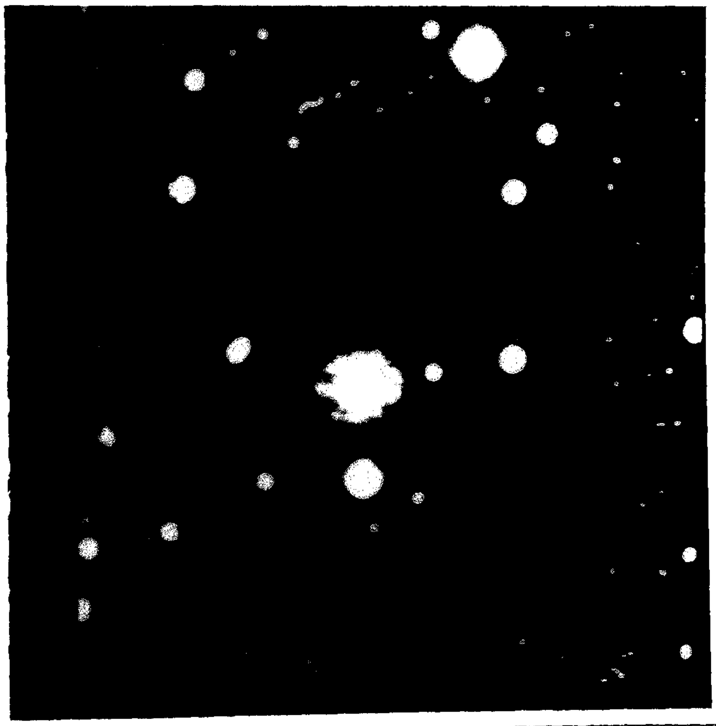

Fig. IV.3.3 T Pyx shell through [O III] emission obtained from ESO on 1987 February 4. North is at the top and east to the left. Scale: 1 mm = 0.98 arcsec.

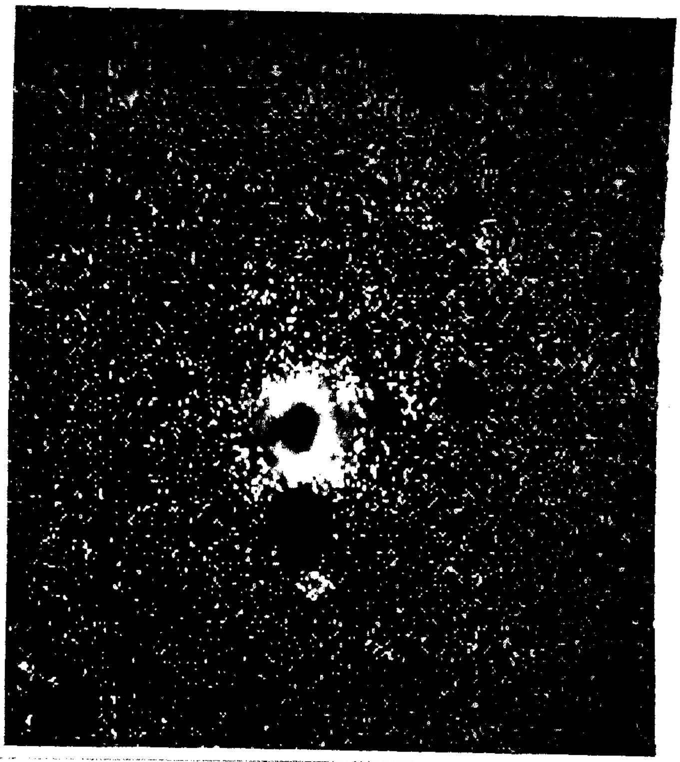

Fig. IV.3.4 [N II]/[O III] ratio image of T Pyx shell. North is at the top and east to the left. Scale: 1 mm = 0.90 arcsec.

north-south direction, but asymmetric along the east-west with very little emission in the east portion of the shell. The region of [O III] emission is more symmetric than Hα+[N II] region. [O III] is stronger than Hα+[N II] in the east direction. A ratio image of Hα+[N II]/[O III] was obtained by dividing the 1987 Hα+[N II] and [O III] images. This is shown in Figure IV.3.4. From this ratio image it is very clear that Hα+[N II] emission is stronger than [O III] emission at all directions but the east. Spectral scans across the northern portion of the shell by Williams (1982) also indicate Hα+[N II] is stronger than [O III] in that region. Also [N II] is stronger than Hα by a factor of ~ 2. The Hα+[N II] emission image is hence predominantly [N II] emission. The difference in the spatial distribution of the [O III] and [N II] emission regions indicates chemical inhomogeneities in the shell.

Intensity cuts through T Pyx were obtained along the north-south as well as along the east-west directions in [N II] images. The angular distance at half-maximum intensity level from the central star of T Pyx was measured in the intensity cuts of 1986, 1987 and 1989 images. The measured angular size of the shell is 13.0 arcsec, 13.1 arcsec and 13.2 arcsec in 1986, 1987 and 1989 respectively. The apparent 0.2 arcsec expansion in 3 years and the expansion velocity of 350 km s^{-1} estimated spectroscopically by Shara *et al.* (1989), imply a distance of 1100 pc for

T Pyx. Spectroscopic observations of the outbursts of T Pyx indicate an ejection velocity of 850 km s^{-1}. Assuming a steady deceleration of the velocity of the shell, the angular size of the shell of 13.0 arcsec is consistent with the 1944 outburst origin of the shell at the estimated distance of 1100 pc. The sizes of the shell could however have a ± 0.1 arcsec measurement error, which means the distance could be twice as large *i.e.* ~ 2200 pc, if the expansion is only 0.1 arcsec in 3 years.

In the intensity cut of the 1987 ESO [N II] image, a fainter extension of the shell is observed, apart from the bright ~ 10 arcsec shell. This faint region extended upto ≈ 18.0 arcsec and appeared symmetric. Shara *et al.* (1989) attribute this faint extension to outbursts earlier than 1944. This faint extension is barely discernible in the [O III] image. The size of this extension is consistent with a 1920 outburst origin, at a distance of 1100 pc for the nova.

The temperature and density conditions in the shell can be obtained from the emission line fluxes. Based on the Hβ measured flux for the northern portion of the shell, $F_{H\beta} = 3.5 \times 10^{-15}$ erg cm^{-2} s^{-1} (Williams 1982) the density of the shell in that region may be estimated as $\log n_e = 1.95^{+0.50}_{-0.25}$ where the upper and lower limits depend on the assumed geometry of the shell. Using this density and the observed ratio of [O III] (4959+5007)/4363, the temperature is estimated to be 2.7×10^4 K. Using the [O II] 3727 Å, [O III] 4363, 4959 and 5007 Å lines we estimate $O^+/H^+ = 3.77 \times 10^{-6}$ and $O^{++}/H^+ = 8.63 \times 10^{-6}$. From [N II] 6584 Å line, we obtain $N^+/H^+ = 1.43 \times 10^{-5}$. Since the abundances in other ionization states of these elements are not known, it is not possible to obtain O/H and N/H, and the above estimates are a lower limit to the abundances. However the density and temperature in the shell and also the spectrum being similar to planetary nebulae, the abundances would be more like solar (Williams 1982). The strength of [N II] emission in the spectrum (Williams 1982; Seitter 1987) as well as in the images indicates a possible overabundance of nitrogen. Nitrogen overabundance is consistent with the thermonuclear runaway outburst models (Starrfield 1989). The mass of the emitting shell may be obtained from the observed Hβ flux, the computed density and volume obtained from the measured angular size of the shell. Using a distance of 1100 kpc we estimate the emitting mass $M_n = 3 \times 10^{-5} M_\odot$ for the northern portion of the shell. The total mass of the shell would thus be $\sim 1 \times 10^{-4} M_\odot$; in good agreement with the estimate of Seitter (1987): $8 \times 10^{-5} M_\odot$.

Table IV.3.2 Journal of spectroscopic observations of T Pyx.

Date UT			Wavelength range Å
1989	Nov	25.91	4500–7600
	Dec	4.93	4500–7600
	Dec	31.91	4500–7600
1990	Jan	2.81	4500–7600
	Feb	21.82	4500–7600
	Mar	30.63	4500–7600
	Mar	31.65	4500–7600
	Apr	1.63	4500–7600

3.2. The Quiescent Spectrum

Spectra of T Pyx in the wavelength range 5500–7600 Å were obtained from VBO during 1989 November to 1990 April. The spectra were obtained using the Photometrics CCD system with the UAG spectrograph and 250 mm camera at the Cassegrain focus of the 102 cm telescope. The 150 l mm^{-1} grating was used to give a resolution of 5.5 Å per pixel. Table IV.3.2 gives the journal of observations.

All spectra were individually de-biased, flat field corrected and extracted following the procedure described in Chapter II. A Fe+Ne comparison source was used for wavelength calibration. Bright night sky emissions due to [N II] and [O I] have been removed from all spectra following the method described in Chapter II. Spectrophotometric standards were used for flux calibration. The flux calibrated spectra were averaged to improve the signal to noise ratio. The region below 5500 Å is very noisy and has hence not been used.

The continuum in T Pyx is very blue as compared to RS Oph and T CrB (Duerbeck & Seitter 1989; Williams 1983; also §IV.1 and §IV.2). The spectrum does not show any signature of the cool component, indicating the secondary in T Pyx is not similar to the secondaries of RS Oph and T CrB. The spectrum appears similar to accretion disc spectra: strong emission lines of hydrogen Balmer series, He I 4471, 4922, 5015, 5876, 6678 Å, He II 3924, 4686, 5411 Å and O II 4639 Å are present superposed over the continuum (Williams 1983; Duerbeck & Seitter 1989).

Figure IV.3.5 shows the mean flux spectrum of T Pyx central star, corrected for interstellar reddening using $E(B-V) = 0.36$ (Webbink *et al.* 1987) and the

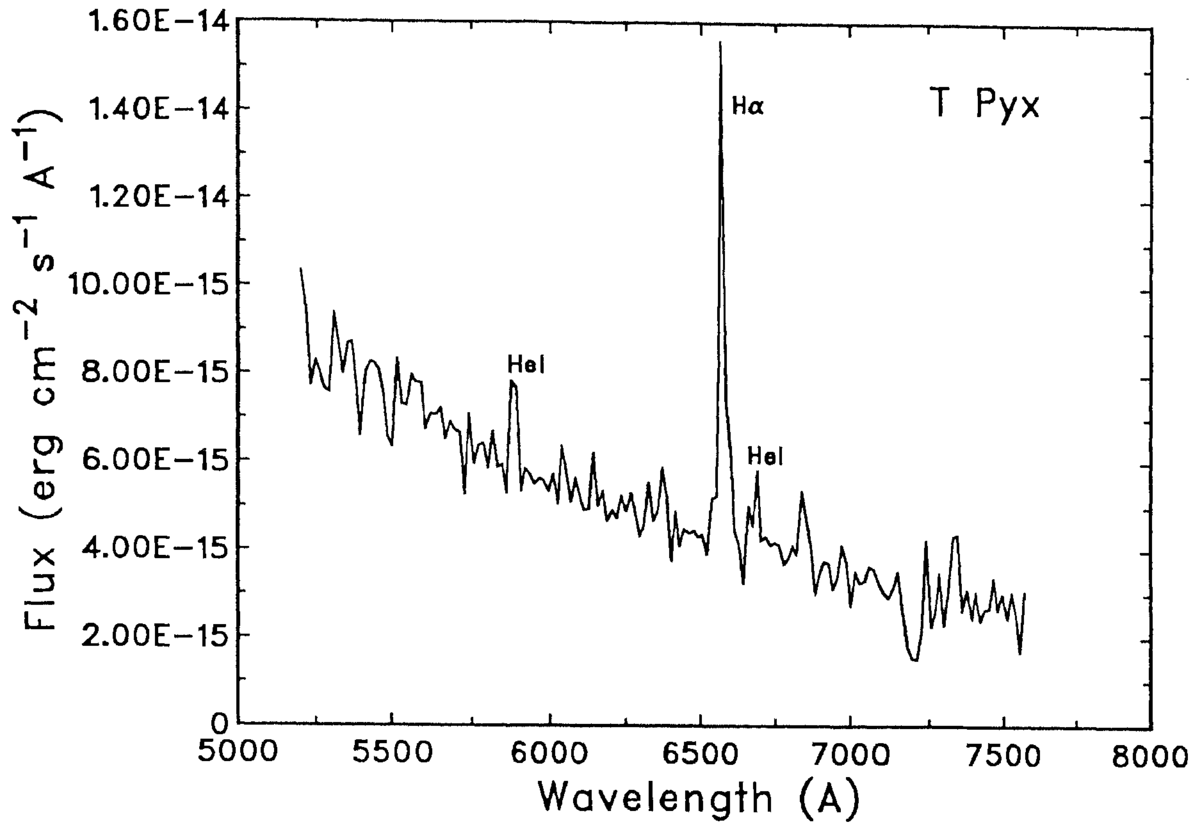

Fig. IV.3.5 Spectrum of T Pyx in the region 5500–7600 Å corrected for $E(B-V)$=0.36. Epoch: 1989 November 25–1990 April 1.

Savage & Mathis (1979) law. The signal-to-noise being poor, only lines of He I 5876, 6678 Å and Hα are seen in the spectrum. The structured appearance of Hα is due to Hα from the disc and [N II] emission from the shell around T Pyx. Helium lines are strong. He II 4686 Å is $\sim$ 1.5 times stronger than Hβ (Williams 1983; Duerbeck & Seitter 1989). The strength of helium lines indicates a very hot ionizing source, which could be the white dwarf primary itself, and/or the accretion disc boundary layer near the surface of the white dwarf, with a likely contribution from the hot, inner region of the accretion disc itself.

The emission line fluxes corrected for interstellar reddening are listed in Table IV.3.3. Also listed in the table are the line fluxes from Duerbeck & Seitter (1989). The Hα line flux (in VBO spectrum) has been corrected for contribution from [N II] as well as Hα emission from the shell. The Balmer decrement is flat with Hα/Hβ $\sim$ 2, similar to GK Per (see §III.4.2), indicating high densities in the emitting medium. From the models of Drake & Ulrich (1980), it is inferred that $T_e \gtrsim 10^4$ K, $n_e \gtrsim 10^{12}$

Table IV.3.3 T Pyx: emission line fluxes corrected for $E(B-V) = 0.36$.

Line identification λ in Å		Flux 10^{-14} erg cm^{-2} s^{-1}
4686	He II	9.2*
4861	Hβ	11.0*
5876	He I	2.9†
6563	Hα	15.7
		20.6*
6678	He I	2.2†
7065	He I	0.7*

* From Duerbeck & Seitter (1989).

† Both VBO and Duerbeck & Seitter (1989).

cm^{-3} in the accretion disc of T Pyx. The mean reddening corrected V magnitude of 14.1 at quiescence (Webbink *et al.* 1987) implies $M_V = +3.9$ at 1100 pc and $M_V = +0.8$ at 4500 pc. Assuming the V flux as entirely due to the accretion disc and using Equation III.1.22, the mass accretion rate $\dot{M}$ may be estimated. Using the value of 27° for inclination as estimated by Shaefer (1990), and a white dwarf mass $\geq 1.3\ M_\odot$, the mass accretion rate is $\dot{M} \sim 3 \times 10^{-9}\ M_\odot$ yr^{-1} for a distance of 1100 pc and $\dot{M} \sim 2 \times 10^{-7}\ M_\odot$ yr^{-1} for a distance of 4500 pc. It has been suggested by Webbink *et al.* (1987) that we are observing the high frequency end of the accretion disc spectrum in the optical region. This appears reasonable since the separation of the system is $\lesssim 1\ R_\odot$. Following §III.2 it is likely that the spectrum turns off earlier than V, and hence the mass transfer rate estimated above is a lower limit.

Using the He I and He II line fluxes together with the hydrogen line fluxes, the helium abundance and the temperature of the central ionizing source can be obtained. The observed He I 5876/7065 ratio of 4.02 lies between $n_e = 10^{11}$ cm^{-3} and $n_e = 10^{12}$ cm^{-3} for an optical depth of He I 3889 Å line $0 \leq \tau(3889) \leq 0.8$ at $T_e = 10^4$ K in the models of Almog & Netzer (1989). Logarithmically interpolating, it is found that observed 5876/7065 ratio is reproduced for $n_e = 4 \times 10^{11}$ cm^{-3}, $\tau(3889) = 0.5$ at $T_e = 10^4$ K. Using the observed line ratios of He I 5876/Hβ, 5876/Hα, He I 7065/Hβ, 7065/Hα, He$^+$/H$^+$ is obtained. Similarly, He II 4686/Hβ line ratio is used to obtain He^{++}/H$^+$. Taking the He I emissivities from Almog & Netzer, interpolated for $n_e = 4 \times 10^{11}$ cm^{-3} and $\tau(3889) = 0.5$, and the hydrogen emissivities from Hummer & Storey (1989), at $n_e = 10^{10}$ cm^{-3} (since emissivities for higher n_e have not been calculated there), a mean $\langle He^+/H^+ \rangle = 0.12 \pm 0.02$ is obtained. Similarly, taking He II emissivities from Hummer & Storey, $He^{++}/H^+ = 0.102$ is obtained. The helium abundance is He/H = 0.22. As in the case of GK Per (§III.4.2), this estimate would be an upper limit for the abundance. Using the observed ratio of He II 4686/Hβ the temperature of the ionizing source is estimated to be $T_s = 5.8 \times 10^5$ K. Duerbeck & Seitter (1989) estimate the temperature to be of the order of 10^5 K. The radius of the source of ionization as derived using Equation III.1.14 is 0.004 $R_\odot$ for an assumed distance of 4.5 kpc, and assuming that only 1% of the radiation is intercepted by the disc. If the distance is smaller and/or the disc intercepts more radiation, the derived radius would be still smaller. Since this value is much smaller than that of a typical white dwarf, it would appear that the line emitting region is not radiation bounded. In such an event the derived temperature is an overestimate.

4. Concluding Remarks

The optical spectroscopic data on RS Ophiuchi obtained at VBO between 32 and 108 days since the 1985 outburst of the nova, and during its subsequent quiescence; spectroscopic data on T CrB during the years 1985–1990; spectrum of the T Pyx system and [N II] images of the nebular extension around it have been presented. Also presented are the images of T Pyx in [N II] and [O III] obtained at ESO by H.W. Duerbeck & his collaborators.

The evolution of the outburst spectrum of RS Oph is similar to the past outbursts, in the narrowing of lines, appearance of coronal and other high excitation lines. The electron density in the ejecta fell from 3.1×10^9 cm^{-3} on day 32 to 1.8×10^8 cm^{-3} on day 108, as deduced from the optical data. The values are consistent with the estimate based on the Si III] 1892 Å, C III] 1909 Å ultraviolet line ratio. The mass of the ejected envelope was $(3.1 \pm 0.6) \times 10^{-6}$ $M_\odot$. A helium abundance of n(He)/n(H)=0.16 has been derived. The temperature in the shock-heated region, estimated from the [Fe XI]/[Fe X] coronal line ratios decreased from 1.5×10^6 K on day 32 to 1.1×10^6 K on day 108. The temperature deduced from different coronal lines mutually differ by ~ 10 percent indicating temperature gradients in the cooling shocked ejecta.

The temperature of the photoionizing source estimated using the hydrogen and helium lines increased from 3×10^4 K on day 32 to 3.6×10^5 K on day 204. The latter estimate agrees with that of Mason *et al.* (1987) based on x-ray observations. Assuming that the geometrical factors permit only a tenth of the ionizing radiation to be absorbed by the envelope, we estimate that the radius of the source decreased from a value of 2×10^{12} cm on day 32 to 6×10^{9} cm on day 204. The radius estimate of day 204 compares well with the radii of white dwarfs. It is difficult to get such a compact emitting region if the accreting star is a main sequence star (M. Kato 1990: preprint). The implied blackbody luminosity decreased from a value of 3×10^{39} erg s^{-1} on day 32 to nearly a constant value of 6×10^{38} erg s^{-1} between days 90–204. The increase in temperature of the ionizing source and a decrease in its radius is similar to the behaviour of classical novae during the constant bolometric luminosity phase following an outburst (Starrfield, Sparks & Truran 1985; Ferland 1979; Krautter & Williams 1988; Martin 1989). The outbursts of RS Oph are most likely powered by thermonuclear runaways on the surface of a white dwarf primary.

The spectra of both RS Oph and T CrB at quiescence are composite, consisting of TiO bands and superposed emission lines. The presence of TiO bands is indicative of a late-type secondary. The spectral type of the secondary, estimated based on the spectral indices of TiO 6180 Å and 7100 Å bands is M1$\pm$1 III in RS Oph and M4$\pm$1 III in T CrB. The energy distribution of RS Oph is much bluer than that of a normal M0-2 III star. This implies contribution from the hot component. The presence of O I 7774 Å in absorption implies an optically thick accretion disc (Friend *et al.* 1988). Assuming steady state accretion disc, an estimated disc spectrum $10^{-3.55}\lambda^{-2.33}$ erg cm^{-2} s^{-1} Å^{-1} was found to account well for the excess in observed fluxes in the optical and infrared J band over a normal M-type star. The accretion disc flux at 5500 Å corresponds to $M_V = -1.4$ mag, a value 0.8 magnitudes brighter than the secondary ($M_V = -0.6$ mag). This estimate is slightly fainter than the estimate of Bruch (1986). The estimated M_V for the accretion disc corresponds to a mass transfer rate $\dot{M} \sim 5 \times 10^{-6}\ M_\odot$ yr^{-1} for a white dwarf with mass approaching the Chandrasekhar limit. In the thermonuclear runaway models for recurrent novae, mass transfer rates of this order imply a recurrence rate of ~ 2 years for the nova outbursts (Starrfield, Sparks & Shaviv 1989).

The absence of significant excess in the spectrum beyond 1.6 μm implies negligible contribution from the accretion disc in that region. In steady state, optically thick discs, the disc spectrum is dependent on the central source temperature and the finite size of the disc. The estimated mass-transfer rate of $5 \times 10^{-6}\ M_\odot$ yr^{-1} implies a temperature $T_* = 8 \times 10^5$ K for the central source. Assuming a turnover in the disc spectrum at H band (1.4 μm), disc radius $R_{\rm disc} \approx 12\ R_\odot$ for $T_* = 8 \times 10^5$ K and $M_{\rm WD} = 1.3\ M_\odot$ is estimated.

No clear evidence exists for the presence of a white dwarf primary in T CrB. However, the similarity between the two systems RS Oph and T CrB and the observed ultraviolet luminosity of T CrB (Cassatella & Selvelli 1989) are suggestive of a white dwarf primary. The energy distribution of T CrB in the optical region observed by us (4500–9200 Å) matches well with a normal M3-4 III star. This indicates negligible contribution from the accretion disc at these wavelengths. A 10 percent contribution to the flux at 5500 Å (as estimated from the mean ultraviolet luminosity) would imply $M_V = +1.4$ mag corresponding to $\dot{M} \sim 10^{-7}\ M_\odot\ {\rm yr}^{-1}$ onto a white dwarf of mass $M_{\rm WD} \geq 1.3\ M_\odot$. The reduced mass transfer rate in comparison with RS Oph appears to increase the recurrence period in T CrB.

The ultraviolet spectrum of T CrB is flatter ($\propto \lambda^0$–$\lambda^{-1.5}$) than a typical accretion disc spectrum. This may indicate that the cutoff due to the inner boundary of the accretion disc is reached $\sim$ 1000 Å. Analysis described in §III.2 leads us to estimate that the accretion disc begins at a few white-dwarf radii and does not reach the surface of the white dwarf. The faintness of RS Oph in the ultraviolet may also be due to a similar cause. These two systems are the widest known nova systems and the specific angular momentum of the accreted matter is about two orders of magnitude larger than in typical novae. The difference in the disc structure may be attributed to this fact.

The emission lines in RS Oph most probably arise in a ring around the secondary formed due to the stellar wind. In T CrB however, the emission lines arise mainly in the accretion disc, and their strengths are found to be variable. Using the Hα equivalent widths, an orbital phase dependence of this variability has been detected. Emission maxima occur at phases 0.93 and 0.53. These maxima are out of phase with the broad band light curve in the blue, which shows minima at phases 0 and 0.5 (Peel 1990). In addition to this orbital phase dependent variation, a long term variation with a period $\sim$ 2400 days has been detected in the Hα light curve. The orbital phase dependent variations in the broad band as well as line emissions indicate two possibilities: (i) geometrical effects as the system is seen from different aspect angles; (ii) physical effects that switch on and off as a function of orbital phase. The coincidence in the occurrence of the two outbursts of T CrB at phase 0.68 is suggestive of some kind of phase switching of the mass transfer. A detailed nearly simultaneous spectrophotometric monitoring of the nova from the ultraviolet to infrared region of the spectrum over an entire orbital period, and modelling in terms of different components is necessary for a clear understanding of this system. It is also desirable to monitor the emission line profiles at good spectral resolution.

The quiescence spectrum of T Pyx is quite different from that of both RS Oph and T CrB. The continuum is very blue and does not show any signature of the cool component, indicating the secondary spectral type and luminosity is earlier than M giants. The spectrum of T Pyx is essentially an accretion disc spectrum. At an assumed mean distance of 2.2 kpc the accretion disc has an $M_V = +2.4$ corresponding to a mass transfer rate of $\sim 10^{-8}\ M_\odot\ \mathrm{yr}^{-1}$, which is a lower limit since the spectrum probably turns over at wavelengths less than V due to a small separation of the system. Helium lines are very strong, with He II 4686 Å ~ 1.5 times stronger than Hβ. The flat Balmer decrement of Hα/H$\beta \approx 2$ indicates densities $\gtrsim 10^{12}$ cm^{-3} and temperatures $\gtrsim 10^4$ K in the accretion disc. From the observed ratios of the helium and hydrogen lines, a helium abundance He/H ≤ 0.22 is estimated. Using the He II 4686/Hβ ratio, the temperature of the ionizing source is estimated to be $T_s = 5.8 \times 10^5$ K. The derived radius of the white dwarf is too small, which suggests that the line forming region is not radiation bound and the estimated temperature is too high.

The shell of T Pyx appears clumpy in [N II] emission. The shell in [N II] is symmetric along the north-south direction, but asymmetric along the east-west, with very little emission in the east. In [O III], the shell is more symmetric than in [N II]. The shell is stronger in [N II] in all directions but the east. The difference in the spatial distribution of the [O III] and [N II] emission regions indicates inhomogeneities in the O/N abundance ratio in the shell. Abundances in the shell are nearly solar with an enhancement of nitrogen. The density in the shell is ~ 100 cm^{-3} and temperature $\sim 3 \times 10^4$ K. The mass of the shell is estimated to be $\sim 10^{-4}\ M_\odot$.

The angular size of the shell of T Pyx is ≈ 13 arcsec. Intensity cuts of the [N II] image through the central star show an expansion of 0.2 arcsec in 3 years, implying a velocity of 320 km s^{-1} at a distance of 1 kpc for T Pyx. This velocity estimate agrees with the 350 km s^{-1} shell velocity detected spectroscopically (Shara *et al.* 1989). For an assumed distance ~ 1 kpc, the angular size of 13 arcsec is consistent with the 1944 outburst origin. A faint symmetric extension of the shell upto ≈ 18 arcsec is seen apart from the bright shell, which can be attributed to the 1920 outburst.

V. Concluding Remarks and Future Prospects

Nova outbursts are understood to take place in interacting binary systems where a white dwarf accretes matter from the Roche-lobe filling secondary through an accretion disc. When a critical amount of matter is accreted, thermonuclear runaway reactions take place on the surface of the white dwarf. The result of the injection of the energy released over such a short duration is the ejection of the envelope (see Starrfield 1989). As the envelope expands, in some cases, there is a nucleation of dust particles. The envelope interacts with the ambient medium which may simply contain the interstellar matter, or also the matter lost through slow wind by the secondary, the matter ejected at the previous outbursts, or even the matter ejected during a previous planetary nebula phase that gave birth to the white dwarf. In some cases the nebula may provide perceptible angular disc many years after the outburst. When the envelope has expanded out, it becomes easier to study all the components of the central system. Observations of outburst and quiescence through all the available windows of electromagnetic radiation — both ground-based as well as satellite-borne — add the vital information needed to construct a more detailed account of the above scenario.

In this chapter specific problems under the general context of the nature and evolution of a nova system are described. In each area the contribution of the present study is summarized, and prospects for the future brought out.

1. The Nova System

Though the interacting binary model of novae is universally accepted, detailed models are available only for a few systems. In particular, one requires the estimates of the mass and composition of the white dwarf, the characteristics of the secondary, the mass transfer rate, the structure of the accretion disc, the composition of the mass transferred, the mass-loss rate from the secondary in the form of steady wind, *etc.* Indeed, it has even been suggested the primary in some recurrent novae is a main sequence star instead of a white dwarf. In the following, individual components are focused upon.

The primary

A direct evidence for the white dwarf can be obtained only from observations in the far ultraviolet, after the short-wavelength turnover of the accretion disc spectrum. Even there it would be difficult to detect it at the mean distance to novae. Recombination lines from the nova envelopes during outburst and the accretion disc at quiescence have been used in the present work to determine the temperature and radius of the source of photoionization.

The temperature of the central source in RS Oph increased from 3×10^4 K early in outburst to 3.6×10^5 K at later epochs. The radius decreased from 9 $R_\odot$ to 0.03 $R_\odot$ during the same period. Thinning out of the inner envelope until the central source becomes bare is thus seen. A similar analysis was not possible at quiescence due to a large contribution to the Balmer lines from the envelope of the cool component. High-resolution observations of the line profiles at different orbital phases will help separation of the emission lines arising in the accretion disc. This can lead to an estimate of the characteristics of the primary. In the case of T CrB the emission lines certainly arise from a region around primary. However, large variations in their strength suggest some non-steady processes are taking place around the primary. Hence no attempt was made here to obtain the characteristics of the primary. More detailed observations are needed before a physical model can be constructed. The central source of Nova Sct 1989 had a temperature of 8.7×10^4 K and radius of 2.8 $R_\odot$, 77 days after outburst. This is identified with the hot white dwarf with an optically thick envelope just as in the case of RS Oph in outburst. Temperature estimates of 1.3×10^5 K for the white dwarf in GK Per and 5.8×10^5 K for the one in T Pyx have been derived, based on the hydrogen and helium emission lines present in the quiescence spectra. The corresponding radii of the white dwarfs are 0.01 $R_\odot$ in the case of GK Per for an assumed distance of 470 pc, and $\ll 0.01$ $R_\odot$ for T Pyx for an assumed distance of 2.2 kpc.

The temperature determination is affected by the following assumptions. (i) The white dwarf is the only source of ionizing radiation. In fact, the boundary layer and the inner regions of the accretion disc may also contribute significantly. The spectral shape of the total ionizing radiation may hence depart from the assumed blackbody radiation. (ii) The line forming region is radiation bound. If not, the H-ionizing radiation would escape preferentially, resulting in a higher estimate of temperature. (iii) Significant contribution to the emission lines may arise from the outer regions of an optically thick accretion disc or from the secondary without irradiation from the white dwarf. The estimate for T Pyx is specifically affected by (ii) as seen from the very low value of the derived radius.

The estimate of radius depends on temperature, and is hence affected by the above uncertainties. In addition, it is also affected by the following factors. (i) The line-emitting region is not spherically symmetric about the central source, and does not intercept all the radiation emitted by it. It appears reasonable to assume that it intercepts about 1 percent of the radiation. The radius varies inversely as the square-root of the fraction intercepted. (ii) The derived radius is proportional to the assumed distance.

The above uncertainties permit only the conclusions that the source of ionization has the dimensions ($R_s \sim 0.01\ R_\odot$) and the temperature ($T_s \sim 10^5$ K) consistent with those of a white dwarf, for RS Oph in late outburst, and GK Per and T Pyx in quiescence. Estimates of the temperature and size of the primary was not possible based on the quiescence observations of RS Oph and T CrB due to uncertainties in the model of line forming region. It should be noted that because of a large separation of binary components in these systems the accreted matter has a large specific angular momentum. This fact would complicate the structure of the inner regions of the accretion disc. The estimates for RS Oph based on outburst observations, however, support the idea that the primary is a white dwarf rather than a bloated main sequence star as suggested by Livio, Truran & Webbink (1986). Better estimates can be obtained only from multiwavelength observations and detailed modelling of the continuum and line emission. Such a study is feasible with the best facilities available on and around the globe.

Though a theoretical relation is avaliable between the mass and radius of a white dwarf (Chandrasekhar 1967), the uncertainties in the radius do not permit an accurate estimation of the mass. It is hence necessary to obtain the mass function from spectroscopic orbits and obtain the mass of the white dwarf using estimates for the mass M_2 of the secondary, and the inclination i of the system to the line of sight. Such studies are feasible with medium and large optical telescopes. The available information suggests that the mass of the white dwarf is $> 0.73\ M_\odot$ in GK Per and possibly $\sim 1.4\ M_\odot$ in the recurrent novae. These estimates are considerably uncertain due to an uncertainty in M_2 and i. Detailed spectroscopic monitoring and modelling can improve the estimates. It is necessary to determine and refine spectroscopic orbits of these systems. Orbits of the emission-line components need to be studied using detailed line profiles (see Selvelli 1989).

The secondary

Based on the spectrophotometric data during quiescence, it has been shown here that the secondaries of RS Oph, T CrB and GK Per are of spectral types M1III, M4III and K0-2IV respectively. Though these determinations do not differ appreciably from the values in literature, the present study has brought out the importance of subtracting out the accretion disc spectrum before the methods of quantitative spectroscopy are employed. All the above systems have evolved secondaries that are bright enough to be observed easily in the red spectrum. The secondary of T Pyx, on the other hand, does not contribute much to the optical spectrum, and is hence not an evolved star. Future attempts at its identification should depend on spectroscopy extending to the near infrared. Our understanding of the secondaries of nova systems in general would be improved considerably from their near-infrared spectroscopy.

The accretion disc and mass transfer rate

The theory of physically thin and optically thick steady accretion discs is sufficiently well developed for a comparison of the observed continuous spectrum. The continuum can be fit well by $f_\nu \propto \nu^{-1/3}$ or $f_\lambda \propto \lambda^{-2.33}$ power laws (see King 1989). It was possible to obtain good fits for RS Oph and GK Per. The observed fluxes in erg cm^{-2} s^{-1} $Å^{-1}$ are $10^{-3.55}\lambda^{-2.33}$ for RS Oph and $10^{-5.02}\lambda^{-2.33}$ for GK Per, with λ expressed in Å units. It is, in principle, possible to obtain a fit for T Pyx, except for the poor signal-to-noise ratio of the present data. Telescopes of aperture greater than 1 m are thus necessary. In the case of T CrB the secondary is much brighter than the accretion disc in the optical region and hence it would be necessary to use the ultraviolet data.

The accretion disc spectrum has turnovers in the ultraviolet due to the finite inner radius of the disc, and in the infrared due to the finite outer radius. With the available ultraviolet data for GK Per, it was possible to determine the inner radius as 10^9 cm; similarly, with the available infrared data for RS Oph, it was possible to determine the outer radius $\sim 10^{12}$ cm. The λ^{-1} ultraviolet spectrum of T CrB suggests the high frequency turnover. The very blue colours of T Pyx suggest that the low frequency turnover is in the blue region of the spectrum itself because of the compact size of the disc. Clearly, it would be rewarding to observe the accretion discs from far ultraviolet to the infrared.

The absolute spectrum of the accretion disc is determined by the product of mass of the white dwarf and the mass accretion rate (Webbink *et al.* 1987). Since the white dwarf mass has a narrow range, the mass transfer rate can be estimated if the distance to the nova can be determined (see §3 below). Mass transfer rates of

$\sim 10^{-6}$, $\sim 10^{-7}$, $\sim 10^{-8}$ and $\sim 10^{-10}$ $M_\odot$ yr^{-1} are estimated for RS Oph, T CrB, T Pyx and GK Per respectively.

Based on the hydrogen and helium line ratios in the spectra of GK Per and T Pyx, it is estimated that the helium abundance is He/H $\lesssim 0.24$ in the accretion discs of these systems. An absorption feature due to O I 7774 Å has been identified in the accretion disc of RS Oph. Detailed model atmospheres of accretion discs are necessary in order to compare these observations, as also of emission line regions of the accretion discs.

The current understanding of the accretion disc is limited to the continuum spectrum of the optically thick discs, and the emission lines from optically thin discs. These ideas are used in the present study. The course of the theoretical studies are taking the direction of modelling absorption lines in optically thick discs that are optically thin to the lines while optically thick to the continuum (Smak 1990). Models of extended atmospheres of accretion discs are likely to become available in near future, and a better comparison of observed profiles of lines in emission and absorption would then be possible. Such studies are also necessary in an attempt to obtain better estimates of the characteristics of the primary.

Spectroscopic studies of dwarf-nova-like outbursts of novae in quiescence will also improve our knowledge of the nature of accretion discs and mass transfer rate since such an outburst is powered by accretion disc instabilities. However, such studies necessarily depend on the efforts of discovery and dissemination of information.

The binary orbit

Spectroscopic orbits are available for GK Per, RS Oph and T CrB. A binary period has been inferred for T Pyx from photometric observations. Fairly good spectral resolution is required for a determination of spectroscopic orbits. Such observations require medium to large size telescopes, and sustained effort in the case of long-period systems such as RS Oph and T CrB.

The absorption line orbits refer to the secondary, whereas at least a part of the emission line is centred around the primary. The orbit of the primary can be determined only after a separation of the emission line component belonging to it. Both the orbits, and an estimate of the inclination of the orbit i to the line of sight are needed before an estimate of the masses of individual orbits can be made. Available methods of determination of i are very inaccurate, in the absence of eclipses. An accurate model of the orbital phase dependent variations of the continuum spectrum and emission lines can constrain the possible range of i. Such variations have been reported in the Hα line from T CrB in the present work. The emission is peaked around phases 0.53 and 0.93. It is important to monitor such variations using a linear detector at good spectral resolution, and also to look for interrelationship between the variations of different lines and the ultraviolet continuum.

Secular variations in the spectra

Long-term variations in the mass transfer rate and in the structure of accretion disc are useful for understanding the cyclic evolution scenario of novae. The class of recurrent novae particularly offer a possibility of observing a complete cycle over a reasonable span of decades. The present investigation has revealed a $\sim$ 2400 day variation in the Hα flux from T CrB. This variation may either be related to the secular changes in the accretion disc — which require to be monitored in the ultraviolet, or in the secondary — such as pulsations, or both. A major fraction of our data is based on photographic spectra with poor photometric accuracy. A linear detector and photometric skies are called for. It is also important to observe the spectrum from the ultraviolet to the infrared.

The ejecta

Observations of the ejecta of a nova explosion in the form of a resolved nebula have manifold interests. The abundances of light elements can be accurately determined by spectroscopic observations of the nebula. Once the nebulosity is resolved, one may look for abundance variations in the nebula — an input yet to enter the models of an outburst. An indication of spatial variations in N/O abundance ratio has been brought out here in the case of GK Per in §III.4.1. It appears that the equatorial plane has an excess of oxygen. Similar indications are also present in T Pyx (§IV.3.1). Spectroscopic confirmation requires large aperture telescopes.

Angular expansion of the shell, together with spectroscopic expansion velocities determined during the outburst provide an accurate estimate for the distance to the nova. A 'nebular parallax' of 1–2 kpc has been determined for T Pyx (§IV.3.1). The expansion was, however, marginally detected over a baseline of 3 years in time. Further monitoring is thus necessary. The use of space telescopes would not only cut down the requirement on the baseline in time, but also the reduced background would enable the identification of individual shells ejected in the past outbursts.

Such an attempt was made by Seitter (1987) from ground-based observations.

In the case of GK Per, the ejected shell is interacting with the remnant of an old planetary nebula (Bode *et al.* 1987; Seaquist *et al.* 1989). The densities in the ambient circumstellar matter in the immediate neighbourhood of the ejecta are higher in the polar region than in the equatorial region. A distance of 470 pc based on early observations was used to determine the initial velocities and decelerations in the equatorial and polar regions using the measured proper motions of knots in the ejecta. The initial velocity was lower in the equatorial regions ($\sim$ 1100 km s^{-1}) in comparison with the polar regions ($\sim$ 1500 km s^{-1}). The higher density ambient medium has decelerated the polar regions more (12.8 km s^{-1} yr^{-1}) than the equatorial region (1.5 km s^{-1} yr^{-1}). The ratio of the equatorial to polar velocity (0.73) is comparable to that deduced for the shell of DQ Her (0.67) based on its images. The shell of DQ Her is expanding relatively freely in the interstellar medium. The observations of structure, expansion parallax and kinematics can be made for a large number of arcsecond size nova shells using space telescopes, and from ground based telescopes using interferometric methods such as speckle interferometry.

It is possible to construct a kinematic model of the ejected shell based on the line profiles observed during the late stages of outburst. An example is provided here in the case of LW Ser (§III.2.3) based on the Hα line profile. The model consists of an equatorial ring and polar cones similar to the ones observed in DQ Her and HR Del among other novae. The optical depth effects were probably still present in the Hα profile. However, it was not possible to obtain either the observations of Hα at later epochs, or of fainter forbidden lines at corresponding epoch, using the 102 cm reflector and the photographic plate. The capabilities have certainly improved since then and it is easier now to obtain more accurate data on novae of similar brightness.

An instance of interaction of the ejecta with high density ambient medium is also provided by the coronal lines in the outburst spectra of recurrent novae. These are produced in a region shocked by the expansion of the envelope into the stellar wind of the secondary. Temperature of $\sim 10^6$ K has been estimated for the shocked region of the ejecta of RS Oph using a few coronal lines in the optical region (§IV.1.1.3). The shocked region is likely to contain regions of differing temperature and densities. Rayleigh–Taylor instabilities may even cause condensations in the shell. A detailed model of such inhomogeneities can be made from the observations of a large number of coronal lines from the ultraviolet to the infrared. Different regions of the ejecta could be ionized to differing degrees. One should use various density and temperature sensitive line ratios to construct a detailed model.

2. The Outburst

The spectra of novae during outburst are the most complicated to interpret. Studies are hence generally restricted to the determination of expansion velocities based on P-Cygni absorption features, qualitative description of the emission line spectra at different times, and a comparison of the spectral evolution with that of a standard nova (§I.1.2). The major hurdles are the high densities, large expansion velocities, non-steady-state evolution, and the variations in the characteristics of the energy source. Synthetic spectra need to be constructed similar to the ones used for supernovae (*cf.* Branch 1990), in order to improve our understanding of the spectral evolution.

Recent models of recombination lines produced in high-density environments and high optical depth conditions (§III.1) have enabled a qualitative inference of physical conditions in Nova Scuti 1989 and RS Oph 1985. In particular, it was found that the density varied as $3.2 \times 10^{11} t_d^{-2.02}$ cm^{-3} in Nova Sct and $8.36 \times 10^{12} t_d^{-2.26}$ cm^{-3} in RS Oph, where t_d is the time measured in days since outburst. The total mass of the shell was estimated as $3.5 \times 10^{-5}\ M_\odot$ for Nova Sct, and $3.1 \times 10^{-6}\ M_\odot$ for RS Oph.

The derived mass in the case of Nova Scuti increased directly with time. This has been explained as an effect of decreasing optical depth that allows one to see deeper into the envelope. Another contributing factor could be the fact that the outer part of the envelope could initially be neutral and the ionization front moves into it as the optical depth of the inner region to Lyman continuum decreases. In the case of RS Oph, the derived mass decreased as $t_d^{-0.3}$. Since the envelope mass is lower in RS Oph than in Nova Sct 1989, and also since RS Oph was observed at epochs later than those of Nova Sct 1989, the mass of its shell should remain constant in time. It has been assumed that the volume of the shell of Nova Sct increased as t_d^3 corresponding to free expansion. In the case of RS Oph, the volume was assumed to increase as t_d^2 corresponding to adiabatic expansion as the shell is interacting with circumstellar matter. The restriction on the constancy of mass suggests that volume varied as $t_d^{2.6}$, *i. e.* intermediate between free expansion and adiabatic expansion. It was possible to obtain the above information because of the availability of recombination line emissivities in high density conditions (Hummer & Storey 1987). However, considerable amount of uncertainity is introduced by the effect of high optical depth in Balmer lines. Detailed photoionization models have been employed in the analysis of emission lines in DQ Her by Matrin (1989). Similar models need to be constructed for other novae also.

In the case of RS Oph, a helium abundance of He/H= 0.16 is estimated, which implies moderate enrichment. He abundances could not be determined in the slow novae LW Ser and Nova Sct 1989 since considerable amount of He is in neutral form. Detailed models of the envelope would be needed before an abundance determination can be made at corresponding stages of the light curve. Abundances are best estimated during the nebular stage when the envelope is like a photoionized nebula though not of perceptible angular size. The systems are normally faint at this stage, and require moderate aperture telescopes for detailed spectroscopy.

The moderately slow novae LW Ser and Nova Sct 1989 exhibit spectral evolution that compares well with other novae of similar speed class. The principal, diffuse enhanced and Orion absorptions at ~ -750 km s^{-1}, ~ -1300 km s^{-1}, and ~ -1800 km s^{-1} could be identified in LW Ser, whereas only one system — probably diffuse enhanced — at -1300 km s^{-1} could be identified in Nova Sct 1989. The principal system had apparently weakened by the time of our early observations. Both these novae are characterized by oscillations in the light curve near maximum. In the case of Nova Sct 1989, the oscillations are more clearly seen as continuum variations rather than variations in the emission lines. The oscillations thus indicate variations in the photospheric radius, indicating inhomogeneities in the shell. Detailed models are required in this direction.

The spectral evolution of the fast nova RS Oph is similar to its past outbursts. The narrowing down of emission lines as the envelope is decelerated by interaction with the circumstellar matter is clearly seen. More continuous spectrophotometric monitoring than presented here are essential for all novae to induce motivation for theoretical modelling.

3. Interstellar Extinction and Distance

Most of the discussion in §1 and §2 above depends on the ability to deredden the observed spectrum. Interstellar colour excess of $E(B-V) = 0.5$ and 0.4 have been estimated for LW Ser and Nova Sct 1989 respectively, based on a comparison of the colours with other novae with known extinction. These estimates are not as accurate as the value available for RS Oph based on ultraviolet and radio observations. Such observations, as also the spectrophotometric observations of the ejecta beyond the nebular stage are necessary for an accurate estimation of extinction.

Whenever absolute fluxes are needed, the estimate of distance becomes important. The most accurate distances are obtained from the infrared and radio expansion parallaxes, and also from the angular size of the expanding nebulosity. An alternative is to study the interstellar extinction, or the 21 cm column density as a function of distance in the direction of the nova. All these methods are equally difficult and require assured time on sensitive telescopes.

Our best estimates of interstellar extinction and distances to LW Ser and Nova Sct 1989 suggest that they are underluminous compared to other novae of similar speed class by 1–2 mag. The interstellar extinction is not likely to be much higher than that estimated, since these novae would rise above the galactic plane in a few kpc. This leaves the possibility that the maxima of these novae were missed, and were 1–2 mag higher than recorded.

At present one depends largely on amateurs for discovery and follow up of the early light curves of novae. Dedicated surveys and immediate photometric and spectroscopic follow up of Galactic novae are desirable. More sensitive surveys in the nearby galaxies like the Magellanic Clouds and M31 should also be carried out, along with spectroscopic follow up on large telescopes. A ten-fold increase of the sample of novae with spectroscopic observations is likely to reveal intrinsic differences in novae of different luminosities in a given speed class.

Publications

Refereed Journals:

Evolution of the Optical Spectrum of SN 1987A in the Large Magellanic Cloud: B.N. Ashoka, G.C. Anupama, T.P. Prabhu, S. Giridhar, S.K. Jain, A.K. Pati & N. Kameswara Rao 1987, *J. Astrophys. Astr.*, **8**, 195.

RESPECT — Software for Reduction of Astronomical Spectra: T.P. Prabhu, G.C. Anupama & S. Giridhar 1987, *Bull. Astr. Soc. India,* **15**, 98.

Spectroscopic Evolution of Nova LW Serpentis 1978 during its Early Decline: T.P. Prabhu & G.C. Anupama 1987, *J. Astrophys. Astr.*, **8**, 369.

The 1985 Outburst of RS Ophiuchi: Spectroscopic Results: G.C. Anupama & T.P. Prabhu 1989, *J. Astrophys. Astr.,* **10**, 237.

Fourier Smoothing of Photographic Digital Spectra: G.C. Anupama 1990, *Bull. Astr. Soc. India* (in press).

Conference Proceedings:

The Optical Spectrum of RS Ophiuchi: G.C. Anupama & T.P. Prabhu 1987, in *RS Ophiuchi (1985) and the Recurrent Nova Phenomenon,* ed. M.F. Bode (Utrecht: VNU Sci. Press) p.17.

The Optical Spectrum of Nova LW Serpentis 1978: T.P. Prabhu & G.C. Anupama 1987, in *Proc. IAU Coll. 93: Cataclysmic Variables: Astrophys. Space Sci.,* **131**, 479.

Further Spectroscopic Observations of SN 1987A: G.C. Anupama, T.P. Prabhu, K.K. Ghosh, B.N. Ashoka, S. Giridhar & N. Kameswara Rao 1988, *Vistas Astr.,* **31**, 261.

Spectroscopic Results of the Recurrent Nova RS Ophiuchi: G.C. Anupama & T.P. Prabhu 1989, in *The Physics of Classical Novae: IAU Colloq. 122,* ed. A. Cassatella (Berlin: Springer) (in press).

Spectroscopic Observations of SN 1987A between 190 and 385 days since Outburst: G.C. Anupama, T.P. Prabhu, B.N. Ashoka, K.K. Ghosh, S. Giridhar, N. Kameswara Rao & S.K. Jain 1989, in *Proc. XI ERAM: New Windows to the Universe* (in press).

References

Allen, C.W. 1973, *Astrophysical Quantities* (London: Univ. London).

Almog, Y., Netzer, H. 1989, *Mon. Not. Roy. Astr. Soc.,* **238,** 57.

Anderson, P.H., Borra, E.F., Dubas, O.V. 1971, *Publ. Astr. Soc. Pacific,* **83,** 5.

Anderson, T.D. 1901, *Harvard College Obs. Circ. No.,* 56.

Andrillat, Y. 1977, in *Novae and Related Stars,* ed. M. Friedjung (Dodrecht: Reidel) p.155.

Andrillat, Y., Houziaux, L. 1982, in *The Nature of Symbiotic Stars,* eds. M. Freidjung & R. Viotti (Dordecht: Reidel) p.57.

Anthony-Twarog, B.J., Payne, D.M., Twarog, B.A. 1989, *Astr. J.,* **97,** 1048.

Antipova, L.I. 1974, *Highlights Astr.,* **3,** 501.

Anupama, G.C. 1990, *Bull. Astr. Soc. India* (in press).

Anupama, G.C., Prabhu, T.P. 1989, *J. Astrophys. Astr.,* **10,** 237.

Arp, H.C. 1956, *Astr. J.,* **61,** 15.

Bailey, J. 1975, *J. Br. Astr. Assoc.,* **85,** 217.

Barbon, R., Mammano, A., Rosino, L. 1968, in *Non-periodic Phenomenon in Variable Stars,* ed. L. Detre (Budapest: Academic Press) p.257.

Bath, G.T. 1978, *Quart. J. Roy. Astr. Soc.,* **19,** 442.

Bath, G.T., Shaviv, G. 1976, *Mon. Not. Roy. Astr. Soc.,* **175,** 305.

Bath, G.T., Shaviv, G. 1978, *Mon. Not. Roy. Astr. Soc.,* **183,** 515.

Beall, J.H., Knight, F.K., Smith, H.A., Wood, K.S., Lebofsky, M., Rieke, G. 1984, *Astrophys. J.,* **284,** 745.

Becker, R.H. 1989, in *Classical Novae,* eds. M.F. Bode & A. Evans (New York: John Wiley) p.215.

Becker, R.H., Marshall, F.E. 1981, *Astrophys. J. (Lett.),* **244,** L93.

Berman, L. 1932, *Publ. Astr. Soc. Pacific,* **44,** 318.

Bessel, M.S. 1986, *Publ. Astr. Soc. Pacific,* **98,** 1303.

Bhatia, A.K., Feldman, U., Doschek, G.A. 1979, *Astr. Astrophys.,* **80,** 22.

Bianchini, A. 1990, *Astr. J.*, **99**, 1941.

Bianchini, A., Hamzaoglu, E., Sabbadin, F. 1981, *Astr. Astrophys.*, **99**, 392.

Bianchini, A., Middleditch, J. 1976, *Inf. Bull. Var. Stars* No. 1151.

Bianchini, A., Sabbadin, F. 1983, *Astr. Astrophys. Suppl.*, **54**, 393.

Bianchini, A., Sabbadin, F., Favero, G.C., Dalmeri, I. 1986, *Astr. Astrophys.*, **160**, 367.

Bohigas, J., Echevarría, J., Diego, F., Sarimiento, J.A. 1989, *Mon. Not. Roy. Astr. Soc.*, **233**, 1395.

Bode, M. 1987, ed., *RS Ophiuchi (1985) and the Recurrent Nova Phenomenon* (Utrecht: VNU Sci. Press).

Bode, M.F., Evans, A. 1983, *Mon. Not. Roy. Astr. Soc.*, **203**, 285.

Bode, M.F., Evans, A. 1989, eds., *Classical Novae* (New York: John Wiley).

Bode, M.F., Evans, A. 1989, in *Classical Novae,* eds. M.F. Bode & A. Evans (New York: John Wiley) p.163.

Bode, M.F., Kahn, F.D. 1985, *Mon. Not. Roy. Astr. Soc.*, **217**, 205.

Bode, M.F., Seaquist, E.R., Frail, D.A., Roberts, J.A., Whittet, D.C.B., Evans, A., Albinson, J.S. 1987, *Nature,* **329**, 519.

Branch, D. 1990, in *Supernovae,* ed. A.G. Petschek (New York: Springer-Verlag), p.30.

Brault, J.W., White, O.R. 1971, *Astr. Astrophys.*, **13**, 169.

Brocklehurst, M. 1971, *Mon. Not. Roy. Astr. Soc.*, **153**, 271.

Bruch, A. 1986, *Astr. Astrophys.*, **167**, 91.

Bruch, A., Duerbeck, H.W., Seitter, W.C. 1981, *Mitt. Astr. Ges.*, **52**, 34.

Campbell, L. 1948, *Harvard Ann.*, **116**, 191.

Cannizzo, J.K., Kenyon, S.J. 1986, *Astrophys. J. (Lett.)*, **309**, L43.

Capaccioli, M., Della Valle, M., D'Onofrio, M., Rosino, L. 1989, *Astr. J.*, **97**, 1622.

Cassatella, A., Gilmozzi, R., Selvelli, P.L. 1985, in *Recent Results on Cataclysmic Variables,* ed. W.R. Burke (Noordwijk: ESA SP-236) p.213.

Cassatella, A., Hassall, B.J.M., Harris, A., Snijders, M.A.J. 1985, in *Recent Results on Cataclysmic Variables,* ed. W.R. Burke (Noordwijk: ESA SP-236) p.281.

Cassatella, A., Selvelli, P.L. 1988, in *A Decade of UV Astronomy with IUE: Proc. Celebratory Symp.,* GSFC, Greenbelt, **1,** p.9.

Catchpole, R.M. 1969, *Mon. Not. Roy. Astr. Soc.,* **142,** 119.

Chanan, G.A., Nelson, J.E., Margon, B. 1978, *Astrophys. J.,* **226,** 962.

Chandrasekhar, S. 1967, *An Introduction to the study of Stellar Structure* (New York: Dover).

Chincarni, G., Rosino, L. 1964, *Ann. Astrophys.,* **27,** 469.

Clegg, R.E.S. 1987, *Mon. Not. Roy. Astr. Soc.,* **229,** 31p.

Cohen, J.G. 1985, *Astrophys. J.,* **292,** 90.

Cohen, J.G., Rosenthal, A.J. 1983, *Astrophys. J.,* **268,** 689.

Collin-Souffrin, S. 1977, in *Novae and Related Stars,* ed. M. Friedjung (Dodrecht: Reidel) p.123.

Corbally, C.J., Garrison, S.J., Garrison, R.F. 1983, in *The MK Process and Stellar Classification,* ed. R.F. Garrison (Toronto: Univ. Toronto), p.277.

Cordova, F.A., Mason, K.O. 1984, *Mon. Not. Roy. Astr. Soc.,* **206,** 890.

Couderc, P. 1939, *Ann. Astrophys.,* **2,** 271.

Crampton, D., Cowley, A.P., Fisher, W.A. 1986, *Astrophys. J.,* **300,** 788.

Crawford, J.A., Kraft, R.P. 1956, *Astrophys. J.,* **123,** 44.

Cropper, M. 1990, *Mon. Not. Roy. Astr. Soc.,* **243,** 144.

de Robertis, M.M., Dufour, R.J., Hunt, R.W. 1987, *J. Roy. Astr. Soc. Canada,* **81,** 195.

Drake, S.A., Ulrich, R.K. 1980, *Astrophys. J. Suppl.,* **42,** 351.

Duerbeck, H.W. 1981, *Publ. Astr. Soc. Pacific,* **93,** 165.

Duerbeck, H.W. 1987, *ESO Messenger,* No. 50, 8.

Duerbeck, H.W., Seitter, W.C. 1979, *ESO Messenger,* No. 17, 1.

Duerbeck, H.W., Seitter, W.C. 1989, in *The Physics of Classical Novae: IAU Colloq. 122,* ed. A. Cassatella (Berlin: Springer) (in press).

Dufay, J., Bloch, M., Bertaud, G., Dufay, M. 1964, *Ann. Astrophys.,* **27,** 555.

Eggen, O.J., Mathewson, D.S., Serkowski, K. 1967, *Nature,* **275,** 400.

Egret, D., Keenan, P.C., Heck, A. 1982, *Astr. Astrophys.,* 106, 115.

Evans, A., Callus, C.M., Albinson, J.S., Whitelock, P.A., Glass, I.S., Carter, B., Roberts, G. 1988, *Mon. Not. Roy. Astr. Soc.,* **234,** 755.

Farragiana, R., Gerbaldi, M., van't Veer, C., Floqust, M. 1988, *Astr. Astrophys.,* **201,** 259.

Feast, M.W., Glass, I.S. 1974, *Mon. Not. Roy. Astr. Soc.,* **167,** 81.

Feibleman, W.A., Aller, L.H. 1987, *Astrophys. J.,* **519,** 407.

Ferland, G.J. 1977, *Nature,* **267,** 597.

Ferland, G.J. 1979, *Astrophys. J.,* **231,** 781.

Ford, H. 1978, *Astrophys. J.,* **219,** 595.

Friedjung, M. 1989, in *Classical Novae,* eds. M.F. Bode & A. Evans (New York: John Wiley) p.187.

Friend, M.T., Martin, J.S., Smith, R.C., Jones, D.H.P. 1988, *Mon. Not. Roy. Astr. Soc.,* **233,** 451.

Frogel, J.A., Persson, S.E., Aaronson, M., Matthews, K. 1978, *Astrophys. J.,* **220,** 75.

Gallagher, J.S., Code, A.F. 1974, *Astrophys. J. (Lett.),* **189,** L23.

Gallagher, J.S., Oinas, V. 1974, *Publ. Astr. Soc. Pacific,* **86,** 952.

Gallagher, J.S., Starrfield, S.G. 1976, *Mon. Not. Roy. Astr. Soc.,* **176,** 53.

Gallagher, J.S., Starrfield, S.G. 1978, *Ann. Rev. Astr. Astrophys.,* **16,** 171.

Garcia, M.R. 1986, *Astr. J.,* **91,** 1400.

Geisel, S.L., Kleinmann, D.E., Low, F.J. 1970, *Astrophys. J. (Lett.),* **161,** L101.

Gerhz, R.D. 1988, *Ann. Rev. Astr. Astrophys.,* **26,** 377.

Gerhz, R.D., Grasdalen, G.L., Hackwell, J.A. 1985, *Astrophys. J. (Lett.),* **298,** L47.

Gerhz, R.D., Grasdalen, G.L., Hackwell, J.A., Ney, E.P. 1980, *Astrophys. J.,* **337,** 835.

Gorbatskii, V.G. 1972, *Sov. Astr.,* **16,** 32.

Gorbatskii, V.G. 1973, *Sov. Astr.,* **17,** 111.

Griffin, R., Thackery, A.D. 1958, *Observatory,* **78,** 245.

Hardie, R.H. 1962, in *Astronomical Techniques,* ed. W.A. Hiltner (Chicago: Chicago Univ. Press) p.178.

Harmanec, P. 1974, in *Late Stages of Stellar Evolution: IAU Symp. 66,* eds. R.J. Taylor & J.E. Hesser (Dodrecht: Reidel), p.195.

Hessman, F.V. 1989, *Mon. Not. Roy. Astr. Soc.,* **239,** 759.

Hjellming, R.M., Wade, C.M. 1970, *Astrophys. J. (Lett.),* **162,** L2.

Hjellming, R.M., van Gorkom, J.H., Taylor, A.R., Seaquist, E.R., Padin, S., Davis, R.J., Bode, M.F. 1986, *Astrophys. J. (Lett.),* **305,** L71.

Horne, K. 1986, *Publ. Astr. Soc. Pacific,* **98,** 609.

Horne, K. 1988, in *New Directions in Spectrophotometry,* eds. A.G.D. Philip, D. Hayes, S. Adelman (Schenectady: L. Davis Press).

Horne, K., Schneider, D.P. 1989, *Astrophys. J.,* **343,** 888.

Hubble, E. 1929, *Astrophys. J.,* **69,** 103.

Hummer, D.G., Storey, P.J. 1987, *Mon. Not. Roy. Astr. Soc.,* **224,** 801.

Hutchings, J.B. 1979, *Astrophys. J.,* **230,** 162.

Hyland, A.R., Neugebauer, G. 1970, *Astrophys. J. (Lett.),* **219,** L11.

Jacobs, V.L., Davis, J., Keeple, P.C., Blaha, M. 1977. *Astrophys. J.,* **211,** 605.

Joy, A.H. 1938, *Publ. Astr. Soc. Pacific,* **50,** 300.

Joy, A.H., Swings, P. 1945, *Astrophys. J.,* **102,** 353.

Kaluzny, J., Chlebowski,T. 1988, *Astrophys. J.,* **332,** 287.

Kastner, S.O. 1976, *Sol.Phys.,* **46,** 179.

Kastner, S.O. 1977, *Astr. Astrophys.,* **54,** 255.

Kastner, S.O., Bhatia, A.K. 1979, *Astr. Astrophys.,* **71,** 211.

Kato, M. 1990a, *Astrophys. J.,* **355,** 277.

Kato, M. 1990b, *Astrophys. J. (Lett.)* (in press).

Kenyon, S.J. 1985, *Symbiotic Stars* (Cambridge: Cambridge Univ. Press).

Kenyon, S.J., Fernandez-Castro, T. 1987, *Astr. J.,* **93,** 938.

Kenyon, S.J., Garcia, M.R. 1986, *Astr. J.,* **91,** 125.

Kenyon, S.J., Webbink, R.F. 1984, *Astrophys. J.,* **279,** 252.

King, A.R. 1989, in *Classical Novae,* eds. M.F. Bode & A. Evans (New York: John Wiley) p.17.

King, A.R., Ricketts, M.J., Warwick, R.S. 1979, *Mon. Not. Roy. Astr. Soc.,* **187,** 77p.

Kovetz, A., Prialnik, D., Shara, M.M. 1988, *Astrophys. J.,* **325,** 828.

Kraft, R.P. 1958, *Astrophys. J.,* **127,** 625.

Kraft, R.P. 1964, *Astrophys. J.,* **139,** 457.

Krautter, J. Williams, R.E. 1988, *ESO Messenger,* No. 54, 33.

Krolik, J.H., McKee, C.F. 1978, *Astrophys. J. Suppl.,* **37,** 459.

Kutter, G.S., Sparks, W.M. 1980, *Astrophys. J.,* **239,** 988.

Lamb, D.Q., Patterson, J. 1983, in *Cataclysmic Variables and Related Objects,* eds. M. Livio & G. Shaviv (Dordercht: Reidel), p.229.

Lance, C.M., McCall, M.L., Uomoto, A.K. 1988, *Astrophys. J. Suppl.,* **66,** 151.

Landini, M., Fossi, B.C.M. 1972, *Astr. Astrophys. Suppl.,* **7,** 291.

Landolt, A.U. 1970, *Publ. Astr. Soc. Pacific,* **82,** 86.

Lee, C.W., Mathieu, R.D., Latham, D.W. 1989, *Astr. J.,* **97,** 1710.

Lindgren, H. 1975, *Rep. Obs. Lund,* No. 6, 15.

Lines, H.C., Lines, R.D., McFaul, T.G. 1988, *Astr. J.,* **95,** 1505.

Livio, M. 1988, in *The Symbiotic Phenomenon,* eds. J. Mikolajewska *et al.* (Kluwer Academic) p.323.

Livio, M. 1989, in *The Physics of Classical Novae: IAU Colloq. 122,* ed. A. Cassatella (Berlin: Springer) (in press).

Livio, M., Shara, M.M. 1987, *Astrophys. J.,* **319,** 819.

Livio, M., Truran, J.W., Webbink, R.F. 1986, *Astrophys. J.,* **308,** 736.

Martin, P.G. 1989, in *Classical Novae,* eds. M.F. Bode & A. Evans (New York: John Wiley) p.73; p.113.

Mason, H.E. 1975, *Mon. Not. Roy. Astr. Soc.,* **170,** 651.

Mason, K.O., Cordova, F.A., Bode, M.F., Barr, P. 1987, in *RS Ophiuchi (1985) and the Recurrent Nova Phenomenon,* ed. M.F. Bode (Utrecht: VNU Sci. Press) p.167.

McLaughlin, D.B. 1936, *Astrophys. J.,* **84,** 104.

McLaughlin, D.B. 1945, *Publ. Astr. Soc. Pacific,* **57,** 69.

McLaughlin, D.B. 1960, in *Stellar Atmospheres,* ed. J.L Greenstein (Chicago:

Chicago Univ. Press) p.585.

Meinel, A.B., Aveni, A.F., Stockton, M.W. 1975, *Catalog of Emission Lines in Astrophysical Objects,* Tech. Rep. No. 27 (Tuscon: Optical Sciences Center, Univ. Arizona).

Minkowski, R. 1943, *Publ. Astr. Soc. Pacific,* **55,** 101.

Mustel, E.R., Boyarchuk, A.A. 1970, *Astrophys. Space Sci.,* **6,** 183.

Nariai, K., Nomoto, K., Sugimoto, D. 1980, *Pub. Astr. Soc. Japan,* **32,** 472.

Netzer, H. 1975, *Mon. Not. Roy. Astr. Soc.,* **171,** 395.

Ney, E.P., Hatfield, B.F. 1978, *Astrophys. J. (Lett.),* **219,** L11.

Nussbaumer, H. 1986, *Astr. Astrophys.,* **155,** 205.

Nussbaumer, H., Schild, H. 1979, *Astr. Astrophys.,* **75,** L17.

Nussbaumer, H., Stencel, R.E. 1987, in *Scientific Accomplishments of the IUE,* ed. Y. Kondo (Dordrecht: Reidel) p.203.

O'Brien, T.J., Kahn, F.D. 1987, *Mon. Not. Roy. Astr. Soc.,* **228,** 277.

O'Connell, R.W. 1973, *Astr. J.,* **78,** 1074.

Ögleman, H., Beurmann, K., Krautter, J. 1984, *Astrophys. J. (Lett.),* **287,** L31.

Ögleman, H., Krautter, J., Beurmann, K. 1987, *Astr. Astrophys.,* **177,** 110.

Oort, J.H. 1951, in *Problems of Cosmical Aerodynamics,* ed. J. Burgess (Ohio: Central Air Documents) p.118.

Orio, M. 1987, *Ph.D Thesis.*

Osterbrock, D.E. 1974, *Astrophysics of Gaseous Nebulae* (San Fransisco: Freeman).

Paczyński, B. 1965, *Acta Astr.,* **15,** 197.

Patterson, J., Robinson, J.L., Nather, R.E. 1978, *Astrophys. J.,* **224,** 570.

Payne-Gaposchkin, C. 1957, *The Galactic Novae* (Amsterdam: North-Holland Publ. Co.).

Payne-Gaposchkin, C. 1977, *Astr. J.,* **82,** 665.

Pease, F.G. 1917, *Publ. Astr. Soc. Pacific,* **29,** 256.

Peel, M. 1985, *J. Am. Assoc. Var. Star Obs.,* **14,** 8.

Peel, M. 1990, *J. Br. Astr. Assoc.,* **100,** 136.

Perrine, C.D. 1902, *Astrophys. J.,* **16,** 249.

Pettit, E. 1946, *Publ. Astr. Soc. Pacific,* **58,** 359.

Plavec, M., Ulrich, R.K., Polidan, R.S. 1973, *Publ. Astr. Soc. Pacific,* **85,** 769.

Porcas, R.W., Davis, R.J., Graham, D.A. 1987, in *RS Ophiuchi (1985) and the Recurrent Nova Phenomenon,* ed. M.F. Bode (Utrecht: VNU Sci. Press) p.203.

Pottasch, S.R. 1959, *Ann. Astrophys.,* **22,** 394.

Pottasch, S.R. 1967, *Bull. Astr. Inst. Neth.,* **19,** 227.

Prabhu, T.P. 1977, *Kodaikanal Obs. Bull. Ser. A,* **2,** 75.

Prabhu, T.P., Anupama, G.C. 1987, *J. Astrophys. Astr.,* **8,** 369.

Prabhu, T.P., Anupama, G.C., Giridhar, S. 1987, *Bull. Astr. Soc. India,* **15,** 98.

Prialnik, D., Livio, M., Shaviv, G., Kovetz, A. 1982, *Astrophys. J.,* **257,** 312.

Prialnik, D., Shara, M.M. 1986, *Astrophys. J.,* **311,** 172.

Reynolds, S.P., Chevalier, R.A. 1984, *Astrophys. J. (Lett.),* **281,** L33.

Ritchey, G.W. 1901, *Astrophys. J.,* **14,** 167.

Robinson, E.L. 1975, *Astr. J.,* **80,** 515.

Robinson, K., Bode, M.F., Meaburn, J., Whitehead, M.J. 1989, in *Dynamics of Astrophysical Discs,* ed. J.A. Sellwood (Cambridge: Cambridge Univ. Press) p.85.

Rosino, L. 1987, in *RS Ophiuchi (1985) and the Recurrent Nova Phenomenon,* ed. M.F. Bode (Utrecht: VNU Sci. Press) p.1.

Rosino, L., Bianchini, A., Rafanelli, P. 1982, *Astr. Astrophys.,* **108,** 243.

Rosino, L., Iijima, T. 1987, in *RS Ophiuchi (1985) and the Recurrent Nova Phenomenon,* ed. M.F. Bode (Utrecht: VNU Sci. Press) p.27.

Rybicki, G.A., Lightman, A.P. 1979, *Radiative Processes in Astrophysics* (New York: John Wiley).

Sabbadin, F., Bianchini, A. 1983, *Astr. Astrophys. Suppl.,* **54,** 393.

Sanduleak, N., Stephenson, C.B. 1973, *Astrophys. J.,* **185,** 899.

Sanford, R.F., 1949, *Astrophys. J.,* **109,** 81.

Savage, B.D., Mathis, J.S. 1979, *Ann. Rev. Astr. Astrophys.,* **17,** 73.

Schaefer, B. 1988, *Astrophys. J.,* **327,** 347.

Schmid, H.M. 1989, *Astr. Astrophys.,* **211,** L31.

Seaquist, E.R., 1989, in *Classical Novae,* eds. M.F. Bode & A. Evans (New York: John Wiley) p.143.

Seaquist, E.R., Bode, M.F., Frail, D.A., Roberts, J.A., Evans, A., Albinson, J.S. 1989, *Astrophys. J.,* **344,** 805.

Seitter, W.C. 1977, in *Novae and Related Stars,* ed. M. Friedjung (Dodrecht: Reidel) p.183.

Seitter, W.C. 1987, in *RS Ophiuchi (1985) and the Recurrent Nova Phenomenon,* ed. M.F. Bode (Utrecht: VNU Sci. Press) p.63.

Seitter, W.C. 1989, in *The Physics of Classical Novae: IAU Colloq. 122,* ed. A. Cassatella (Berlin: Springer) (in press).

Seitter, W.C., Duerbeck, H.W. 1987, in *RS Ophiuchi (1985) and the Recurrent Nova Phenomenon,* ed. M.F. Bode (Utrecht: VNU Sci. Press) p.71.

Sekiguchi, K. *et al.* 1990, *Mon. Not. Roy. Astr. Soc.,* **246,** 78.

Selvelli, P.L. 1989, *Mem. Soc. Astr. It.,* **60,** 151.

Shaefer, B.E. 1990, *Astrophys. J. (Lett.),* **335,** L39.

Shara, M.M. 1989, *Publ. Astr. Soc. Pacific,* **101,** 5.

Shara, M.M., Livio, M., Moffat, A.F.J., Orio, M. 1986, *Astrophys. J.,* **311,** 163.

Shara, M.M., Moffat, A.F.J., Williams, R.E., Cohen, J.G. 1989, *Astrophys. J.,* **337,** 720.

Sharpless, S.L. 1956, *Astrophys. J.,* **124,** 342.

Shaviv, G., Starrfield, S. 1988, *Astrophys. J.,* **335,** 383.

Shcherbakov, A.G. 1977, *Sov. Astr. Lett.,* **3,** 244.

Shields, G.A., Ferland, G.J. 1978, *Astrophys. J.,* **225,** 950.

Shylaja, B.S. 1986, *Ph.D Thesis.*

Smak, J. 1990, in *Structure and Emission Properties of Accretion Discs: IAU Colloq. 129* (in press).

Snijders, M.A.J. 1987, in *RS Ophiuchi (1985) and the Recurrent Nova Phenomenon,* ed. M.F. Bode (Utrecht: VNU Sci. Press) p.51.

Snijders, M.A.J., Batt, T.J., Roche, P.F., Seaton, M.J., Morton, D.C., Spoelstra, T.A., Blades, J.C. 1987, *Mon. Not. Roy. Astr. Soc.,* **228,** 329.

Solf, J. 1983, *Astrophys. J.,* **273,** 647.

Starrfield, S. 1988, in *Multiwavelength Astrophysics,* ed. F.A. Cordova (Cambridge: Cambridge Univ. Press) p.159.

Starrfield, S. 1989, in *Classical Novae,* eds. M.F. Bode & A. Evans (New York: John Wiley) p.39.

Starrfield, S., Sparks, W.M., Shaviv, G. 1989, *Astrophys. J. (Lett.),* **325,** L35.

Starrfield, S., Sparks, W.M., Truran, J.W. 1976, in *Structure and Evolution of Close Binary Systems: IAU Symp. 73,* eds. P. Eggleton, S. Mitton, & J.A.J. Whelan (Dordercht: Reidel) p.155.

Starrfield, S., Sparks, W.M., Truran, J.W. 1985, *Astrophys. J.,* **291,** 136.

Starrfield, S., Truran, J.W., Sparks, W.M., Kutter, G.S. 1972, *Astrophys. J.,* **176,** 169.

Stockmon, H.S., Schmidt, G., Lamb, D.Q. 1988, *Astrophys. J.,* **332,** 282.

Stratton, F.J.M., Manning, W.H. 1939, *Atlas of Spectra of Nova Herculis 1939,* (Cambridge: Solar Phys. Obs.).

Strittmatter, P.A., Woolf, N.J., Thompson, R.I., Wilkerson, S., Angel, J.R.P., Stockman, H.S., Gilbert, G., Grandi, G., Larson, H., Fink, U. 1977, *Astrophys. J.,* **216,** 23.

Swings, P., Struve, O. 1941, *Astrophys. J.,* **94,** 291.

Swope, H. 1940, *Harvard Bull.,* No. 913, 11.

Szkody, P., Dyck, H.M., Capps, R.W., Becklin, E.E., Cruickshank, D.P. 1979, *Astr. J.,* **84,** 1359.

Taylor, A.R., Davis, R.J., Porcas, R.W., Bode, M.F. 1989, *Mon. Not. Roy. Astr. Soc.,* **237,** 81.

Truran, J.W. 1982, in *Essays in Nuclear Astrophysics,* eds. C.A. Barnes, D.D. Clayton & D.N. Schramm (Cambridge: Cambridge Univ. Press) p.467.

van den Bergh, S., Younger, P.F. 1987, *Astr. Astrophys. Suppl.,* **70,** 125.

Vogt, N. 1982, *Mitt. Astr. Ges.,* **57,** 79.

Vogt, N. 1989, in *Classical Novae,* eds. M.F. Bode & A. Evans (New York: John Wiley) p.225.

Walker, A.R. 1977, *Mon. Not. Roy. Astr. Soc.,* **179,** 587.

Walker, A.R. 1979, *Publ. Astr. Soc. Pacific,* **91,** 46.

Walker, M.F. 1954, *Publ. Astr. Soc. Pacific,* **66,** 230.

Wallerstein, G., Garnavich, P.M. 1986, *Publ. Astr. Soc. Pacific,* 98, 875.

Warner, B. 1975, *Mon. Not. Roy. Astr. Soc.,* **170,** 219.

Warner, B. 1976, in *Structure and Evolution of Close Binary Systems,* eds. P. Eggleton, S. Mitton & J.A.J. Whelan (Dordercht: Reidel) p.85.

Warner, B. 1983, in *Cataclysmic Variables and Related Objects,* eds. M. Livio & G. Shaviv (Dordercht: Reidel) p.155.

Warner, B. 1989, in *Classical Novae,* eds. M.F. Bode & A. Evans (New York: John Wiley) p.1.

Watson, M.G., King, A.R., Osborne, J. 1985, *Mon. Not. Roy. Astr. Soc.,* **212,** 917.

Weaver, H. 1974, *Highlights Astr.,* **3,** 509.

Webbink, R.F. 1976, *Nature,* **262,** 271.

Webbink, R.F. 1989, in *The Physics of Classical Novae: IAU Colloq. 122,* ed. A. Cassatella (Berlin: Springer) (in press).

Webbink, R.F., Livio, M., Truran, J.W., Orio, M. 1987, *Astrophys. J.,* **314,** 653.

Whitney, B.A., Clayton, G.C. 1989, *Astr. J.,* **98,** 297.

Williams, G. 1983, *Astrophys. J. Suppl.,* **53,** 523.

Williams, R.E. 1977, in *Interaction of Variable Stars with their Environment,* eds. R. Kippenhahn, J. Rahe & W. Strohmein (Bamberg: Remeis-Sternwarte) p.242.

Williams, R.E. 1981, *Sci. American,* **244,** 96.

Williams, R.E. 1982, *Astrophys. J.,* **261,** 170.

Williams, R.E. 1989, in *The Physics of Classical Novae: IAU Colloq. 122,* ed. A. Cassatella (Berlin: Springer) (in press).

Williams, R.E., Ney, E.P., Sparks, W.M., Starrfield, S., Truran, J.W., Wyckoff, S. 1984, *Mon. Not. Roy. Astr. Soc.,* **212,** 753.

Wu, C.-C., Panek, R.J., Holm, A.W., Raymond, J.C., Hartmann, L.W., Swank, J.H. 1989, *Astrophys. J.,* **339,** 441.

Yamashita, Y., Ichimura, K., Nakagiri, M., Norimoto, Y., Maehara, H., Miyajima, K. 1977, *Publ. Astr. Soc. Japan,* **29,** 527.